Geotechnical Properties of Coal and Mine Pillar Design in the Greymouth and Reefton Coalfields, West Coast, South Island

---

A thesis
submitted in partial fulfilment
of the requirements for the Degree
of
Master of Science in Engineering Geology
at the
University of Canterbury
by

Dean Michael Harris

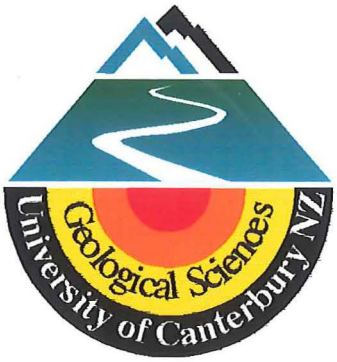

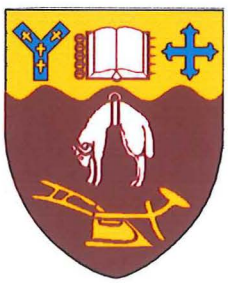

University of Canterbury
2002

Frontispiece

Coal mining,
which began in a small way,
has developed into an industry of great consequence,
that promises to be even more important in the future.

Percy Gates Morgan
The Geology of the Greymouth Subdivision,
North Westland.
New Zealand Geological Survey Bulletin No. 13
1911

Abstract

This project has estimated coal strength in selected parts of the Greymouth and Reefton Coalfields in order to better estimate the size of pillars needed to maintain stability of the underground workings. Coal strength in known to decrease with increasing rank, and the Greymouth Coalfield displays to a very high rank gradient increasing from west to east. The mines assessed by this study were the Bishop Block, Strongman No. 2, Spring Creek, Roa and Terrace (Reefton Coalfield) Mines.

Core samples could not be obtained from all locations so 63.5mm cubes and point load tests were used, and compared to a control group of with a known UCS/cube relationship, in order to develop an equation from which a $UCS_{equivalent}$ value could be determined.

Coal strength drops from 24 MPa in the west (Strongman No. 2 E seam) to 1.3 MPa in the east of the coalfield (Roa mine Kimbell seam). Other coal properties also shows changes corresponding to changes in coal strength including carbon, volatile matter, ash, and the degree of cleating. Ash is the only one of these which is not related to increasing rank. Cleat frequency, which increases with coal rank has the most significant effect on coal strength.

The equations of Bieniawski and Salamon-Munro have been used for pillar strength calculations with panel pillars designed to a factor of safety of 1.6. Optimum pillar sizes for each of the locations in this study have been calculated, but small changes to these sizes may be necessary depending on local conditions such as faults and sheared zones. Pillar design must take into account the chance of pillar shearing once seam dip increases above 20° as the shear strength becomes greatly reduced with increasing seam dip. Coal from the Spring Creek Mine shows a high degree of anisotropy and so pillars have been designed for specific seam dips at this location.

Bearing capacity of the fireclay in the Terrace Mine is greatly reduced with increasing seam dip and overburden thickness, thus increasing the chances of floor heave. Pillars need to be of adequate size so as not to transfer excess overburden load to the mine floor, which would result in floor heave.

Table of Contents

Part 1. Chapters 1-5

Chapter 1. Introduction

Chapter 2. Laboratory Estimation of Coal Strength

Chapter 4. Pillar Design

Chapter 5. Mining Implications

Chapter 6. Summary and Conclusions

Part 2. Appendices

Appendix 1.

Appendix 2. Unconfined Compressive Strength Determination of Cores Samples

Appendix 3. Unconfined Compressive Strength Determination of Cubes Samples

Appendix 7. Shear Strength

Appendix 8. Proximate Analysis Data

Appendix 9. Pillar Design

List of Figures

List of Tables

Abbreviations used in Text

ASTM	American Society for Testing Materials
CCS	Cube compressive strength
DH	Drill hole
E/OC	Strongman No. 2 mine E seam (Samples taken from opencast mine)
E/UG	Strongman No. 2 mine E seam (Samples taken from underground)
FOS	Factor of safety
GCL	Greymouth Coal Ltd
$I_{a(50)}$	Strength anisotropy index
$I_{s(50)}$	Point load strength index
ISRM	International Society for Rock Mechanics
JRC	Joint roughness coefficient
L/D ratio	Length/Diameter ratio
MNU	Spring Creek Main Upper seam
Mt	Million tonnes
R^2, r^2	Correlation coefficient of a data set
RMR	Rock mass rating system of Bieniawski (1989)
SC/D	Spring Creek Mine D seam
SC/MNU	Spring Creek Mine Main Upper seam
SM/D	Strongman No. 2 Mine D seam
SM/E/OC	Strongman No. 2 Mine E seam (Samples taken from opencast mine)
SM/E/UG	Strongman No. 2 Mine E seam (Samples taken from underground)
RoMax	Mean maximum vitrinite reflectance
UCS	Unconfined compressive strength
$UCS_{equivalent}$	Estimated unconfined compressive strength value
w_{eff}	Effective width of a mine pillar
w/h	Width/height ratio for mine pillars

Acknowledgements

I must give a huge thank you to Solid Energy International for the financial support and the locations which made this project possible. Thanks for all the coal samples which were a pretty fundamental part of the project, and to the Solid Energy staff who helped me out along the way during my work.

Thank you to my supervisor Dave Bell for answering my questions, proof reading all of my chapters, and for giving me guidance along the way. You made sure that my story made sense to more people than just me. Those red pens sure came in handy didn't they. Fortunately you didn't get to see this page or I would still be sitting here fixing the gramm'r and spellin. Thanks to my co-supervisor Laurie Richards for the original topic for this thesis and for the contacts at Solid Energy to make it happen. Thanks also for the guidance along the way when I started to get lost and not know what I was doing, and for answering all my questions.

To Jonny McNee who helped me collect and carry my first lot of samples from the Strongman No. 2 mine, when I didn't really know what I wanted. Thanks for all the information and maps that you provided me with. They were an invaluable part of this project. I would have gotten lost on the Bishop Block bush bash without you and Rob there to help. Thanks to you both for scoring the helicopter to get those samples out of there. It would have killed me otherwise.

To Rob Boyd for helping collect the samples from Spring Creek and crashing around up in the bush of the Bishop Block. It was quite an entertaining day up there, capped off by having to crash start the truck because 'someone' left the lights on. Can you thank those two guys who gave us a ride out of Spring Creek. That saved my poor little arms carrying all that coal. Thanks for answering all my email question so promptly, and reading the draft of this little story. You must not be working hard enough.

Other Solid Energy staff that need a big thanks are the following: Dingy (Kevin) Pattinson for providing me with samples, feasibility studies, mining history, proximate analyses and everything else that I needed to know about the Terrace mine. Stu Henley for supplying me with previous strength test results and other things that I required, and for reading the draft of my thesis. Dean Fergusson and Richard Campbell form Huntly who also gave me some information that I couldn't find anywhere else.

Thanks to the Francis Mining Co Ltd for letting me collect samples from the Roa mine, and to Paul Caffyn who took me there to collect them and for the reports any other stuff that you supplied me with.

Thanks to all of the Geology Department technical staff, Cathy Knight, John Southward, Rob Spiers and Arthur Nichols, for helping me out with different things along the way, showing me how things worked and generally sorted out any problems that I had.

Thanks to Nigel and Jane Newman who between them supplied me with various reports that I required, conducted vitrinite reflectance tests, got proximate analyses done, and shared their vast amount of knowledge about the properties and problems of coal.

A special thanks to Amanda for putting up with me while all this was going on, the bad moods, always being tired and busy. Thanks also for taking the photos when I couldn't get your camera to work (Stupid thing), and for helping me to sort out the mountain of paper at the very end. A big thanks to Amanda's parents, Bev and Garry for giving me somewhere to stay when I had nowhere else to live.

A final thanks to Tim Clark who has been through this before and once gave me the encouraging words 'just when you think you can see the light at the end of the tunnel, you realise it's a train coming from the other direction'. Thanks Timee, much appreciated.

Thank you to anybody that I may have forgotten. Sorry that you got left out, but those of you who know me well will know that my memory is not that good anymore. I'm getting old.

Part 1

Chapters 1-6

Chapter 1. Introduction

1.1 Project Formulation

1.1.1 Location of Study Area

This project is based in two separate areas of South Island, New Zealand. The Greymouth Coalfield, where the majority of the study is based, is a 100km^2 area of North Westland on the West Coast of the South Island, 10km north of Greymouth (Figure 1.1). The Terrace Mine is situated at the south-western limit of the Reefton Coalfield, on the outskirts of the Reefton Township, North Westland c. 80km to the north-west of Greymouth (Figure 1.2). Coal mined in the Greymouth Coalfield is largely contained in the Morgan and Rewanui Coal Measures of the Paparoa Group (Figure 1.3), with the early years of mining in this region concentrated on the Brunner Coal Measures. Coal from the Reefton Coalfield is mined exclusively from the Brunner Coal Measures.

1.1.2 Background

Two things that are very important in underground mining are safety of the workforce and profitability of the mine. The main safety issues in underground mining arise from the possibility of ignition of methane gas, spontaneous combustion of coal, and roof or pillar collapse. One aim of this study is to provide a method of determining a stable pillar size. To achieve this the strength of the coal must be accurately determined, roof-supporting pillars designed to the optimum size meeting the conditions present in each mine.

This thesis project arose because of a lack of any significant coal strength data for the Greymouth Coalfield, and for the Terrace mine in Reefton. Testing had been conducted on samples from the Bishop Creek Block, Roa, Spring Creek and Strongman No. 2 Mines (as well as other locations not included in this project), but there were usually too few tests to provide a valid estimate of the coal strength in these areas. This study will assist Solid Energy Ltd and Francis Mining (owners of the Roa Mine) with pillar sizing in their

currently operation mines, and with the planned new underground mine in the Bishop Block.

The Greymouth Coalfield presents a large challenge in the form of steeply dipping seams (seam dips are commonly up to 35° in the Greymouth Coalfield) and a very high rank gradient which increases eastwards from high-volatile bituminous C near the coast (Spring Creek and Strongman No. 2 Mines) to low-volatile bituminous at the western margin of the coalfield (Roa Mine). The increase in rank corresponds to a rapid decrease in coal strength which results from an increase in the cleat frequency, so a new set of conditions are present in each new mine developed.

In the Reefton Coalfield seam dips are generally up to 25°. The Terrace Mine has experienced problems in the past with pillar punching, where the bearing capacity of the floor is not sufficient to meet the load imposed upon it by the overburden load transferred through the pillars. This problem was apparently due to pillars being made a constant size of 20m x 20m regardless of depth (Field, 1998).

This study reviews different methods (both standardised (ISRM) and unconventional) of estimating coal strength in order to determine which methods are most accurate. Experimental coal strength estimation techniques used in this study include the use of volatile matter, ash and fixed carbon contents, along with coal rank and the rarely used cube compressive strength test. The data obtained is then applied to pillar sizing for each of the five locations tested (Bishop Block, Roa, Spring Creek, Strongman No. 2 and Terrace mines) with the aim of making a safer working environment for Solid Energy staff.

1.1.3 Thesis Objectives

The specific aims of this project are:

1) Determine the extent of any relationship between coal rank and strength, and establish the causes of such a relationship: - Decreasing coal strength with increasing coal rank is a well-recognised worldwide trend that this author believes to be largely related to increasing cleat frequency with increasing coal rank. The Greymouth Coalfield is an ideal area to study this relationship given the very high west-east gradient of increasing rank present in the Morgan, Paparoa and Dunollie Coal Measures. Rank also increases with increasing burial depth (0.32% Ro/km (Boyd and Lewis, 1995) – 0.91% Ro/km (Ward, 1997)).

2) Establish a relationship between unconfined compressive strength and point load strength for each seam studied: - The UCS = $24.I_{s(50)}$ relationship was shown by a previous study (Caffyn, 1987) to to be invalid for some areas of the coalfield. For coal strength to be determined accurately and cheaply in the future (e.g. by point load tests) this relationship needs to be determined for each location.

3) Establish a database of the geotechnical properties of coal in the Greymouth Coalfield: - Little is known about the strength or other coal properties in the Greymouth Coalfield (or the majority of New Zealand), so the establishment of a database of coal properties for reference during future mine development is considered very useful.

4) Determine to what extent pillar geometry affects coal pillar strength: - Coal mine pillars are usually square or rectangular in plan. Rectangular pillars are stronger but more coal is retained in the pillar. Analysis of stress distribution and studying pillars with varying geometries will help to determine the optimum configuration for maximum safe extraction.

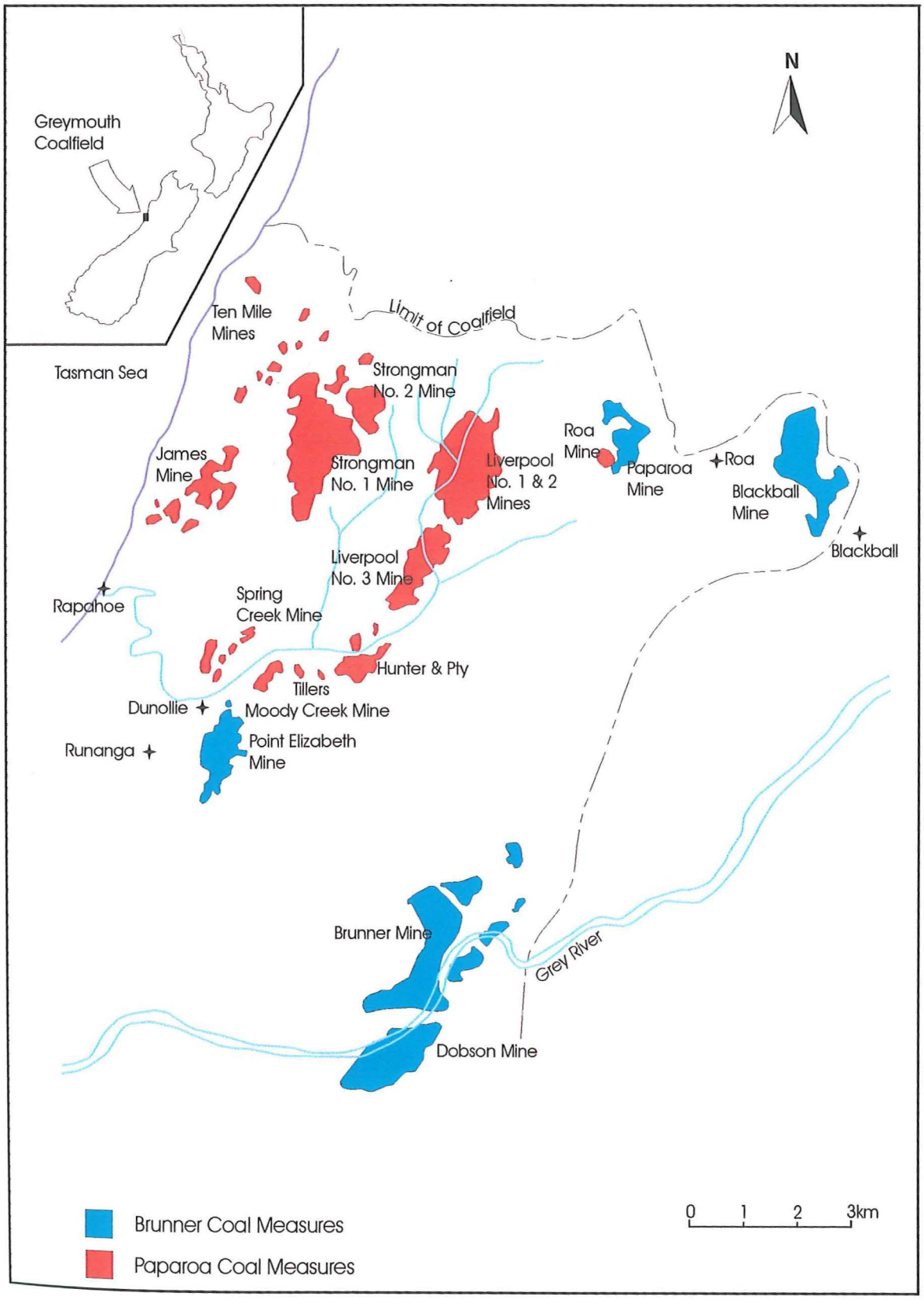

Figure 1.1. Location map, Greymouth Coalfield (modified from map provided by Solid Energy Ltd).

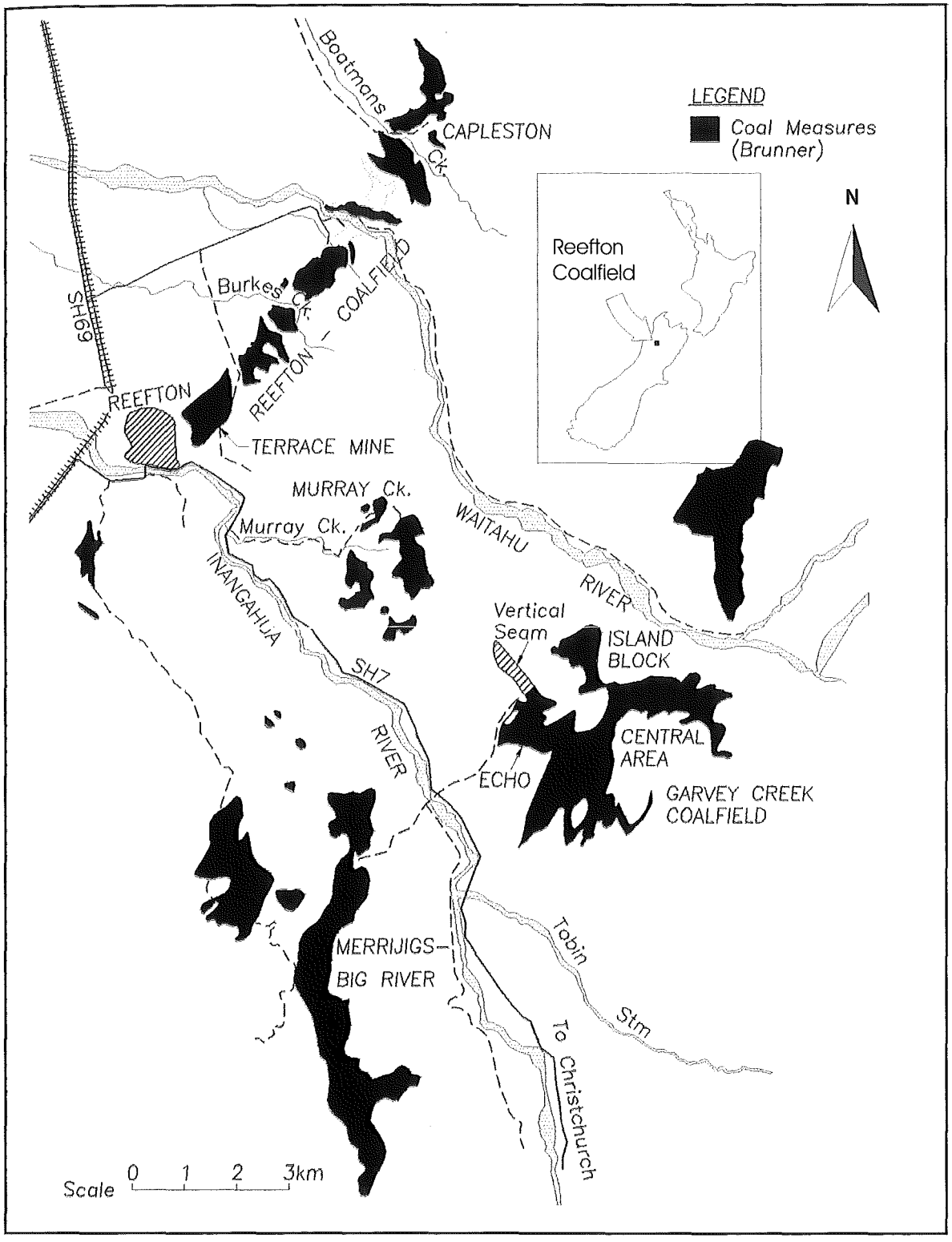

Figure 1.2. Location map, Reefton Coalfield (modified from map provided by Solid Energy Ltd, drawn by S. Todd).

1.2 Greymouth Coalfield

1.2.1 Geology of the Study Area

Almost all bituminous coal in New Zealand is found on the West Coast of the South Island within the upper Cretaceous to Paleocene Paparoa Coal Measures and Eocene Brunner Coal Measures (J. Newman, 1985; Edbrooke, 1999).

The Greymouth Coalfield is part of a southwards-plunging, asymmetrical anticlinorium, with many steeply dipping faults and secondary folds traversing both limbs. A simplified stratigraphic column for the Greymouth Coalfield is presented in Figure 1.3. Coal deposits are distributed in many seams through five coal bearing rock formations, separated by barren units (Gage, 1952). Coal has been mined from all but the lowest of them, being the Jay Coal Measures which contains no mineable seams. Four of these coal-bearing units are contained within the Paparoa Coal Measures while the uppermost coal-bearing unit is contained within the Brunner Coal Measures. The coal seams dip steeply with dips usually exceeding 15° (J. Newman, 1985), and are of limited extent with the largest 3 km long by 1.5 km wide.

The Paparoa Coal Measures are characterised by rapid lateral variations in thickness, and by lateral and vertical variations in lithology (J. Newman, 1985) caused by deformation occurring which the coal measures were being deposited. Some units, including the Jay and Dunollie Coal Measures may increase in thickness by over 330m across only 1 km.

Coal rank also varies vertically, increasing with increasing burial depth from 0.32% Ro/km (Boyd and Lewis, 1995) to 0.91% Ro/km (Ward, 1997). The Paparoa Coal Measures are most widely exposed in the Greymouth Coalfield, but also occurs to the in the Pike River Coalfield and at Kowhitirangi to the south (Bowman *et al.*, 1984).

Formation	Group	Age	Thickness	Major Mines	Seams
Brunner Coal Measures	Brunner	Late Paleocene - Eocene	30-130m	Brunner	
Dunollie Coal Measures	Upper Paparoa	Paleocene	<330m	Point Elizabeth, Hunter and Party	
Goldlight Formation			<200m		
Rewanui Coal Measures	Middle Paparoa	Late Cretaceous	<370m	Strongman No. 1 and 2, Spring Creek, Roa	C, D, E,F, Main, Kimbell, Ramages
Waiomo Mudstone	Lower Paparoa		25-65m		
Morgan Coal Measures			15-65m in west <470m in east	Liverpool No. 1, 2 and 3, Roa	Morgan, Sub-Morgan
Ford Formation			<170m		
Jay Coal Measures			0-500m		
Hawks Crag Breccia	Pororari	Mid Cretaceous			
Greenland Group		Late Cambrian - Early Ordovician	unknown		

Legend

- Coal seam
- Gradational contact
- Unconformity
- Structural contact on basement
- Unconformable contact on basement

Figure 1.3. Simplified schematic stratigraphic column for the Greymouth Coalfield (modified after Ward, 1997. Not drawn to scale).

The coal bearing fluvial units of the Paparoa Coal Measures are the Dunollie, Rewanui, Morgan, and the Jay Coal Measures, which are separated by the barren lacustrine mudstones of the Goldlight, Waiomo and Ford Formations (Figure 1.3). The Paparoa Group was formed on a peneplained surface during an early phase of rifting at the beginning of the break-up of Gondwana (Kamp, 1986. Bishop, 1992). As the separation of Gondwana began, north-west/south-east trending narrow fault bounded basins formed and rapidly subsided. Peat accumulated in those basins starved of clastic sediment (Bowman *et al*, 1984).

The Hawks Crag Breccia (Pororari Group) is a lensoidal unit which was deposited in pre-existing depressions of the underlying Greenland Group (Nathan, 1978). The local basement is the Greenland Group (Late Cambrian-Early Ordovician), which is a strongly folded and faulted greywacke and argillite unit of unknown thickness (Gage, 1952). This is overlain by the Jay Formation which is the lowest in the coal measure sequence and contains three recognised lithologies (breccia, conglomerates and sandstone). Coal seams of 1-2.5m thickness (none of which is mineable) are restricted to the sandstone unit and only outcrop in the Roa district (Gage, 1952).

The second coal measure unit in the sequence is the Morgan Coal Measures in which two facies are recognised; 1) conglomerates, sandstones, shales, coal seams, and 2) igneous conglomerate and tuff. With the exception of the Brunner Formation, the Morgan Coal Measures is the most widespread coal-measure unit in the coalfield. The sandstones and conglomerates are representative of deltas which advanced across the infilled Ford Formation lakes (Gage, 1952). A carbonaceous horizon is present in all locations in one of two forms. The first is the Morgan seam which ranges from a few centimetres to 10m thick and has previously been mined at the Liverpool and Paparoa Mines. The second type is alternating carbonaceous shale and coal with thicknesses greater than 15m, which contains the Sub-Morgan seam.

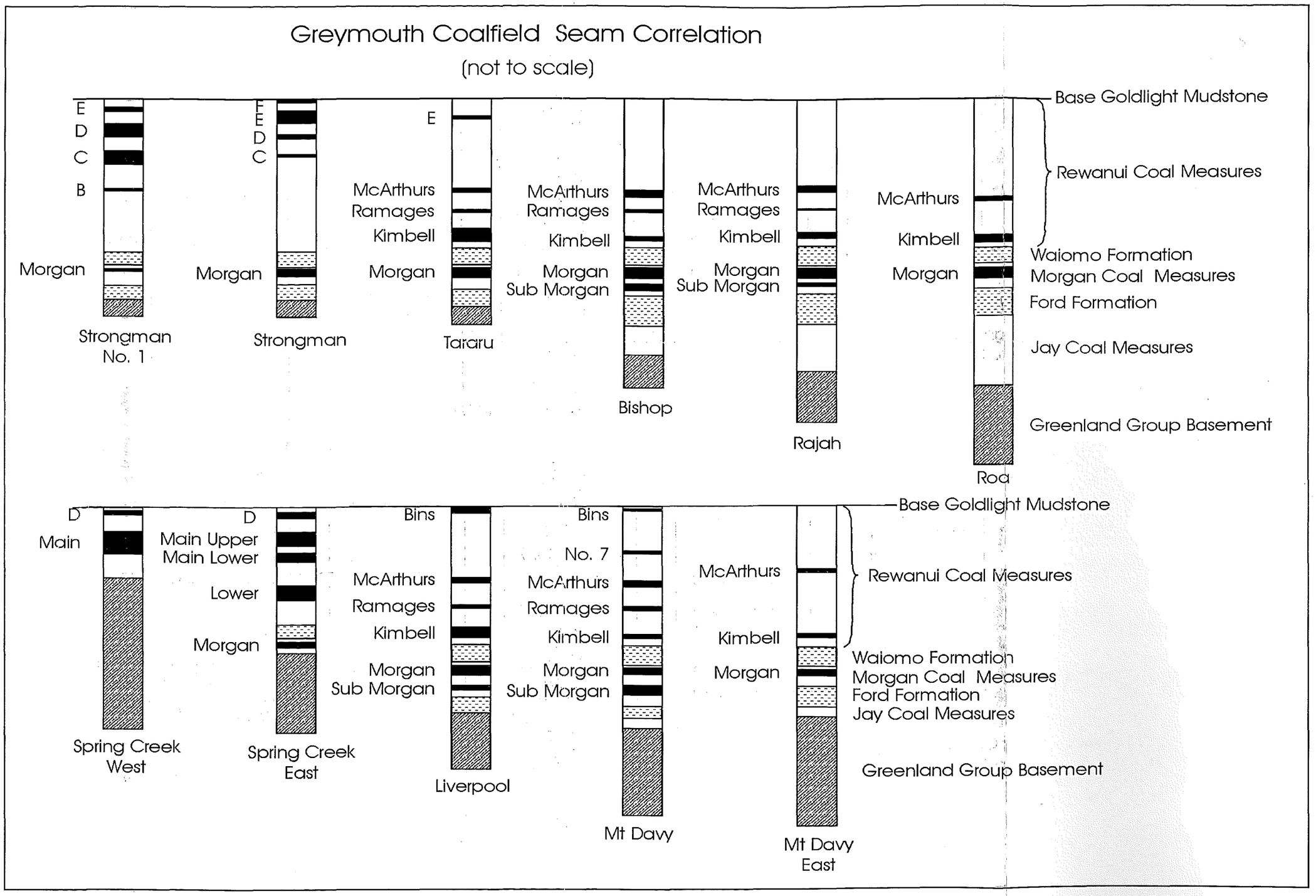

Figure 1.4. Greymouth Coalfield seam correlation showing all seams involved in this study (Original drawing compiled by S. Henley, drawn by S. Todd. Modified by this study; Not drawn to scale).

The Rewanui Coal Measures contain the majority of the seams that have been worked in the Greymouth Coalfield, including most of the seams sampled in this study (Figure 1.4). Seams are typically up to 10 m thick, but can be up to 35 m thick locally (e.g. Main seam at Spring Creek), and have a maximum lateral extent of 1.5 km (Edbrooke, 1999). The Rewanui Coal Measures are the thickest coal bearing stratigraphic unit across the majority of the coalfield apart from in the west, where the Jay Coal Measures become very thick.

The Dunollie coal measures occur in the northwest of the coalfield and contain two coal seams. The lower seam is thin and of limited extent. The upper seam has been worked by numerous mines, including the Point Elizabeth State Mine. The Dunollie Coal Measures represent the final infilling of the Paparoa basin with the end of deposition coming at the cessation of spreading in the Tasman Sea at ~60Ma (Nunweek, 2001).

The Brunner Coal Measures are more widespread and thin compared to the Paparoa Coal Measures (J. Newman, 1985) with deposits extending into Hokitika and Nelson. They are the first major unit associated with a marine transgression at the end of the Eocene and are comprised largely of sandstone, conglomerate and carbonaceous mudstone. In most places the Brunner Coal Measures contains only one workable seam (Gage, 1952), though many thinner lensoidal seams are known to occur (Nathan, 1978).

1.2.2 Mining History

Coal was first discovered in the Greymouth Coalfield in 1848 by Thomas Brunner on the banks of the Grey River (Morgan, 1911). The first coal mine opened at Brunner in 1864, with the coal mostly used to supply ships travelling from Greymouth to Nelson. Following the decline of the gold industry in 1877, the coal export trade became increasingly important allowing the community of Greymouth to prosper (Gage, 1952). More than 100 mines have operated in the Greymouth Coalfield since this time, working both the Paparoa and the Brunner Coal Measures, almost all having been large underground mines including the Brunner, Liverpool, Paparoa, Spring Creek and Strongman State Mines (Anon, 1996). The Liverpool No's 1, 2, 3 and Strongman No. 1 are the largest to have worked the Greymouth Coalfield with a total production of 4.8 M/t and 5.3 M/t

respectively. Annual production of the Strongman No. 2 mine is c. 0.42 M/t. Very little opencast mining has taken place due to steep topography and thick overburden. Approximately 0.5% of the current reserves are considered opencastable. The majority of mines are of limited extent and are fault bounded. These faults often have large throws ($\leq$200m), and dip steeply (few < 50°) making development across them impossible.

The Strongman No. 1 Mine which opened in 1939 finally closed shortly before the opening of the new Strongman No. 2 mine immediately to the east in 1994. The No. 1 mine worked the C, D and E seams of the Rewanui Coal Measures, with the No. 2 mine continuing today working the D, E and F seams. Two large mines (Strongman No. 2 and Roa) are currently being worked in the Greymouth Coalfield with activity at the Spring Creek Mine due to resume in the near future (all three are in the Paparoa Coal Measures). More than 30 Mt of coal has been produced from the Greymouth Coalfield with current production c. 0.437 Mt/yr (B. Winfield, pers. comm.).

More than 100 miners have been killed in mine accidents in the Greymouth Coalfield. As far as the author is aware, the majority of these deaths resulted from explosions, and none as the result of pillar collapse. The largest single tragedy to occur in this region was the 1896 Brunner Mine disaster where 66 deaths resulted from a single explosion. In the early days when coal was mined by blasting and hand shovelling was a commonly used technique in coal mining and so deaths caused by accidental explosions were more common. With the advent of advanced mining machinery blasting is only now required for to break up overburden in opencast mines, and so the frequency of gas explosions is decreased significantly making for a much safer working environment. This is also due to good ventilation practice and not allowing fine material (prone to explosion) to build up in working areas.

1.3 Reefton Coalfield

1.3.1 Geology of the Study Area

The Reefton Coalfield is situated within the Brunner Coal Measures bordering the east side of the Grey-Inangahua depression (Suggate, 1957). The coalfield is an area 10km long by 1km wide to the northeast of the town, with a small area to the south (Figure 1.2). The coal measures are generally undisturbed by faulting, with all known faults having displacements of less than 10m (Field, 1998). Most known faults were discovered during mining activity due to a thick covering of gravels (80-85m thick in area above the Terrace Mine) over much of the region obscuring fault traces which pre-date the last glaciation, from which the gravels were derived.

The coal measures, which are typically 135m thick in the area of the Terrace Mine (Figure 1.5), consist of mudstone interbedded with sandstone and coal, and with some marine sediments near the top of the unit which results in the seams having higher sulphur contents due to leaching (c. 1.3% sulphur). Significantly younger glacial outwash gravels directly overlie the coal measures in the area around the Terrace Mine. Six coal seams are recognised, with the No. 4 and No. 2 Upper being the most extensive and economically important (Field, 1998).

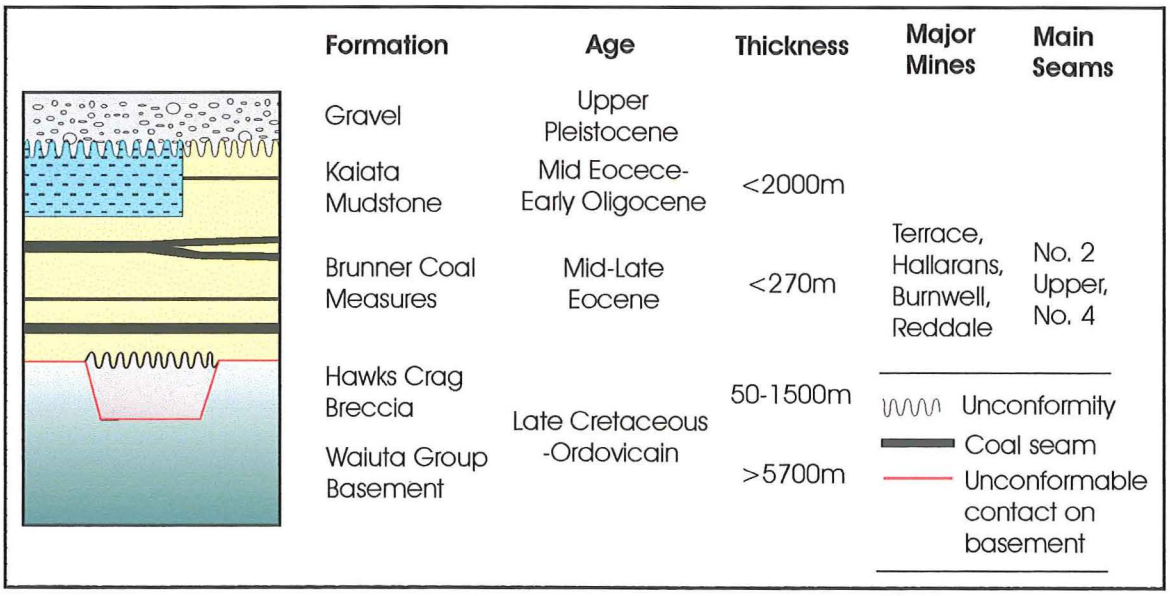

Figure 1.5. Simplified schematic stratigraphic column for the Reefton Coalfield (not drawn to scale).

1.3.2 Mining History

Coal mining commenced in the Reefton District in the 1870's with the majority of the coal produced from the small-scattered mines being used to power steam plants for gold batteries (Suggate, 1957). Until the 1950's most Reefton mines were small, undercapitalised and worked by hand (Fowke, 1998) using bord and pillar methods. Mine boundaries were drawn without consideration of geological boundaries, including faults and outcrop, thus hindering systematic mining (Fowke, 1998).

Six seams have been worked in this area, being No's. 1-4 and splits of the No. 1 and 2 seams, with the No. 4 seam the lowest in the stratigraphic column. The No. 2 and 4 seams were the most commonly worked as they are thicker, and the No. 4 seam had low sulphur and ash contents. Workings in the No. 1 seam were very localised.

The Terrace Mine was opened in 1939. This originally worked both the No. 2 and 4 seams, as there was little demand for No. 4 seam coal in the early days due to its soft nature. The Terrace mine now only works the No. 4 seam. Coal from the No. 4 seam is known to be highly prone to spontaneous combustion, and so many mines in the Reefton Coalfield have been abandoned throughout the years because of fires.

The Burkes Creek Mine (1898-1952) working the No. 2 seam was previously the only mine in the Reefton Coalfield to exceed 200m depth. All mines in the No. 4 seam which exceeded 140m in depth experienced problems with floor heave and pillar crush and creep. This is mostly due to pillars being made a standard size of one chain square (20m by 20m) regardless of depth (Field, 1998). The Terrace Mine (annual production c. 66,000 tonnes) workings are currently at a depth of 170m and will extent to 260m in the next stage of development.

1.4 Previous Work

This review of previous work in the Greymouth Coalfield concentrates on that which is relevant to this project. For a comprehensive review of other geological work in this area reference should be made to Ward (1997).

Strength testing in some form has previously been conducted on samples taken from each of the coal seams studied in this project, with the exception of the No. 4 seam at the Terrace Mine and the Morgan seam in the Bishop Block. Strength testing is, however, not a common occurrence, with only a limited number of unconfined compressive strength and point load tests being conducted, usually during the exploration phase.

Limited uniaxial compressive strength testing has been conducted by the Ministry of Works (reported in Caffyn, 1987) on the D and E seams of the Strongman No. 2 Mine. One and two tests were conducted from each seam respectively on samples taken from drill hole #689 and #690 (Map 1). These drillholes are in close proximity to sampling locations for this study. All three of these tests were performed on samples with L/D ratio too low (< 2) to be valid (as per ISRM standard. Brown, 1981), and so have been corrected empirically to an L/D of 2.0 for comparison with the results of this study (Section 2.2.2). A series of ten point load tests on E seam coal, as well as other lithologies, were carried out during the 1986 drilling programme in the portion of the Doherty Block where the Strongman No. 2 Mine is now located.

Six unconfined compressive strength tests have previously been conducted on coal from the Spring Creek Mine. Five of these were from the Main Upper seam (MNU) and one from the Main seam. No indication is given of the dimensions of the specimens used, therefore these results have been disregarded by this study.

The University of Canterbury has conducted two uniaxial tests and a series of point load tests on coal from the Kimbell seam (DH #848; Map 1) in the Bishop Block (Richards, 2000). Point load tests were also carried out on these samples to get a $UCS/I_{s(50)}$ relationship for this seam.

A series of point load and direct shear tests were conducted by Bell (1993a) on samples from the Kimbell seam at the Roa Mine. Bell used a different UCS/$I_{s(50)}$ relationship to that developed in this study, but the final UCS value is similar for both series of tests.

The in-situ strength of the No. 4 seam at the Terrace Mine has been estimated from unconfined compressive strength test results conducted on coal samples taken from the Kupakupa seam at the Huntly East Mine (Field, 1998. Mills, 1986) which is of a similar nature but slightly higher rank. However, no previous strength testing has been conducted in this seam.

1.5 Sampling and Testing Programme

1.5.1 Sample Collection

Lump samples of coal have been collected from various locations throughout the Greymouth and Reefton Coalfields. These were collected from underground at most locations, apart from the Bishop Block where samples were taken from outcrop. Sampling locations for the Greymouth Coalfield are shown on Map 1 (in map pocket). The location of Terrace Mine samples is shown on Figure 1.2. Lumps as large as possible (between 150mm×150mm and 300mm×300mm) were taken to ensure that the cores drilled from them would be of great enough length to conform to the ISRM standards.

Moisture content was kept as close to field values as possible by sealing all samples in plastic bags at the sampling location. After preparation of the samples, they were replaced in the plastic bags until testing. Moisture content was determined by drying the samples in a low temperature (40°) oven for 4 days to ensure the samples were completely dry. Lump samples from all locations were packed in boxes filled with polystyrene chips for transportation from their respective sample locations to the laboratory.

The E seam at the Strongman No. 2 mine was sampled both underground and from the opencast stockpile. This seam was sampled in two locations because of a significant rank difference between the E seam underground (E/UG) and what is found in the opencast

(E/OC). The relative rank, RoMax, is 0.63% (high volatile bituminous C) and 0.70% (high volatile bituminous B) vitrinite reflectance for E/UG and E/OC respectively, which is due a 'coalification jump' in vitrinite (a common rank indicator) near the eastern margin of the mine (McNee, pers. comm.). A coalification jump is a rapid change in coal chemistry which vitrinite macerals experience four times, the first of which occurs in the high-volatile bituminous stage as seen here.

Samples of Strongman No. 2 D seam were taken from underground in close proximity to (c. 150 m from) the Doherty Fault, which is a prominent reverse fault separating the northern most workings of the Strongman No. 1 mine from the smaller Strongman No. 2. The fault is not considered to have affected the amount of shearing in the samples, but the dip of the seam increases sharply towards the fault.

Lump samples from the Bishop Block were taken from the Kimbell seam and the upper split of the Morgan seam. The Kimbell seam was sampled from two separate locations due to a significant difference in appearance of the coal at each location. The first, in the north of the Bishop Block, was a small adit cut 2-3m into the outcrop during a previous sampling trip by Solid Energy personnel. Coal from the Bishop Block is sufficiently weathered when sampled from outcrop that it would be expected to influence the strength significantly. The coal at this location displayed a great deal more shearing throughout the seam than the same seam outcropping further south. The second sample site was an outcrop c. 500m south of the first. Samples of the Morgan seam were taken from an adit similar to that for the Kimbell seam.

1.5.2 Preparation and Testing

Testing has been conducted as closely as possible to the ISRM suggested methods set out in Brown (1981). Test methods used on each seam are summarised in Table 1.1. Departures from the prescribed methods have been noted in the text. All calculation of means and standard deviations in this study were conducted by disregarding the highest and lowest values to disregard extreme values as recommended by Brown (1981). 54mm

(NX) diameter core was drilled from lump samples using a core barrel mounted on a drill press in the Rock Mechanics Laboratory at the University of Canterbury.

Unconfined compressive strength (UCS) and point load strength tests are the most commonly performed strength tests on coal. Coal strength is most commonly determined in order to estimate pillar stability for underground mines. Because of the brittle nature of coal UCS tests cannot always be performed, and subsequently the point load test is often used to provide an estimated value of UCS. The UCS/point load strength relationship has therefore been established at each location. Cube samples were used to indirectly determine the UCS/point load strength relationship where core samples were not available.

1.6 Thesis Organisation

This study has been split into five chapters, with each being an almost discrete part of the study. Chapter Two represents the laboratory component of the research presenting the strength testing results and the corresponding analysis and interpretation of it. Chapter Three shows how coal strength varies with coal properties such as rank, fixed carbon and ash contents. Chapter Four deals with the problem of pillar design and the applicability of different design methods to the different situations encountered in this study. Chapter Five gives the overall conclusions of this study and recommendations for further work.

Chapter 2. Laboratory Estimation of Coal Strength

2.1 Introduction

> "Since coal is not a continuous solid material but contains various discontinuities such as cracks, cleats and bedding planes, the strength of coal is of necessity a statistical value depending on how many and what types of discontinuities are present." - Bieniawski (1968, p. 325).

The principal objective of a producing underground mine is to achieve maximum coal extraction under safe conditions (Jeremic, 1985). For an underground operation, this requires the strength of the coal seam to be accurately determined. The compressive strength of coal is an important part of most pillar design equations, and thus is an important part in determining how much coal which can be safely extracted from a particular mine. As coal strength increases, less material needs to be retained in pillars to maintain stability of the workings, and consequently the economic viability of the mine is increased, though other factors such as seam dip, faulting and overburden thickness must also be taken into account.

Very little strength testing has been conducted previously on coal from the Greymouth Coalfield (Section 1.4), with the majority of that being point load index tests. It is thought by this author that point load testing alone does not give reliable strength information, so it was important from a safety point of view to obtain unconfined compressive strength (UCS) data for calibration and comparison purposes. The objectives of this testing programme are therefore:

1) To provide a reliable database of coal strength for each of the locations involved in this study, using both confined and unconfined testing methods along with others methods including strength trends with coal rank, ash, volatile matter and fixed carbon contents.

2) To determine the Hoek-Brown parameters of the coal from triaxial testing in areas where core can be obtained, and to determine the Mohr-Coulomb failure envelope.

3) To derive a method for establishing an unconfined compressive strength value for coal in areas where no core is available, and which is more appropriate for the Greymouth Coalfield than the currently available methods of coal strength determination, including the unconfined compressive strength and point load strength tests.

Bieniawski (1968) reported that the compressive strength of coal is one of the most difficult properties to establish experimentally due to a number of factors, including specimen size and shape, anisotropy, loading rate and moisture content. This was reflected in the wide range of strengths seen in each seam examined in this study. The majority of authors who have worked with coal, including St George (1995) and Townsend *et al.* (1977), confirm the difficulty of obtaining samples of the required size and getting meaningful results from them. Mills (1986) reports only being able to test two samples from 5m of drill core.

A large amount of variation in the results is common when determining coal strength because of cleating (joints in coal) in core-sized samples (Figure 2.1). Most rock types do not have visible defects in core-sized samples other than bedding and foliation. Gale and Mills (1995) suggest that unconfined coal strength varies by at least ± 60% with respect to the mean UCS value. In hard rocks compressive strength can also be highly variable, especially in coarse grained sedimentary rocks where Lucas (2002) reports variations from the mean of ± 100%, but a reduction grain size gives a corresponding reduction in the variation which is typically less than ± 30%.

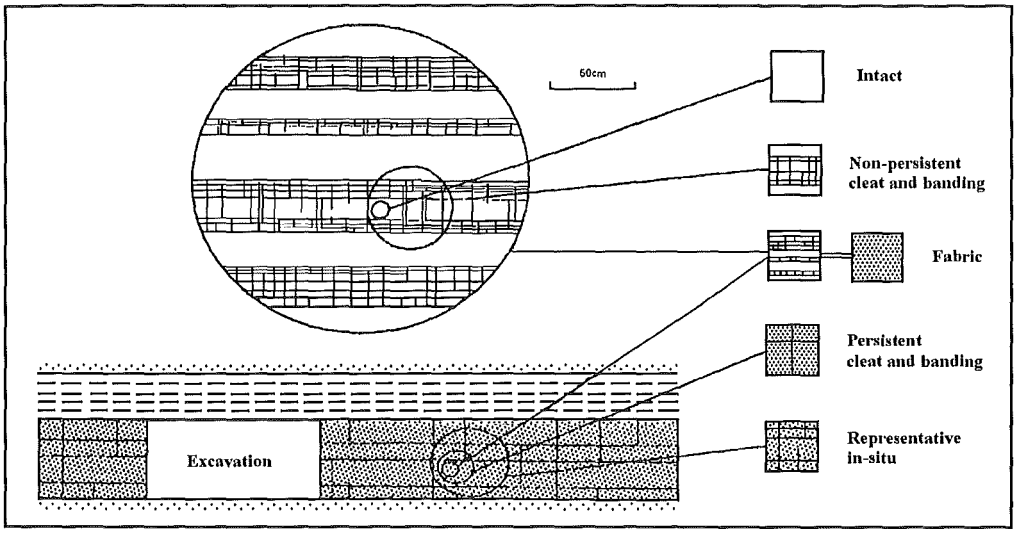

Figure 2.1. Appearance of coal at different scales. Transition from defects seen in-situ to those seen in laboratory-sized samples (modified after Trueman and Medhurst, 1994; Medhurst and Brown, 1998).

This chapter is divided into sections, each comprising a separate strength test. Each section has then been further divided into sub-headings outlining test methods used, results, mode of failure, and factors influencing the results including bedding/banding, cleating, moisture content and anisotropy. Test methods used for each seam involved in this are shown in Table 2.1. All tests (other than point load and shear) were conducted using the same 1500 kN loading frame.

Location	Seams tested	Coal Rank (% RoMax)	Forms of Testing Used					
			UCS	Triaxial	Cubes	Point Load	Shear	Brazilian
Bishop Block	Morgan, Kimbell	0.87, 0.89			×	×		
Roa	Kimbell	1.76			×	×		
Spring Creek	D, MNU	0.64, 0.62	×	×	×	×		×
Strongman No. 2	D, E/UG, E/OC	0.63, 0.63, 0.70	×	×	×	×	×	×
Terrace	No. 4	0.48			×	×		

Table 2.1. Testing methods used for each seam studied.

2.2 Unconfined Compressive Strength Determination for Core Samples

2.2.1 Methodology and Scope

The unconfined compressive strength (UCS) test is the most common value quoted for rock strength (Brook, 1993. St George, 1995) as it is the most consistent and reliable method of determining rock strength. This test is not representative of in-situ coal

strength, but there are methods of estimating the in-situ strength from UCS values (presented in Chapter 4), and so the UCS test been used in this study wherever possible. UCS testing in this study has been carried out with the intention of using the data for pillar design in underground coal mines (Chapter 4). All mine pillar strength prediction equations (Section 4.3) use this parameter in some way, so it was important to establish it at each location. Some authors, including Bieniawski (1967, 1968) and Bieniawski and van Heerden (1975), repeatedly claim that large-scale in-situ tests are the only way to accurately determine coal strength. From a practical point of view, however, and taking into account the inherent variability seen in coal strength values, this author believes that laboratory strength values are equally valid if properly conducted and evaluated.

Unconfined compressive strength tests could only be conducted on samples taken from the Spring Creek and Strongman No. 2 mines. Coal from other seams sampled in this study contained too many defects for the required core to be obtained. In these cases, UCS was determined by developing a strength prediction equation (Section 3.6) from the results obtained in this study. All unconfined compressive strength tests were conducted on 54mm (NX) core, which was drilled from coal blocks in the laboratory.

Lump samples taken from the Spring Creek and Strongman No. 2 mines often had one or two dominating cleats which cut through the entire sample. These cleats would often cause a core to break into two or more large pieces during preparation. These pieces were usually not long enough for use in either unconfined or triaxial compressive strength tests. This problem was encountered when cutting cubes from the Terrace mine samples also. Other seams (Bishop Block, Roa) had smaller and more frequent cleats which had the same effect. This means that the weakest samples are not represented in the strength tests and the strengths of each seam may be overrepresented.

The coal studied was not strong enough to allow failure to occur within 5-10 min, so a loading rate of 0.5 MPa/s was used to conform to the ISRM standard. Samples were trimmed as straight as possible, but could not be made parallel in all cases due to the fragility of the samples. Pells and Ferry (1983) conducted tests to determine the effects of non-parallel ends, as well as other parameters specified in the ISRM guidelines, in an attempt to do away with what they termed was 'needless stringency' for weak lithologies.

They showed that samples with ends non parallel by up to 2° gave no significant strength difference from those tested according to the ISRM standard.

2.2.2 Discussion of Results

2.2.2.1 Data Summary

The results of the uniaxial compression testing on the Strongman No. 2 and Spring Creek samples are summarised in Table 2.2 and the complete set of results are presented in Appendix 2. Of the five seams tested by this method, those from Spring Creek are the weakest with mean σ_c = 8.9 and 7.0 MPa. The E seam opencast (E/OC) is similar with σ_c = 10.7, but the D and E seam underground (E/UG) from the Strongman No. 2 mine are significantly stronger with σ_c = 17.1 and 24.8 MPa respectively. Each seam tested shows a large range of strength values with high standard deviations. The largest range of value was shown by the Strongman D seam where σ_c ranged from 0.5-31.6 MPa. The strength range shown by the E/UG seam (7.4-30.4 MPa) is deceptive as only one sample recorded a strength value < 19.5 MPa.

This scatter shown in the results is due to a number of reasons. The first is that samples were loaded at a range of bedding orientations. This produces low compressive strength values when β = 20°-60°, and values closer to the actual compressive strength (when β = 90°) when β is outside this range. The mean strength of each seam can be classified as weak (5-25 MPa) according to Hoek and Brown (1997, see Table 2.3) with the range largely confined to this classification also.

Location	No. Tests	UCS ave. (MPa)	Range	Std Dev	L/D Ratio ave.	W %	E_{dyn} (GPa)	Poisson's ratio, ν	Bedding orientation, β
Spring Creek									
D seam	7	8.9	5.9 - 17.6	2.97	2.49	9.43	-	-	15°-90°
Main Upper seam	11	7.0	3.6 - 13.6	2.68	2.69	7.55	-	-	5°-85°
Strongman No. 2									
D seam	16	17.1	0.5 - 31.6	6.85	2.48	3.23	1.78†	0.42†	0°-90°
E seam (UG)	6	24.8	7.4 - 30.4	3.31	2.78	3.26	1.96†	0.44†	-
E seam (OC)	9	10.7	7.5 - 21.5	4.73	2.46	4.06	-	0.26‡	0°-90°

Table 2.2. Summary of unconfined compressive strength test results. † Refers to values determined from P and S wave velocity. ‡ Refers to values determined from strain gauges.

Grade	Term	Uniaxial Compressive Strength (MPa)	Point Load Index (MPa)	Field estimate of strength	Examples
R6	Extremely strong	> 250	> 10	Specimen can only be chipped with a geological hammer	Fresh basalt, chert, diabase, gneiss, granite, quartzite
R5	Very strong	100-250	4-10	Specimen requires many blows of a geological hammer to fracture it	Amphibolite, sandstone, basalt, gabbro, marble, rhyolite, tuff
R4	Strong	50-100	2-4	Specimen requires more than one blow of a geological hammer to fracture it	Limestone, marble, phylitte, sandstone, schist, shale
R3	Medium strong	25-50	1-2	Cannot be scraped or peeled with a pocket knife. Specimen can be fractured with a single blow from a geological hammer	Claystone, concrete, schist, shale, siltstone
R2	Weak	5-25	†	Can be peeled with a pocket knife with difficulty, shallow indentation made by firm blow with point of a geological hammer	Chalk, rocksalt, potash, coal
R1	Very weak	1-5	†	Crumbles under firm blows with the point of a geological hammer, can be peeled with a pocket knife	Highly weathered or altered rock, coal
R0	Extremely weak	0.25-1	†	Indented by thumbnail	Stiff fault gouge

Table 2.3. Classification of rocks according to compressive strength (modified after Hoek and Brown, 1997). All coal types tested in this study are classified as weak (R2) or very weak (R1). † Point load tests on rocks with a uniaxial compressive strength below 25 MPa are likely to yield ambiguous results (Hoek and Brown, 1997; Hoek *et al.* 1998).

2.2.2.2 Spring Creek Samples

A total of eighteen unconfined compressive strength tests were performed on coal from the D and Main Upper seams. Six of these were below the 2.5 L/D ratio required by the ISRM standard, but no tests were conducted on samples with L/D ratios less than 2.29. the range of results was similar for both seams (D seam 5.9-17.6 MPa; Main Upper 3.6-17.6 MPa), with the mean σ_c values of 8.9 (D) and 7.0 MPa (MNU) below the median for both seams. Standard deviation of the D seam (2.97) is almost equal to that of the Main Upper at 2.68. The Main Upper seam shows a coefficient of variation of 38% where as the D seam has a variation of 33% (see appendix A1.2 for calculation method). A large amount of scatter is present in the results, which is common in coal due to its anisotropic and discontinuous nature.

2.2.2.3 Strongman No. 2 Samples

Thirty-one unconfined compressive strength tests were conducted on Strongman No. 2 coal cores. The D and E seams were tested, with the strength of the E seam being determined from coal taken from both the underground (E/UG) and opencast (E/OC) mines due to a significant rank difference (Section 1.5.1). All of the E/OC samples had L/D ratio > 2.5 (conforming to the ISRM standard), but fourteen of the E/UG and D seam samples were tested with a minimum L/D of 2.09 as samples of sufficient length could not be obtained. The results are summarised in Table 2.2. At the time of testing all samples had moisture contents of 2.9%-3.5%, so little strength variation should result from this. The loading direction is unknown in many of the samples due to difficulty in determining bedding orientation as it is not prominent in these samples. Even though bedding and microfracturing is not evident on a macroscopic scale, it may exist on a smaller scale not visible to the naked eye, and thus the samples cannot be assumed to be isotropic and homogeneous.

The E/UG seam is the strongest of the Strongman No. 2 samples with σ_c = 24.8 MPa, followed by the D (17.1 MPa) and E/OC (10.7 MPa) seams. The D seam had a much greater spread in the results than the two E seam populations ranging from 0.5-31.6 MPa, compared to 7.4-30.4 (E/UG) and 7.5-21.5 (E/OC). The coefficient of variation is also highest in the D seam at 40% reflecting the results spread of 30 MPa. The E/OC and E/UG seams showed significantly lower coefficients of variation with 31% and 19% respectively. This results from the cleat frequency which was highest in the D seam and lowest in E/UG.

A surprisingly large strength difference exists between the E/OC and E/UG samples. The E/UG samples displayed significantly less cleats than E/OC specimens, except for one sample which contained a great deal of cleats and subsequently recorded a low strength (7.4 MPa). A number of other E/UG samples broke along cleats during sample preparation so could not be tested. The resulting lack of defects in the samples that were tested has caused the mean strength of E/UG samples to be biased towards the higher side of the

expected strength range (σ_c = 24.8 MPa, range 7.4-30.4 MPa), and significantly higher than the D seam samples which are of the same rank.

Samples breaking during preparation are not confined to coal however, and for this reason Laubscher (1990) suggests that samples tested in the laboratory are commonly better quality than the average rock material. Laubscher recommends that UCS data should be reduced by up to 20% to give a more representative value. Because of the number of samples which broke during preparation in this study, the proportion of weaker samples tested is not a representative selection of actual coal strength, which is especially true in the E/UG seam. The author of this study believes therefore that some degree of strength correction is appropriate, but the extent to which this correction is applied is difficult to determine.

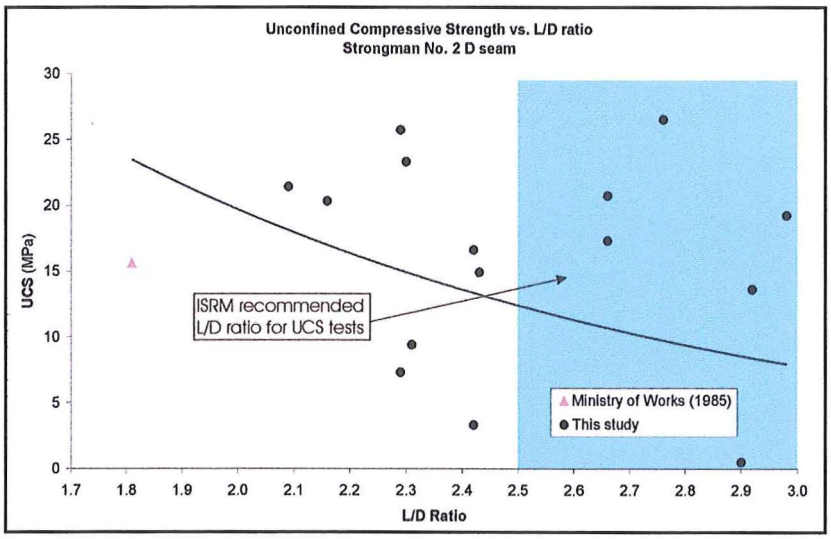

Figure 2.2. Decrease in unconfined compressive strength with increasing L/D ratio for Strongman No. 2 D seam. Shaded area shows ISRM recommendations for L/D ratio.

Strongman No. 2 D seam samples show a slight strength decrease with increasing L/D ratio, but the trend is very weak (r^2 = 0.09; Figure 2.2). No significant trends are seen when L/D is plotted against strength for the E/UG seam samples, and the E/OC samples show a slight increase in strength with increasing sample length, though the trend is this seam is also weak (r^2 = 0.174; Figure A2.4, Appendix 2). Therefore difference between average L/D ratio for the two seams (E/OC = 2.78, E/UG = 2.46) is not a factor in the strength difference between the two, and the difference in the amount of cleats is the most

significant factor. Hence, if samples are tested within the ISRM suggested length guidelines (L/D 2.5-3.0) then no appreciable strength differences can be expected.

One unconfined compressive strength test has previously been conducted by MWD (1985) on D seam coal and two from the E seam. These samples were taken from drill hole #690 (Map 1), which is located in the eastern part of the Strongman No. 2 mine. This drill hole is within 150m of where the D and E/UG seam samples for this study were taken, so direct comparisons can reasonably be made. These tests were on cores much shorter than the ISRM standard required, so have been corrected to an L/D ratio of 2.0 by the ASTM (1979) equation:

$$\sigma_c / \sigma_m = \frac{1}{0.88 + 0.24(D/L)} \qquad (2.1)$$

where σ_c = Corrected UCS with L/D = 2

σ_m = Measured UCS of a non-standardised sample (MPa)

D = Specimen diameter (mm)

L = Specimen length (mm)

The ISRM recommends that L/D is 2.5-3.0 for UCS testing, but as there are no methods available to correct samples to this range, equation 2.1 has been used. This gives the D seam sample strength of 15.4 MPa, with 13.9 and 15.2 MPa for the two E seam samples. The D seam result is very similar to that found in this study where the average UCS value was 17.1 MPa, and was well within one standard deviation of ± 6.85 MPa. However, the E seam results are much higher in this study than those previously tested. This most likely arises from the lack of defects seen in the E/UG samples of this study. It is unclear what core size was used in the previous tests, but it is assumed to be either NX or HQ, as these are common exploration drill core sizes. Since HQ is only slightly larger than NX, strength differences should be minimal from this source.

The strength of Strongman No. 2 coal, which is the strongest in this study, is slightly higher than the Kupakupa seam in both the Huntly East and West mines, but is generally weaker than coal from elsewhere in the world. This is partially due to the age of the coal, which in this study is Upper Cretaceous-Eocene for the Greymouth Coalfield and Eocene for the Reefton Coalfield. Coal which is younger is generally weaker, and New Zealand coals are quite young by world standards. New Zealand Coals have a higher percentage vitrinite macerals than overseas coal (S. Henley, pers. comm.) which tends to be higher in inertinite and have higher ash contents, both of help to increase the strength of the coal.

2.2.3 Mode of Failure

Samples of Spring Creek D seam coal failed in a variety of ways, with axial splitting, cataclasis and shearing equally represented (following the terminology in Hawkes and Mellor, 1970, as shown in Figure 2.3). Shearing was most common in the D seam which displayed the most prominent banding, and it tends to occur when bedding is inclined 30-60° to loading direction. Not all samples could be loaded parallel to bedding due to difficulties obtaining intact samples. However, in mine pillars, bedding will often be inclined to the direction of applied overburden stress due to the seam dip (up to 35°), thus β = 55-90°. When bedding was either perpendicular or parallel to loading direction, failure was often seen to occur by a combination of axial splitting and cataclasis. Cataclasis is the dominant failure mechanism in samples with no cleats.

Where no defects were present spalling or slabbing from the sides of the samples was common producing an hourglass shape which is a common mode of brittle failure (Figure 2.3d). The relatively solid end segments remaining showing the effects of end constraint by the loading platens (Hawkes and Mellor, 1970). Brittle failure and axial splitting was the most common mode of failure in samples from the Strongman No. 2 Mine. Shearing was much less common due to the absence of the distinct bedding planes seen in Spring Creek samples.

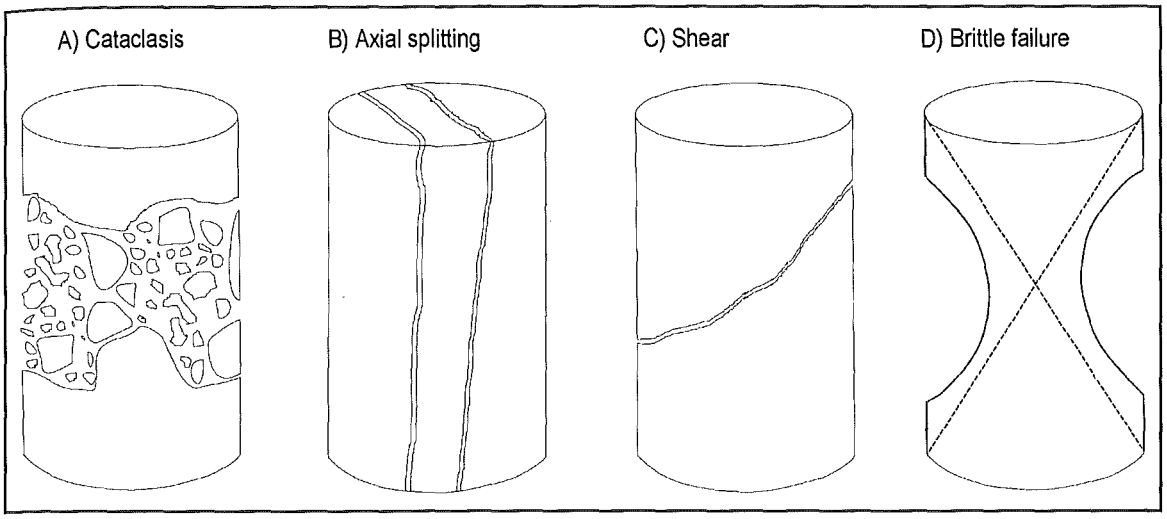

Figure 2.3. Idealised diagrams showing common modes of failure seen in UCS testing. A) Cataclasis:-Internal crumbling by formation of multiple cracks in the direction of the applied load. B) Axial cleavage:-Vertical splitting, in which one or more major cracks split the sample along the loading direction. C) Shearing:-Shearing of test specimen along a single oblique plane (after Hawkes and Mellor, 1970). D) Brittle failure:-Hourglass shape leaving relatively solid end segments.

2.2.4 Influence of Cleating and Banding

Cleats in coal are the equivalent of joints in rock. The samples which displayed more frequent (closely spaced), and open cleating tended to have lower strengths and greater variability in the results than those containing fewer defects. A large amount of scatter in results is normal for coal, with some authors such as Unrug *et al.* (1987), who studied the strength of individual layers within coal seams, reporting variations of up to 100% of the mean strength in a 1.3 m seam.

Strongman No. 2 D seam and E/OC samples frequently contained one large cleat or many smaller defects. The defects would often dictate how and where the sample failed. Samples with only minor or no defects would often fail by cataclasis in an hourglass shape at high strength (Figure 2.3d). These specimens fail in the centre in this manner because this is where frictional forces imposed by the platens are at a minimum (Hansen *et al*, 1962). E/OC samples tended to contain more large and dominating cleats, with cataclasis still the main failure mechanism, but at a lower strength than the D seam.

Significant defects were largely absent in E/UG samples and this shows in the high strength result (mean σ_c = 24.8 MPa; Table 2.2). Six samples were tested from the E/UG seam, of which five showed no cleating. These samples recorded strengths of 19.5-30.4 MPa. One sample displayed through going open cleats like those of the D and E/OC seams, and subsequently recorded a much lower strength of 7.4 MPa. All other E/UG samples which displayed open cleats broke during samples preparation, which results in the weakest samples not being tested. Consequently the strength of this seam is significantly over estimated. The actual strength of this seam is more likely to be similar to those for the Strongman D seam where σ_c = 17.1 MPa.

Samples tested in this study which showed little or no defects, consistently recorded the highest strengths (often 20-30 MPa). The two weakest core samples tested in this study, which recorded UCS strengths of 0.5 and 3.3 MPa, both from the Strongman No. 2 D seam, were very extensively cleated, whereas the average for this seam was 17.1 MPa. Mills (1986) reports that cleats do not appear to affect the strength behaviour of core specimens.

There is general agreement in the literature that the in-situ strength of coal is significantly less than that tested in the laboratory (Bieniawski, 1967; Pariseau, 1977; Hustrulid, 1976). Larger samples are more likely to contain defects which will have a detrimental effect on coal strength than are laboratory-sized specimens (Figure 2.1). Depending on the spacing of defects, some small samples may not contain any defects at all, so a somewhat higher strength is recorded. This was convincingly shown by Bieniawski's (1968) work on the compressive strength of coal cubes where the smaller samples recorded the highest strengths.

The D and Main Upper seams are of similar rank (0.64% and 0.62% RoMax respectively) to the D and E seams of the Strongman No. 2 Mine (0.65% RoMax for D and E/UG seams), but displayed considerably lower strength. The D and Main Upper seams show a clearly defined alternation of dull (clarain) and bright (vitrain) bands, with the banding (equivalent of bedding) more pronounced in the D seam (compare Figures A2.5a and A2.5c, Appendix 2). Occasional fusain bands also occur, and these are soft and often

pulverised, thus representing layers of minimal strength (Jeremic, 1985). The vitrain bands are most prominent with clarain bands of up to 2mm thick interspersed between them (Figure 2.4 and Figures A2.5, A2.6, A2.7, Appendix 2). The bands appear to be evenly spaced, with the clarain bands usually 1-2mm thick and often of lenticular shape. This banding has a considerable effect on the strength by providing additional weakness planes when samples are not loaded perpendicular to bedding. This weakness is induced by a significant strength difference between the bands, as the bright vitrain bands are softer and weaker, whereas the dull clarain bands are finer material which is harder and stronger.

Clarain is described as a semi-hard, semi-bright coal by Jeremic (1985) with an unconfined compressive strength of 7-18 MPa. Vitrain is said to be a brittle and bright coal, which is well cleated with a UCS value of 1-7 MPa. Strengths of the individual macerals could not be determined in this study as the individual bands are too thin (< 6mm). Failure was frequently observed at the intersection between a bright and dull band within the sample, with some failure planes stepping down through bedding (Figure 2.4a and b). Coal strength may therefore be partly a function of maceral type, and the close alternation of bands of different maceral types which represent additional weakness planes. Different maceral types have different cleat frequencies and cleat orientations. Cleats are more distinct (open), frequent in the brighter macerals (including vitrain), and are less frequent in the dull macerals such as clarain which may help to explain why clarain has a higher compressive strength.

Despite more prominent banding in the D seam, the average strength (8.9 MPa) was still higher than the Main Upper seam (7.0 MPa). Standard deviations were similar with 2.97 and 2.68 for the D and MNU seams respectively. The strength range is higher in the D seam (5.9-17.6 MPa) compared to that of MNU (3.6-13.6 MPa) even though less samples were tested (7 of D, 11 of MNU). The Main Upper seam samples show significantly larger and more numerous cleats than D seam specimens, which appears to have had the most significant effect on the strength causing a difference of c. 20% between the two seams.

The difference in the L/D ratio between the two seams does not appear to be of significance in this difference (average L/D = 2.69 for Main Upper compared to 2.49 for the D seam) as neither seam shows any strength trend with increasing specimen length (r^2

= 0.01 for both seams; Figures A2.1 & A2.2, Appendix 2). As specimen length increases the constraining effects of the loading platens are less effective than in a shorter sample, therefore providing a more accurate estimate of UCS is given.

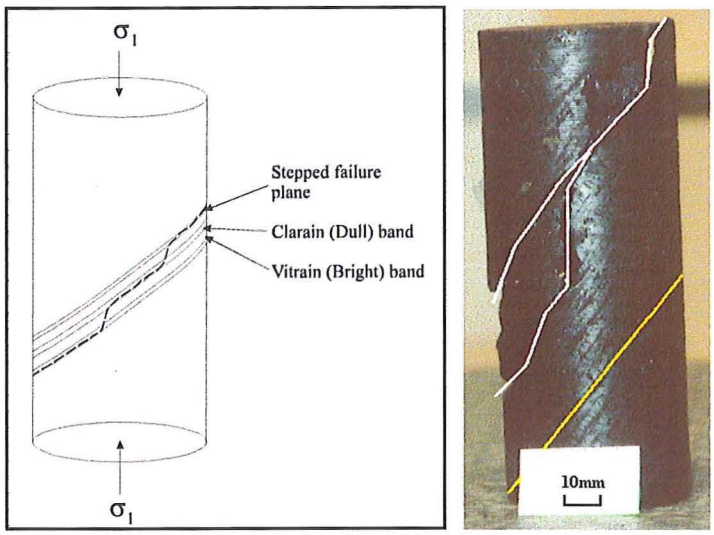

Figure 2.4. Stepped failure through bedding planes seen in some Spring Creek coal. A) Idealised diagram showing a typical stepped shear failure. B) Stepped failure in D seam coal (white line). Bedding orientation shown by yellow line.

2.2.5 Influence of Moisture Content

All samples were tested as close to natural moisture content as possible, since changes in moisture content can significantly affect the strength of the samples. In most rock types an increase in moisture content would be expected to give a lower strength value for various reasons including:

-Water acts as a lubricant along defect surfaces (including joints and cleats).
-Moisture softening of some constituent within the rock.
-Decreased void volume resulting in excess pore pressures.
-Differential hydrostatic pressures between interconnected and non-interconnected areas of the specimen (after Kennedy, 1988).

Figure 2.5 shows the strength of Spring Creek coal plotted against moisture content. Moisture contents in this study ranged from 1-18%. A very weak trend (r^2 = 0.115) of increasing coal strength with increasing moisture content can be seen from this, therefore moisture content may have the opposite effect on coal strength to hard rock. However, the trendline shown in Figure 2.5 could be placed in a number of directions (shown by dashed

lines) resulting in widely varied interpretations. Hawkes and Mellor (1970) note that the effects of moisture content are greatest at low moisture contents.

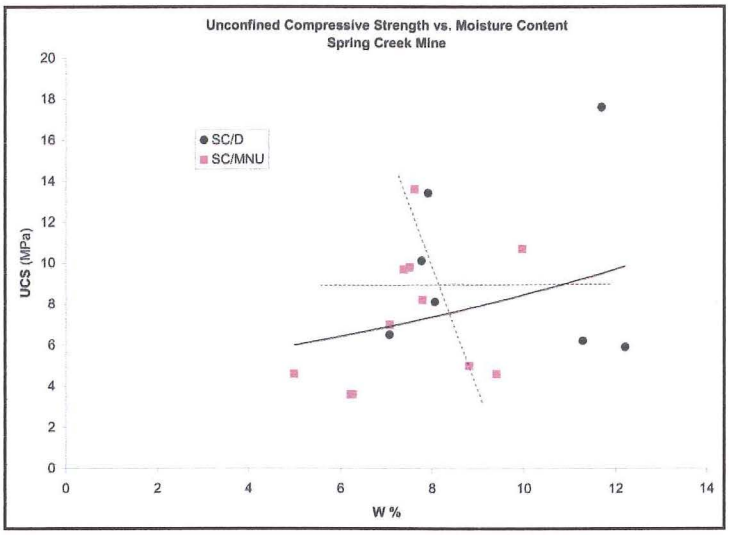

Figure 2.5. Relationship between moisture content and unconfined compressive strength for Spring Creek samples. A very weak trend can be seen, but the trendline could be placed in a number of directions and still get the similar r^2 values as shown by the dashed line.

2.2.6 Strength Anisotropy

Spring Creek D seam specimens were loaded at a range of orientations with respect to bedding for ease of sample preparation. Because intact samples were very difficult to obtain, cores were drilled from whichever orientation it was most likely to yield an intact sample. Many of the lump samples were not large enough for samples of the required length to be taken perpendicular to bedding. Figure 2.6 shows that maximum strength occurs when loading is at an angle, β (Figure 2.7), less than 15° or greater than 80° to bedding, and minimum strength occurs at $\beta = 35^\circ$ ($r^2 = 0.608$). This is consistent with other rock types where minimum strength is commonly seen when $\beta \cong 30\text{-}40^\circ$ (Anderson, 2001; Broch, 1983; Hoek and Brown, 1980, 1997; Kwasniewski, 1993; Ramamurthy, 1993). Hoek and Brown (1980) state that for angles of $\beta \cong 15\text{-}50^\circ$ failure occurs on discontinuities, but for angles other than this failure occurs through intact rock and in this case across bedding.

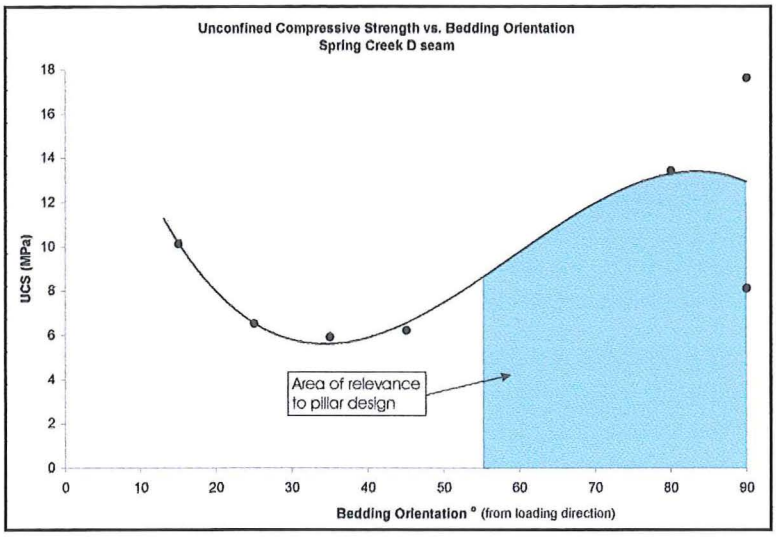

Figure 2.6. Variation of unconfined compressive strength resulting from changes in loading direction with respect to bedding orientation, β. Shaded area shows the loading directions likely to be encountered in mine pillars using a maximum seam dip of 35° seen in the Strongman No. 2 mine.

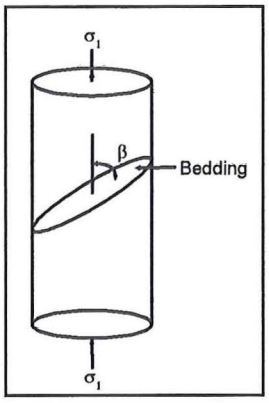

Figure 2.7. Orientation of bedding, β, with respect to loading direction σ_1.

The anisotropy is a significant feature in the Spring Creek mine as the dip of the seams increases significantly from an average of 6-12° to the west in the eastern portion of the mine to 12-28° in the west. Where the dip is low β is close to 90° and thus strength is high. As the dip angle increases β will approach 60° and correspondingly the strength will drop.

The results of strength tests on Spring Creek D seam samples plotted in Figure 2.6 may not be relevant for pillar design as there are several β orientations outside of those expected within the mine. Seam dip in the Spring Creek mine is generally 6-28° (β = 62-84°). The mean σ_c value when β = 90° is 12.9 MPa, slightly lower than the value for β = 80° of 13.4 MPa taken from Figure 2.6. What Figure 2.6 shows is the even when β = 90°

there is a high degree of variability in the strength data, with the lowest value (8.1 MPa) being similar to those when β = 25-45° (5.9-6.5 MPa). Therefore any coal strength value quoted is only a best estimate and an accurate determination of coal strength may be a myth.

The type of anisotropy is defined by the shape of the curve when UCS is plotted against bedding angle, β (Ramamurthy, 1993). Anisotropy occurs in three different types: i) U-type anisotropy; ii) shoulder-type anisotropy; and iii) undulatory type anisotropy (Figure 2.8). It is difficult to determine the type of anisotropy displayed in Figure 2.6 due to no samples being tested with $\beta = 0°$, but it appears likely to be U-type by comparison with Figure 2.8. Ramamurthy (1993) reports undulatory type is found predominantly in coal as this arises from the presence of more than one set of weakness planes crossing each other. These defects are referred to as the face and butt cleats. Their spatial orientation is dependant on the paleostress environment, but they are always approximately perpendicular to each other. Figure 2.8 shows that U-type and undulatory-type anisotropy are similar, apart from a flattening of the undulatory-type curve between c. β = 45-60°. Given the weakness of bedding planes seen in samples from the Spring Creek Mine, this flattening in the curve is unlikely to form, thus U-type anisotropy is to be considered more likely. Shoulder type anisotropy can also be discounted as weakness of bedding planes would cause the axial splitting mode of failure to dominate when bedding is orientated parallel to loading direction. This would make the high strength required at this orientation unlikely to form.

Anisotropy ratio can be classified further by a numerical value, R_c (Table 2.4), which is the ratio of tests results perpendicular and parallel to bedding. Anisotropy showed up much better in the UCS tests rather than the point load tests (Table 2.7). The R_c classification only takes into account loading perpendicular and parallel to bedding planes, but when samples are loaded at different orientations the true anisotropic nature of coal can be seen. Figure 2.6 also shows the at any one bedding orientation the strength can still be highly variable and assigning a numerical value such as R_c may not be appropriate for coal.

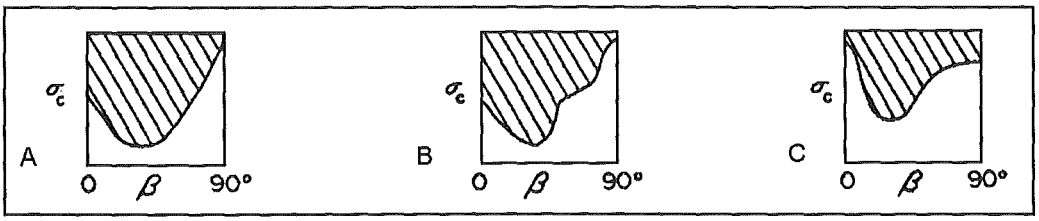

Figure 2.8. Types of Anisotropy. A) U type; B) Undulatory type; and C) Shoulder type (after Ramamurthy, 1993).

Anisotropy ratio, R_c	Class
1.0-1.1	Isotropic
>1.1-2.0	Low anisotropy
>2.0-4.0	Medium anisotropy
>4.0-6.0	High anisotropy
>6.0	Very high anisotropy

Table 2.4. Classification of anisotropy (after Ramamurthy, 1993).

2.2.7 Other Parameters

Strain gauges were attached to two E/OC samples in order to examine performance under load and determine values for Young's modulus and Poisson's ratio. Four strain gauges were attached to each sample; two radial and two axial (Figure A2.9). A radial strain gauge on one sample failed when a piece of the sample broke off prior to failure. This sample was consequently disregarded for calculation of Young's modulus and Poisson's ratio.

Location	Seam	Author	E_{ave} (GPa)	E_t (GPa)	E_{dyn} (GPa)	ν
Strongman No. 2	E/OC	This study	3.9	2.9	1.78	0.28-0.42
	E	Caffyn, 1987	1.7	-	-	-
	D	This study	-	-	1.96	0.44
	D	Caffyn, 1987	1.1	-	-	-
Ohinewai		Murray & Orr, 1985	0.9-2.0	-	-	-
Huntly	Kupakupa	Mills, 1986	-	-	-	0.40

Table 2.5. Summary of Young's Modulus and Poisson's Ratio determined by this and other studies of New Zealand coal.

The average Young's modulus, E_{av}, calculated from the average slope of the stress-strain compression curve (Figure 2.9) was calculated as 3.9 GPa, while the tangent Young's modulus, E_t (calculated at 50% of the ultimate stress) is 2.9 GPa. However, this was calculated from the results of one sample so may not be a reliable estimate. Poisson's ratio was calculated to be 0.28. Dynamic Young's Modulus, using P and S waves, was

determined for two samples from each of the Strongman No. 2 D and E seams to be 1.78 and 1.96 GPa respectively, with corresponding Poisson's ratios of 0.42 and 0.44. Due to the discontinuous nature of the coal, the P and S waves used in determining these properties would not penetrate through most of the samples from Strongman No. 2, and none of the Spring Creek samples.

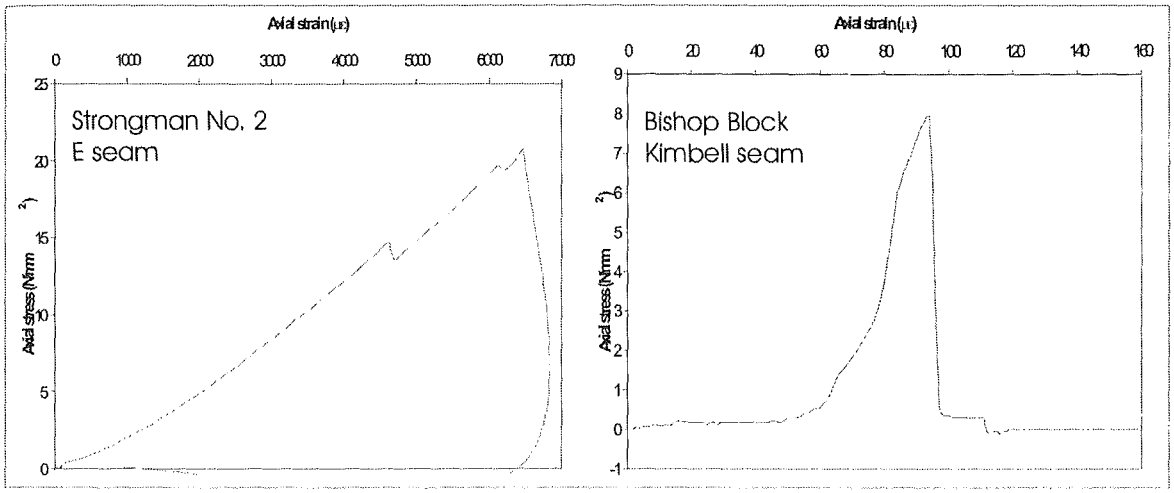

Figure 2.9. Comparison of compression curves for Strongman No. 2 E seam (this study) and the Bishop Block Kimbell seam (after Richards, 2000).

The slope of the axial stress-axial strain plot is dependant of rock properties and rate of loading (Hawkes and Mellor, 1970). If the slope of the plot is a straight line, then the sample is said to be perfectly elastic. A comparison of compression curves for the Strongman No. 2 E seam and the Bishop Block Kimbell seam (after Richards, 2000; sample from DH #848, Map 1) are presented in Figure 2.9 and show that the lower rank E seam coal takes a great deal more strain over a larger stress range than the Kimbell seam. The E seam coal behaves in an almost perfectly elastic manner once the axial strain increases above 2000με (as seen from the linear trendline). There is one small dip in the trendline when axial strain reached 4500με which is related to a small amount of spalling from the sample. The Kimbell seam shows a short, sharp increase in axial stress which shows that this coal behaves in a much more plastic manner.

E_t was determined to be 1.7 GPa for E seam coal and 1.1 GPa for D seam by the Ministry of Works (Caffyn, 1987), from samples with L/D ratios of 1.14-1.81. elastic properties of rocks and coal change with sample length. Very short samples (such as the reported by

Caffyn, 1987) behave in a much more brittle manner than those with L/D of 2.5-3.0 and subsequently are considered too short to have any significance.

Jeremic (1985) states that soft coal shows a decrease in strength and modulus of elasticity with increasing mine depth. This has been estimated as a strength decrease of 25%, and a 50% reduction in modulus of elasticity for coal at a depth of 250m relative to that at the surface. Medhurst and Brown (1998) found that Poisson's ratio showed no apparent trends with change in sample size, so values can be applied directly to in-situ coal.

2.3 Unconfined Compressive Strength Determination for Cube Samples

2.3.1 Methodology and Scope

Bieniawski (1968), who conducted a large number of tests on cubical specimens of South African coal with side lengths ranging from 19mm to 1.52m, conducted the most comprehensive work on compressive strength of coal cubes. The strength decreasing rapidly as the specimen size increased until sample size reaches 457mm (18") at which point it decreases more slowly, before becoming constant above 1.52m (60"). Pariseau (1977) determined the size at which no further strength reductions occur is 0.9m for U.S coals. Bieniawski (1968) found that there was also a minimum size of 63.5mm (2 ½") beyond which no further strength differences occur.

Cube compressive strength was determined for each seam studied in this project (other than Strongman No. 2 D seam), as it proved significantly easier to obtain samples for this than for unconfined compressive strength tests on cores from the weakest seams. Cubes with a side length of 63.5mm (2 ½") were tested using the same loading frame as the triaxial and UCS tests. This size was chosen for two reasons; 1) cutting cubes of a larger size from the lump samples proved too difficult due to the presence of defects and the generally weak nature of the coal; and 2) after testing cubes with side length ranging from 19mm (0.75") to 1.52m (60"), Bieniawski (1968) concluded that for cubes smaller than 63.5mm, the strength became essentially constant, although this will vary from seam to seam depending on coal properties. Bieniawski goes on to suggest that the minimum size

is due to the size of the sample being smaller than the least distance between defects, but does not explain why a maximum size for constant strength exists. Spacing between defects decreases with increasing coal rank, and were commonly 5-10mm apart in samples of Bishop Block and Roa coal which had a rank of high volatile bituminous A and low volatile bituminous respectively.

Because of the difficulty of preparation of specimens, especially from the weaker coals, some allowances needed to be made in terms of exact sample size. In most cases samples have a side length of 63.5 ± 2mm. No correction has been made for this size difference, but it is expected that the effects are minimal. Townsend *et al.* (1977) also experienced difficulties preparing perfect cubic specimens so used a range of width to height (*w/h*) and width to depth (*w/d*) of:

$$0.95 < w/h < 1.05$$
$$0.95 < w/d < 1.05$$

Anything outside this range was not considered. The aim of the cube strength tests was to use the results in deriving a formula to predict the unconfined compressive strength of coal in areas where core cannot easily be obtained (Section 3.6). Reliable strength comparisons could also be made between each of the seams by using this method.

Often a defect within the cube samples would cause a corner of the sample to break off during sample preparation. Because of the difficulty of obtaining perfect samples, these corners were filled with Plaster of Paris. Townsend *et al.* (1977) used a guideline where if 10% or more of the cross sectional area of the sample was missing the sample would be disregarded. 10% of the cross sectional area is equivalent to c. 400mm^2 for samples tested in this study. The plaster ensured that when the samples were tested the loading would occur over the entire cross sectional area of the sample. Plaster capping was more common in the weaker samples. Because of the small amount of plaster used on the affected samples there should be no significant bias in the strength test results.

Pells and Ferry (1983) conducted unconfined compressive strength tests on weak (c. 50 MPa) sandstone cores which were capped using concrete cylinder sulphur capping. They discovered that the capped samples were on average 6% weaker than the uncapped samples. Pells (1993) suggests that the use of capping materials is often the only way of obtaining test specimens in some friable rocks, and that the practice is almost universally used for testing concrete cylinders. The use of Plaster of Paris for capping coal specimens has also been reported by Mills (1986). In testing of large coal blocks ($\leq$2m) Bieniawski used a mixture of cement and sand to account for surface irregularities.

2.3.2 Results and Discussion

2.3.2.1 Summary

The complete set of cube strength test results is presented in Appendix 3, and are summarised in Table 2.6. The mean cube compressive strength (CCS) varied from 3.0 MPa for the Roa mine to 20.0 MPa for the Strongman No. 2 E seam. Mean strengths of the Morgan and Kimbell seams of the Bishop Block were low at 3.3 MPa and 7.8 MPa respectively, while the D (19.8 MPa) and Main Upper (19.9 MPa) seams from Spring Creek were very similar to the E seam (20.0 MPa). The range of results in individual seams is generally low, but the spread of results is skewed with the mean occurring at the lower of the results range in all seams. The average percentage difference of the lowest and highest strength values from the mean is 30% and 84% across each of the seven seams. The greatest range occurs in the Morgan seam with deviations of -64% and +112% from the mean strength.

Location	Seam	No. Tests	Mean compressive strength (MPa)	Range	Std Dev.	W %
Bishop Block	Kimbell seam	9	7.8	4.4-13.7	1.7	3.34-5.35
	Morgan seam	7	3.3	1.2-7.0	2.1	3.00-6.71
Roa	Kimbell seam	7	3.0	2.4 - 5.8	0.5	0.96-2.90
Spring Creek	D seam	5	19.8	12.1 - 38.0	5.0	6.63-9.68
	Main Upper seam	7	19.9	13.5 - 32.7	6.2	4.66-7.37
Strongman No. 2	E seam (OC)	7	20.0	15.5-35.6	3.8	2.13-6.30
Terrace	No. 4 seam	6	13.0	10.2 - 20.4	1.5	10.60-13.58

Table 2.6. Results of compressive strength tests on coal cubes.

2.3.2.2 Bishop Block

Seven samples were tested from the Morgan seam and nine from the Kimbell. These samples were affected by weathering, which has significantly affected the strength of the samples. Unweathered samples were unavailable as there are no mining activities currently in this area. The Kimbell seam gave a CCS value of 7.8 MPa with a range of 4.4-13.7 MPa and a relatively low standard deviation of 1.7 MPa. The Morgan seam returned a much lower CCS value of 3.3 MPa and range of 1.2-7.0 MPa. The standard deviation was however higher in the Morgan seam which is a result of two distinct strength populations being represented, which is shown graphically in Figure 2.10.

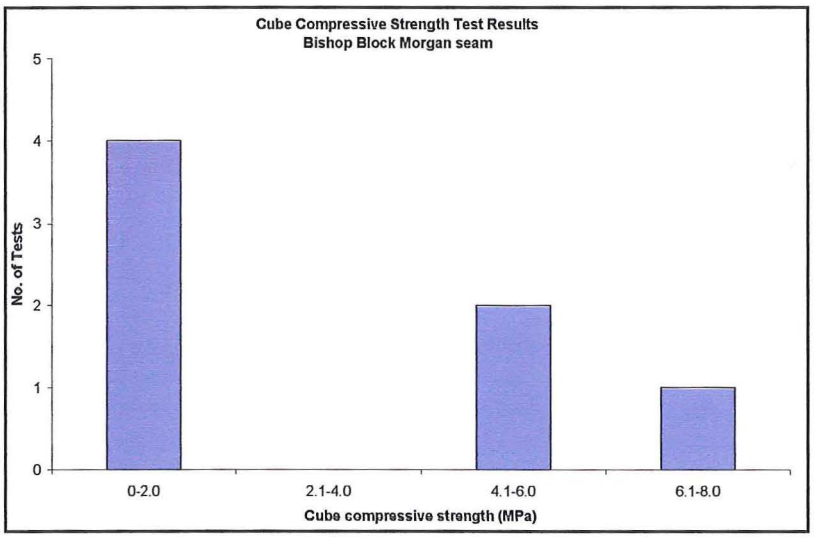

Figure 2.10. Frequency of cube compressive strength results from the Bishop Block Morgan seam showing the two distinct strength populations.

The coefficient of variation was quite low in the Kimbell seam at 22%, but much greater in Morgan seam at 64% owing to the two strength populations. Four of the Morgan seam samples, comprising the lower strength population of Figure 2.10, failed plastically, whereby they took a small amount of load (c. 4.6-8.1 kN) at which point the load began to decrease without a definite peak being recorded, while the samples continued to shorten and dilate. This yielding behaviour for the Morgan seam coal led to one population with cube compressive strengths (CCS) of 1.2-1.7 MPa whilst the other had strengths of 5.3-7.0 MPa. These failed by crushing the corners of the samples similar to those of higher strength. No such strength bias was seen in the in the Kimbell seam.

Does this apply to coals?

Both the Kimbell and Morgan seam samples displayed grade II weathering (slightly weathered) according to the ISRM (1981) description (Table A1.1). The weathering of the Kimbell seam coal appeared more penetrative, with a thin film of clay was found on some defect surfaces after failure. Jeremic (1985) notes that weathered coal is more plastic and gives poorly defined peak strength, with yielding observed over a range of loads without clear failure. The Morgan seam, which appeared to be much less weathered took little load, gave unreliable strength results, did not produce a definite peak, and behaved in a similar manor to Roa coal.

how does the oxidation of coal affect its strength.

2.3.2.3 Roa

The Kimbell seam was the only seam sampled at the Roa mine. Because of the weakness of this coal, five of the seven samples needed to have a corner capped with plaster. This seam is the highest rank (low volatile bituminous) and lowest strength coal in this study, with a CCS of 3.0 MPa. The strengths recorded ranged from 2.4-5.8 MPa and had a standard deviation of only ±0.5 MPa. The give a coefficient of variation of only 16% which is very low compared to most of the other seams. Moisture content when tested is insignificant at 1.8%, and slightly lower than field moisture content of 3.1%.

2.3.2.4 Spring Creek

The average cube compressive strength of the two seams tested from the Spring Creek Mine is almost identical at 19.8 MPa in the D seam and 19.9 MPa for the Main Upper seam. The range of strengths (D = 12.1-38.0 MPa; MNU = 13.5-32.7 MPa) is higher in the D seam, but the coefficient of variation is slightly higher in the Main Upper seam at 31% compared to 25% for the D seam. This variation is significantly lower than for the corresponding core samples and is likely to be representative of loading direction in the cube samples. The core samples were loaded at a variety of orientations (β = 10-90°), whereas the cube samples were loaded predominantly with β = 55-90°. Due to difficulties experienced in sample preparation, where many of the samples broke along cleat planes, sufficient samples with $\beta = 90°$ could not be prepared. Spring Creek coal gives the highest coefficient of variation of all seams tested, and is probably a function of the very

pronounced bedding seen in this coal. Moisture content is high with 8.4% and 6.5% for the D and Main Upper seams respectively. Only two samples from each of the Spring Creek seams needed to have plaster caps on an edge.

2.3.2.5 Strongman No. 2

Only cubes from the Strongman No 2 E seam opencast were used for cube testing, due to no samples of the D seam being available, as no mining activity was occurring in this seam when cube samples were being collected. The strength of the seven E seam cubes was the same as those from Spring Creek at 20.0 MPa, but had a lower standard deviation and coefficient of variation (19%) which may be related to the absence of prominent banding resulting in fewer planes of weakness in the E seam. All but two of the cubes required plaster on a corner. Bedding orientation for all but one sample was β = 80-90°, while the other sample had $\beta = 0°$.

2.3.2.6 Terrace

Only six samples from this seam could be tested due to the fragility of the samples. The average strength of the No. 4 seam (13.0 MPa) is close to the bottom end of the strength range (10.2-20.4 MPa). This seam has a very low standard deviation and coefficient of variation (11.5%), resulting from the lack of cleats in this low rank coal. All samples of the No. 4 seam were oriented with the loading axis 80-90° to bedding, and tested with an average moisture content of 11.7%.

2.3.3 Mode of Failure

Many of the cubes failed by crushing one corner or one side of the sample. In mine pillars stress is concentrated on the edges and corners of the excavation (Figure 4.7), so it is perhaps not surprising that cubical samples should fail in the same manner as they are of similar shape. In many cases a central core of the cube remained largely intact, though fractured. This central core has also been reported by Bieniawski (1968) who suggested this could sometimes remain quite solid.

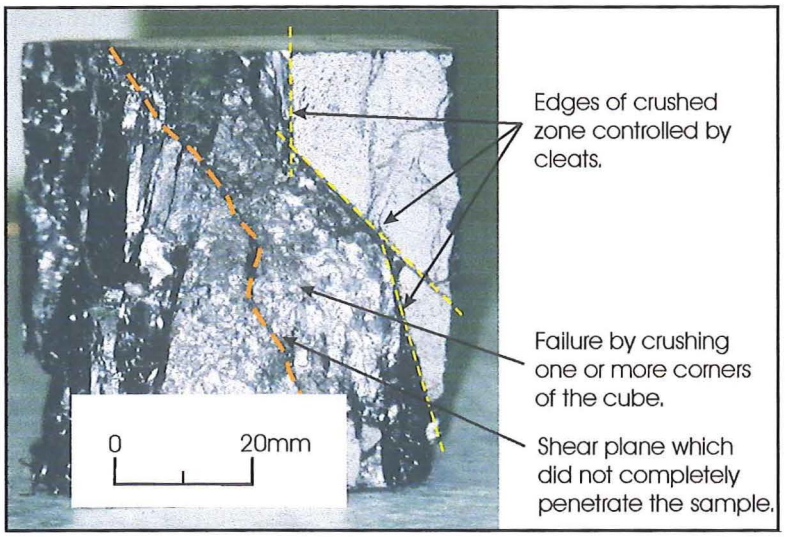

Figure 2.11. Common mode of failure in strong cube samples where one or more corners of the cube is crushed. Sample shown is from the Spring Creek Main Upper seam. Loading direction parallel to bedding, but this has no bearing on the failure mode, as samples of all orientations showed this type of failure.

The mode of failure in the samples containing few defects was a double pyramid shape similar to that described by Bieniawski (1968). The double pyramid shape (Figure 2.12) comes about by the same mechanism as the hourglass shape in cylindrical samples (Section 2.2, Figure 2.3d), whereby the ends of the sample are constrained by the platens, so it must fail through the centre where frictional forces are least.

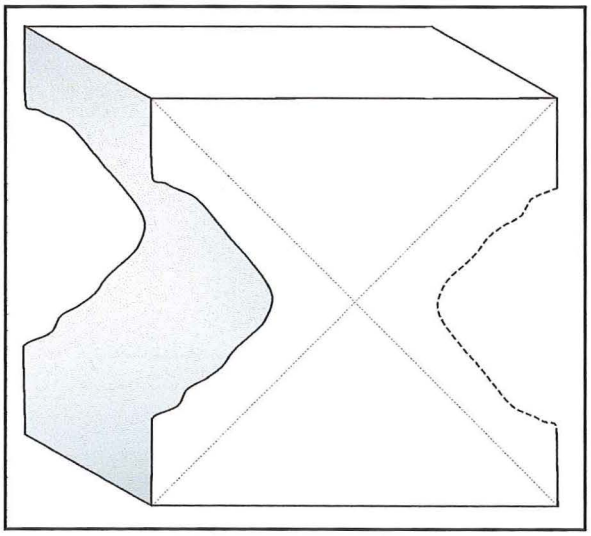

Figure 2.12. Double pyramid cube failure mechanism described by Bieniawski (1968) displayed in cube samples with few cleats. Often only one side of the double pyramid would form in samples from this study. This is a brittle failure mechanism similar to that seen in core samples (Figure 2.3d).

Cubes of coal from the Kimbell seam (at the Roa Mine) did not fail in the same elastic-brittle manner as all other coal type tested in this study, which is a reflection on the softness of the coal. Instead, the samples deformed plastically, showing a considerable amount of shortening and lateral dilation during the compression tests as shown in Figure 2.13. Although obvious bulges could be seen in the sides of the samples, the amount of shortening is much greater than the amount of lateral expansion (and is similar to yielding failure in mine pillar; Figure 4.13c). One sample shortened by 20%, while expanding laterally by only 5%. These samples only took a small amount of load (8-10kN), but once this point was reached they continued to deform (shorten and dilate) with the sample still largely intact. If loading continues the sample will continue to deform slowly to a point where it crumbles into small fragments c. 1-2mm in diameter. Medhurst and Brown (1998) report that when coal is loaded beyond its peak strength irreversible deformation will occur and it will begin to soften.

After loading the Roa samples often displayed a large number of sub-vertical to vertical cracks concentrated on the edges and corners of the sample, and there are a result of a large amount of lateral dilation. These were cut by sub-horizontal cracks which are much fewer in number. The samples became very fragile and prone to disintegration upon touching. This behaviour was not displayed in any other seams.

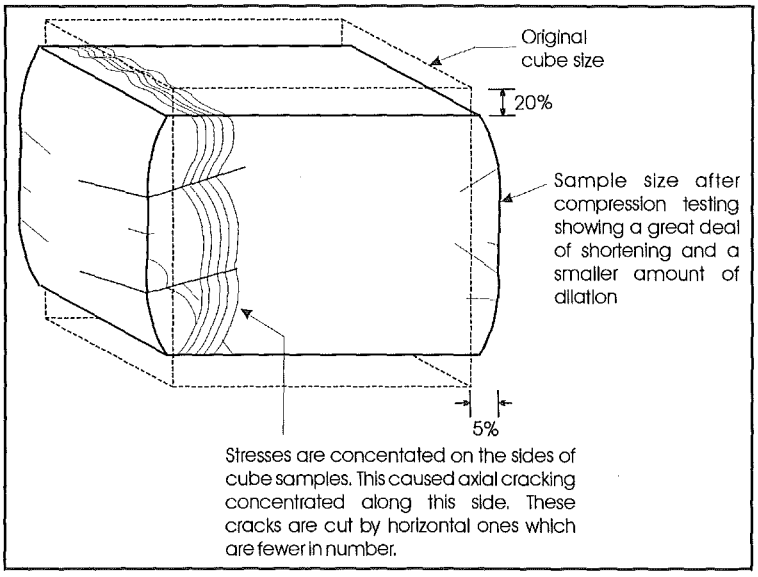

Figure 2.13. Common mode of failure observed in cube samples from the Roa Mine which behave plastically. Samples shorten and dilate resulting in axial cracking and bulging of the sides.

2.3.4 Influence of Bedding and Banding

The Kimbell and Morgan seams of the Bishop Block had quite different appearances to each other. The Morgan seam coal showed greater alternation of vitrain and durain, with durain bands up to 22mm thick. Vitrain is the dominant component and contains more cleats, whereas the cleats in durain are few and run approximately perpendicular to those in vitrain in this seam. Overall the Morgan coal is less cleated than the Kimbell, which often had cleat spacings of <5mm. The dominating cleats were often orientated parallel to bedding, which N. Newman (pers. comm.) suggests is an unusual feature most likely related to weathering. The failure mechanism was similar to each of the other seams in this study, with crushing of one or more corners and axial splitting with occasional shear planes.

Samples from the Kimbell seam (Roa Mine) were prepared and loaded at a range of orientations with respect to bedding purely for ease of sample preparation. One sample loaded with $\beta = 30^{\circ}$ was the strongest of all Roa samples by 50% with a strength of 5.8 MPa (mean 3.0 MPa). This was highly unexpected considering the findings of the UCS tests on cores (Section 2.2. Figure 2.6), and of many other authors who showed that when $\beta = 30^{\circ}$ the lowest strengths are usually recorded.

The Kimbell seam shows a prominent alternation of durain and vitrain bands similar to those seen in the D seam at Spring Creek. The durain bands in this seam were up to 6mm in thickness, which is much thicker than those of Spring Creek. Coal from the Roa mine shows a moderate correlation between strength and bedding orientation having a r^2 value of 0.82. This trend shows that the lowest strengths are recorded when bedding is perpendicular and parallel to bedding orientation, though the difference is small (c. 15%). This is the opposite to the effect seen in the Spring Creek D seam core samples when the minimum strengths occurred when $\beta = 35^{\circ}$. All others seams tested show no significant strength trends with bedding orientation, each having an r^2 value < 0.5.

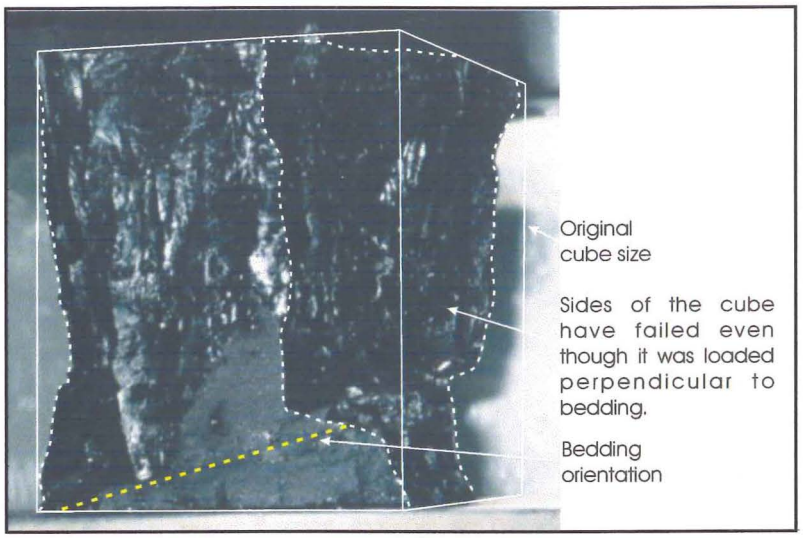

Figure 2.14. Bedding in coal cubes does not appear to have a significant effect on the mode of failure of cube strength.

As with the core samples, alternating vitrain and clarain bands were common in the cubes of Spring Creek coal. Bedding did not appear to be a factor in the failure of the cubes as it was with the cores. Instead, failure often occurred perpendicular to bedding by either crushing of one side or a corner. These failures did not appear to be along major defects within the sample as occurred in the core specimens, though defects must have played a role in giving the sample an overall weakness.

2.3.5 Influence of other Factors

The No. 4 seam of the Terrace Mine was the lowest rank coal tested in this study with a vitrinite reflectance of 0.48% (sub-bituminous B). Accordingly there were fewer cleats in samples taken from this seam than any other, as the proportion of cleats is a function of coal rank as illustrated in Figure 3.2. This lack of cleats had a significant effect on the scatter of results. The standard deviation was low and the resulting coefficient of variation was the lowest seen in this study at 11.5%.

One sample of the No. 4 seam, which contained only minor defects, failed in an explosive manner leaving only relatively small pieces. This same type of failure was reported as characteristic of small and medium sized samples tested by Bieniawski, though the samples used in his study were substantially stronger than those in this study, possibly due

to a lower number of cleats in the Bieniawski samples. Samples displaying less cleats are more likely to fail by this explosive mechanism due to a lack of weakness planes. The double pyramid failure mechanism seen at Spring Creek was displayed in some samples from the No. 4 seam, but failed to form completely (Figure 2.12). Only one side of the double pyramid would form, leaving a wedge type shape in one side of the sample.

The dominant cleats are parallel to bedding in the Strongman No. 2 samples. Often they are quite open. The distribution of cleats varied widely from having few cleats to being extensively cleated in a cubic pattern (spacing ranges from c. 5-30mm). The samples with fewer cleats yielded significantly higher strengths.

Moisture content of Bishop Block coal (c. 3.0-6.7%) is higher than that from the Strongman mine (2.1-6.3%) even though a lower moisture content would be expected due to the rank. This is due to the degree weathering which introduces moisture to samples.

2.4 Point Load Strength Index

2.4.1 Methodology and Scope

The main advantage of the point load test is that it can be conducted in the field on unprepared specimens with portable equipment (Bieniawski, 1975) or as a quick and cheap laboratory test, whereas unconfined compressive strength tests tend to be expensive, time consuming (Broch, 1983) and samples are difficult to prepare when dealing with weak lithologies. More tests can be conducted on the same sized sample using the point load test rather than UCS. Broch and Franklin (1972) proposed the point load test should replace the UCS test as the standard strength classification although that will not happen. It is important to conduct some unconfined compressive strength tests to define the relationship between UCS and $I_{s(50)}$ for each lithology (or seam) because of the large amount of variability shown in $I_{s(50)}$ results, and because the UCS/$I_{s(50)}$ and CCS/$I_{s(50)}$ relationships vary across the coalfield (Sections 3.3 and 3.4).

Coal from all locations had point load tests conducted on samples taken from failed cube specimens, or from the same lump sample as the cube sample was taken. Core and cube samples were taken from different blocks as the samples were collected at different times. Point load tests on failed core specimens were conducted on coal from Spring Creek and Strongman No. 2 mines only.

The majority of point load tests were conducted using the irregular lump method, as per ISRM suggested method detailed in Brown (1981), at the moisture content of the corresponding core or cube sample. Point load testing on irregular lump samples is commonly regarded as the least accurate method of determining point load strength (Bieniawski, 1975. Broch and Franklin, 1972) due to liberties taken with sample volume i.e. sample volume cannot accurately determined due to its irregular shape. Axial tests were therefore conducted whenever possible. Brook (1993) suggests that cores taken from coal measure rocks are not suitable for diametral type tests due to the large number of bedding planes producing erratic results. No diametral tests were conducted in this study.

Often the irregular lump samples were such that they were smaller than required according to ISRM standard, but due to the nature of the coal being tested they needed to be used to allow a representative number of samples to be tested. In general a minimum size, D (the distance between the platens), of 15mm was adopted, but in the case of the Roa mine, three samples smaller than this were tested to get sufficient samples for the $CCS/I_{s(50)}$ correlation (section 3.4).

Axial samples were prepared by two methods. The first was to take the off cuts from UCS core samples which were trimmed to conform to the ISRM standard of L/D between 2.5-3.0. The second method was to prepare axial test samples from cores that were too short for UCS testing. The point load tests could then be correlated to UCS test cores taken from the same block sample.

2.4.2 Results and Discussion

The point load strength data is separated into two separate components. Table 2.7 summarises the results of irregular lump tests on failed cube samples and Table 2.8 gives the results of axial and irregular lump tests on cube samples. The complete set of results is presented in Appendix 4. The problem with conducting point load tests on such a weak material (UCS <25 MPa) is that it is likely to yield ambiguous results (Hoek and Brown, 1997; Hoek *et al.* 1998).

Location	Seam	No. Tests	$I_{s(50)}$ (MPa)	Range	$I_{a(50)}$
Bishop Block	Kimbell	60	0.21	0.06 - 0.42	
	Morgan	44	0.17	0.06 - 0.47	1.01
Roa	Kimbell	23	0.13	0.06 - 0.23	1.16
Spring Creek	D	20	0.57	0.19 - 0.99	0.99
	Main Upper	38	0.51	0.07 - 1.10	1.16
Strongman No. 2	E/OC	44	0.51	0.22 - 1.48	1.06
Terrace	No. 4	31	0.45	0.07 - 1.32	0.86

Table 2.7. Results of point load tests conducted on failed cube samples using the irregular lump method.

Location	Seam	No. Tests	Type	$I_{s(50)}$ (MPa)	Range
Spring Creek	D	42	Lump	0.48	0.14 - 1.16
	Main Upper	75	Lump	0.56	0.10 - 1.34
Strongman No. 2	D	26	Lump	0.85	0.27 - 1.38
		45	Axial	0.50	0.14 - 1.14
	E seam (UG)	22	Lump	1.12	0.42 - 2.17
		17	Axial	0.54	0.05 - 0.98
	E seam (OC)	39	Axial	0.61	0.11 - 1.30

Table 2.8. Results of point load strength tests conducted on failed core samples using either the irregular lump or axial test method.

2.4.2.1 Samples from Cubes Specimens

All seams show a large range of point load strengths. The spread of results increases with increasing strength. Samples from the Kimbell and Morgan seams of the Bishop Block, and samples from the Roa mine have the lowest $I_{s(50)}$ values of 0.21, 0.17 and 0.13 MPa respectively. Accordingly these three seams also have the lowest strength ranges with 0.06-0.42 MPa (Kimbell), 0.06-0.47 MPa (Morgan) and 0.06-0.23 MPa (Roa). These are the only seams with a narrow range of strength values. The result for the Kimbell seam at the Roa mine reported in this study are significantly different to those of Bell (1993a) who reports a mean $I_{s(50)}$ of 0.066 MPa.

Samples taken from Spring Creek, Strongman No. 2 and the Terrace Mines had much higher mean $I_{s(50)}$ values. These were 0.57 and 0.51 MPa for the Spring Creek D and Main Upper seams, 0.51 MPa for the E seam (OC) and 0.45 MPa for the Terrace Mine. The Spring Creek D seam gave the lowest spread in results of these four seams (0.19-0.99 MPa) followed by the Main Upper seam (0.07-1.10 MPa), No. 4 seam (0.07-1.32 MPa) and the E seam (0.22-1.48 MPa).

Strength anisotropy, $I_{a(50)}$, is calculated as the ratio of $I_{s(50)}$ values determined perpendicular and parallel to bedding. This has been calculated for most of the seams tested in this study (Table 2.7). In many of the point load tests the samples were quite small and it was often impossible to determine bedding orientation, so $I_{a(50)}$ was generally determined from 5-10 samples per seam. Broch and Franklin (1972) suggest that most rocks are anisotropic to some extent even though they may not contain visible weakness planes. It appears that direction of loading, whether perpendicular of parallel to bedding, does not have much effect for point load tests as the $I_{a(50)}$ values are all very low ranging from 0.86-1.16. Caffyn (1987) reported $I_{a(50)} = 1.50$ for the Strongman No. 2 E seam. Using the classification of Ramamurthy (1993) (Table 2.4) these coals are classified as isotropic to having low anisotropy.

A significant feature is that the Spring Creek D seam gives an $I_{a(50)}$ value of 0.99, i.e. being isotropic, when it is clear from Figure 2.6 that this seam displays a high level of anisotropy. The point load strength test does not show the true anisotropy of rocks because samples are only tested parallel and perpendicular to bedding. The true anisotropy of rocks is revealed when they are loaded at a range of orientations in UCS tests, which show that the minimum strength occurs when β = c. 35°, while the maximum strengths occur when β = 0° & 90°. It is not surprising then that $I_{a(50)}$ values may be close to 1.0 when the point load test is used. It may be possible to investigate anisotropy more accurately using the axial point load test and loading samples at a range of orientations, but this has not been attempted in this study.

2.4.2.2 Samples from Core Specimens

Both axial and irregular lump testing methods were used for Strongman No. 2 coal, while only the irregular lump method was used for Spring Creek samples. Results of these tests are summarised in Table 2.8. Large differences between the results of the two tests methods can be seen in the Strongman D and E seams. The D seam had a mean strength of 0.85 MPa in the lump tests (0.27-1.38 MPa) compared to 0.50 MPa for the axial test (0.14-1.14 MPa). Results for E/UG are higher with 0.85 MPa for lump samples (0.42-2.17 MPa) and 0.54 MPa for axial tests (0.05-0.98 MPa). Only axial tests were conducted on core samples from the E/OC seam. These had a point load strength of 0.61 MPa ranging from 0.11-1.30 MPa. The range as strengths is highest using the lump test which has an average spread of 1.28 MPa compared to 1.04 MPa for samples tested axially.

The results of axial tests on E/UG and E/OC samples of 0.54 MPa and 0.61 MPa respectively correspond well to the 0.60 MPa for axial tests on E seam coal reported by Caffyn (1987) and 0.54 MPa by MWD (1985).

The difference in strengths recorded between the two tests methods is attributable to the inaccuracies in determining the volume of samples used in the irregular lump method. The volume of axial samples can be determined accurately as the sample is of uniform shape. By their nature, irregular lump samples are non-uniform shapes. Standard practice is to make one measurement of samples thickness and two of sample width, so large inaccuracies are easily introduced.

The spread seen in the results of point load tests becomes much more significant when it is applied to the UCS = $24.I_{s(50)}$ relationship. The relationships between point load strength and both UCS and CCS have been developed in sections 3.3 and 3.4 respectively.

2.5 Triaxial Compressive Strength

2.5.1 Methodology and Scope

Triaxial compressive strength tests were conducted on NX sized core prepared from lump samples taken from the Spring Creek and Strongman No. 2 mines to establish the Hoek-Brown and Mohr-Coulomb failure criteria for each seam. These tests were conducted using a Hoek and Franklin cell to provide the confining pressure (Figure A5.1, Appendix 5). No triaxial tests have previously been conducted on Greymouth coal, and as far as the author is aware the only other triaxial tests on New Zealand coal are by Mills (1986).

Samples used in the triaxial testing had flat but not necessarily parallel ends (flat to within c. 2°), due to the fragility of the samples. This has been shown to have little influence on the overall results of the testing by Pells and Ferry (1983) as discussed in section 2.2.1. One sample from Spring Creek D seam was tested with L/D ratio of 1.98. This was corrected to an L/D ratio of 2.0 using the ASTM (1979) method as detailed in section 2.2.2. The value obtained by using the correction was only 0.1 MPa (0.2%) weaker than that determined in the original test, and likely to be well within the margin of error. All other samples were tested in accordance with the ISRM recommendations.

From field monitoring of coal pillar loading in Bulli Mine, NSW, Australia, Gale and Mills (1995) determined that if a confining pressure of 4 MPa could be maintained in the core of a coal pillar, then this pillar could support an overburden stress of 30-35 MPa. They estimate that this confinement could be provided by 1.5m of failed coal around the edges of the pillar, which is held in place by friction against the roof and floor, provided the roof and floor strata are of sufficient strength. Coal from the Bulli Mine is similar in strength to the D seam of the Spring Creek Mine with c. σ_c = 10 MPa, but is of significantly higher rank (S. Henley, pers. comm.).

As the coal seams in this study were relatively shallow (<300m), a maximum confining pressure of 6 MPa was used in the triaxial testing. Confining pressures of 2, 4 and 6 Mpa should encompass the majority of situations encountered in these mines where the

overburden stress on each pillar is expected to be < 10 MPa. These σ_3 values were chosen using the Hoek and Brown (1997) guidelines for confining pressures where $0<\sigma_3<0.5\sigma_c$. These σ_3 values fit Strongman No. 2 coal better than Spring Creek where $0.5\sigma_c$ is 3.5 and 4.45 MPa for both the Spring Creek seams. This puts the σ_3 = 6 MPa outside of the Hoek and Brown guidelines.

Tests were undrained, as the effects of pore pressure build up were not expected to be significant due to low moisture contents of 7% for Spring Creek and 3% for Strongman No. 2 samples at the time of testing. Field moisture contents are higher than this with 12-13% moisture for the Spring Creek Mine and c. 7% for the Strongman No. 2 Mine.

Six triaxial compressive strength tests over the three different confining pressures were conducted for each of the two seams sampled at the Spring Creek mine (Table 2.9). Ten triaxial tests were conducted on each of the D and E/OC seams from Strongman No. 2. Three tests for each seam were at confining pressures of 2.0 MPa and 6.0 MPa with the remaining four tests at 4.0 MPa.

2.5.2 Results and Discussion

Results from triaxial testing are summarised in Table 2.9. When σ_3 = 2 MPa the Main Upper and Strongman D seams, which were the weakest from their respective mines, become the strongest. For Spring Creek coal σ_1 = 28.0 Mpa in the D seam compared to 44.6 MPa when σ_3 = 2 MPa, while the strengths are similar in the D (40.6 MPa) and E (38.1 MPa) seams of Strongman No. 2. When σ_3 increases to 4 and 6 MPa much smaller strength increases are seen (c. 3-8MPa), except the Spring Creek D seam which continues to increase by >10 MPa. Even with the influence of confining pressure, there is still a great deal of variation in the tests results. For example the range in the Strongman D seam results when σ_3 = 4 MPa (σ_1 = 35.2-62.7 MPa) is sufficient to encompass the results for σ_3 = 6 MPa (σ_1 = 52.9-62.6 MPa), and the spread is almost as great as that seen in the UCS tests (section 2.2.2). In general the scatter in the results decreases with increasing confining pressure as it becomes more difficult for the samples to expand laterally and

thus fail on defects of certain orientations. Cohesion, c, and friction angle, ϕ, are very similar in each of the four seams tested where c = 1.91-2.78 MPa and ϕ = 48.6-51.5°.

Location	No. Tests	σ_3 (MPa)	σ_1 (MPa) mean	σ_1 range	σ_n (MPa)	τ (MPa)	c (MPa)	ϕ	m_i	r^2	W (%)
Spring Creek											
	2	2	28.0	23.3-32.7	5.10	8.5					
D seam	2	4	41.2	40.2-44.0	8.50	12.1	2.11	48.6°	14.6	0.94	7.41
	2	6	52.1	46.7-57.5	11.50	15.0					
	2	2	44.6	34.1-55.0	6.40	12.9					
Main Upper seam	2	4	47.9	47.3-48.4	8.50	13.3	1.91	51.5°	18.3	0.87	5.94
	2	6	54.0	52.6-55.3	10.90	14.6					
Strongman No. 2											
	3	2	40.6	30.7-48.2	7.00	12.8					
D seam	4	4	45.2	35.2-62.7	11.10	13.8	2.78	50.4°	17.1	0.82	3.23
	3	6	57.1	52.9-62.7	12.70	17.1					
	3	2	38.1	25.4-48.9	6.40	11.8					
E seam	4	4	46.1	42.6-51.6	9.10	13.7	2.47	50.8°	18.4	0.91	3.26
	3	6	57.9	53.0-66.2	12.30	16.9					

Table 2.9. Triaxial compressive strength results for Spring Creek and Strongman No. 2 mines.

Strength of coal from the Spring Creek and Strongman No. 2 mines is significantly different in UCS tests, but with increasing confining pressure the strengths become increasingly similar. The Main Upper seam gains the most strength under confinement becoming stronger than the Spring Creek D seam when σ_3 = 6 MPa, suggesting that it has a more discontinuous structure than the D seam which was reflected in the UCS tests. The rapid strength increase of coal with increased confining pressure becomes very significant in the behaviour of mine pillars (Section 4.3) as the pillar core gains significant strength from the confinement given by the zone of failed coal around the perimeter.

Triaxial strength showed no significant trends with changes in bedding orientation at confining pressures of σ_3 = 2 and 4 MPa. When σ_3 = 6 MPa there is a moderate trend (r^2 = 0.593) where the weakest samples had bedding orientations of 25-35°. The drop is strength was c. 15% at these orientations, and 10% when β = 0° compared to when β = 90°.

2.5.3 Modes of Failure

The mode of failure changes from one of cataclasis and axial splitting in uniaxial compression to one of shearing in triaxial compression. Often failure planes did not propagate completely through the samples as seen in UCS testing, but rather a series of

cracks would form extending only part way through, preventing the samples taking more load (Figure 2.15). As the confining pressure increases, incomplete failure becomes more common, and the angle of the shear plane steepens, deviating further from the horizontal (Figure 2.15).

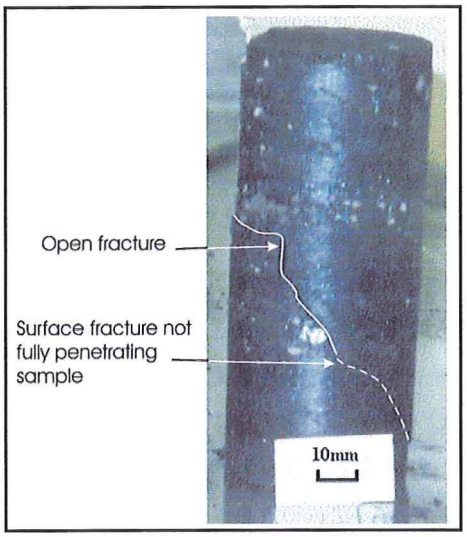

Figure 2.15. Incomplete failure of some triaxial test specimens. Sample shown in figure is from the Strongman No. 2 D seam (σ_3 = 4 MPa).

Shearing was common along a weakness plane such as a cleat or a bedding plane. Failure would often start as a steep angled shear failure, then intercept a low angle bedding plane then continue along this weakness plane. This weakness plane was most commonly a dull (clarain) band in Spring Creek coal, though it was also present in some Strongman No. 2 samples where banding was not common. The shearing plane ranged from being smooth to stepped, and in one case was a pronounced curve. Bedding plane failure was sometimes seen, though most commonly in Spring Creek samples which had more pronounced bedding. This was dependant on β and tended to occur when β = 0-30°. D seam samples were loaded with β = 20-90° and Main Upper seam samples had β = 0-10° & 90°. β could only be determined in two samples of Strongman D seam and was 20° & 90° while it ranged from 0-90° in the E seam.

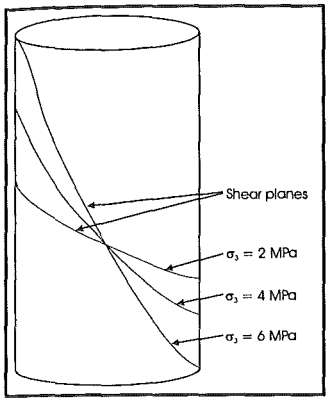

Figure 2.16. Steepening of the shear plane angle in triaxial test specimens as the confining pressure, σ_3, increases.

2.5.4 Cohesion and Friction Angle

The Triaxial test results have been analysed using the 'Rockdata' program (Figure 2.17; Table 2.9), which was used to calculate values for c, ϕ and the Hoek-Brown parameter m_i. The friction angle, ϕ, is very high at low confining pressures, but decreases with increasing confining pressure to give a non-linear failure envelope which is a reflection on the discontinuous structure of coal. The ϕ value was very similar in all seams, with a range of 48.6-51.5° for confining pressures of 2-6 MPa. This is quite high for coal seams around the world, with Abel (1988) suggesting that ϕ usually in the range 25-50° for coal. Mills (1986) reported ϕ = 38° for Huntly coal at confining pressures of 2-8 MPa, which is similar to reported friction angles of 42° (Atkinson and Ko, 1977) and 35° (Wilson, 1980) for U.S coal, with 35° also reported by Atkinson and Ko for some British coals. Indian coals tend to have very high friction angles of 45-67° as reported in Sheorey *et al.* (1989).

Cohesion was higher in the Strongman No. 2 samples than Spring Creek, which is a function of the lower moisture content in Strongman No. 2 samples. Increased moisture lowers the cohesion and friction angles by providing lubrication along weakness planes. Cohesion increases with confining pressure while friction angle falls, though there is no individual relationship between cohesion and friction angle (r^2 = 0.0003).

The values for the Hoek-Brown constant m_i were similar in four seams. In the Spring Creek D and Main Upper seams m_i = 14.6 & 18.3, and for the D and E seams of Strongman No. 2 m_i = 17.1 & 18.4 respectively. The values determined by this study compare well to those quoted by Hoek and Brown (1997) for coal (m_i = 8-21). Hoek and

Brown do note, however, that these are only estimates. Triaxial tests on some Australian coal by Medhurst and Brown (1998) yielded values of m_i lower than this study (≤ 16.7), but they did show a trend of lower values with increasing coal rank. The same trend is found in samples taken from the Spring Creek and Strongman Mines shown graphically is Figure 2.18 ($r^2 = 0.734$; $y = 0.0002x^2$-$0.0118x$+0.762).

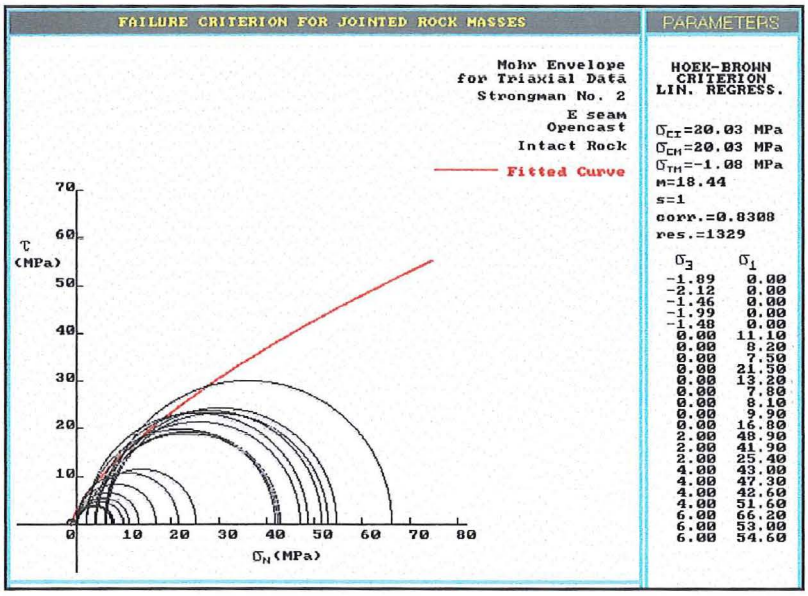

Figure 2.17. Example of Mohr envelope for the Hoek-Brown Criterion of the Strongman No. E seam, developed from triaxial and Brazilian testing. Mohr envelopes for each of the seams tested in this study are presented in Appendix 5, Figures A5.2-A5.9.

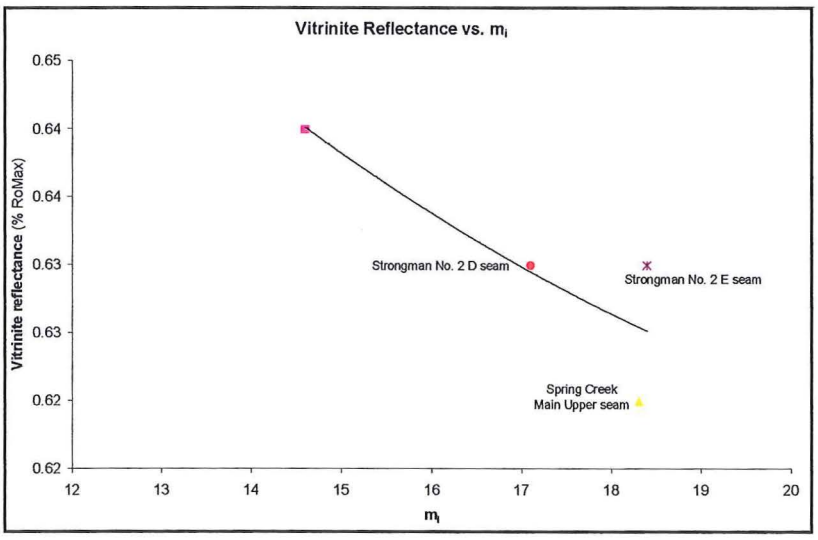

Figure 2.18. Vitrinite reflectance vs. the Hoek-Brown parameter m_i which shows a distinctive increase with decreasing coal rank. Medhurst and Brown (1998) found a similar relationship in some Australian coals

2.6 Brazilian (Indirect Tensile Strength) Test

The Brazilian test was only conducted on the Spring Creek and Strongman No. 2 mine samples where core could be obtained, and it was tested as per the ISRM standard method (Brown, 1981). The test method and apparatus are described in Appendix 6. This test was used primarily to constrain the lower end of the Mohr envelope (Figure 2.17), thereby providing a more accurate estimate of cohesion and friction angle values. The advantage of the Brazilian test is that it generally has a lower standard deviation than the UCS test.

Mean tensile strengths had a tight range of 1.44–1.82 MPa (Table 2.10) over all of the seams tested. Standard deviations are also similar ranging from ± 0.26 to ± 0.43 MPa. The tensile strength showed an increase with UCS (Figure 2.19), though the trend is very weakly confined with $r^2 = 0.164$.

Location	Seam	No. Tests	σ_t (MPa)	Range	Std Dev.	$I_{s(50)}/\sigma_t$
Spring Creek	D	12	1.62	0.68-2.42	0.41	0.35
	Main Upper	12	1.44	0.75-2.93	0.26	0.35
Strongman No. 2	D	8	1.45	0.57-1.98	0.29	0.59
	E/OC	5	1.79	1.46-2.12	0.27	0.28
	E/UG	12	1.82	0.46-2.58	0.43	0.62

Table 2.10. Results of Brazilian (Indirect tensile strength) tests.

Many samples were loaded perpendicular to bedding and failed by one or more vertical cracks. In many of the Strongman No. 2 samples bedding orientation could not be determined as there is no distinctive banding. Moisture contents at the time of testing were 3% for the Strongman No. 2 samples and 7% for Spring Creek. The coefficient of variation was approximately half of that seen in UCS testing ranging from 15-25%. The tensile strength shows a very weak correlation to UCS (Figure 2.19). It does, however, correlate better than point load strength in most cases, but point load strength has the significant advantage of not needing core samples.

The ISRM (1985) suggested method for determining point load strength states that the point load strength is approximately 0.8 times the Brazilian tensile strength for hard rock samples. Values for this study are much lower, with a range of 0.28-0.62 (ave. 0.44). Both seams from the Spring Creek seams have $I_{s(50)}/\sigma_t$ values of 0.35, with the higher values

coming from the Strongman D (0.59) and E/UG seams (0.62). This reflects the UCS/$I_{s(50)}$ relationships where the conversions are also higher in the Strongman No. 2 mine.

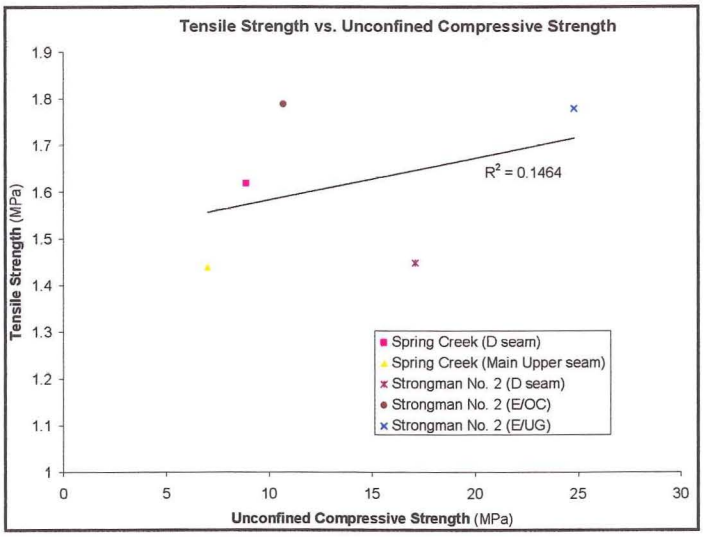

Figure 2.19. Tensile strength vs. unconfined compressive strength. There appears to be a trend between the two but the r^2 value is low at 0.146.

2.7 Shear Strength of Discontinuities

Slip on defects is largely controlled by the shear strength of the discontinuities involved. The shear strength of cleat planes was tested for samples of Strongman No. 2 D and E seam coal by the direct shear method using a portable shear box. Blocks of coal were cut from lump samples for this purpose. Each sample was tested three times, at a different normal load where σ_n = 2.5, 5.0, and 7.5 kN according to the ISRM suggested outlined in Brown (1981). σ_n = 7.5 kN was equivalent to low maximum normal load of 2.4 MPa which is considerably lower than overburden pressure, but because of the weakness of the samples, higher normal loads were not a viable option. The cleats tested were unweathered and had no visible filling of any kind.

Seam	No. Tests	Friction angle ϕ (°)		Cohesion (MPa)		r^2	JRC
		average	range	average	range		
SM/D	5	24.1	18.3-26.6	0.33	0.02-0.48	0.80	8-18
SM/E	5	13.4	11.6-15.9	0.26	0.10-0.43	0.38	4-16

Table 2.11. Summary of values determined by shear strength testing.

The discontinuities being tested showed a large range of roughness, as measured by the joint roughness coefficient (JRC). Cleat planes are rough surfaces which are highly variable. Roughness can cause shear strength to be a directional property (Brady and Brown, 1993), depending on whether the roughness varies in only one direction, or in all directions across the plane being sheared. Roughness varies in all directions across cleat planes, and were always rough in the low rank coals (such as Strongman No. 2 and Spring Creek), though the tend to become smoother as the coal rank increases. A slight increase in shear strength is seen with higher JRC values, but not as much as would be seen in some other rocks types. Because coal is soft, the roughest parts of the defect are more easily sheared off, hence lessening the effects of the roughness. The JRC values ranged from 8-18 for Strongman No. 2 D seam and 4-16 for the E seam. The higher overall JRC values in the D seam would make shearing along the cleat planes more difficult resulting in a higher friction angle. The lower JRC values in the E seam may therefore be partially responsible for the low friction angle of 13.4°.

Friction angle of the specimen is calculated from the slope of the failure envelope as $\phi =$ 24.1° for the D seam ranging from 18.3-26.6° (Figure 2.20). The E seam showed a significantly lower mean friction angle of 13.4° ranging from 11.6-15.9° (Figure A7.2, Appendix 7). The cohesion of the D and E seams was calculated to be 0.33 MPa and 0.26 MPa respectively, with ranges of 0.02-0.48 MPa and 0.10-0.43 MPa.

The peak shear stresses have been plotted against normal stress for the Strongman D seam in Figure 2.20. Five tests were conducted on samples taken from this seam, but only three displayed an increasing shear stress as the normal stress increased. The other two samples (not plotted in Figure 2.20) showed a decreased shear stress as the normal stress increased. Because coal is soft and brittle the roughest parts of the shear surface are easily sheared off resulting in this decreased shear stress. The D seam has the strongest correlation value of the two seams for the plot of τ vs. σ_n with $r^2 = 0.808$, compared to $r^2 = 0.380$ for the E seam.

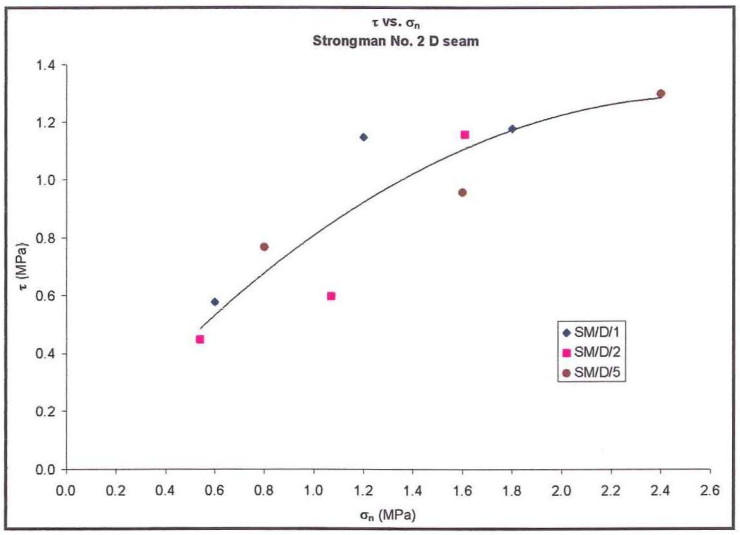

Figure 2.20. Shear stress, τ, vs. normal stress, σ_n, for Strongman No. 2 D seam samples. Discontinuities display a wide range of shear strengths. A similar plot for the E seam in presented in Appendix 7.

The friction angles determined by this study are very similar to those determined by Bell (1993b) for samples of the Kimbell seam at the Roa mine (24°) and the Morgan seam from Mt Watson (25°), so the friction angle appears to be relatively constant across the coalfield, apart from the E seam at Strongman No. 2 which is significantly lower at 13°.

Shear stress along defects increases with increasing dip due to decreases in the normal load. The simplest and most likely scenario is that shearing would occur along or parallel to bedding. Analyses of pillar failure by shearing along bedding or cleat planes are presented in section 4.5.2.

2.8 Synthesis

2.8.1 Compressive Strength of Core Samples

- Cores were very difficult to obtain, so UCS and triaxial strength was only tested for samples from Strongman No. 2 and Spring Creek. All coal is this study can be classified as very weak (1-5 MPa) to weak (5-25 MPa) according to the Hoek and Brown classification (Table 2.3). Average UCS ranges from 7.0 MPa to 24.8 MPa (Table 2.12). Large scatter in results is common for coal with strength variations of

$\pm 100\%$ of the mean from a single seam. There is a weak trend in some seams of lower strength with increasing sample length.

Location	UCS ave. (MPa)	Range	Std Dev	E_{dyn} (GPa)	Poisson's ratio, ν
Spring Creek					
D seam	8.9	5.9 - 17.6	2.97	-	-
Main Upper seam	7.0	3.6 - 13.6	2.68	-	-
Strongman No. 2					
D seam	17.1	0.5 - 31.6	6.85	1.78†	0.42
E seam (UG)	24.8	7.4 - 30.4	3.31	1.96†	0.44
E seam (OC)	10.7	7.5 - 21.5	4.73	-	0.26

Table 2.12. Summary of UCS test results

- Failure mechanism in core samples is dependant on the number and orientation of cleats and the orientation of bedding with respect to the loading direction. Samples which contained more cleats were significantly weaker than those containing fewer defects. Bedding planes are weak, especially in Spring Creek samples, and when these are inclined to the loading direction a significant strength decrease and change in the failure mechanism is observed. Increasing number of cleats resulted in lower strengths and greater variability in the results. Shearing is common when bedding planes are inclined to the loading direction. When bedding is perpendicular, or when there are few cleats in the sample cataclasis tends to dominate. Axial splitting is most common when loading direction is parallel to the loading direction.

- Moisture content was found to have a slight influence of the strength of the samples. Instead of the expected decrease in strength with increasing moisture content (as would occur in most rock types), the strength of the Spring Creek core samples was seen to increase slightly.

- Coal in this study displays U-type anisotropy with strength decreasing to a minimum when $\beta \cong 35^{\circ}$. The anisotropy is considered low when comparing loading parallel and perpendicular to bedding (as in $I_{a(50)}$) but more anisotropy is apparent when then whole range of bedding orientations is considered.

- Young's modulus and Poisson's ratio were generally low and difficult to determine. P and S waves often did not penetrate the coal due to its discontinuous structure and the bedding in the samples from Spring Creek. One value for Young's Modulus was determined from the use of strain gauges to be 2.9 GPa. This is higher than the dynamic Young's Modulus but limited results limit their use.

2.8.2 Compressive Strength of Cube Samples

- Average compressive strength of cube samples is approximately twice that of core samples and ranges from 3.0 (Roa) to 20.0 MPa (Strongman N0. 2 E/OC). Less scatter was present in the cube strength results resulting from the decreased role of bedding in the failure mechanism.

- Samples from the Bishop Block were weathered and subsequently gave unreliable strengths values c. 50% lower than expected. Samples from the Roa mine deformed in a plastic manner without recording a definite peak strength, rather than brittle failure as observed in all other seams which is a reflection on the soft and sheared nature of this coal.

Location	Seam	Mean compressive strength (MPa)	Range	Std Dev.
Bishop Block	Kimbell seam	7.8	4.4-13.7	1.7
	Morgan seam	3.3	1.2-7.0	2.1
Roa	Kimbell seam	3.0	2.4 - 5.8	0.5
Spring Creek	D seam	19.8	12.1 - 38.0	5.0
	Main Upper seam	19.9	13.5 - 32.7	6.2
Strongman No. 2	E seam (OC)	20.0	15.5-35.6	3.8
Terrace	No. 4 seam	13.0	10.2 - 20.4	1.5

Table 2.13. Summary of cube compressive strength test results.

- Cubes from the other seams tended to fail in the same manner as coal pillars whereby one or more corners of the sample were crushed with a central core remaining largely intact. Bedding orientation had little effect on the failure mechanism of cube samples and shows no strength trends, though cleat frequency is still a significant feature.

2.8.3 Triaxial Compressive Strength

- Less scatter and increasing similarity of the results from all seams is seen with increasing confining pressure in the triaxial tests. With increasing confining pressure the mode of failure changes to become dominantly shearing, with the angle of shearing steepening with increased σ_3.

- A tight range of cohesion (1.91-2.78 MPa) and friction angles (48.6-51.5°) were seen in the results of the triaxial testing with no apparent relationship between the two. Cohesion is low and seen to decrease with increasing moisture content. Friction angles are quite high compared to other coal seams around the world.

2.8.4 Point Load, Brazilian and Shear Strength Tests

- Point load tests results, like all others test types, had a large range of values (Table 2.14) which is very significant when applied to the UCS = $x.I_{s(50)}$ relationship where the spread of result becomes even greater. Ambiguous results are expected for point load tests when UCS is <25 MPa. Using the irregular lump method also contributed to the inaccuracies and the spread in the results. Low strength anisotropy was seen in the point load results with $I_{a(50)}$ ranging form 0.86-1.16. It was however difficult tot determine bedding orientation is many of the samples used in this test.

Location	Seam	$I_{s(50)}$ (MPa)	Range	$I_{a(50)}$	σ_t (MPa)	Range	Std Dev.
Bishop Block	Kimbell seam	0.21	0.06-0.42		-	-	-
	Morgan seam	0.17	0.06-0.47	1.01	-	-	-
Roa	Kimbell seam	0.13	0.06-0.23	1.16	-	-	-
Spring Creek	D seam	0.57	0.19-0.99	0.99	1.62	0.68-2.42	0.41
	Main Upper	0.51	0.07-1.10	1.16	1.44	0.75-2.93	0.26
Strongman No. 2	E seam (OC)	0.51	0.22-1.48	1.06	1.79	1.46-2.12	0.27
Terrace	No. 4 seam	0.45	0.07-1.32	0.86	-	-	-

Table 2.14. Summary of point load and Brazilian strength testing

- A tight range of tensile strengths were seen in Brazilian testing (Table 2.14), with little variation between each of the seams. The tensile strength has a low correlation with both unconfined compressive strength and point load strength.

- Friction angle in the Strongman No. 2 D seam (24°) is consistent with previous testing conducted in other seams throughout the Greymouth Coalfield, but the E seam (13°) is substantially lower. A slight increase in the shear strength of coal was seen with increasing joint roughness (JRC). This is only low due to the roughest parts of the sample being easily sheared of due to the soft and brittle nature of the coal.

Chapter 3. Relationship between Coal Strength and other Properties

3.1 Introduction

The Greymouth Coalfield has a very high rank gradient, increasing from high-volatile bituminous C in the west to low-volatile bituminous in the east over a very short distance of c. 10 km (Figure 3.1). Wellman (1952) suggests that the rank increase over 6km in the Greymouth Coalfield is similar to that over 1300km in some parts if the world. When sediments were being deposited in the Greymouth Coalfield the basin was subsiding, with the subsidence becoming increasingly rapid towards the eastern margin of the coalfield. This subjected the coals to increasingly higher temperature and pressure towards the east resulting in this rank gradient. Increasing rank of coal is reported by Jeremic (1985), St George, (1995) and Pashin *et al.* (1999), amongst others, to have a detrimental effect on coal strength. This is due to a number a factors, the most important of which is an increase in cleat frequency and increased softness of the coal with increasing rank. There is also inconclusive evidence that strength is related to the fixed carbon, volatile matter and ash contents of coal. The aim of this chapter is to determine if it is possible to estimate coal strength with a reasonable degree of certainty from each of the coal rank parameters, namely volatile matter, fixed carbon, and vitrinite reflectance.

A significant step forward in coal strength determination for the Greymouth Coalfield developed by this study is an equation estimating the unconfined compressive strength using more input parameters than just the point load strength. This method was alluded to in Chapter Two and is presented in section 3.6. This method relates the unconfined compressive strength of core and cubes to the point load strength to more accurately determine a UCS strength value where no core samples can be obtained. By using this method the important $UCS/I_{s(50)}$ relationship can be determined for areas where it could otherwise only be estimated.

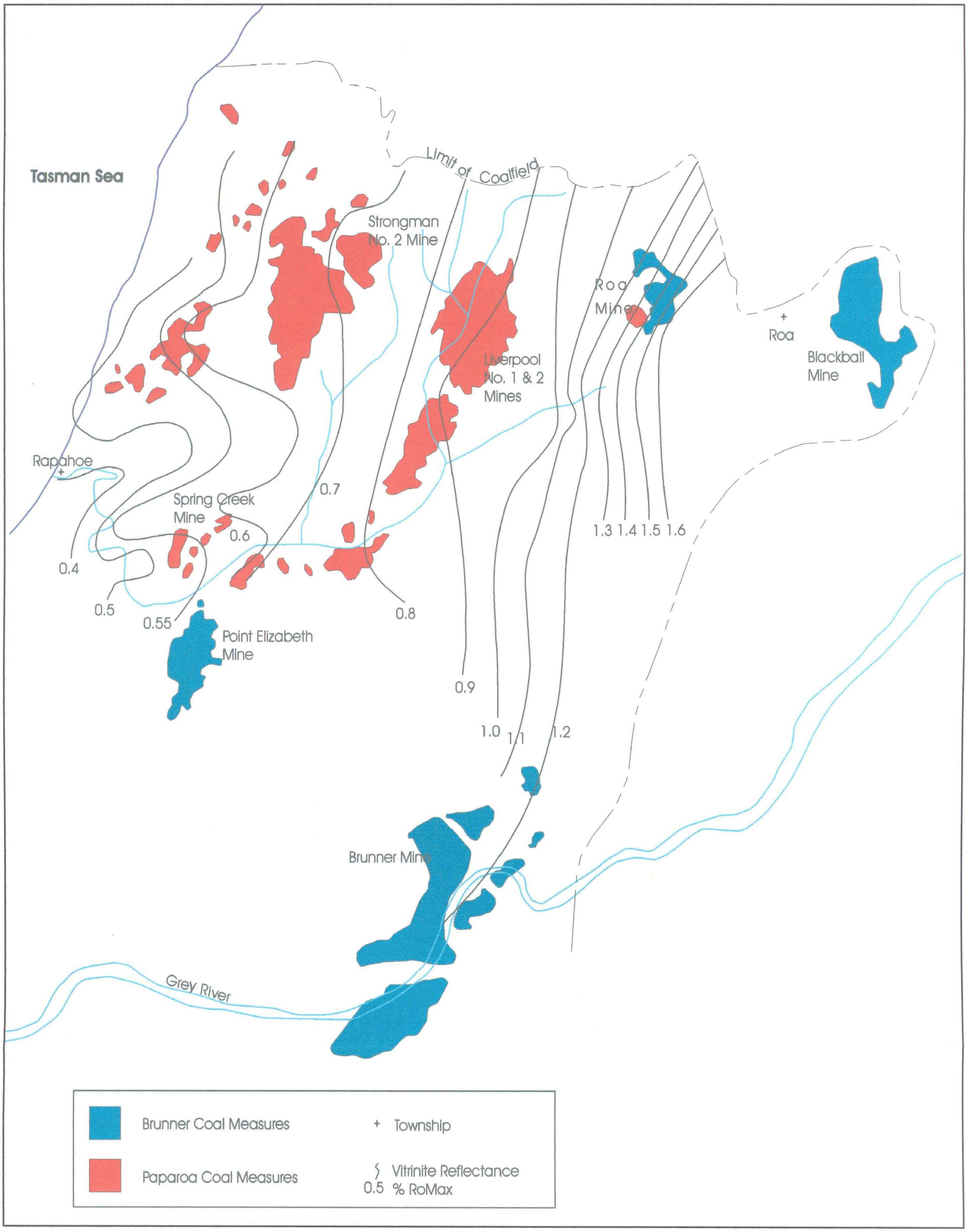

Figure 3.1. Vitrinite reflectance trend across the Greymouth Coalfield. Base map modified from map provided by Solid Energy International Ltd. Vitrinite reflectance data from Bowman *et al.* (1984, Part 1, Plan 45).

Outcrop samples of coal from the Bishop Block was sufficiently weathered that the cube compressive strength (CCS) values recorded as sufficiently different than that which would be expected in unweathered samples. This strength reduction was largely due to clay infilling of some cleat planes within the samples. The UCS strengths to be used in this chapter have been estimated from Richards (2000; unless otherwise stated) who gives UCS for the Kimbell seam as 8 MPa. A UCS value for the Morgan seam was not reported by Richards, but is estimated here to be c. 7 MPa given the slightly lower strength tests results found in this study (Section 2.3.2).

Four different methods of representing coal strength are given in this chapter. To avoid any confusion each method has been defined as follows:

UCS = Unconfined compressive strength (MPa) determined on 54mm (NX) diameter core (section 2.2).

CCS = Cube compressive strength (MPa) of 63.5mm coal cubes (section 2.3).

$UCS_{equivalent}$ = A value of UCS determined indirectly by using equations, but not directly from strength testing.

$I_{s(50)}$ = Average point load strength of a particular seam (MPa; section 2.4).

3.2 Relationship between Coal Strength and Coal Rank

3.2.1 Rank Variation in the Greymouth Coalfield

Coal rank is a measure of the degree of alteration (metamorphism) that the organic material has undergone. The alteration process is termed coalification and results in the coal undergoing various physical and chemical changes. These changes are governed primarily by increasing temperature, time and pressure which inhibits chemical reactions. Changes include decreases in moisture, volatile matter, hydrogen and oxygen content and increases in vitrinite reflectance, carbon content and specific energy. The properties from which coal rank can be estimated are given in Table 3.1. Although temperature is very important in the coalification process, most coals have been exposed to temperatures less than 200°C (Gillard and Moore, 1999). Coal rank is affected by age, temperature, depth of

burial and the tectonics of the basin. Because of the large number of influences, coal rank cannot be precisely determined and no one method is a completely reliable (J. Newman, 1985; Quick, 1992).

Coal rank can be estimated by a large number of methods with vitrinite reflectance being the most commonly quoted value, owing to the fact that chemical and optical properties of vitrinite alter more uniformly during coalification than those of the other maceral groups (Stach *et al.*, 1982). Vitrinite reflectance is a particularly good indictor of coal rank above medium-volatile bituminous, but can be used over the entire range of this study as shown in Table 3.1. Other parameters including volatile matter, moisture and ash contents are all indicative of the degree of alteration.

Table 3.1 shows the moisture content has become relatively constant and has little influence in the range of this study, apart from the range of the Terrace Mine (RoMax = 0.48%) where the moisture content is high. A consistent decrease in volatile matter and corresponding increase in carbon content are useful rank indicators, though volatile matter is also controlled by coal type. The changing chemical structure of the coal as volatile matter is released is thought to be responsible for the increasingly plastic behaviour of the coal (section 2.2.7) as coalification progresses (N. Newman, pers. comm.).

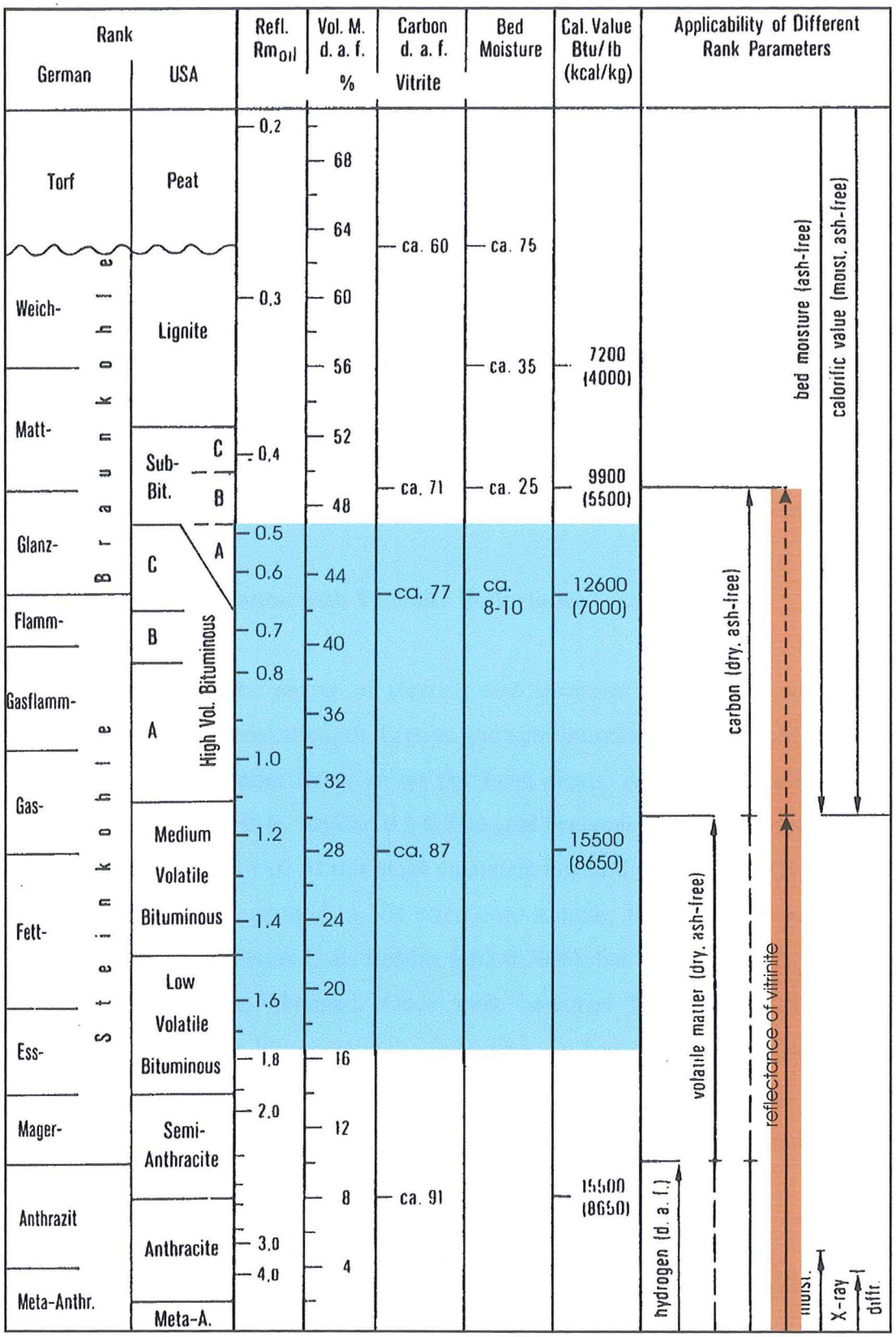

Table 3.1. Coal classification according to the German (DIN) and North American (ASTM) terminology (after Stach *et al.*, 1982). Blue shaded area shows the range of coal ranks covered by this study. Red shaded area shows the effective range of the vitrinite maceral as an indicator of coal rank.

Because the coals in the Greymouth Coalfield are relatively young, very high rank coals (e.g. anthracite) are absent, as they are for the majority of New Zealand coalfields. Figure 3.1 gives the general trend of the rank gradient across the coalfield, which increases sharply in the east near Roa. This is partially due to the coalification jump which occurs at 1.25% vitrinite reflectance (medium-volatile bituminous), where loss of volatile matter from the inertinite group causes a transformation to vitrinite. The gradient based on vitrinite reflectance values is prone to local variation due to differences in coal type influencing the measured reflectance value (Newman and Newman, 1992) where coal type is largely dependant maceral characteristics and volatile matter content. The rank of the D and Main Upper seams of the Spring Creek Mine, for example, give higher vitrinite reflectance values than would be predicted from Figure 3.1 given the location, though still accurate, due to different vitrinite types present in this area (J. Newman, pers. comm.).

3.2.2 Coal Strength Variation with Vitrinite Reflectance

As coal rank increases, the degree of cleating also increases (Figure 3.2) which has a detrimental effect on the coal strength. Lignite and sub-bituminous coals (RoMax c. 0.27-0.55%) are deformable under stress so do not form cleats. As rank increases to high-volatile bituminous C and B (c. RoMax 0.5-0.8%) coal becomes more brittle and cleats are formed to accommodate stress. At this stage cleats are few and well defined (N. Newman, pers. comm.). Cleats are common in NX sized core samples from the Strongman No. 2 Mine (high-volatile bituminous C-B; RoMax 0.63-0.70%), but samples which contain no cleats can sometimes be obtained. Once rank becomes higher still (high-volatile bituminous A–low-volatile bituminous) the fracturing can become so intense that the coal becomes friable, such as that from the Kimbell seam of the Roa Mine (RoMax c. 1.76%). This coal, however, is affected by shearing induced by the Roa-Mt Buckley Fault zone.

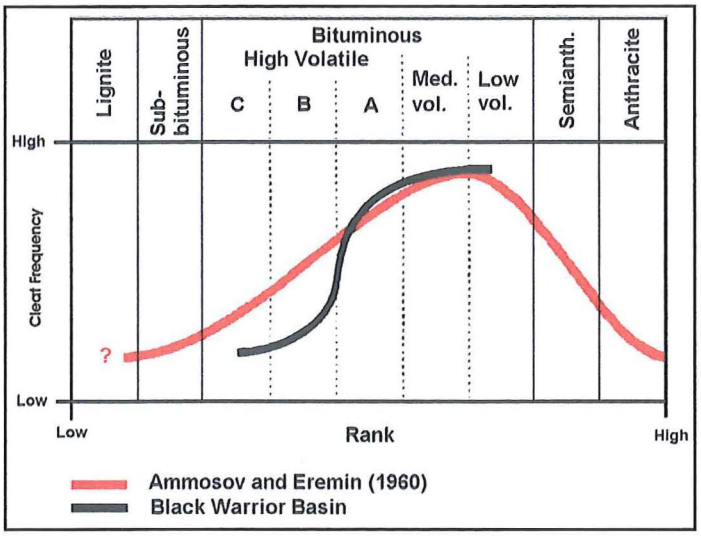

Figure 3.2. Relationship of cleat frequency to coal rank (after Pashin *et al.*, 1999). Cleat frequency is highest at medium-low volatile bituminous rank, then declines as the rank increases further.

There is a strong trend of decreasing coal strength with increasing rank in the Greymouth Coalfield, which is shown graphically in Figures 3.3a and b. As rank increases from c. 0.60% vitrinite reflectance (sub-bituminous A/high-volatile bituminous C) in the west of the coalfield, to a maximum of c. 1.80% (low-volatile bituminous) in the east there is a corresponding large drop in point load and unconfined compressive strengths. UCS drops from a maximum of 24.8 MPa (0.64% RoMax) to 1.3 MPa (1.76% RoMax) in the highest rank coal corresponding to a 2.1 MPa drop in unconfined compressive strength for each 0.1% increase in vitrinite reflectance. The trend is however weakly constrained at low vitrinite reflectance values (0.62-0.65%).

Point load strength shows a similar trend to UCS and is less variable at low rank, but is more variable throughout the middle rank values (RoMax 0.87-1.20%) where there is a large amount of variability introduced by the Bishop Block and Mt Watson values. This is especially true of the value for the Kimbell seam reported in Richards (2000) which plots significantly above the values determined by this study. This is likely due to the weathering of the point load samples of this study, whereas those of Richards were taken from drill core so weathering would not have been a factor.

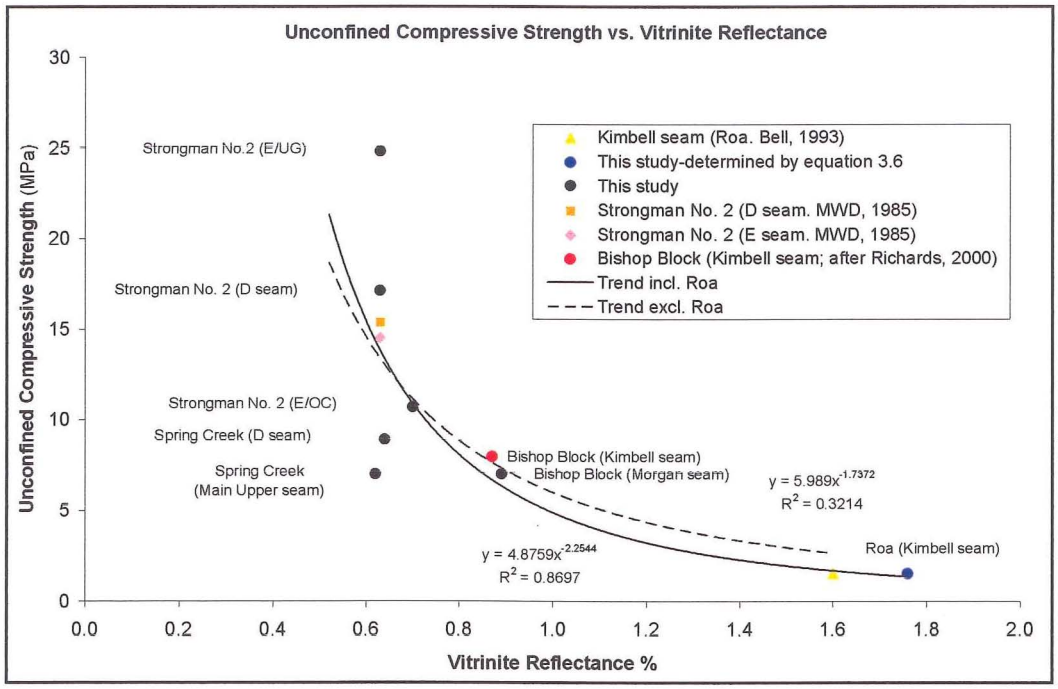

A)

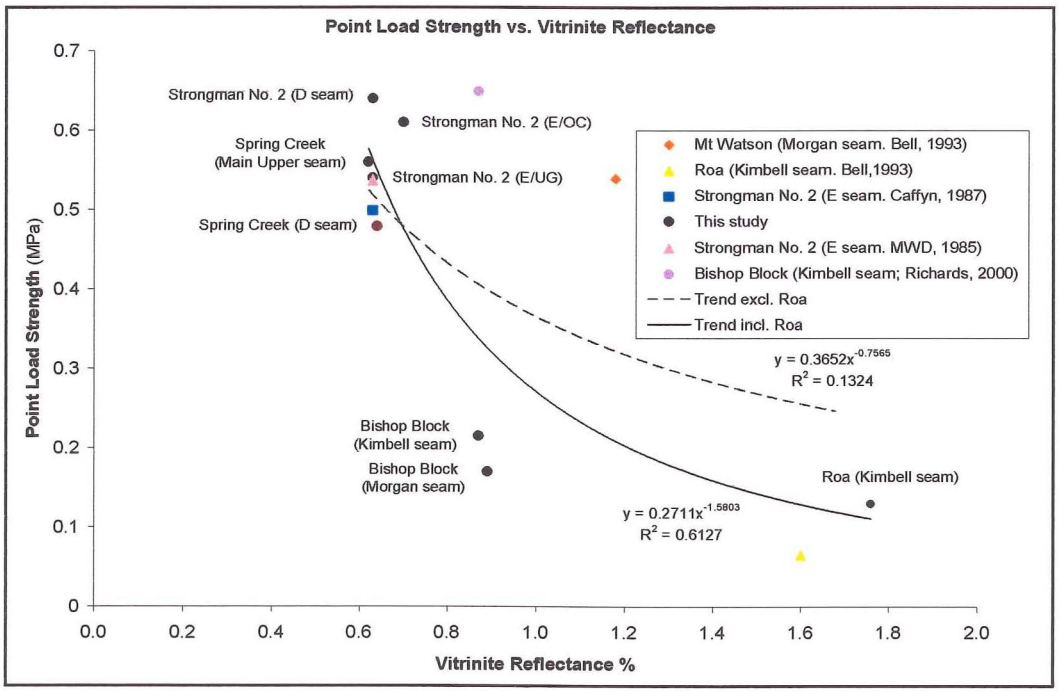

B)

Figure 3.3. Plots of coal strength vs. vitrinite reflectance. A) Unconfined compressive strength vs. vitrinite reflectance. UCS value for the Roa Mine estimated from equation 3.13. B) Point load strength vs. vitrinite reflectance. The Terrace mine coal has not been included in these diagrams as it is from a separate coalfield, and thus subject to a different set of formation and stress conditions.

In both plots the Roa mine appears to be an outlying point constraining the trendline which would otherwise show less of a trend. When trendlines are plotted both including and excluding the Roa data point for the plot of UCS vs. vitrinite reflectance, the trendlines are both very similar. The trend inclusive of Roa (solid line) has a substantially higher r^2 value of 0.870 compared to $r^2 = 0.321$ for the trendline excluding (dashed line) the Roa Mine. The two trendlines are described by the following relationships:

Including Roa: $y = 4.8759x^{-2.2544}$ $(r^2 = 0.870)$ (3.1)

Excluding Roa: $y = 5.989x^{-1.7372}$ $(r^2 = 0.321)$ (3.2)

In the plot of point load strength vs. vitrinite reflectance (Figure 3.3b) the Roa Mine again appears to be the outlying irregular data point. Plotting the trendlines including (solid line) and excluding (dashed line) Roa shows significantly different relationships in this case. The dashed line ($r^2 = 0.132$) becomes largely constrained by the data points of the Strongman No. 2 and Spring Creek mines with the Bishop Block plotting a long way from the trendline. The trend inclusive of the Roa mine gives a much higher r^2 value of 0.613 and is more encompassing of the data points, especially the Bishop Block.

Including Roa: $y = 0.2711x^{-1.5803}$ $(r^2 = 0.613)$ (3.3)

Excluding Roa: $y = 0.3652x^{-0.7565}$ $(r^2 = 0.132)$ (3.4)

While there is a definite trend of decreasing strength with increasing coal rank, the relationship is at times not well constrained as seen in Figure 3.3a. Large variations in strength are commonplace when the rank is low. There are not enough results for vitrinite reflectance of 0.9-1.6%, and therefore this cannot be used as an accurate predictor of compressive strength. The r^2 value is significantly higher for UCS than point load strength, with values of 0.870 and 0.624 respectively. With this relatively high correlation value it is thought to be reasonably accurate to estimate compressive strength from equation 3.1 (except at low rank) derived from Figure 3.3a.

The Terrace Mine has been excluded from Figures 3.3a and b because it is from a different coalfield to the rest of the data. While the trends of decreasing coal strength with increasing rank seen in these plots are recognised worldwide across individual coalfields, they do not necessarily transfer between coalfields, as all coalfield are of different ages and formed under different conditions. The rank of coal from the Terrace Mine (RoMax 0.48%) is significantly lower than any other coal from this study and so based on the trends seen in Figures 3.3a and b would be expected to have significantly higher strengths. However, the strength of the No. 4 seam is substantially lower. The Reefton Coalfield, in which the Terrace Mine is located, shows a west-east rank gradient (with a much smaller change than the Greymouth Coalfield) which extends into the neighbouring Garvey Creek Coalfield (location shown in Figure 1.2). Coal rank increases from high-volatile bituminous C in the Reefton Coalfield to high-volatile bituminous A in the Garvey Creek Coalfield (Barry *et al.*, 1994). These coalfields would therefore be expected to show a strength trend similar, but independent, to that of the Greymouth Coalfield. Investigation of the trend for the Reefton and Garvey Creeks Coalfields is beyond the scope of this study.

There are a number of reasons for this drop in strength. One reason, and possibly the most important, is the increased presence of cleats as rank increases (Figure 3.2). Cleats begin to form with the onset of bituminous rank because of the changing coal properties. Three types of cleats are formed; 1) endogenous cleavage, 2) exogenic cleavage, and 3) induced cleavage (related to mining activity). Cleats reach a maximum abundance when rank reaches low-volatile bituminous (Pashin *et al.*, 1999), which is equal to the rank of Roa coal. Cleat frequency then declines through semi-anthracite to anthracite.

Endogenous cleavage forms perpendicular to bedding planes as the result of shrinkage due to moisture loss as the material is buried and compacted, and with the release of volatile matter. Exogenic cleavage results from external tectonic forces and is dependant on the tectonic history of the coal. Induced cleavage originates during mining activities with redistribution of the stress regime to areas of increased load and of stress release.

The development of cleats is obvious when looking at coals of differing rank sampled in this study. Some cleats were present in Terrace coal (sub-volatile bituminous; RoMax 0.48%) but these are relatively faint and widely spaced. In Spring Creek coal the cleats became more prominent and greater in number. Strongman No. 2 samples tended to have larger open cleats which were widely spaced (30-70mm), though for samples of E/OC the cleats were not as open and spaced 5-40mm apart. Although the Strongman No. 2 samples were more cleated and of marginally higher rank, they were still stronger than those samples taken from Spring Creek. Coal from the Bishop Block is extensively cleated, with spacings of 5-10mm. Coal from the Roa Mine is extensively cleated and friable.

Cleats are always best developed in the bright parts of bituminous coal, and are less distinct, more widely spaced, or even non-apparent in durain (Evans and Pomeroy, 1966). In coal from the Greymouth Coalfield, cleats in the bright and dull parts of the coal often had different orientations. This was especially so in Bishop Block samples, where cleats in durain bands would form parallel to bedding while cleats in vitrain were predominantly perpendicular to bedding.

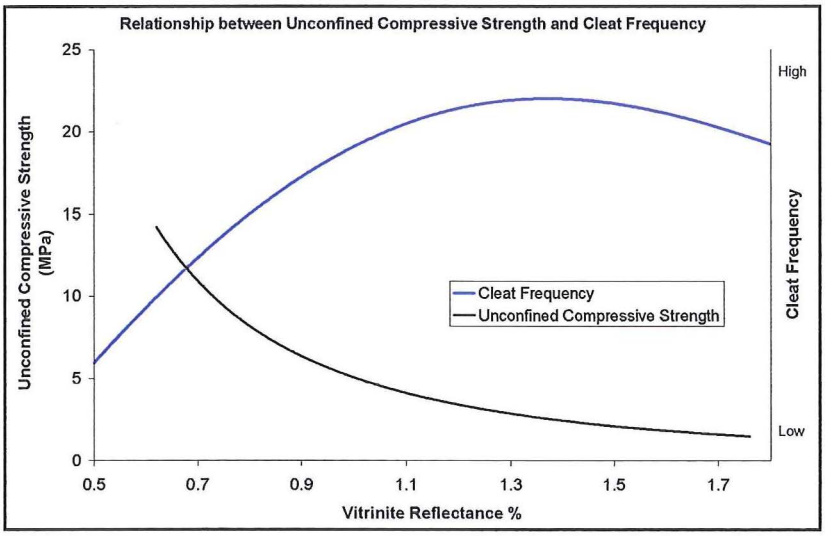

Figure 3.4. Relationship between unconfined compressive strength and cleat frequency. Cleat frequency curve modified after Ammosov and Eremin (1960).

By superimposing Figure 3.2 on Figure 3.3a the true relationship between unconfined compressive strength and cleat frequency can be seen (Figure 3.4). Coal strength decreases rapidly until cleat frequency reaches a maximum when vitrinite reflectance is c. 1.4%.

Though cleat frequency declines from vitrinite reflectance of 1.4% onwards, coal strength does not begin to increase again. Instead the strength drop is more gradual owing to the changing chemical structure making the coal softer and more brittle.

3.2.3 Unconfined Compressive Strength and Coal Constituents

3.2.3.1 Fixed Carbon Content

Carbon content increases slowly with increasing coal rank due to volatile matter and moisture being driven off during the chemical reactions that the carbonaceous matter undergoes during increased coalification, and correspondingly there is an associated steady decrease in coal strength as shown in Figure 3.5. The range of fixed carbon contents for each seam is summarised in Table 3.2. Coal strength is a maximum (24.8 MPa) with the low carbon content of 54% in the E/UG seam. Coal strength then shows a rapid decrease as the carbon content steadily increases. Coal strength is lowest in the Roa Mine (1.32 MPa) when the carbon content is highest (78.2%). The range of carbon contents within each seam is low, usually from 1 to 2%. The decrease in coal strength becomes slower, but still significant as carbon increases. R^2 at 0.894 is very high for this trend which can be described by equation 3.5.

$$UCS_{equivalent} = 4\times10^{11}x^{-6.04} \qquad (3.5)$$

where: x = carbon content (%)

Location	Seam	Ash (%)		Volatile Matter (%)		Fixed Carbon (%)	
		Average	Range	Average	Range	Average	Range
Bishop Block	Kimbell	1.77	1.0-3.1	35.9	34.2-38.4	58.9	58.2-59.8
	Morgan	1.94	1.8-2.2	37.9	37.8-38.0	58.2	57.7-58.7
Roa	Kimbell	1.94	1.2-3.3	19.1	18.8-19.3	78.2	77.0-79.3
Spring Creek	D	1.16	0.9-1.8	38.7	37.9-39.4	55.8	55.1-56.4
	Main Upper	1.82	1.3-2.2	40.9	40.2-41.6	53.6	53.1-54.0
Strongman No. 2	D	2.2	-	41.0	-	54.0	-
	E/OC	1.65	1.0-2.1	39.7	39.1-40.8	55.9	55.0-56.9
	E/UG	2.2	-	41.0	-	54.0	-

Table 3.2. Ash, volatile matter and fixed carbon contents of each seam.

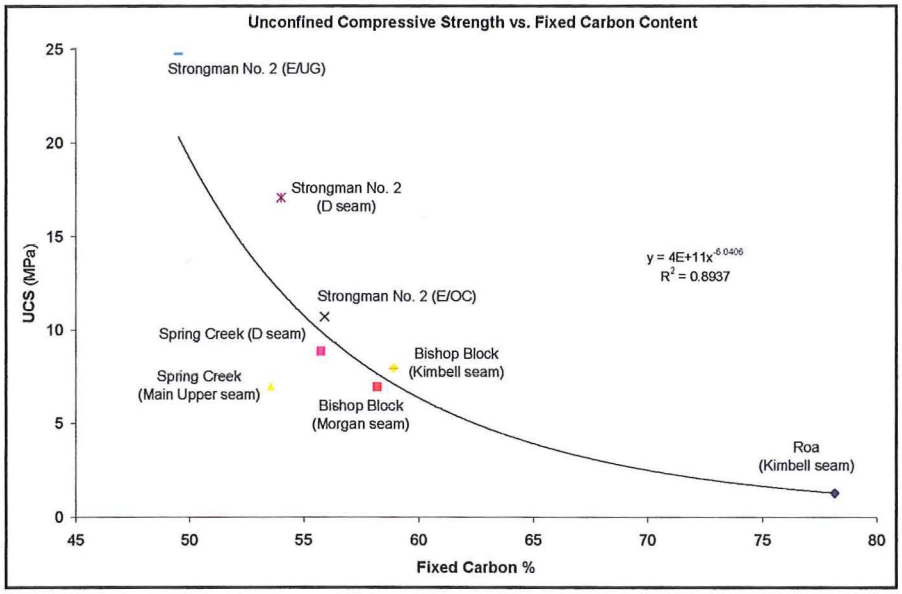

Figure 3.5. Plot of unconfined compressive strength vs. fixed carbon content for each seam studied. UCS value for the Roa Mine estimated from equation 3.13.

3.2.3.2 Ash Content

Unlike carbon and volatile matter, ash content is not affected by increasing coalification, and subsequently this is the only property which is independent of the effect of cleats. Samples with ash contents ranging from 1.16-2.20% (Table 3.2), and unconfined compressive strengths of 1.3-24.8 MPa, were tested in this study. The spread in ash contents of individual seams is low ranging from 0.4% in the Morgan seam to 2.1% in the Kimbell seam for both the Bishop Block and Roa Mine. The ash content of coal has been demonstrated by some authors, including Szwilski (1987), to have an effect on its strength properties. The difference between the samples with the highest and lowest compressive strengths comes about with only a 1% increase in the ash content (Figure 3.6). The correlation coefficient, r^2, between ash content and coal strength is low at 0.200. Strongman No. 2 E/UG and Roa Mines are outlying points in Figure 3.6, but all of the other seams plot relatively close to the trendline. A $UCS_{equivalent}$ strength can be estimated from Figure 3.6 by the following equation:

$$UCS_{equivalent} = 9.65x - 7.11 \qquad (3.6)$$

where: x = ash content (%)

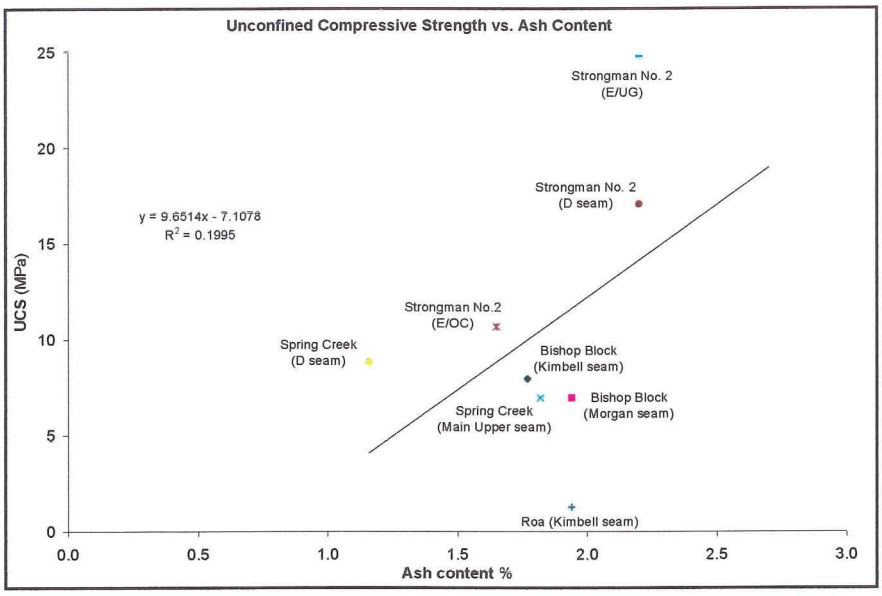

Figure 3.6. Unconfined compressive strength vs. ash content. UCS value for the Roa Mine estimated from equation 3.13.

3.2.3.3 Volatile Matter

The amount of volatile matter in coal decreases steadily with increasing rank as the result of volatile matter being driven off during the chemical reactions occurring during coalification. The variations in volatile matter seen in the coals of this study were not large compared to those of the unconfined compressive strength, but a definite decrease in UCS can be seen as the volatile matter decreases (Figure 3.7). Volatile matter has a maximum range within seams of 4% (Bishop Block Kimbell seam), but is usually only 1.5% (Table 3.2). Coal strength shows a steady almost linear increase with increasing volatile matter, from 1.3 MPa in the Roa Mine (volatile matter = 19.1%) to 24.8 MPa for the Strongman No. 2 E/UG seam where volatile matter is 41%. This trend has also been reported by Ghose *et al.* (1964). The release of volatile matter causes the coal to shrink and thus is a partial cause of cleat formation, which in turns causes a drop in strength giving the relationship in Figure 3.7. The r^2 of the trendline shown in Figure 3.7 value is high at 0.800 and can be described by equation 3.7. The Strongman No. 2 E/UG seam is an outlying point in this plot which reduces the r^2 value. This is due to the strength of the E/UG seam being overestimated in the strength testing program (section 2.2.2). Many of the E/UG samples were free of defects which led to them having very high strengths. The actual strength is estimated to be much closed to that of the Strongman No. 2 D seam as

shown by the Ministry of Works and Development (1985), who reported that the D seam is c. 1 MPa stronger than the E seam.

$$UCS_{equivalent} = 0.0002x^{2.976} \quad (3.7)$$

where: x = volatile matter content

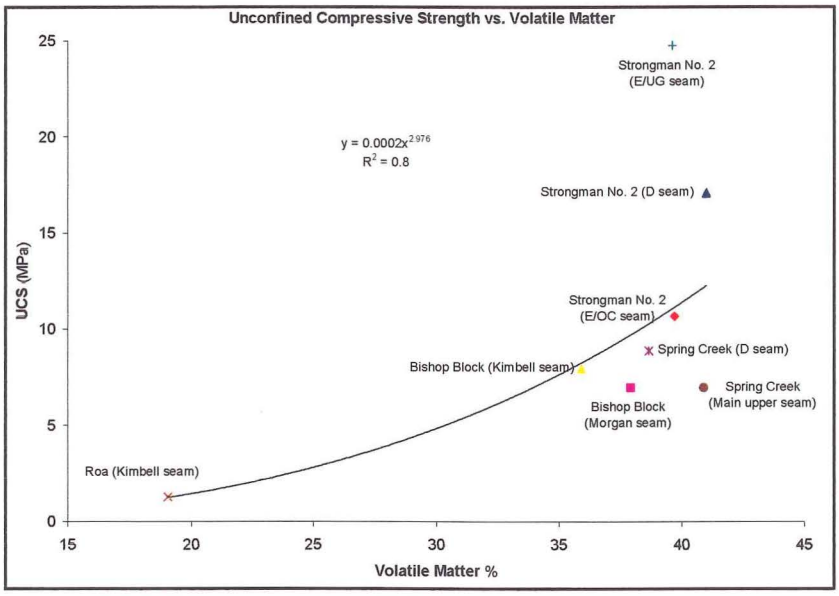

Figure 3.7. Unconfined compressive strength vs. Volatile matter. UCS value for the Roa Mine estimated from equation 3.13.

3.3 Relationship between UCS and Point Load Strength

3.3.1 Introduction and Background

UCS vs. $I_{s(50)}$ relationships were only determined directly from testing for each of the two seams studied at the Spring Creek and Strongman No. 2 Mines. This was done to establish any deviation from the standard relationship developed by Broch and Franklin (1972) where UCS = 24.$I_{s(50)}$. This multiplier is known to vary widely in all rock types between 9 and 45 (Anderson, 2001; Chapple, 1998). Caffyn (1987) reported that multiplier for coal varies across the Greymouth Coalfield from seam to seam, so establishing a value that is unique to each seam studied is quite important. Point load testing can then be used as a

cheap and easy alternative to UCS testing for determining the unconfined compressive strength.

The original work on this correlation was conducted by D'Andrea *et al.* (1965) who conducted compressive strength tests on nineteen different rock types. The results were plotted against eight other rock properties including point load strength, Young's modulus and Poisson's ratio to determine which parameters could accurately predict compressive strength. D'Andrea *et al.* conclude that only point load strength could alone be used as an accurate compressive strength prediction. D'Andrea reported UCS = $16.I_{s(50)}$ using 25mm point load samples.

Broch and Franklin (1972) continued the work of D'Andrea *et al.* by conducting uniaxial compressive strength and point load tests on ten different rock types using 38mm core. The results of the point load tests were corrected to give a reference diameter of 50mm. However, the same correction was not applied to the UCS tests, which is shown to be significant by Bieniawski (1975) who tested three different core diameters resulting in significantly different results for each. The multiplier in 42mm diameter core is reported as 21, compared to 18 for 21.5mm core.

Using 54mm core Bieniawski, combined with the results of D'Andrea *et. al.* and Broch and Franklin, determined that UCS is equivalent to 23.5 (rounded to 24) times the point load strength. Broch and Franklin proposed the point load test replace the unconfined compressive strength test as a means of classifying rocks. One of their reasons for this is less scatter shown in point load test results than the corresponding compressive strength tests. This is not supported by Bieniawski (1975) or by this study. The average coefficients of variation for point load tests conducted on samples from the Spring Creek D seam were 50% compared to 35% for UCS, which is still high, but reflective of coals discontinuous nature. However, point load tests can be useful and convenient if some UCS tests have been conducted for correlation, especially if limited samples are available.

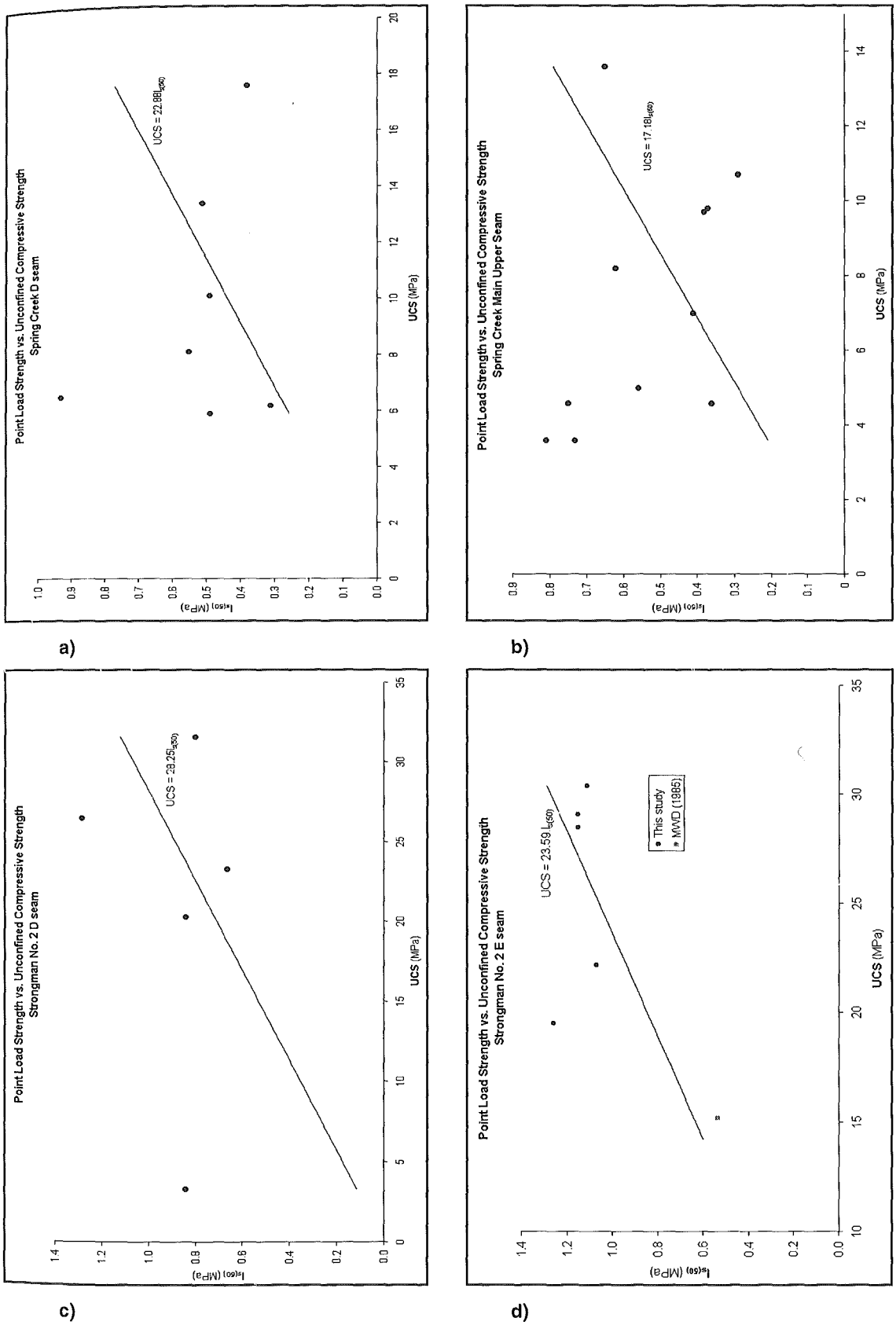

Figure 3.8. Plots of point load strength vs. UCS. a) Spring Creek D seam; b) Spring Creek Main Upper seam; c) Strongman No. 2 D seam; d) Strongman No. 2 E seam. These plots show a great deal of variation of both point load and UCS strengths.

3.3.2 Results and Discussion

The $UCS/I_{s(50)}$ ratio of the Spring Creek D and Strongman E seams have similar ratios of 22.88 and 23.59 respectively (Table 3.3). The Main Upper and Strongman D seams are significantly different with ratios of 17.18 and 28.25. Plots of point load strength vs. UCS are presented for each of the four seams in Figure 3.8a-d. The Spring Creek Main Upper seam has the most variable results of the four seams. It has a low range of UCS values, but the corresponding range of point load strengths is very high (Figure 3.8b), but all seams show large variations. Only the Strongman E seam gave a positive r^2 value which was also low (0.22) meaning that all of these multipliers are unreliable. These $UCS/I_{s(50)}$ ratios therefore should not be used. In general the D seams of both the Spring Creek and Strongman No. 2 D seams show reasonable trends. However, in both plots there is one data point which plots a long way from the trendline which decrease the r^2 values significantly.

Location	Seam	$UCS/I_{s(50)}$ ratio	r^2
Spring Creek	D seam	22.88	-1.47
	Main Upper	17.18	-2.46
Strongman No. 2	D seam	28.25	-2.59
	E seam (UG)	23.59	0.219

Table 3.3. $UCS/I_{s(50)}$ ratio, as determined from cores, of Spring Creek and Strongman No. 2 samples.

When the results of point load strength vs. unconfined compressive strength are plotted for the Spring Creek D and Main Upper seams along with the Strongman No. 2 D and E seams, the equation of the trendline is given as $UCS = 23.9.I_{s(50)}$ (Figure 3.9). Significant scatter can be seen in this plot especially at low compressive strengths, where Hoek and Brown warn that point load strength results are likely to be ambiguous. Due to this scatter Figure 3.9 has a negative r^2 value of -0.266, making the plot somewhat meaningless.

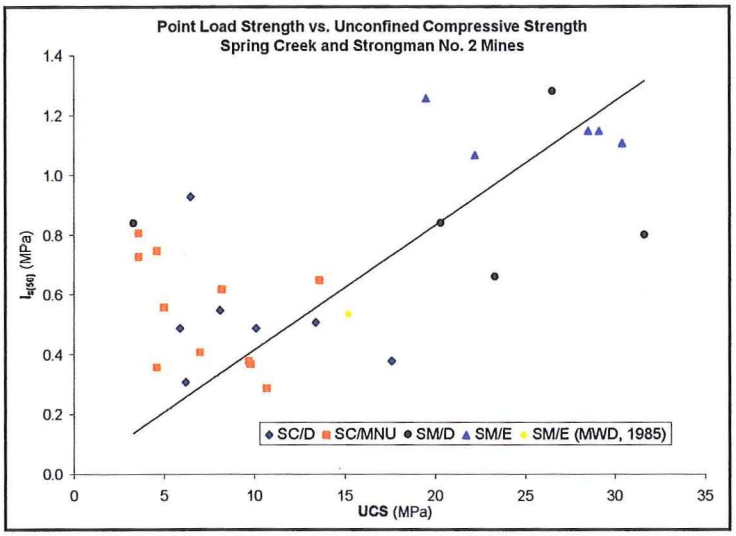

Figure 3.9. Point load strength vs. unconfined compressive strength for Spring Creek and Strongman No. 2 Mines. When all results are plotted together the relationship is equal to that determined by Bieniawski (1975). † Ministry of Works and Development UCS value corrected to L/D ratio of 2.0 using equation 2.1.

3.4 Relationship between CCS and Point Load Strength

The ratio of cube compressive strength to point load strength has been determined for all seams (other than Strongman No. 2 D seam). The results of this are summarised in Table 3.4. The values of the $CCS/I_{s(50)}$ ratio range from 27.62 for the Morgan seam, to 46.08 for the Main Upper seam. As with the $UCS/I_{s(50)}$ ratio the trends are very weak with the Spring Creek D seam and the Morgan seam recording the only positive r^2 values (0.33 and 0.83 respectively).

Location	Seam	$CCS/I_{s(50)}$	r^2
Bishop Block	Kimbell	42.74	-1.89
	Morgan	34.48	0.83
Roa	Kimbell	27.70	-4.28
Spring Creek	D	37.45	0.33
	Main Upper	46.08	-0.87
Strongman No. 2	E (Opencast)	42.00	-0.57
Terrace	No. 4	33.11	-0.29

Table 3.4. Summary of $CCS/I_{s(50)}$ ratios

Each seam shows a much lower spread in the results of cube samples than for UCS cores as shown by Figures 3.10a-g. The results for most seams other than the Bishop Block plot close to the trendline other than one or two data points. The Bishop Block samples show the largest spread of results which is related to the weathering.

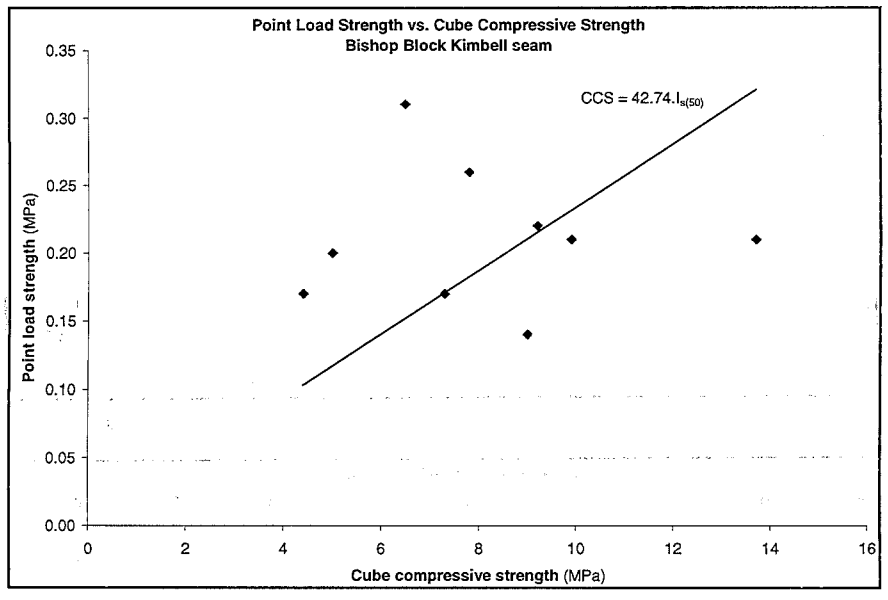

a)

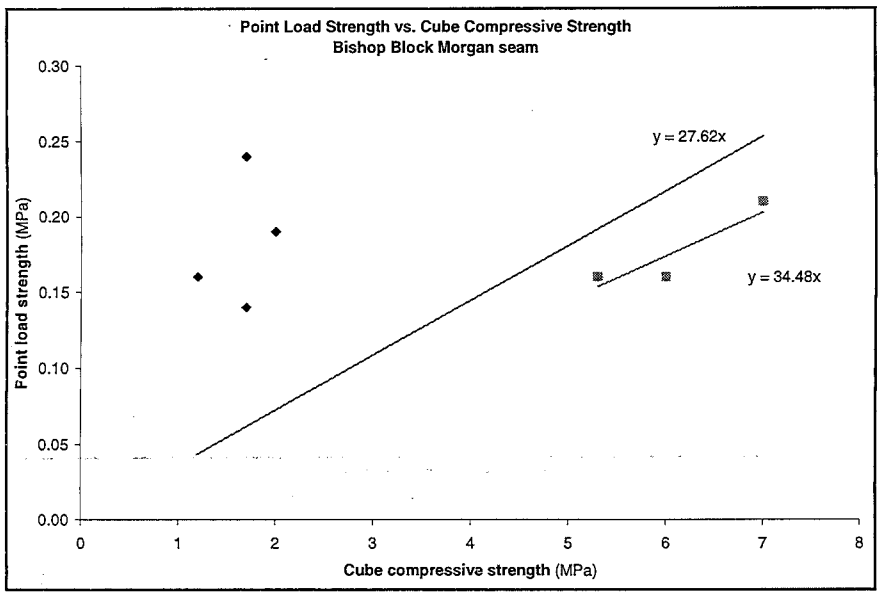

b)

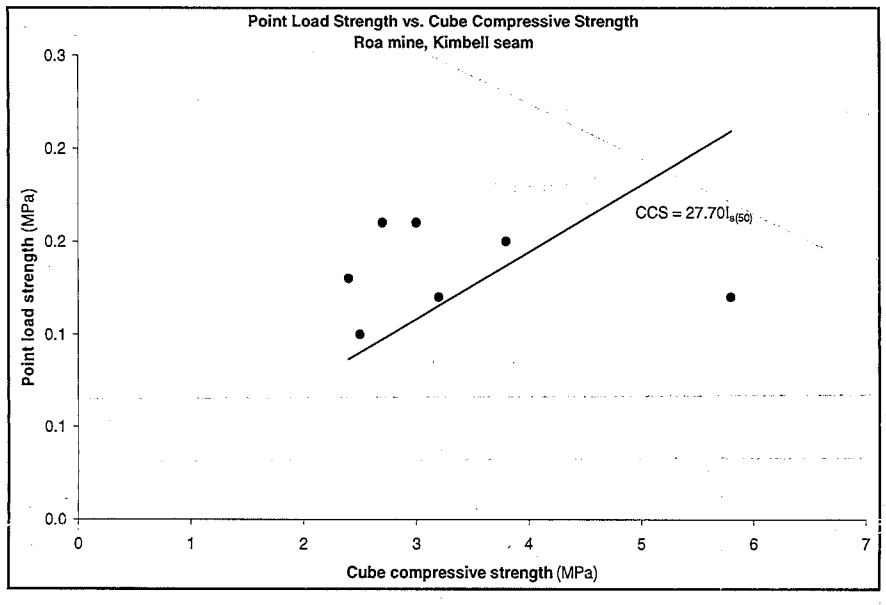

c)

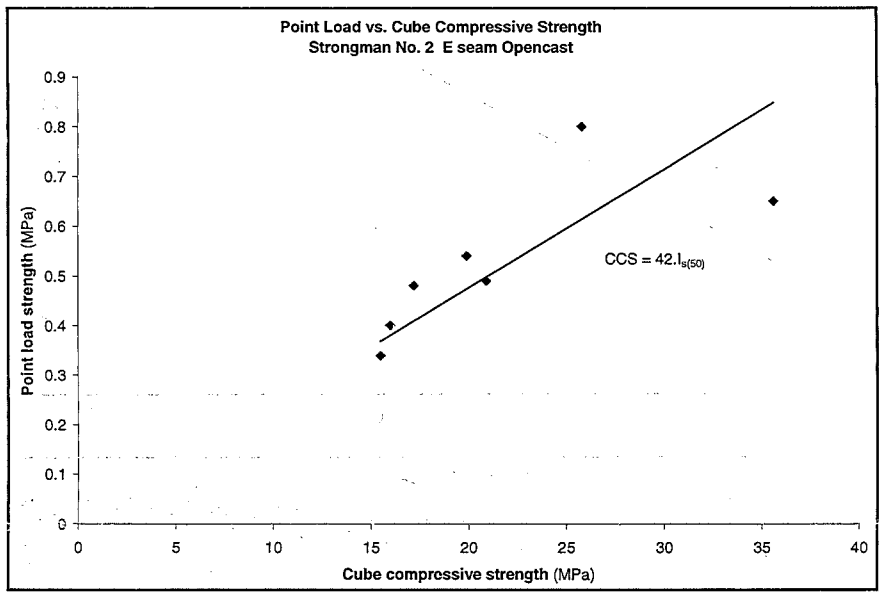

d)

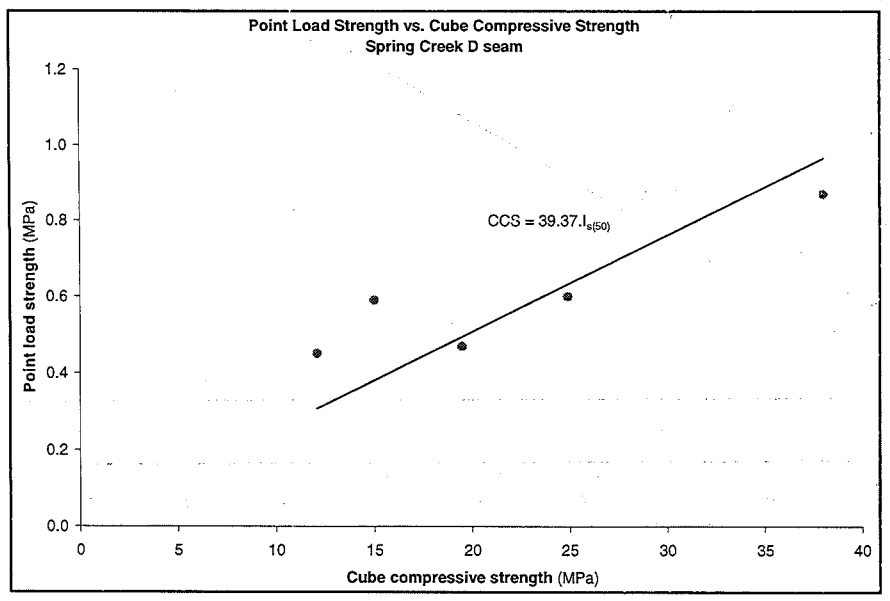

e)

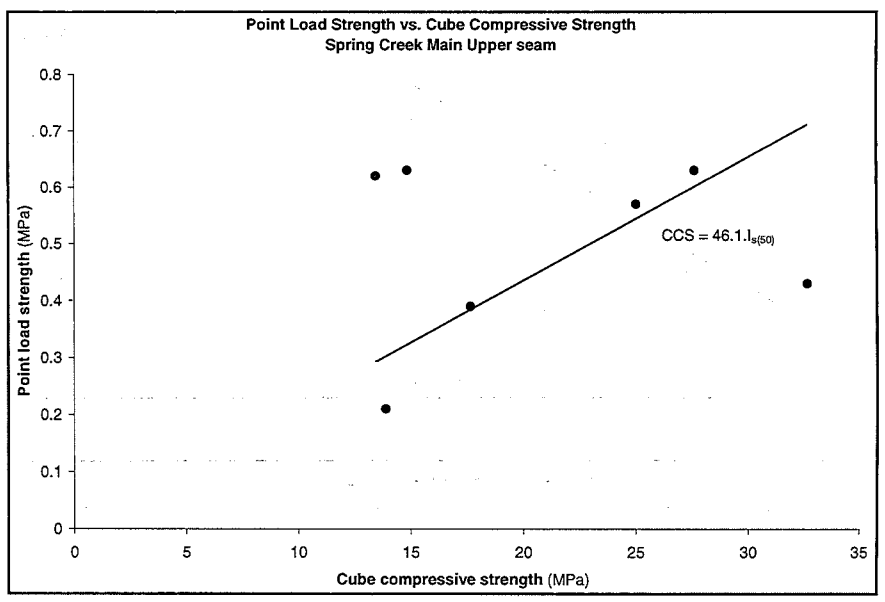

f)

g)

Figure 3.10. Plots of point load strength vs. cube compressive strength. a) Bishop Block, Kimbell seam; b) Bishop Block, Morgan seam; c) Roa Mine, Kimbell seam; d) Strongman No. 2, E seam opencast; e) Spring Creek, D seam; f) Spring Creek, Main Upper seam; g) Terrace Mine, No. 4 seam.

The spread for the Morgan seam was spread into two distinct populations. The lower strength population behaved in a plastic manner described earlier in section 2.3.2.2. The second population behaved in a brittle manner and is considered the more valid of the two. Subsequently two values for the $CCS/I_{s(50)}$ ratio were determined (Figure 3.10b). The lower value ($y = 27.62x$) takes into account both populations. The higher value ($y = 34.48x$), considered the more valid, takes into account only the population with the higher strength values. By disregarding the lower strength population of the Morgan seam shown in Figure 3.10b, the r^2 value of the $CCS/I_{s(50)}$ ratio increases from 0.027 to 0.830 for the Morgan seam.

3.5 Relationship between UCS and CCS

Cube compressive strength is plotted against UCS in Figure 3.11 for the Spring Creek D and Main Upper seams, along with E/OC from Strongman No. 2, to determine any correlation between the two strength values. This plot shows a weak trend of CCS increasing slowly with a much larger increase in UCS (shown by the blue trendline), though the correlation is low with $r^2 = 0.237$. Townsend *et al.* (1977) conducted cube strength tests on various U.S coals and determined that cube strength and the UCS/cube strength relationship are both highly variable.

The orange trendline in Figure 3.11 shows the CCS/UCS ratio which declines as CCS increases, but has a very low r^2 value of 0.167. The CCS values are on average 2.3 times higher than the UCS strengths determined earlier in section 2.2, but range from 1.87-2.84. Hansen *et al.* (1962) found a similar relationship by conducted compressive strength tests on cylinders and cubes of concrete.

Strength differences occur between cores and cubes largely due to the extra friction imposed on the ends of the samples by the loading platens (Hansen *et al*, 1962; Medhurst and Brown, 1998). Townsend *et al.* (1977) found that cylinders were 20-30% weaker than cubical specimens of the same cross-sectional area. Using this data and equation 3.8 (from Singh, 1981), Richards (2002) estimated the strength of a 25mm cube (a value used in

some popular pillar strength equations) to be c. 3.5 times that of a 54mm core. The author of this study estimates this value to be closer to 4.

$$UCS = 44.8 \times \left(\frac{L}{25.4}\right)^{-0.59} \text{ MPa} \qquad \text{(Singh, 1981)} \qquad (3.8)$$

where L = cube side length (mm)

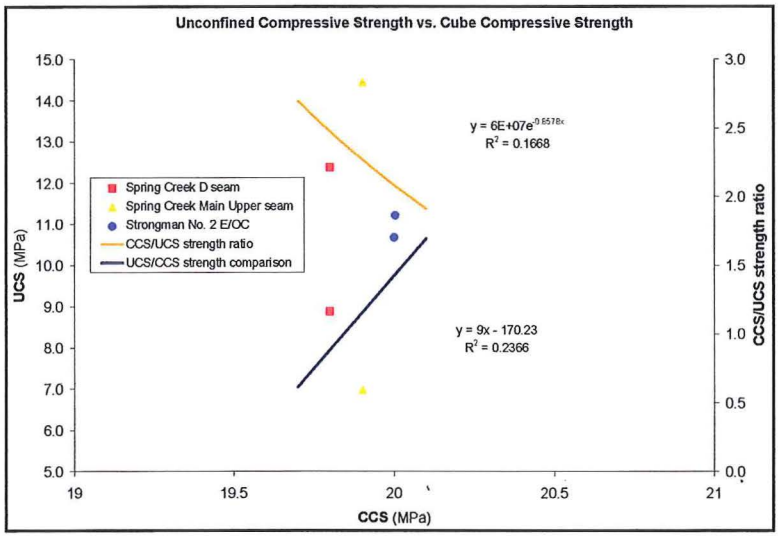

Figure 3.11. Cube compressive strength vs. UCS. The blue trendline shows the comparison of UCS to CCS which has a weak trend with r^2 = 0.237. The orange trendline shows the ratio of CCS to UCS which declines as coal strength increases and has a weaker trend of r^2 = 0.167.

3.6 Determining Unconfined Compressive Strength without Cores

3.6.1 Introduction

Unconfined Compressive Strength (UCS) is the most quoted strength value used in rock mechanics. Core samples for UCS testing could not be obtained for many of the seams studied, so another method needed to be established from which to derive a UCS value. Point load testing is a commonly used alternative, but the UCS = $24.I_{s(50)}$ (for 54mm core) relationship has proved to be invalid for the majority of coal in the Greymouth Coalfield (Section 3.3).

The solution was to conduct compressive strength tests on 63.5mm (2 ½") cubes, and point load tests on the resulting failed samples. The rationale for this was to relate the results to UCS test results so that an equation relating each parameter could be developed. This could then be applied in areas where no core samples could be obtained. The derivation of this equation is presented in section 3.6.2.

3.6.2 Derivation of Strength Prediction Equation

To establish the equation from which $UCS_{equivalent}$ values could be calculated, a benchmark was needed from a location where core, point load and cube test samples could be obtained. Samples from Spring Creek D and Main Upper seams and Strongman No. 2 E seam, opencast, were used as the control group for this. The results of this testing were compared to the UCS results obtained from cores taken from the same seams, resulting in a multiplier y:

given by $$y = \frac{UCS_{control}}{CCS_{control}} \tag{3.9}$$

where: $UCS_{control}$, $CCS_{control}$ = known compressive strength values for 54mm core and 63.5mm cubes (MPa; sections 2.2 and 2.3).

The value of y was found to be 0.45 and 0.35 for the D and MNU seams respectively, and 0.53 for Strongman No. 2 E seam, which gives an average value for y of 0.44.

A second multiplier, z, is then derived from the slope of the trendline from the plot of point load strength vs. cube compressive strength (Figures 3.10a-g). z was established for each locality sampled in this project (except Strongman No. 2 D seam), and the values are summarised in Table 3.5.

$$z = \frac{CCS}{I_{s(50)}} \tag{3.10}$$

where: $I_{s(50)}$ = point load strength (MPa)

Location	Seam	UCS (MPa)	CCS (MPa)	y=UCS/CCS	$z=CCS/I_{s(50)}$
Bishop Block	Kimbell	*3.9*	7.8	-	42.74
	Morgan	*2.1*	3.3	-	27.62
Roa	Kimbell	*1.6*	3.0	-	27.70
Spring Creek	D	8.9	19.8	0.45	37.45
	Main Upper	7.0	19.9	0.35	46.08
Strongman No. 2	E (Opencast)	10.7	20.0	0.53	42.00
Terrace	No. 4	*6.5*	13.8	-	33.11

Table 3.5. Summary of UCS and cube strengths, as well as factors *y* and *z* for each of the sample localities involved in development of equation 3.12. Results in Italics refer to those determined by equation 3.13 (i.e. $UCS_{equivalent}$) and not by strength testing.

z performs the same function as the multiplier, 24, in the $UCS = 24I_{s(50)}$ relationship. By replacing 24 with z gives the following relationship:

$$CCS_{equivalent} = \left(\frac{CCS}{I_{s(50)}}\right).I_{s(50)} \qquad (3.11)$$

where: $\left(\frac{CCS}{I_{s(50)}}\right) = z$

$I_{s(50)}$ = the point load strength of the seam or sample being studied.

Equation 3.11 gives a value for $CCS_{equivalent}$, which is an estimated value of the cube compressive strength for a 63.5mm cube. The multiplier y is then used to convert the strength value from a $CCS_{equivalent}$ to a $UCS_{equivalent}$ compressive strength value (equation 3.12). This estimate should be more reliable than point load strength alone because of the input of results from a compressive strength test.

Thus $$UCS_{equivalent} = y\,(z.I_{s(50)}) \qquad (3.12)$$

where: $y = \frac{UCS_{control}}{CCS_{control}}$

$$z = \frac{CCS}{I_{s(50)}}$$

The bonus of using this equation is that a value for $UCS_{equivalent}$ compressive strength value can be estimated for weak seams where no core samples are available. $I_{s(50)}$ in equation 3.12 can either be the point load strength of an individual sample or the average of an entire seam. Using point load strength values for individual samples is the more desirable alternative, as the point load strength is known to be highly variable (section 2.4). By using c. 10 point load samples a range of $UCS_{equivalent}$ values could be ascertained, thereby providing a better picture of the seams strength.

3.6.3 Applicability of the Method

As far as the author is aware, no other relationship of the type presented in equation 3.12 has been proposed for any other coalfield. Equation 3.12 was used to back calculate the strengths of the Spring Creek D and Main Upper seams and the E seam of the Strongman No. 2 Mine from which it was developed to check how well $UCS_{equivalent}$ compared to actual UCS test results. The results of these calculations are presented in Table 3.6. Each UCS test result from section 2.2 had a corresponding point test result (Figures 3.8a-d). These point load test results were used in the calculation of $UCS_{equivalent}$ to give a range of strength estimates which could then be compared to the variation seen in other test methods.

Location	Seam	$UCS_{equivalent}$ ave. (MPa)	Range	Std dev.	Difference from UCS (%)	Coefficient of Variation %		
						Eqn 3.12	UCS	$I_{s(50)}$
Spring Creek	Main Upper	10.86	7.3-15.2	2.74	+ 55	25	38	55
	D	8.00	6.2-9.2	1.08	- 10	12	33	44
Strongman No. 2	E/OC	11.25	5.7-18.5	2.83	+ 5	25	31	44

Table 3.6. Comparison of $UCS_{equivalent}$ (from equation 3.12) to other methods of coal strength determination.

Equation 3.12 gives $UCS_{equivalent}$ values of 10.86 and 8.00 MPa for the Spring Creek Main Upper and D seams respectively, and 11.25 MPa for the E seam. These values over represent the strength of the Main Upper and E seams by 64% and 5% respectively, and underestimate the strength of the D 10%. The value for the Main Upper seam has a very large error, and so this value is obviously invalid, but the values for the other two seam are similar to those determined in the laboratory (E/OC = 10.7 MPa; D = 8.9 MPa). The coefficient of variation in the result using equation 3.13 is low in the D seam (12%), but

while it is significantly higher in the Main Upper and E seams (both 25%), it is still lower than the corresponding values for UCS (31-38%) and point load tests (44-55%) in all cases.

A modification has been made to equation 3.12 in order to reduce the error for the Main Upper seam. An exponent of 0.945 for the multiplier, z, has been introduced into the equation in order to reduce the effect of z, as this value has a low r^2 value in most cases, and so is the likely cause of the errors that exist in $UCS_{equivalent}$ values. The exponent also serves to spread the errors more evenly across the seams, rather than a very large error on one seam and small errors on all others. This then results in more accurate overall estimate of coal strength.

$$UCS_{equivalent} = y\,(z^{0.945}.I_{s(50)}) \qquad (3.13)$$

Location	Seam	$UCS_{equivalent}$ ave. (MPa)	Range	Std dev.	Difference from UCS (%)	Coefficient of Variation %		
						Eqn 3.13	UCS	$I_{s(50)}$
Spring Creek	Main Upper	8.80	5.9-12.3	2.74	+ 26	30	38	55
	D	6.56	5.1-7.6	0.89	- 26	14	33	44
Strongman No. 2	E/OC	9.16	4.7-15.05	2.30	- 16	25	31	44

Table 3.7. Comparison of $UCS_{equivalent}$ (from equation 3.13) to other methods of coal strength determination.

This revised equation reduces the overestimation of the Main Upper seam's strength to 26%, but consequently underestimates the strength of the D and E seam by 26% and 16% respectively, which are significantly higher than in equation 3.12 however, the spread of the error is more favourable. A comparison of the errors for equations 3.12 and 3.13 with respect to laboratory values is given in Table 3.8.

Location	Seam	UCS_{actual} (MPa)	Difference from UCS_{actual} (%)		
			Eqn 3.12	Eqn 3.13	UCS = $24I_{s(50)}$
Spring Creek	Main Upper	7.0	+ 55	+ 26	+ 91
	D	8.9	- 10	- 26	+ 29
Strongman No. 2	E/OC	10.7	+ 5	- 16	+ 36

Table 3.8. Comparison of strength differences from laboratory values for equations 3.12, 3.13, and the UCS = $24.I_{s(50)}$ relationship.

Table 3.8 shows that equation 3.13 is provides a significantly better estimate of UCS than the UCS = 24.$I_{s(50)}$ relationship. Using the 24 times multiplier overestimate the strength of the Main Upper seam by 91% compared to 26% using equation 3.13. The errors are of similar magnitude using either method for the D seam, with +29% and -26% for the 24.$I_{s(50)}$ method and equation 3.13 respectively, but the strength is either over or underestimated depending on the method used. This is also true for the E seam, but by the using equation 3.13 the error is reduced by 20%.

It must be kept in mind that no method of estimating coal strength is perfect due to its inherent strength variability. Equation 3.13 methods does need to be used with caution as it still has significant error attached, but from looking at Table 3.8 the advantage in using this method in place of UCS = 24.$I_{s(50)}$ is clear.

3.6.4 Estimates of UCS/Point Load Strength Ratio

One benefit of equation 3.13 is that it can be used to determine the $UCS_{equivalent}/I_{s(50)}$ ratio of each seam (Table 3.9), which is seen as a convenient and cost effective method of strength estimation. When a $UCS_{equivalent}$ value has been determined, it can be related to the average point load strength of each particular seam to determine that seam's $UCS_{equivalent}/I_{s(50)}$ relationship, thereby allowing point load strength to be used in future coal strength determinations.

Location	Seam	$UCS_{equivalent} = x.I_{s(50)}$	
Bishop Block	Kimbell	*15.30*	
		13.8-14.3	Richards (2000)
	Morgan	*12.48*	
Roa	Kimbell	*10.15*	
Spring Creek	D	22.88	
	Main Upper	17.18	
Strongman No. 2	D	28.25	
	E	23.31	
		$(8.8.I_{s(50)}) + 11$	Caffyn (1987)
Terrace	No. 4	*12.02*	

Table 3.9. Summary of $UCS/I_{s(50)}$ relationships. Values in italics refer to those values derived from equation 3.13. *x* is the multiplier which is used to estimate UCS from point load strength.

Table 3.9 gives the $UCS_{equivalent}/I_{s(50)}$ ratios for each seam involved in this study. These have a large range from 10.15 for the Roa Mine up to 28.25 for the Strongman No. 2 D seam. Values in italics are determined by using equation 3.13 whereby the strength estimated by this method ($UCS_{equivalent}$) is divided by the average point load strength of each particular seam to give a $UCS_{equivalent}/I_{s(50)}$ ratio. Multipliers for the Spring Creek and Strongman No. 2 Mines are taken from the plots of point load strength vs. UCS given in Figures 3.8a-d.

This method of determining coal strength is more applicable in the Greymouth Coalfield than the $UCS = 24.I_{s(50)}$ method which is commonly employed, as this method takes into account some aspect of the strength of each seam other than point load strength which is prone to large errors in such weak strata. While the $UCS = 24.I_{s(50)}$ may be applicable in some parts of the coalfield, it can be seen from Figure 3.12 that the $UCS/I_{s(50)}$ relationship is a function of coal rank. As the rank increases there is a corresponding decrease in the $UCS/I_{s(50)}$ ratio, and so the ratio will decrease from west to east across the coalfield. As with Figures 3.3a & b the outlying point appears to be the Roa Mine. Trendlines both including (solid line) and excluding (dashed line) the Roa Mine have been plotted. The trendlines show equal r^2 values of 0.71, but are described by different equations which are presented as follows:

Including Roa: $y = 14.28x^{-0.8353}$ (3.14)

Excluding Roa: $y = 11.503x^{-1.4517}$ (3.15)

A reasonable approximation of the $UCS/I_{s(50)}$ relationship can be made from the trendline, but more investigations need to be conducted for samples with vitrinite reflectance from 0.9-1.7% to accurately determine the trend at higher ranks. Samples in this region were beyond the scope of this study for three reasons; 1) samples would only be available from outcrop. Experience gained from Bishop Block outcrop samples showed that the degree of weathering renders them unusable for strength testing; 2) the sampling areas are only accessible by foot and requires the use of a helicopter to remove the samples; 3) no development currently planned for this area (Refer Rajah Block in Map 1). This lack of data for medium rank results in a moderate r^2 value of 0.713.

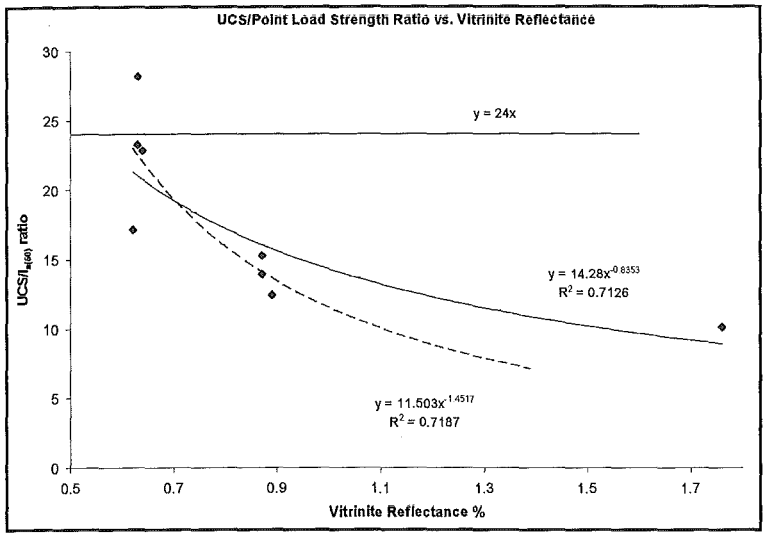

Figure 3.12. Relationship between UCS/$I_{s(50)}$ ratio and vitrinite reflectance. The ratio decreases with increasing coal rank.

3.7 Synthesis

- A number of factors appear to contribute to changes in, or are useful predictors of, coal strength including carbon and volatile matter content, rank, degree of cleating and age of the coal.

- Coal strength drops rapidly with increasing coal rank. There are two reasons for this: 1) cleat frequency increases from very few at rank of high-volatile bituminous C through to a maximum at med-low volatile bituminous before declining rapidly as rank approaches anthracite; and 2) as coal rank increases the coal becomes increasingly soft and deforms plastically. This trend shows up stronger in UCS results (Figure 3.3a) had one of the highest r^2 values seen in this study ($r^2 = 0.870$), as thus is considered to be one of the best methods of estimating unconfined compressive strength (equation 3.16).

$$UCS_{equivalent} = 4.88x^{-2.25} \qquad x = \text{vitrinite reflectance \%} \qquad (3.16)$$

- The drop in coal strength as the rank increases is predominantly caused by a steady increase in cleat frequency with increasing rank until medium-low volatile bituminous, at which point the cleat frequency begins to decline. The corresponding

strength drop is at first rapid and then declines as the rank increases. Strength continues to drop as cleat frequency declines as the changing chemical structure makes the coal behave plastically.

- Variations in fixed carbon and volatile matter contents of coal come about with increasing coalification and correspond to the strength variations. The changes in fixed carbon and volatile matter do not cause, but occur parallel to, changes in the coal strength with increasing coalification.

- Ash content however is an independent property related to the depositional regime and thus does not change with coalification. The evidence presented in this study is inconclusive as to whether changes in ash content cause changes in coal strength, but the trend of coal strength increasing with ash content is apparent in Figure 3.6 though the r^2 value of 0.200 is very low. The correlation is low due to two outlying points, but ash is a useful independent property for making strength estimates for each of the other seams. The trend is descried by equation 3.17.

- Volatile matter and carbon content both show very strong trends with changes in the compressive strength of coal. Volatile matter increases with increasing coal strength with and r^2 value of 0.800. Increasing carbon content corresponds to a rapid decrease in coal strength with an r^2 value of 0.894. These trends are not the cause of the change in coal strength, but are useful predictors of it and the trends can be described by equations 3.18 and 3.19.

$$UCS_{equivalent} = 9.65x\text{-}7.11 \quad \text{where x = ash content (\%)} \qquad (3.17)$$

$$UCS_{equivalent} = 0.0002x^{2.98} \quad \text{where x = volatile matter (\%)} \qquad (3.18)$$

$$UCS_{equivalent} = 4\times10^{11}x^{-6.04} \quad \text{where x = carbon content (\%)} \qquad (3.19)$$

- An equation for predicting $UCS_{equivalent}$ values more accurate than using UCS = $24.I_{s(50)}$ has been established by this study. When the seams are plotted individually the multiplier can range from 12-28, though the r^2 value in many cases is low or negative, making them of little or no use. The afore mentioned equation is presented as follows:

$$UCS_{equivalent} = y\ (z.I_{s(50)}) \tag{3.20}$$

$$UCS_{equivalent} = y\ (z^{0.945}.I_{s(50)}) \tag{3.21}$$

Equation 3.20 overestimates the strength of weak coal, so a revision was made to curb this effect in the form of equation 3.21 which is not as accurate as UCS testing, but provides a useful estimate of coal strength where no core samples are available.

- From equation 3.21 $UCS_{equivalent}/I_{s(50)}$ ratios for each seam studied were established. These ratios vary widely across the coalfield and decrease with increasing coal rank. They can be estimated from equation 3.22 which is taken from Figure 3.12 with an r^2 value of 0.71.

$$UCS_{equivalent}/I_{s(50)} \text{ ratio} = 12.28x^{-0.84} \quad \text{where } x = \text{vitrinite reflectance} \tag{3.22}$$

- $UCS/I_{s(50)}$ ratios developed from UCS testing had very low or negative r^2 values due to the scatter seen in the results. Correlation values could be greatly increased by removing an extreme value in most cases, but the compressive strengths estimated by these ratios will still have a large margin of error and thus should not be used.

- Equations 3.16-3.19 and 3.21 are all potentially useful methods of estimating coal strength. While they are not intended to replace the use of the unconfined compressive strength, they may at times be not only more convenient but also equally as accurate. A combination of at least two of these methods should be used to estimate coal strength so that two $UCS_{equivalent}$ values can be compared to eliminate any results which are clearly incorrect.

Chapter 4. Pillar Design

4.1 Introduction

> "...I merely want to emphasize the complexity of pillar design such that it is unreasonable at present to stipulate a cookbook type pillar design formula for all occasions" - Syd S. Peng (1993 p. 1053. Reply to an article by J. I Mathis, 1993).

Geological conditions in the Greymouth coalfield, including steep topography and steeply dipping seams, limit the amount of opencast mining which can be conducted such that c. 0.7% of the total resource is considered opencastable (Barry *et al*, 1994. Edbrooke, 1999). The geology also confines underground mining to the use of the room and pillar technique, which is the most adaptable to the changing ground conditions.

Room-and-pillar mining is the oldest form of mining (Jeremic, 1985), and is still the method by which the majority of coal is mined worldwide. In this method the pillars are the element of the coal mine carrying the weight of the overburden (Yardley, 1996; Figure 4.1). The aim of effective pillar design is to provide roof support and maintain a safe working environment whilst committing as little resource to the pillars as possible. The expected life of the pillar will depend on its function. If they are to be removed on retreat, they may be needed for some months only, while pillars supporting shafts or haulage routes will likely be required for the life of the mine. If subsidence of the ground surface needs to be avoided, they may remain permanently (i.e. barrier pillars). To achieve the stability requirements it is very important to have a sound design procedure and a thorough understanding of how the pillars, and the coal of which they are composed, will perform under load.

The aims of this chapter are to 1) calculate the minimum required pillar sizes using the coal strength data of Chapter Two in combination with appropriate pillar design equations and factors of safety; and 2) investigate bearing capacity (floor heave) problems in the

Terrace mine and size pillars to minimise the effects of this problem which often results from the use of undersized pillars.

Different pillar types have different functions and corresponding differing factors of safety are used in their design (Hebblewhite *et al.*, 1986). Barrier, rib, yield, and panel (production) pillars are the main types of pillars used in coal mining.

Barrier and rib pillars are solid coal pillars with length significantly greater than their width (Hebblewhite *et al.*, 1986). These are designed to high FOS (~2.0) for long term stability, as they often must remain stable for many years. The pillars separate development panels within the mine to prevent areas of widespread pillar collapse, to isolate fires and to provide ventilation. Barrier pillars are also left around the edges of the mine workings where a seam outcrops, or when the seam passes under a stream.

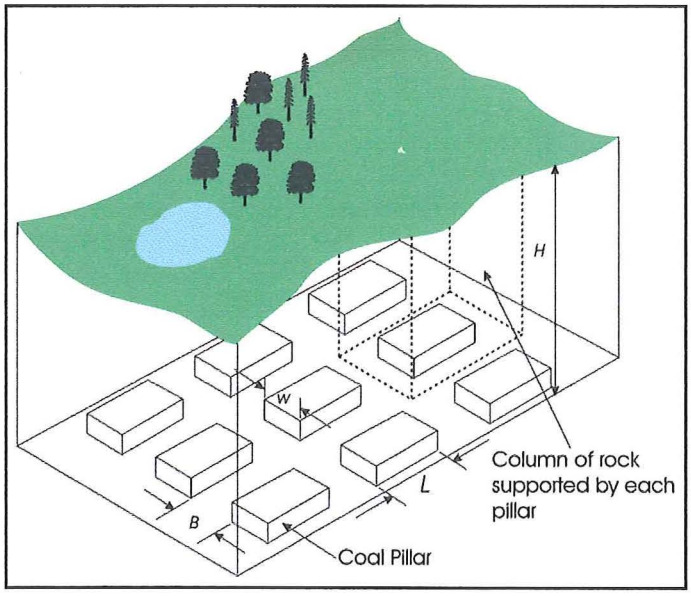

Figure 4.1. Typical layout of room and pillar mining, and the parameters involved in determining the average pillar stress by the tributary area method.

Panel (or production) pillars are much smaller than barrier pillars, and are used in the panels where mining is occurring. These are usually square or rectangular in cross section and designed to a lower FOS of 1.6 (Beamish and Vance, 1989; Salamon and Munro, 1967; Wagner, 1992; Yardley, 1996) as they are required for much shorter periods from a

few months to a few years until pillar extraction begins during retreat mining when pillar failure is allowed to occur.

Yield pillars are most commonly used during retreat mining where the panel pillars are being extracted. In this case yield pillars are smaller remnants of the panel pillar and have a FOS of <1 (i.e. they are unstable). They are designed to fail in a controlled manner following pillar extraction. For these to be designed properly, a thorough understanding of the deformation characteristics of the coal pillar and the roof rocks needs to be taken into account. Due to time constraints this is beyond the scope of this study.

4.2 Pillar Load

4.2.1 Background

Before the size of a pillar can be calculated, the pillar load (the average stress on each pillar) needs to be determined, and this is dependent on thickness and density of overburden as well as the pillar size and extraction ratio. There are two main approaches, the tributary-area approach (equations 4.1 and 4.2) and elastic-deflection theory (equation 4.4).

4.2.2 Tributary Area Approach

The tributary area method is a very simplified method of determining the load acting upon a mine pillar. The pillar load is dependant on the shape of the pillar with different load being exerted on rectangular and square shaped pillars and is calculated as follows:

$$S_p = \frac{0.025H(w+B)(L+B)}{w.L} \qquad (4.1)$$

where: S_p = pillar load (MPa)
w = pillar width (m)
H = depth below surface (m)
B = entry width (m)
L = pillar length (m)

Extraction ratio, e, is calculated by the following equation:

$$e = 1 - \frac{w.L}{(w+B)(L+B)} \tag{4.2}$$

where: e = extraction ratio (percentage of resource extracted).

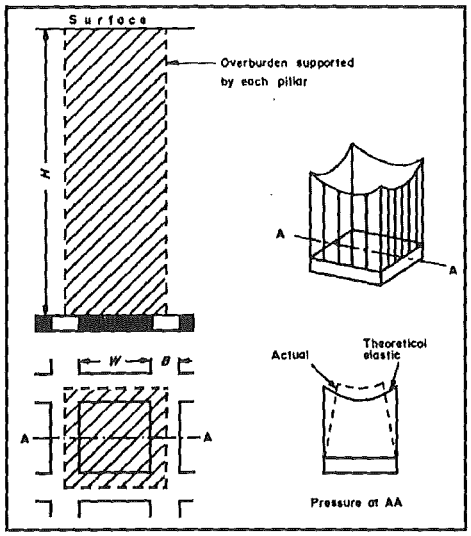

Figure 4.2. Pillar load according to the tributary area method (after Sheorey, 1993). Note how the load is concentrated on the corners and sides of the pillar.

The simplicity of the method is the reason it is so popular, but this has its problems. There are a number of assumptions associated with the tributary area approach as noted by Bieniawski (1984), including 1) the seam is only subjected to a constant vertical pressure; 2) each pillar supports the column of rock immediately above the pillar plus a portion of the room area equal to that shared by all neighbouring pillars (as illustrated by Figures 4.1 and 4.2); and 3) the load is uniformly distributed over the cross-sectional area of the pillar. These conditions generally cannot be met due to non-uniform stress distributions which leads to the overestimation of pillar load. However the tributary area method is more commonly used, due to the over complication of the elastic deflection approach (section 4.2.3), and has been adopted as the method of choice in this study. Yardley notes that the Tributary Area Method is valid for seam dips up to 1V:4H (~14°) if width of mined out panel is at least equal to the depth below the surface. Trumbachev and Melnikov (1964)

give a method of calculating the pillar load when seam dip increases above 14° which can be calculated as follows:

$$S_p = 0.025H\left(\frac{w+B}{w}\right)^2(\cos^2\alpha\text{-m }\sin^2\alpha) \qquad (4.3)$$

where: α = angle of seam dip

m = a constant

The tributary-area method is said (Hustrulid and Swanson, 1981) to overestimate the pillar load by c. 40%, while Coates (1966) showed the elastic-deflection theory to give result about 40% lower than the tributary area method, thus giving what should equate to the actual pillar load. Gale and Mills (1995) conducted field measurements of pillar strength and suggest that the difference between measured values and stress predicted by the tributary area method is insignificant for practical purposes.

The expected pillar stress has been calculated for all overburden depths likely to be encountered in the Greymouth and Reefton Coalfields, and for extraction ratios of 5-75 %. These are presented in appendix 9.1 (Table A9.1) and summarised in Table 4.1.

Location	Seam	Depth of workings (m)	Initial extraction (%)	Overburden stress (MPa)
Bishop Block	Kimbell	20-120	40-70	1.67-5.00
	Morgan	20-150	30-70	1.67-5.36
Roa	Kimbell	20-170	5-25	0.67-4.47
Spring Creek	D	200-220	25-35	7.33-7.69
	Main Upper	250-300	20-30	8.93-9.38
Strongman No. 2	D	50-170	45-70	4.17-7.73
	E	50-120	45-70	4.17-5.45
Terrace	No. 4	170-260	9-14	4.94-7.14

Table 4.1. Summary of overburden stress and percentage initial extraction for each location involved in this study.

4.2.3 Elastic Deflection Theory

The elastic-deflection theory takes into account many more variables than the tributary area method, resulting in a more accurate estimate of the overburden load. Consequently, the method is vastly more complex. Coates (1966) gives the following equation for the elastic-deflection theory (taken from Bieniawski, 1984):

$$\frac{S_p}{S_v} = \frac{\Delta S_p}{S_v} + 1 \qquad (4.4)$$

where: S_p = total pillar load

S_v = virgin vertical stress

ΔS_p = pillar load due to mining which is calculated as follows:

$$\Delta S_p = \frac{2R - kh(1-w)(1-x^2+h) - wp(khn)}{hn + \pi(1-R)(1+1/N)(1+h/1-x^2)/2 + 2Rb'(1-w)\pi}$$

where, for plane strain:

$M = E/(1-\nu^2)$

$w = \nu/(1-\nu)$

$k = \sigma_h/\sigma_v$

$b' = b/L$

$x = x^*/l^*$

$h = h^*/l^*$

$n = M/M_p$ (p subscript denotes pillar rock value)

where: E = Young's Modulus of the roof rock (psi)

ν = Poisson's Ratio

σ_h = horizontal stress acting on the seam (psi)

σ_v = vertical stress acting on the seam (psi)

b = width of the pillar (feet)

R = radial distance from centre (feet)

L = breadth of mining zone (feet)

x^* = displacement in x direction

h^* = pillar height (feet)

l^* = pillar length (feet)

N = number of pillars

Due to the complexity of this method, it has been avoided by most authors who prefer instead to deal only with the tributary area method. For this reason there is very little analysis of this method in the literature.

4.2.4 Approach Used

The elastic-deflection theory method is said to have good correlation with field measurements of stress distribution (Bieniawski, 1984), but due to the complexity of the elastic-deflection method, the tributary area method is vastly more popular in the mining industry. The tributary area method gives more conservative results (Bieniawski, 1984) which accounts for variability in thickness and density of the overburden, and gives are greater margin or error for pillar design factor of safety calculations helping to account for coal strength variability.

The elastic-deflection theory approach requires values of Young's modulus and Poisson's ratio for the roof rocks. Due to time constraints, properties of roof rocks were not determined by this study, so the elastic-deflection theory could not be used by this study.

4.3 Pillar Strength

4.3.1 Background

Pillar strength can be heavily influenced by a number of factors including: 1) Uniaxial and tensile strength of coal; 2) *w/h* ratio of the pillar (*h* = height of the pillar); 3) pillar size or volume; 4) shape in plan; and 5) pre-excavation horizontal stresses (Sheorey, 1993). Bieniawski (1967) states that pillar strength is 'the ultimate load bearing capacity per unit area based on the weakest cross-section'.

There is general agreement over the confined core concept whereby the unconfined coal adjacent to the roadways fails and provides confinement for the pillar core, thus increasing its strength (Figure 4.3). This method takes into account the roles that roof and floor rocks have in pillar strength by confining failed coal adjacent to excavations. Coal adjacent to the excavation is in an unconfined state and because the stresses are highest in this area, this coal fails first. Load must then be redistributed towards the pillar core which can support this new load if it sufficiently confined (Salamon, 1992). Yielding around the pillar edges will continue until the pillar core is sufficiently confined to support the new

load. The failed coal is confined by the roof and floor rocks, thereby providing confinement for the pillar core.

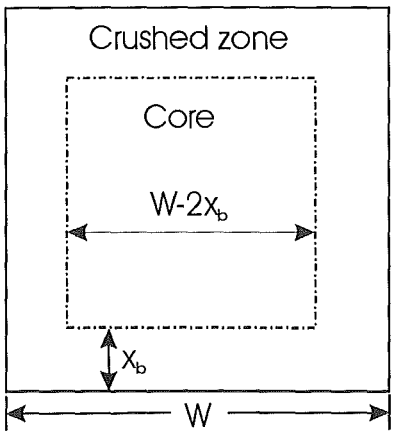

Figure 4.3. Schematic illustration of the confined core concept showing the crushed zone of a coal pillar which provides confinement for the pillar core (modified after Salamon, 1992). The pillar core is the component which supports the overburden load. By the confined core concept the core can support greater load as it is in a state of triaxial confinement.

There are divided opinions of the roles that floor and roof strata play in amplifying the confined core system. Gale and Mills (1995) are advocates of this system and suggest that the empirical methods are more idealised (simplified) methods which are adequate when coal is the weakest unit in the sequence, and thus the influence of roof and floor rocks is lessened. This author believes that empirical methods are a simple and effective means of determining pillar strength which give results equally as valid as those of analytical techniques. The analytical techniques preferred by Gale and Mills require a very thorough understanding of all components of the system, such as strength and behaviour under load of roof and floor rocks, which is often not available from a practical point of view and is beyond the scope of this study.

4.3.2 In-Situ Strength Estimation from Laboratory Testing

Because of the reduction of strength with increasing sample size known as the size effect (Section 2.1, Figure 2.1), there is a need to estimate the in-situ strength of coal for each seam. The point at which no further strength reductions of coal cubes and pillars are obtained by increasing the specimen size is termed the critical size. Bieniawski (1968)

deemed this to be 1.5m for South African coal, and Pariseau (1977) concluded that for U.S coal the critical size was 0.9m. St George (1995) notes that the critical size value is a property of the structure and nature of the coal mass, and will vary from seam to seam. Many authors have adopted the 0.9m critical size for their studies, and due to practical limitations 0.9m has been used for this study also. By using equation 4.5, any errors introduced by using 0.9m should be minimal. Hustrulid (1976) developed an equation from which in-situ (critical size) strength, σ_1, could be calculated from laboratory-determined values of σ_c where:

$$\sigma_1 = \frac{k}{\sqrt{36}} \qquad \text{for pillars with height} > 0.9\text{m.} \tag{4.5}$$

where: σ_1 = in-situ coal strength. Strength of a coal cube >0.9m.

Hustrulid suggests that k should be determined from tests on 76mm (3") cubes, but Bieniawski (1984) states that it can be determined by the Gaddy constant, k, where:

$$k = \frac{145\sigma_c\sqrt{\frac{D}{25.4}}}{145} \tag{4.6}$$

where: k = constant determined for actual pillar material (modified after Gaddy, 1956),

σ_c = unconfined compressive strength (MPa),

D = diameter of cylindrical sample or cube side length (mm).

Table 4.2 summarises values for the Gaddy constant, k, and in-situ coal strength σ_1. σ_1 is the coal strength value used in many pillar strength equations which varies between 0.32 MPa (Roa) and 6.03 MPa (E/UG) which is c. 24% of the UCS value. UCS values have been determined by Harris (2002) using either UCS testing or equation 3.13. In the case of the Bishop Block, strength tests conducted by Harris (2002) were deemed to be unreliable due to the degree of weathering of the samples (section 2.3). Richards (2000) reported a UCS value for the Kimbell seam of 8.0 MPa from two UCS tests on 61 mm core. This value has been adopted here for pillar design applications, along with a slightly lower

value for the Morgan seam (7.0 MPa) which was shown to be slightly weaker by this study (Section 3.6, Table 3.4). Strength values for the Morgan seam were not reported by Richards.

Location	Seam	UCS (MPa)	k	σ_1 (MPa)
Bishop Block	Kimbell†	8.0	11.7	1.9
	Morgan‡	7.0	10.2	1.7
Roa	Kimbell*	1.3	1.9	0.3
Spring Creek	D	8.9	13.0	2.2
	Main Upper	7.0	10.2	1.7
Strongman No. 2	D	17.1	24.9	4.2
	E/UG	24.8	36.2	6.0
Terrace	No. 4*	5.4	7.9	1.3

Table 4.2. Summary of in-situ coal strength, σ_1, estimated using equations 4.5 and 4.6. † UCS strength value taken form Richards (2000) as weathering affected test results of this study. ‡ Morgan seam was weaker than Kimbell in this series of testing, but not tested by Richards. * Values determined by equation 3.13.

4.3.3 Review of Pillar Strength Equations

Bieniawski (1984), Hustrulid (1976) and Sheorey (1993) have conducted comprehensive reviews of pillar design formulae, and give highly varied opinions on which method is best. It is beyond the scope of this study to review design formulas in as much detail as these studies have, and only those formulae that are most commonly used and those which are applicable to the conditions encountered in this study are therefore discussed.

Pillar strength equations either developed from case studies of failed and stable pillars, or by conducting a number of large-scale in-situ tests, are preferred by most authors as these methods are less prone to error than methods involving scaling strength values from laboratory to in-situ values. Simplicity of use is also a factor, as introducing too many variables will introduce more error.

Pillar design formulas, which are mostly developed for South African and U.S coal seams, follow the same basic premise of involving *w/h* ratios along with compressive strength and/or a constant representing a particular coal seam. These follow two general forms:

$$\sigma_p = \sigma_1(a + b\frac{w}{h}) \qquad \text{and} \qquad \sigma_p = \sigma_1\left(\frac{w^a}{h^b}\right)$$

where: a, b are constants

σ_p = Pillar strength

σ_1 = In-situ coal strength from equation 4.5

Many pillar strength equations are only valid over a certain range of *w/h* ratios (generally 2-8), or begin to underestimate the pillar strength as *w/h* ratios increase (especially when *w/h* >5) due to increasing confining pressures in the pillar core giving the pillar greater strength. The centre of the pillar (core) is essentially in a state of triaxial confinement with σ_3 considered to be in the order of 4 MPa on average (Gale and Mills, 1995). The confinement is provided by failed coal around the pillar edges. As pillar size increases more confinement is development and so the centre becomes stronger. Coal rapidly gains strength from increased confinement (Section 2.5, Figure 2.18) and continues to do so until very high confining pressures (at least $\sigma_3 \leq 160$ MPa according to Gale and Mills, 1995). The triaxial confinement can only develop if the failed coal has some residual strength. Coal in this study showed a 7-19 MPa strength increase for every 1 MPa increase in confining pressure (over the range σ_3 = 2-6 MPa), though the increases become smaller as confinement increases. Gale and Mills (1995) found the increase of compressive strength to be c. 4 MPa for every 1 MPa increase of σ_3 for confinements of up to 40 MPa. The significance of this is best explained using an example from Gale and Mills (1995, pp. 21-22) for Bulli coal from the Southern Coalfield, Australia:

> "When the roadways are driven, the coal in the immediate rib, which is then unconfined, becomes loaded to greater than 11 MPa (the overburden load) and, because its unconfined strength is only 8 MPa it fails. Although failed, this coal provides some confinement to coal further into the pillar and thereby increases the strength of the coal deeper into the pillar.
>
> If this coal is also overloaded, it too fails, and by failing provides greater confinement to intact coal further into the pillar. This process continues until, either the confinement...generates sufficient strength...to support the imposed load...or all the coal in the pillar has failed."

Sheorey *et al.* (1987) suggest that at high triaxial confinements, which can occur in the centre of coal pillars with high *w/h* ratios, the uniaxial compressive strength has little bearing on rock failure, and that pillar strength formulae should reduce the influence of UCS as *w/h* ratio increases.

The following is a list of the most popular and best understood pillar design equations. These have been reviewed and comparisons made of selected formulae in order to determine the most appropriate for use in pillar design for the Greymouth and Reefton Coalfields.

Bauschinger 1876 $$\sigma_p = \sigma_1 (0.778+0.222\frac{w}{h})$$ (4.7)

Holland 1964 $$\sigma_p = \frac{k\sqrt{w}}{h}$$ (4.8)

Salamon and Munro 1967 $$\sigma_p = K\frac{w^{0.46}}{h^{0.66}}$$ (4.9)

Bieniawski 1967 $$\sigma_p = \sigma_1 (0.64+0.36\frac{w}{h})$$ (4.10)

Holland 1973 $$\sigma_p = \sigma_1\sqrt{\frac{w}{h}}$$ (4.11)

Logie and Matheson 1982 $$\sigma_p = \sigma_1(0.64+0.36\frac{w}{h})^{1.4}$$ (4.12)

Salamon and Wagner 1985 $$\sigma_p = \sigma_1\frac{R^{0.5933}}{V^{0.0667}}\left[\frac{0.5933}{e}\left[\left(\frac{w/h}{R}\right)^e - 1\right]+1\right]$$ (4.13)

where: e = the rate of strength increase = 2.5

σ_1 = in-situ coal strength as per equation 4.5

w, h = pillar dimensions (m)

$K = \frac{k}{\sqrt{12}}$ and k is as per equation 4.6

V = volume of pillar (m^3)

R = critical w/h ratio = 5

σ_p = pillar strength (MPa)

The aforementioned equations are for the design of square pillars. For application to rectangular pillars, the effective width, w_{eff}, is used in place of w in pillar strength formulas.

$$w_{eff} = \frac{4A}{C} \tag{4.14}$$

where: A = pillar area (m), and C = pillar circumference (m)

In 1876, Bauschinger proposed a strength formula (Equation 4.7) based on sandstone cores which was later replicated by Johnson (1897), Obert and Duval (1967), Hustrulid (1976) and Wang *et al.* (1977). This equation is very similar to equations by other authors including Bunting (1911), Bieniawski (1967, 1968, 1984; Equation 4.10), Sorensen and Priseau (1978) and Van Heerden (1973). Bieniawski (1967) conducted 16 in-situ tests on coal pillars in the Witbank Coalfield, South Africa, and developed equation 4.10 which is still one of the most common methods of pillar strength prediction and is valid for w/h from 1-5 and $w > 1.5$m.

The Holland-Gaddy Formula (Equation 4.8) was introduced by Holland in 1964, and was an extension of Gaddy's (1956) work on the uniaxial compressive strength of coal cubes. Bieniawski (1983) showed this gave very conservative (low) estimates of pillar strength. Sheorey (1993) found that this equation underestimated pillar strength at all w/h ratios, where as other equations tend to only underestimate strength at higher w/h ratios. This equation gave many stable pillars a FOS of much less than 1, and thus in not considered suitable.

The Salamon-Munro (1967) formula (Equation 4.9) is based on the work of Holland (1964) and Greenwald *et al.* (1939), and was developed by studying failed and stable coal pillars in South African coal mines. 125 pillars were studied to develop this formula, of which 27 had failed. Work by Gavin (1995) found that similar relationships are applicable to Australian coal. The problem with this formula is that it is only applicable to square pillars with *w/h* ratios < 4.

The squat pillar formula (Equation 4.13) was developed by Salamon and Wagner (1985) to replace the use of the popular formulae of Bieniawski (1984; Equation 4.10) and Salamon and Munro (1967; Equation 4.9) when *w/h* increases to 5 and above (*w/h* = 5 is the division between squat and slender pillars) because the strength estimates of these equations become too conservative at this point. Madden and Hardman (1992) consider the values of *R* and *e* to be quite conservative.

Equation 4.10 has undergone revision (Equation 4.12) by Logie and Matheson (1982) for application to squat pillars (*w/h* > 5), but Sheorey (1993) mentions that by doing this, two separate values are determined when *w/h* = 5, so suggests equation 4.12 should be used. Sheorey goes on to suggest that a value of 1.5 be used for the exponent in place of 1.4. The author of this study believes that an exponent of 1.5 would overestimate the pillar strength considerably. Figure 4.4 shows that with an exponent of 1.4, equation 4.12 already gives pillar strength estimates c. 10% higher than equation 4.13 of Salamon and Wagner, and over three times higher than any other equation. Using an exponent of 1.5 will only increase this difference further.

4.3.4 Comparison of Selected Pillar Strength Equations

Comparisons of the pillar strength formulae presented in Figures 4.4, 4.5.and 4.6 have been conducted using the in-situ strength of Strongman No. 2 D seam coal for the purposes of the evaluation. From Figure 4.4 it can be seen that the predictions of Bauschinger (1876) and Holland (1973) are very similar. The equations of Bieniawski (4.10, 4.12), Salamon-Munro/Wagner (4.9, 4.13) are also similar to each other, with Bieniawski's equation being the more conservative until *w/h* exceeds 4. The Holland-

Gaddy formula (equation 4.8) is the most conservative of all in its predictions giving pillar strength estimates c. 50% lower than the Bauschinger (Equation 4.7) and Holland (Equation 4.11) methods. All equations, other than the Holland-Gaddy formula, predict similar strengths until $w/h \approx 4$, where the equations of Bauschinger and Holland begin to underestimate the strength produced by the high w/h ratios. The Bieniawski and Salamon squat pillar formulas, however, show that pillar strength increases substantially as w/h increases, due to the high confining pressures in the pillar core.

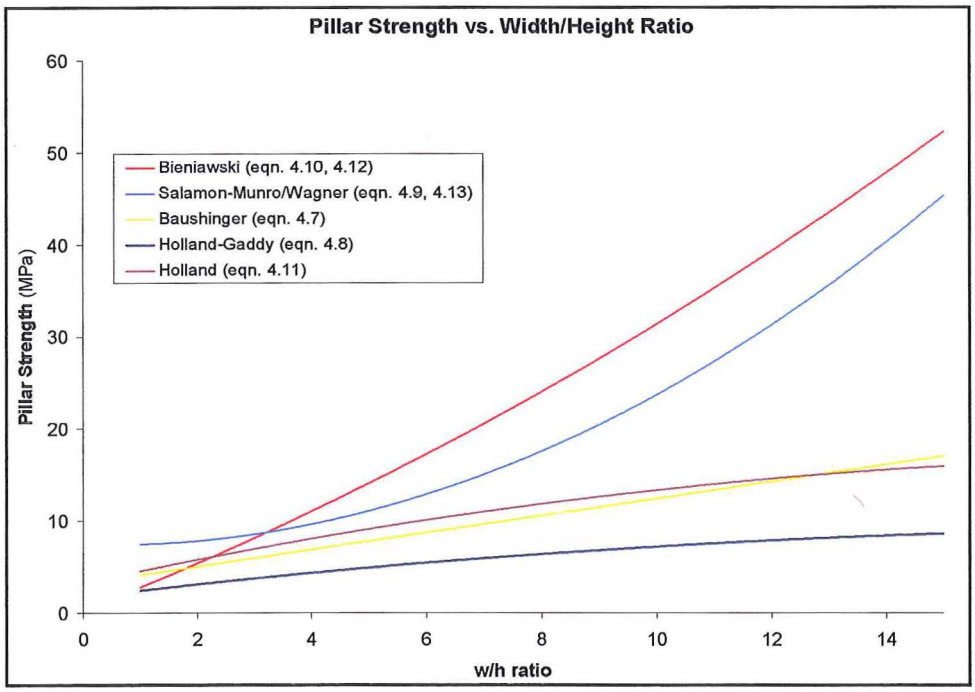

Figure 4.4. Comparison of common pillar strength equations using the strength of Strongman No. 2 D seam for evaluation with a mining height of 3m. D seam was chosen for the purposes of comparison. 3m mining height is a standard mining height where continuous miners are used. Bieniawski - Equation 4.10 used for *w/h* < 5 and equation 4.12 used for *w/h* ≥ 5. Salamon-Munro/Wagner - Equation 4.9 used for *w/h* < 5 and equation 4.13 used for *w/h* ≥ 5. Factor of Safety = 1.6 in all cases as this is standard for panel/production pillars in coal mining.

Figures 4.5 and 4.6 are comparisons between the slender and squat pillar formulas of Bieniawski and Salamon-Munro/Wagner respectively, and show the increased strength predicted by using the squat pillar formula. The Salamon-Munro slender pillar formula gives results slightly higher over all w/h ranges than the corresponding formula from Bieniawski. The equations of Salamon-Munro (4.9) and Bieniawski (4.10) are said to underestimate pillar strength as w/h ratio increases, especially when w/h >6 (Madden,

1988). Wagner (1992) cautions the use of the Salamon squat pillar formula outside the range for which it has been tested, reporting that this method has been used successfully for mining heights of 2.0m at 550m depth, and 2.5m at 250m depth.

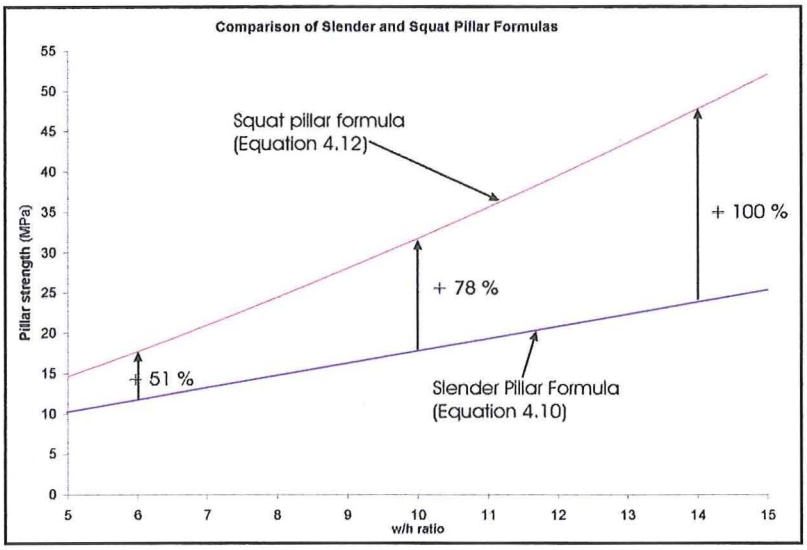

Figure 4.5. Comparison of the slender and squat pillar formulas of Bieniawski showing the increase in pillar strength predicted by the squat pillar formula.

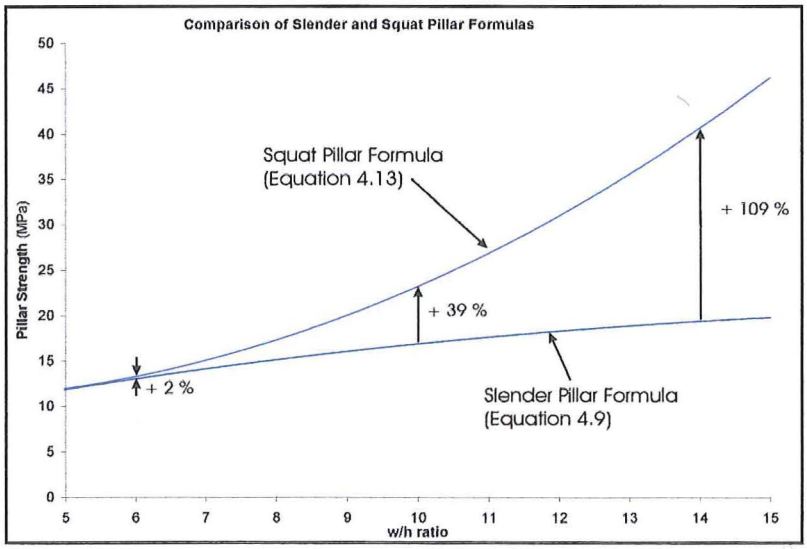

Figure 4.6. Comparison of the slender and squat pillar formulas of Salamon-Munro/Wagner showing the increase in pillar strength predicted by the squat pillar formula.

The strength equations which have been selected in this study are equation 4.9 and 4.10 along with their corresponding squat pillar formulas. These were selected for the following reasons: 1) They are the most commonly used and best understood methods; 2) They have undergone substantial analysis in the literature; 3) Neither equation gives extreme values

in Figure 4.4; and 4) Both equations show the expected significant increase in pillar strength with increasing *w/h* ratios. This allows smaller pillars to be used, thereby increasing the initial extraction percentage while maintaining the required factor of safety of 1.6.

4.4 Pillar Design in the Greymouth and Reefton Coalfields

4.4.1 Background

Pillar design involves the determination of pillar dimensions for the maximum extraction of coal while maintaining stability of the workings and the safety of the workforce. Pillar design can take two different forms. The most common, and the approach in this study, is to use pillar strength formulas such as those presented in section 4.3.2. The second approach is to use the so-called 'finite element structural analysis method'. This approach is vastly more complex, taking into account the strength of the roof and floor materials, and requires a much greater knowledge of each component in the system. Some authors are opposed to pillar strength formulas purely because they do not take into account floor conditions, and thus strong pillars may fail by punching into the floor. The author agrees that it is unwise to ignore the effects of floor materials completely, so this has been dealt with separately in section 4.7. The finite element method is considered to be beyond the scope of this thesis because time constraints prevented the required analysis of roof and floor rocks required to design pillars by this method. The author also believes that the finite element method is not yet well enough understood, with considerable debate as to the confinement in the core of the coal pillar which is partially dependent on the strength of the roof and floor rocks (Salamon, 1992).

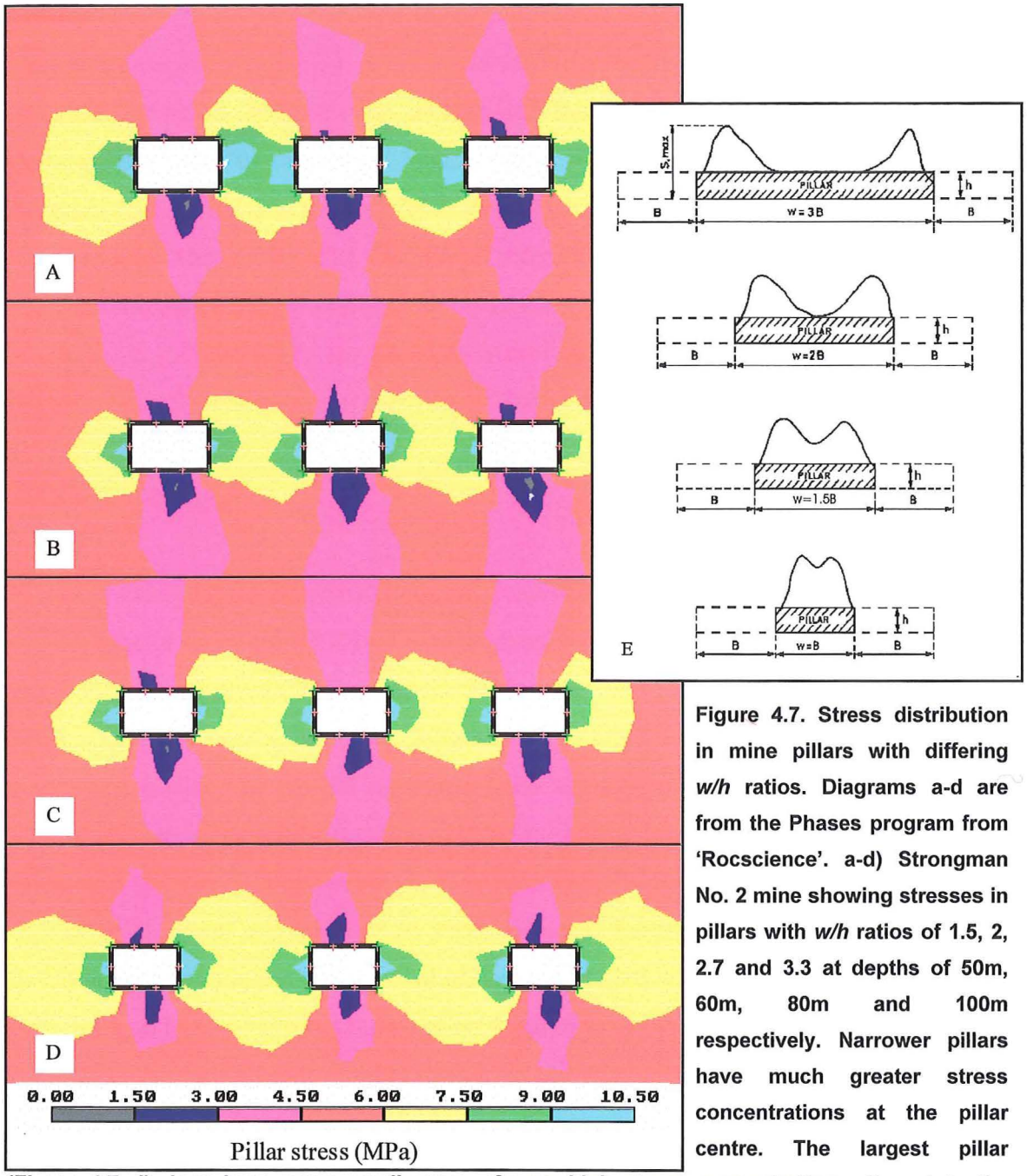

Figure 4.7. Stress distribution in mine pillars with differing *w/h* ratios. Diagrams a-d are from the Phases program from 'Rocscience'. a-d) Strongman No. 2 mine showing stresses in pillars with *w/h* ratios of 1.5, 2, 2.7 and 3.3 at depths of 50m, 60m, 80m and 100m respectively. Narrower pillars have much greater stress concentrations at the pillar centre. The largest pillar (Figure 4.7 d) does have some small areas of very high stress concentration adjacent to the excavation, but these dissipate rapidly. White areas are excavations; e) Schematic diagram showing how applied stress is concentrated in the pillar as *w/h* ratio changes (after Holland, 1958).

The level of stress within a pillar is determined by the overburden depth and percentage extraction of the coal. The way this stress is distributed through the pillar is determined by the *w/h* ratio, seam dip, and pillar shape in plan. As pillar width and *w/h* ratio increases the stress in the centre of the pillar decreases, while the stress in the sides and corners of the excavation remains relatively constant (Figure 4.7). The edges of the pillar where the

stress is concentrated will form the outer yield zone, while the centre where the stress is least will comprise the solid core, which is the main load-bearing portion of the pillar. As *w/h* ratio increases the core zone widens and the yield zone becomes less significant, enabling the pillar to take more load. This is illustrated in Figure 4.7a-d where *w/h* increases from 1.5–3.3 at depths which they would be used (50m, 60m, 80m and 100m). Even though the overburden thickness increases, the pillar stress adjacent to the excavation remains largely constant and is highest at mid height of the excavation. This is where the highest stress in the pillar are recorded. The stress in the centre of the pillar decreases rapidly with increasing *w/h* ratio (Figure 4.6e).

4.4.2 Pillar Design

Factor of safety (with regard to pillars) is a ratio of pillar strength to pillar load (equation 4.15). A factor of safety (FOS) <1 is considered to be unstable, while a FOS value of 1.0 has a 50% probability of failure. As the FOS value increases, the probability of workings being stable increases accordingly. Pillars in this study have been designed to a factor of safety of 1.6 which means the estimated pillar strength is 60% higher than the expected load upon that pillar, which accounts for the variability of coal strength, and accordingly, pillar strength. Hebblewhite *et al.* (1997) estimate that this equates to a failure probability of 3 in 1000, which is considered an acceptable risk. Investigations by Bieniawski (1984) in US coal mines suggest that no coal pillars have failed with FOS >1.3. Similar work by Salamon and Munro (1967) gave no pillar failures with FOS >1.5. Both authors estimated the FOS using their respective pillar design equations.

$$\text{FOS} = \frac{Pillar\ strength}{Pillar\ load} \qquad (4.15)$$

The optimal sizes for square pillar for each of the seams studied are presented diagrammatically in Figure 4.8a-g (map pocket), and are summarised in Table 4.3. The pillars have been sized using the squat and slender variations of equations 4.9 and 4.10. These figures show the smallest square pillar that can be used at any depth likely to be encountered (c. 25-300m) during the mining of each respective seam giving a FOS = 1.6. These design charts are valid for seam dips of up to 20°, but no account has been made for

the effect of seam dip on the coal strength (i.e. the average strength of each seam has been used) which in some cases can be very pronounced (Figure 2.6). When seam dip is above 20° pillar strength becomes increasingly dependant on the shear strength of the seam. In steeply dipping seams the pillar may fail by shearing when the seam dip exceeds the friction angle of the weakness planes which is c. 24° for coal in the Greymouth Coalfield. This is detailed in section 4.5. Pillar sizes for main roadways are given in Table 4.4.

Location	Optimum Square Pillar Size (m) Bishop Block		Roa	Spring Creek		Strongman No. 2		Terrace
Seam	Kimbell	Morgan	Kimbell	D	Main Upper	D	E	No. 4
Depth (m)								
20	6.0	6.2	13.5					
30	7.6	7.7	18.6					
40	8.8	9.6	22.8					
50	10.4	11.6	26.5					
60	11.8	13.2	29.7					
70	13.3	14.4	32.7			6.7	6.7	
80	13.9	15.5	35.6			7.5	7.5	
90	14.3	16.7	38.3			8.4	8.4	
100	15.3	18.1	40.8			9.1	9.1	
110	16.4	19.4	43.3			10.0	10.0	
120	17.4	20.6	45.5			10.8	10.8	
130		21.8	47.8			11.5	11.5	
140		23.0	49.9			12.3	12.3	
150		24.0	52.2	20.9		13.3	13.3	
160		24.8	54.2	22.0		14.3	14.3	
170			55.8	23.9		15.1	15.1	28.0
180				23.8		15.9	15.9	29.1
190				24.7				30.1
200				25.5	27.6			31.3
210				26.2	28.4			32.3
220				27.1	29.1			33.2
230				27.8	29.9			34.2
240				28.5	30.6			35.1
250				29.2	31.2			36.1
260					32.1			37.1
270					32.8			
280					33.4			
290					34.1			
300					34.9			

Table 4.3. Optimum square pillar size for production (panel) pillars.

The pillar design charts presented in Figure 4.8 (map pocket) use roadway widths of 5m and mining heights of 3m for Strongman No. 2, Spring Creek and Bishop Block. Roadways 2m wide and a mining height of 3m have been used for the Terrace mine, while roadways of 2m and a mining height of 2.5m have been used for the Roa mine. These pillar sizes will need to be modified to take into account localised effects such as faulting and sheared zones which could not be considered in this study.

Location	Optimum Square Pillar Size for Main Roadways (m)							
	Bishop Block		Roa	Spring Creek		Strongman No. 2		Terrace
Seam	Kimbell	Morgan	Kimbell	D	Main Upper	D	E	No. 4
Depth (m)								
20	6.8	7.5	18.8					
30	9.0	10.1	24.1					
40	11.3	12.6	28.7					
50	13.3	13.9	32.8			7.9	7.9	
60	14.6	14.2	36.4			9.0	9.0	
70	15.9	15.7	39.8			10.1	10.1	
80	17.3	17.4	43.1			11.2	11.2	
90	18.9	19.2	46.1			12.3	12.3	
100	20.2	20.7	48.9			13.4	13.4	
110	21.6	23.6	51.6			14.5	14.5	
120	22.8	24.9	54.3			15.6	15.6	
130		26.1	56.9			16.7	16.7	
140		27.4	59.2			17.8	17.8	
150		28.5	61.7	25.4		19.0	19.0	
160		29.6	64.1	26.4		20.0	20.0	
170			66.3	27.5		20.9	20.9	33.7
180				28.4		21.9	21.9	34.8
190				29.3				36.1
200				30.1	32.6			37.2
210				31.1	33.6			38.3
220				31.8	34.6			39.4
230				32.8	35.6			40.6
240				33.6	36.4			41.6
250				34.3	37.3			42.7
260					38.1			43.6
270					38.9			
280					39.7			
290					40.6			
300					41.3			

Table 4.4. Optimum square pillar size for main roadways

Pillar size in general shows a steady increase with increasing overburden thickness. Pillar size requirements tend to increase more rapidly when the overburden thickness is low (<60m), but depends on the coal strength. The most rapid size increases are greatest in the Roa Mine which has the lowest compressive strength seen in this study ($UCS_{equivalent}$ = 1.3 MPa). An overburden thickness of 50m requires an increased pillar size of 1m for every further 3m increase in depth. When the depth increases to 150m a 1m increase in pillar size is required every 4m. Pillar size requirements for each of the other locations increases at a relatively constant rate. Spring Creek and Strongman No. 2 Mines require a 1m pillar width increase only with every c. 10m increase in overburden depth.

Equation 4.10 (Bieniawski) gives lower estimate of the required pillar size when the *w/h* ratio is low (c. 5), but when the *w/h* increases to above 5 the squat pillar formulas are used. At this point the Salamon equation becomes the more conservative. This continues until the *w/h* ratio increase to above 16 where the Bieniawski equation once again gives the lowest estimates (Figure 4.8g).

No pillars have been designed with $w/h < 2$ in this study due to the increased risk of failure in pillars of such dimensions. There is evidence from around the world of pillars with $w/h < 2$ failing even though they may have been designed to a high factor of safety (>1.5). This most likely results from either the presence of through going local defects and/or spalling from the sides of the pillar. In such a narrow pillar the failed coal around the pillar edges is likely to be insufficient to provide confinement to the pillar core. Figure 4.7a illustrates the level of stress at the centre of a pillar with $w/h = 1.5$. The stress here is 80% of the maximum stress present in the pillar compared with 70% when $w/h = 2$ and 50% when $w/h = 3.3$. Given this high level of stress, spalling would be expected to penetrate much deeper into the centre of the pillar than would occur in a larger pillar. Much lower stress levels are present in the roof and floor than the pillar sides. Stress is usually 1.5-3.0 MPa in the centre of the floor, and are usually slightly higher in the roof (c. 2.0-3.5 MPa). At the mid-height of the pillars adjacent to the roadway stresses can be as high as 10.5 MPa.

4.4.3 Shape Effect

The effect of using different pillar geometries has been investigated using examples involving the slender and squat pillars. The Kimbell seam from the Bishop Block and the Spring Creek D seam were analysed using six pillar geometries (one square and five rectangular) with a roadway width of 5m and mining height of 3m. It can be seen from Tables 4.5 and 4.6 that no advantage in terms of extraction ratios can be gained by using rectangular pillars. For the Spring Creek D seam at a depth 200m, a 24m square pillar would yield 31.5% extraction with FOS = 1.75 using equation 4.9 (This is over-designed and only used for the purpose of an example. Refer to Figure 4.8c for actual optimum size). If a rectangular pillar of 22m x 26m is used, the pillar volume is $12m^3$ lower (c. 1%) giving an initial extraction of 31.7%. This is a 0.2% extraction increase but gives a slightly lower FOS of 1.74.

Pillar strength is calculated using pillar width (square pillars) or effective width (rectangular pillars), so any decrease in the pillar width needs to be accompanied by an increased length to maintain the pillars load carrying capacity. This however a more

favourable stress distribution, a lower initial extraction percentage is obtained and so it is not a viable option.

Pillar Dimensions (m)	Pillar Volume (m^3)	Extraction Ratio %	Pillar Stress (MPa)	w_{eff} (m)	Pillar Strength (MPa) (Eqn 4.10)	Pillar Strength (MPa) (Eqn 4.9)	FOS (Eqn 4.10)	FOS (Eqn 4.9)
10x10	300	55.5	2.81	10.00	3.86	5.00	1.37	1.78
8x12.5	300	56.0	2.84	9.76	3.80	4.96	1.34	1.75
8x12	288	56.6	2.88	9.60	3.76	4.92	1.31	1.71
8x11	264	57.7	3.02	9.26	3.68	4.84	1.22	1.60
7x13	273	57.9	2.97	9.10	3.64	3.64	1.23	1.62
7x12	252	58.8	3.04	8.84	3.57	4.74	1.17	1.56

Table 4.5. Estimates of pillar strength and factor of safety for the Bishop Block Kimbell seam using different pillar geometries at a depth of 50m.

Pillar Dimensions (m)	Pillar Volume (m^3)	Extraction Ratio %	Pillar Stress (MPa)	w_{eff} (m)	Pillar Strength (MPa) (Eqn 4.10)	Pillar Strength (MPa) (Eqn 4.9)	FOS (Eqn 4.10)	FOS (Eqn 4.9)
24x24	1728	31.5	7.30	24.00	12.81	9.05	1.75	1.24
23x25	1725	31.5	7.30	23.96	12.79	9.06	1.75	1.24
22x24	1584	32.6	7.41	22.96	12.18	8.65	1.64	1.17
22x25	1650	32.1	7.36	23.40	12.45	8.83	1.69	1.20
20x27	1620	32.5	7.41	22.98	12.20	8.63	1.65	1.16
22x26	1716	31.7	7.32	23.83	12.71	8.97	1.74	1.23

Table 4.6. Estimates of pillar strength and factor of safety for the Spring Creek D seam using different pillar geometries at a depth of 200m.

Results of underground tests on coal pillars by Wagner (1974) showed that pillars with rectangular cross section are about 40% stronger than square pillars of the same width and height. This suggests that the empirical formulas used by this study do not adequately take into account the increased strength of a rectangular pillar. Figure 4.9 illustrates the load bearing capacity of square pillars as opposed to long slender pillars. Pillar spalling occurs around the unconfined edges where roadways are cut through. These edges represent areas of minimal strength and consequently load bearing capacity. By eliminating the dividing roadway there are fewer unconfined edges allowing spalling to penetrate less of the pillar, and thus the pillar is able to carry a great deal more load. This, however, compromises the extraction ratio making rectangular shaped production pillars impractical, but this is an important concept for barrier pillars.

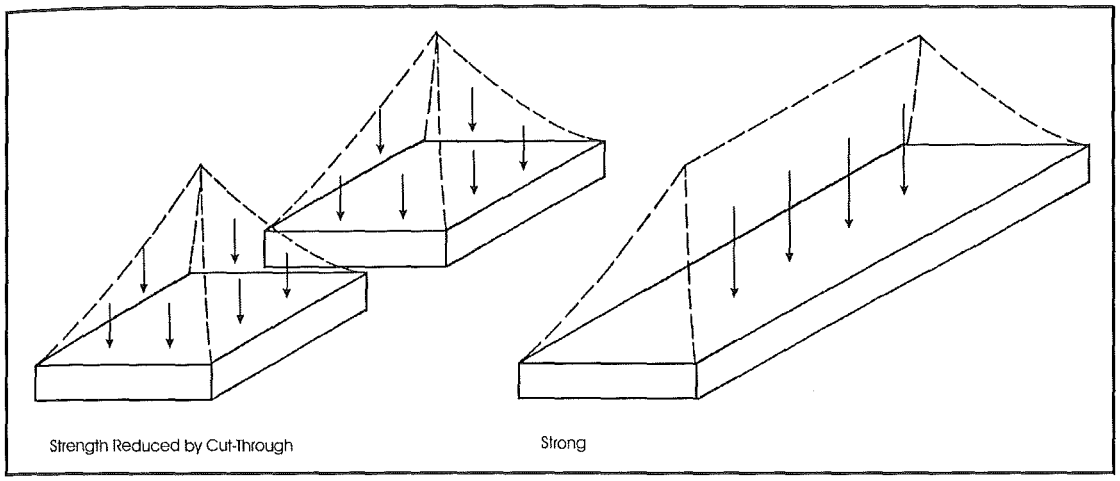

Figure 4.9. Load distribution through square and rectangular pillars (after Gale and Mills, 1995).

4.5 Pillar Design in Dipping Seams

4.5.1 Background

Coal seams in the Greymouth and Reefton Coalfields dip at various angles, usually between 10-30°. The room-and-pillar mining technique is effective up to dips of 30° (Brady and Brown, 1985), but the pillar strength equations presented earlier are not valid once seam dip reaches 20° as this is approaching the friction angle of defects in coal which is c. 24° (section 2.7). When seam dip exceeds 20° the chance of the pillar shearing along the contact with the floor rocks, shearing through the pillar itself, or along intra seam shears needs to be taken into account. In most cases some coal is retained in the mine floor and so shearing will be largely dependant only friction angle of the coal. Coal retained in the floor will often be extracted upon retreat during pillar extraction, or will be retained in the floor due to bearing capacity issues.

4.5.2 Analysis of Pillar Shearing

For this analysis, two cases will be used. The worst case scenario where a continuous shear plane though the pillar is assumed, such as a bedding plane shear. This will use a friction angle of 24° which is the value for a single continuous plane determined by direct shear (section 2.7). The best case scenario is where shear failure occurs on a series of interconnected defects such as cleats. This has a much higher friction angle of c. 50°

determined by triaxial testing (section 2.5). Both of these friction angles appear to only vary by ± 2° across the coalfield, although the friction angle of coal (for a single failure plane) from the Spring Creek mine was not tested by this study, but it is expected to be lower due to alternate banding present at this location. The factor of safety against pillar shearing can be estimated from the following equation:

$$F = \frac{cA + (W\cos\beta)\tan\phi}{W\sin\beta} \qquad (4.16)$$

where: c = cohesion (MPa) ϕ = friction angle

A = pillar area β = angle of seam dip

W = pillar weight = γh (including the weight of the pillar and the overburden it supports)

Example 4.1: The Strongman No. 2 D seam has been presented here as an example using a depth of 100m and a pillar size of 10m ×10m, with the seam dipping at 10°.

c = 0.33 MPa $W = \gamma h$ = 2486 kN

A = 10m×10m = 100m^2 β = 10°

γ_{coal} = 12.0 kPa, $\gamma_{overburden}$ = 24.5 kPa. ϕ = 24°

h_{coal} = 3m, $h_{overburden}$ = 100m.

$$F = \frac{0.33\times100 + (2486\cos10)\tan24}{2486\sin10} = \frac{1123}{432} = 2.60$$

Table 4.7 gives the factor of safety against pillar shearing for seam dips of 5-35°. For the worst case scenario where failure occurs on one continuous plane (ϕ = 24°), the factor of safety falls below 1.6 (same as pillars are designed to) when the seam dip exceed c. 16° which is low for many of the seams in the Greymouth and Reefton Coalfields. If a single failure plane is to be assumed (this is unlikely) the factor of safety drops to 0.66 for a seam dip of 35°.

Seam Dip	Factor of Safety $\phi = 24^\circ$	$\phi = 50^\circ$
5°	5.24	13.78
10°	2.60	6.84
15°	1.71	4.50
20°	1.26	3.31
25°	0.99	2.59
30°	0.80	2.09
35°	0.66	1.73

Table 4.7. Factor of safety against shear failure in pillars at different seam dips. $\phi = 24^\circ$ is the worst case scenario where there is one continuous failure plane. $\phi = 50^\circ$ is the best case scenario where the failure is controlled by a series of discontinuous but interconnected defects.

A much more likely scenario is to assume that there are a series of smaller discontinuous but interconnected weakness plane along which shearing may occur. From triaxial testing (section 2.5) the friction angle for such a situation was deemed to be c. 50°. This scenario sees the factor of safety increase significantly, only falling below 2.0 when seam dip exceeds 30° and does not fall below 1.6 in the range of seam dips expected in the Greymouth and Reefton Coalfields.

As overburden thickness increases the pillar size also must increase. If the pillars are designed according to the optimum size as given by Figure 4.8, the factor of safety against shearing appears to remain relatively constant irrespective of depth.

4.5.3 Optimum Pillar Size for Specific Dip Intervals

Coal strength is a function of loading direction and so the strength of a dipping coal seam may be significantly different from the strength of a horizontal seam. Coal is weaker in dipping seams due to the slip occurring along bedding planes. A detailed analysis of the effect of loading direction on coal strength for the Spring Creek D seam is presented in Figure 2.6. This resulted in the use 5° dip intervals when designing pillars for the Spring Creek D seam (Figure 4.10). The Spring Creek Mine displays a large range of seam dips ranging from 6-28°. As seam dip increases, slip at the intersection between bands becomes more likely, but will still depend on the friction angle and cohesion. There is not enough detailed information is available for other seams to design pillars for specific seam dips. The strengths of the two Spring Creek seams are expected to show the greatest variation

with changing seam dip due to the prominent banding. Less variation in coal strength with seam dip would be expected in other seams where the banding is less evident. More investigation needs to be conducted for these seams before pillars can be designed for specific seam dips such as those shown in Figure 4.10.

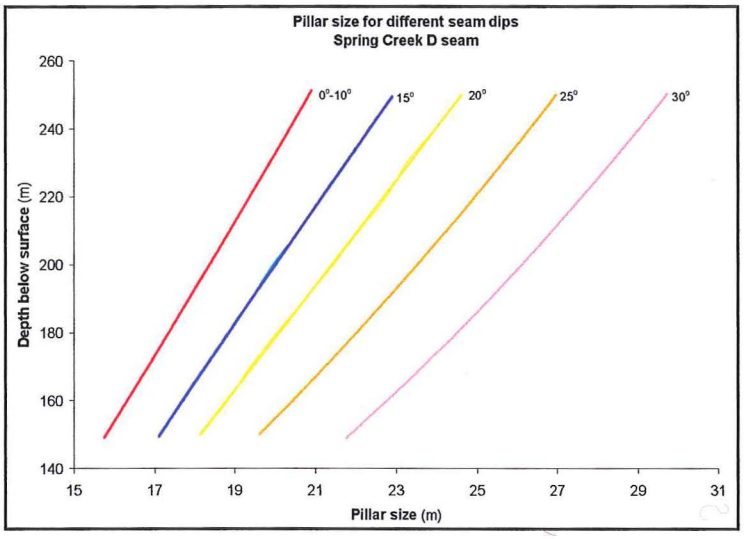

Figure 4.10. Pillar sizes for Spring Creek D seam at different seam dips. This plot uses the mean values of the Bieniawski (equation 4.12) and Salamon (equation 4.13) methods. Individual plots are given in Appendix 9, Figure A9.1a-e. Strength difference for each seam dip is derived from Figure 2.6. Coal strength is considered to be constant when seam dip is 0-10° and then decreases with increasing seam dip.

In the Spring Creek D seam a dip of 25° ($\beta = 65°$) would decrease the coal strength by up to 25% (Figure 2.6). This seam requires an increase in pillar size of 1.9m (on average) for every 5° increase in seam dip, but this increases slightly with increasing depth (Figure 4.10). Therefore at the maximum expected seam dip (c. 28°) a pillar c. 6m larger would be required than for the lowest seam dips (c. 6°). The detailed information required for estimating pillar size at specific seam dip was only available for the Spring Creek D seam.

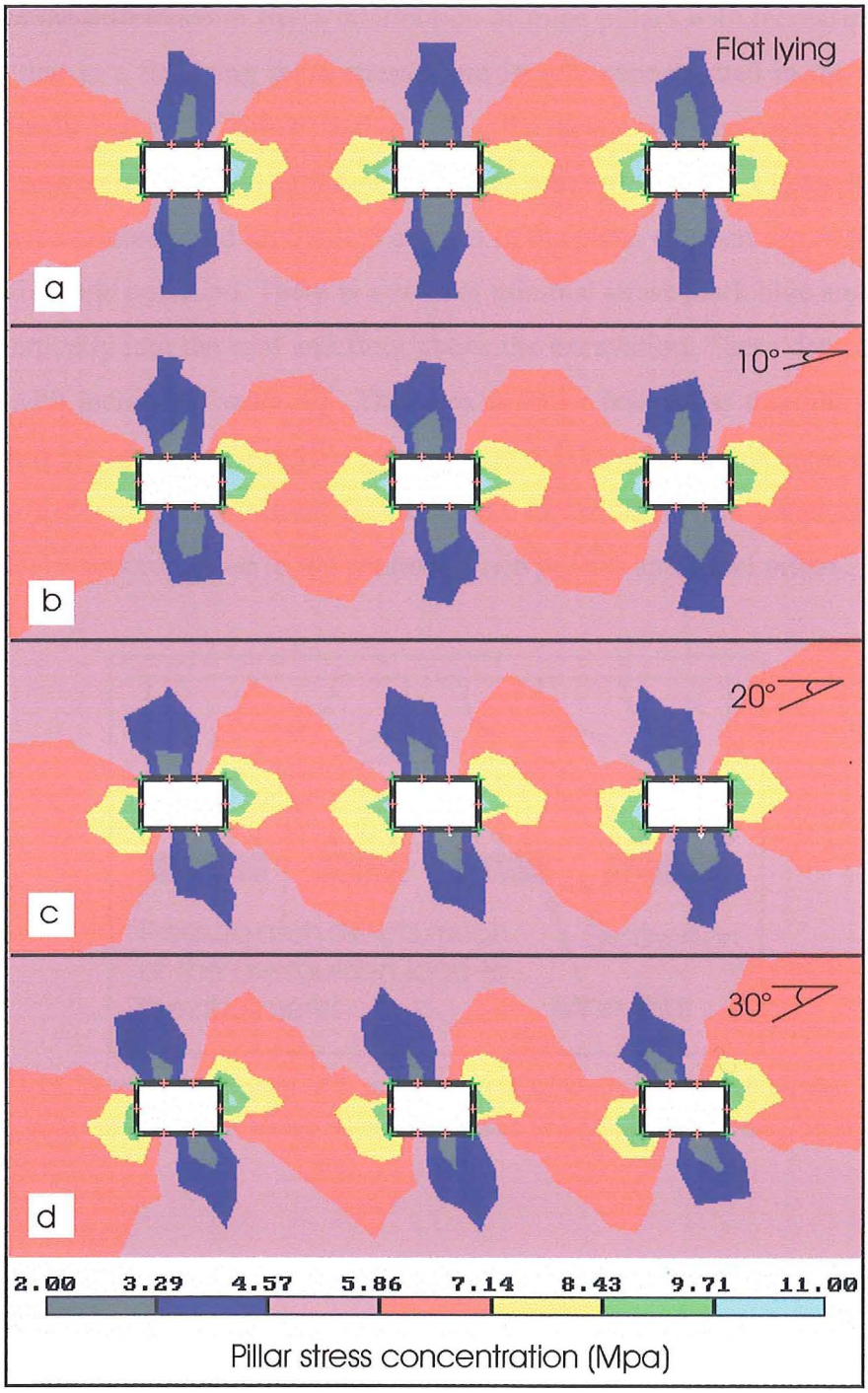

Figure 4.11. Stress distribution through mine pillars with increasing seam dip. a) seam dip 0°; b) seam dip 10°; c) seam dip 20°; d) 30°. The Strongman No. 2 D seam with a 10m square pillar is used here as an example. White areas are excavations (roadways). Stress becomes increasingly concentrated on the corners of the excavation as the seam dip increases.

Pillars in inclined seams often fail in a different manner to those in horizontal seams (Coates, 1965) due to the different stress distributions which are concentrated near the floor on the up-dip side of the pillar and at the roof on the down-dip side. Figure 4.11

demonstrates the difference in stress distribution of mine pillars with increasing seam dip. This shows that in a flat lying seam stresses are largely concentrated in the walls of the excavation contributing to pillar spalling. As the seam dip increases the zones of maximum stress concentration (light blue and green areas of Figure 4.11) are reduced. The stresses become concentrated on the two corners in the plane of seam dip, while the other two corners become unloaded. There is a zone of minimal stress (dark blue and grey areas) extending vertically into the roof and floor above the excavation. These decrease in width and height with increasing seam dip. This area is under less stress than the surrounding country rock (pink areas; 2.0-4.5 MPa compared to 4.5-5.9 MPa). This areas of low stress exist due to a pressure arch which forms across the width of the panel (Figure 4.12) redirecting the overburden load to the abutments (rib pillars) and panel pillars.

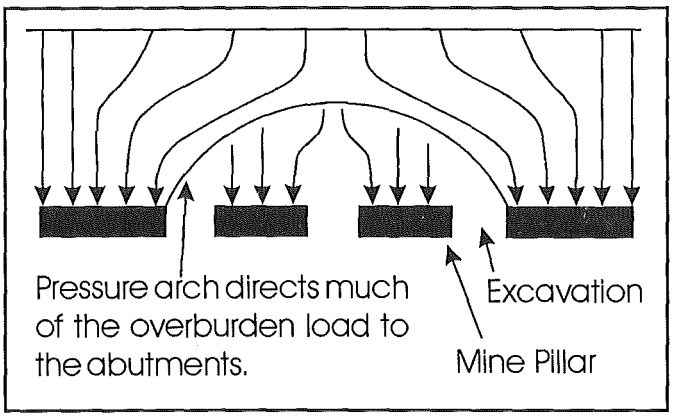

Figure 4.12. Schematic diagram of a pressure arch which redirects overburden stress causing areas of low stress above mine excavations (modified after Yardley, 1996).

4.6 Pillar Failure

4.6.1 Background

Documentation of pillar failure is very difficult to find for any coalfield, and the author could only obtain reports specific pillar failures at one location within New Zealand coalfields, being the Liverpool mines (section 4.6.3). Crushing of coal pillars in the Paparoa mine (adjacent to the Roa mine in this study; Map 1) was reported by Gage (1952, p. 116) 'owing to the softness of the coal', where the pillars continually crush and roof and floor squeeze together. Places driven to full width may close up almost entirely'. This

most likely occurred simply because the pillars were not large enough given the weakness and sheared nature of the coal in this area. Floor heave is known to have occurred in the Terrace Mine and the Liverpool No. 2 and 3 Mines. A detailed review of bearing capacity problems in the Terrace Mine is presented in section 4.7. Not enough details were available to study this problem in the Liverpool Mines.

4.6.2 Modes of Failure

Three dominant modes of pillar failure can be observed in mine pillars, all of which were seen whilst determining the unconfined compressive strength of coal cubes (section 2.3). Fretting or spalling (Figure 4.13a) was the most common type of failure, while yield (slow plastic deformation; Figure 4.13c) was commonly observed in the softer coals, especially from the Roa mine (UCS = 1.6 MPa). Pillar shearing (Figure 4.13b) occurs less often and is largely confined to narrow pillars (*w/h* <3). Pillar fretting is common due to stress concentration occurring at the edges and corners of the pillar (Figure 4.7). This will often strengthen the core of the pillar rather than leading to complete pillar failure (Section 4.3.1), especially at higher *w/h* ratios (>~5). Wagner (1992) illustrated that the depth to which spalling penetrated the pillar was dependent on the factor of safety to which the pillar was designed, and was largely independent of overburden thickness.

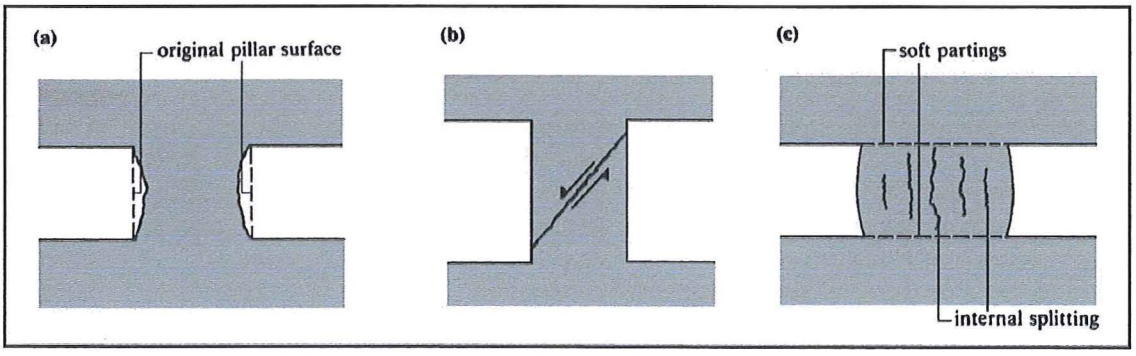

Figure 4.13. Common modes of pillar failure (after Brady and Brown, 1985). a) Pillar fretting = Spalling from the sides of the pillar, and occurs in massive rock with high *w/h* ratios; b) Inclined shear failure, which occurs in jointed rock with low *w/h* ratios; c) Pillar yield by axial splitting within the pillar, which occurs in soft highly deformable rock.

The collapse of one pillar will cause load transfer onto the surrounding pillars, which may in turn collapse (Hoek and Brown, 1980) due to inability to support the increased load. Many deaths have been caused worldwide by the collapse of multiple pillars induced by load transfer after the failure of a few. As an extreme example of this, in 1960 4400 pillars collapsed in a five minute period and 7500 collapsed within a few hours killing all 437 underground workers at the Coalbrook Colliery in South Africa (Hebblewhite *et al*, 1997). Mines are now divided into panels separated by rib pillars which are wider than standard pillars, and extend the length of the panel. These rib pillars isolate each panel limiting the extent of major collapse events. Pillars with *w/h* ratios >10 are unlikely fail except for punching into the floor or roof in very weak strata (Wagner, 1974; Galvin, 1992). Pillars of such dimensions in this study occur in the Roa, Terrace and Spring Creek mines.

No pillars with *w/h* ratio below 2 should be used at any location for long term support while a panel is being developed. There is evidence worldwide of pillar with such dimensions, even with adequate factors of safety (>1.5; Bell and de Bruyn, 1999; Wagner, 1992), failing for a multitude of reasons. Narrow pillars are more prone to shearing along local defects. The high stress concentrations present in the sides of the excavations are also able to penetrate further into the core of the pillar (Figure 4.7) which supports the majority of the overburden load. When the strength of the pillar core is compromised by excessive spalling, the risk of pillar failure is increased. Work by Madden and Hardman (1992; reported in Bell and de Bruyn, 1999) on mine pillars in South Africa showed that 60% of failed cases had width/height (*w/h)* ratios < 2 and no failures were noted with *w/h* >4. Studies of more than forty pillars in Indian coal mines by Sheorey *et al.* (1987) showed no failures with *w/h* > 3, and the average *w/h* ratio for stable cases was 3.10. Since publication of the 1967 Salamon and Munro equation, three pillar failures have been observed with FOS >1.5, all of which had *w/h* < 2 (Wagner, 1992).

4.6.3 Liverpool Mines

Pillar failure has occurred in the Liverpool No. 2 mine, whilst floor heave has occurred in both the Liverpool No. 2 and 3 mines (both of which are now closed; Figure 1.1). Yardley (1993) concluded that these failures could be 'attributed to poor mining practices, in

particular inadequate pillar sizes'. Yardley notes three locations where the pillars had a factor of safety < 1.6 with *w/h* of 4.7-7.0 (Table 4.8; calculated using the Salamon-Munro method).

Section	Depth (m)	Pillar Width used (min)	*w/h*	FOS (Yardley, 1993)	Required pillar size
Andersons Dip (LP2)	344	12-15m	5.6-7.0	1.2-1.4	24m
4A Coal Dip (LP2)	442	15m	7.0	1.1	27.5m
Custs Dip (LP2)	330	10-15m	4.7-7.0	1.1-1.5	23.5m
Morgan Seam (LP3)	350	20m	9.4	1.6	25m
Sub-Morgan Seam (LP3)	309	17m	8.0	1.7	23m

Table 4.8. Pillar sizes used and those required in the Liverpool Mines pillar failure. LP2 = Liverpool No. 2 mine. LP3 = Liverpool No. 3 mine.

Back calculations conducted by this study from the factor of safety and pillar dimensions given by Yardley determined that a σ_c of c. 20.0 MPa was used the strength of the coal seam. This author believes that this strength is vastly overestimated and a new value of σ_c = 10.0 MPa (estimated from Figures 3.1, 3.3a and b) is believed to be more representative, though still high. From this value the pillar sizes required to give the recommended factor of safety of 1.6 were calculated. These range from 23.5-27.5m depending on the depth of the seam (Table 4.8). Table 4.8 shows the minimum pillar width that was used at each location, but Yardley alludes to a 20m×20m pillar being most commonly used, which he suggests is stable to a depth of 350m. Calculations by this study estimate that pillars of these dimensions would only be stable to a depth of 245m. A lack of cohesion and friction angle data prevents an analysis of the floor heave problems at these locations.

4.7 Bearing Capacity Failure of Floor Rocks

Bearing capacity failure is the inability of floor rocks within a mine to carry the overburden load transferred through the mine pillars. Pillars push downward into the floor and the weak floor strata is squeezed out, resulting in floor heave (Figure 4.14). Rockaway and Stephenson (1982) suggest that once this occurs the load previously carried by the failed pillar is transferred to the surrounding pillars where the same may occur. This effect may lead to complete closure of roadways if not effectively designed against. Floor heave

commonly occurs in coal mines throughout the world as many have a weak floor material termed 'fireclay' beneath the coal.

Floor heave is a considerable problem in the No. 4 seam of the Terrace mine. Pillar crushing was seen as early as 1949 (when mining depth was 213m) while floor heave was first reported in 1951 (Fowke, 1998). The floor consists of a weak fireclay or fine-grained mudstone (UCS_{dry} = 5.7 MPa) which loses a considerable amount of its strength (estimated to be ~50% by Field, 1998) upon saturation. This effect is termed moisture softening and is defined by Marino and Choi (1999) as:

> 'The reduction in the strength and stiffness of the rock as the result of an increase in moisture content of the overall mass'.

Field reports that floor heave was especially bad when coal was mined down to the fireclay contact, or when areas of the mine were flooded to control heating (the No. 4 seam is said to be the most susceptible to spontaneous combustion in New Zealand). To combat the problem of floor heave 1m of coal is retained in the floor, preventing excess moisture reaching the mudstone. In the past, before adequate mine design was carried out, mine pillars were sized as 20m x 20m irrespective of depth. Yardley (1998) reports floor heave of 0.6m at a depth of 215m, but gives no indication of how recently this may have occurred. In Yardley's calculation of the FOS against floor heave no account was made for the effect of seam dip on the bearing capacity.

When looking at bearing capacity in mines, the problem can be treated as a soil mechanics problem, and the pillar and floor treated as a shallow foundation type situation, where the overburden is the applied load, Q. By applying the bearing capacity formula given by Brady and Brown (1985) as Equation 4.17, the strength of the floor can be determined with regard to the load applied to it. Thus, once optimum pillar width has been determined (Section 4.4) the bearing capacity needs to be calculated in order to determine if the floor is strong enough. The applied bearing pressure must not exceed the safe bearing capacity, q_s, which is the ultimate bearing capacity, q_{ult}, divided by an appropriate factor of safety (Barnes, 1995). An FOS of 2.0 is recommended by Bieniawski (1992). This value however cannot be achieved at the Terrace mine, especially as the dip increases.

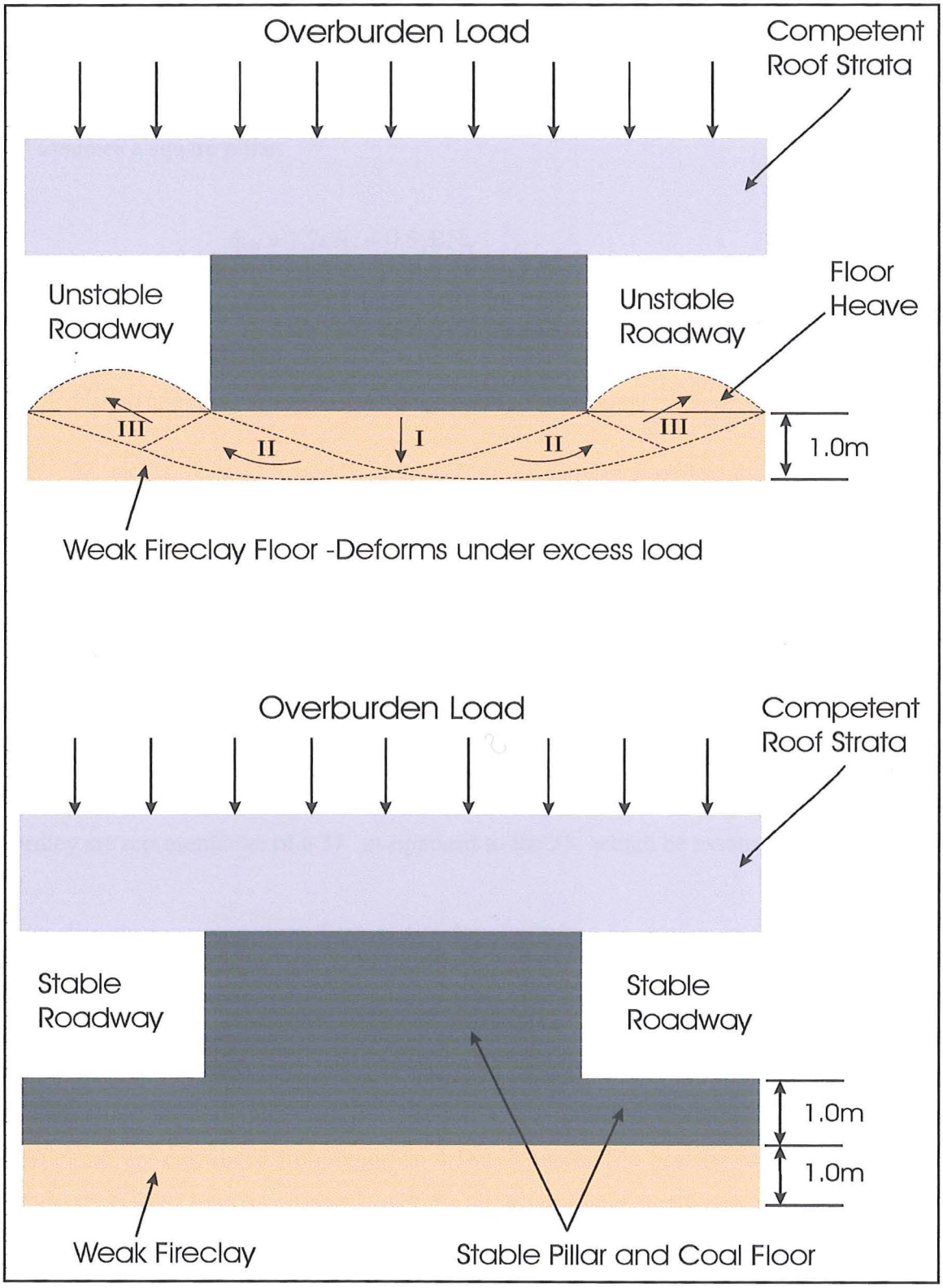

Figure 4.14. Schematic diagram of the effects of weak floor strata resulting in bearing failure of coal pillars in the Terrace mine. Top figure shows occurrence of floor heave after the fireclay floor becomes saturated and loses its strength (modified after Barnes (1995) and Brady and Brown (1985)). Bottom figure shows mitigation of this effect by leaving one metre of coal in the floor, thus not allowing the fireclay to become saturated.

It is beyond the scope of this study to investigate the properties of the fireclay, hence values for cohesion and friction angle are taken from Yardley (1998). The bearing capacity of a mine floor is calculated using equation 4.17 (after Brady and Brown, 1985) and assumes a square pillar.

$$q_{ult} = 1.2cN_c + 0.5\gamma BN_\gamma \qquad (4.17)$$

where: c = cohesion of fireclay (162 kPa dry† and 84 kPa saturated†).

$N_c = (N_q\text{-}1)\cot\phi$, $N_\gamma = 1.8(N_q\text{-}1)\tan\phi$, and $N_q = \left(\frac{1+\sin\phi}{1-\sin\phi}\right)e^{\pi\tan\phi}$

N_c = 46.1, N_γ = 33.9, and N_q = 33.3. Bearing capacity coefficients as function of ϕ.

ϕ = Friction angle of fireclay (35°)‡.

B = pillar width (m)

γ = unit weight of fireclay = 19.62 kPa.

† Calculated by back analysis from values reported in Yardley (1998). Yardley reports a c_{dry} value of 127 kPa calculated using values of N_c = 55 and N_γ = 40 which were too high for the assumed friction angle resulting in a lower value of cohesion. The values used by Yardley are representative of a 37° as opposed to the 35° which he assumed.

‡ Not directly measured from Terrace fireclay, but taken as similar to that of the Huntly mine (after Yardley, 1998).

Dip of No. 4 seam at Terrace mine is typically 15-25°, so the bearing capacity has been calculated for 5° intervals (15°, 20° and 25°). For inclined loads the bearing capacity coefficients are calculated from equation 4.18a, b and c. The bearing capacity coefficient N_γ' drops rapidly with increasing seam dip as it is related to friction angle. As the dip approaches the friction angle N_γ' drops further. This effect is amplified when the friction angle is low, as it only takes a small increase in seam dip to have a significant effect on N_γ'. The coefficients N_c' and N_q' and related to the seam dip only, and so drop more slowly.

$$N_c' = \left(1-\frac{\alpha}{90}\right)^2 N_c, \quad N_q' = \left(1-\frac{\alpha}{90}\right)^2 N_q, \quad N_\gamma' = \left(1-\frac{\alpha}{\phi}\right)^2 N_\gamma \qquad (4.18a, b \text{ and } c)$$

where: α = angle of inclination of applied load from the normal to the seam (Figure 4.15)

when dip $= 15^\circ$ $N_c' = 32.0, N_q' = 23.1, N_\gamma' = 11.1$

$= 20^\circ$ $N_c' = 27.9, N_q' = 20.1, N_\gamma' = 6.2$

$= 25^\circ$ $N_c' = 24.0, N_q' = 17.4, N_\gamma' = 2.8$

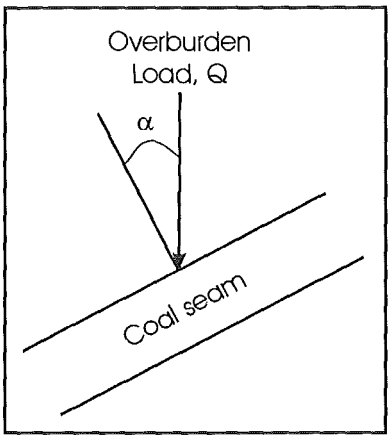

Figure 4.15. Angle of inclination, α, of the applied load from the normal to the seam.

Example 4.2: Bearing capacity of the Terrace mine floor when: Seam depth 170m, pillar width 28.0m, seam dip 15°, assuming mudstone dry. The factor of safety for depths of 170-260m and seam dips of 15°, 20°, and 25° are presented in Table 4.9.

$$q_{ult} = 1.2cN_c' + 0.4\gamma BN_\gamma'$$
$$= (1.2\times162\times32.0) + (0.5\times19.62\times28\times11.1)$$
$$= 9263.4 \text{ kPa}$$

$$F = \frac{q_{ult}}{Q} = \frac{9263}{4400} = 2.11$$

where Q = overburden load (kN)

Example 4.2 shows that at a depth of 170m (current depth of workings) and a seam dip of 15° the optimum pillar size taken from Figure 4.8f gives a factor of safety against bearing capacity failure of 2.11. However for the same depth but with a seam dip of 25° the FOS

falls to 1.24, well below the recommended value. When the depth of workings increases to 260m (next stage of development) the FOS falls almost to a value of 0.84 when seam dip is 25°. This means that pillars have a greatly increased risk of failure by punching into the floor, and the solution to this therefore is to increase pillar size to maintain floor stability. Figure 4.16 gives factor of safety values for the optimum pillar size (taken from Figure 4.8f) for seam dips of 15°, 20° and 25°. These show a steady decline in the factor of safety with increasing depth, and when the seam dip is 25 it is difficult to maintain a FOS value >1.

Depth (m)	Pillar size	Seam Dip 15°	20°	25°
		Factor of safety		
170	28.0	2.11	1.62	1.24
180	29.1	2.04	1.57	1.19
190	30.1	1.95	1.49	1.13
200	31.3	1.84	1.40	1.06
210	32.3	1.79	1.36	1.02
220	33.2	1.72	1.30	0.97
230	34.2	1.66	1.25	0.93
240	35.1	1.60	1.21	0.90
250	36.1	1.57	1.18	0.87
260	37.1	1.51	1.13	0.84

Table 4.9. Optimum pillar size taken from Figure 4.8f for seams dips of 15°, 20° and 25° with the corresponding factors of safety against bearing capacity failure. For the worst case of 260m depth and 25° seam dip there is very little safeguard against bearing capacity failure. The pillar size values are the average of the Bieniawski and Salamon methods taken from Figure 4.8f.

If pillars at depths of 260m are designed to the optimum size as per Figure 4.8f, problems with bearing capacity should be expected, especially as the dip approaches the maximum expected value of 25° as the FOS falls to 0.84. It would take exceptionally large sized pillar to get the FOS above an acceptable value for a seam dip of 25° when overburden is 260m thick.

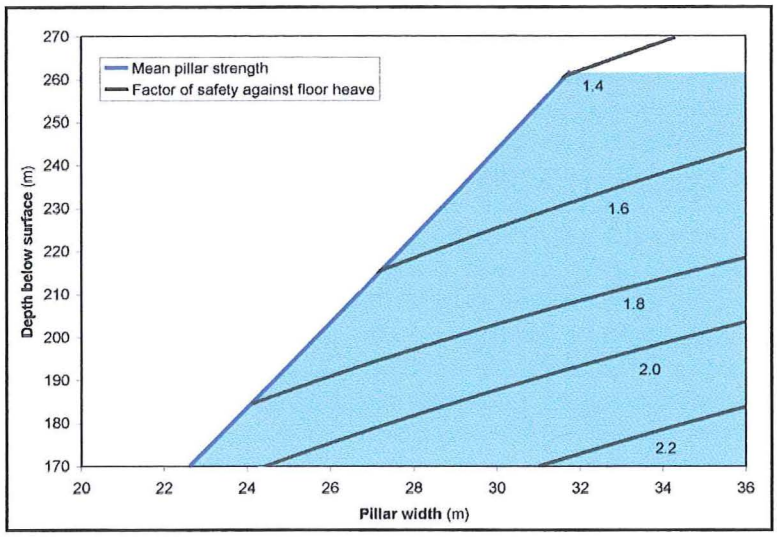

a)

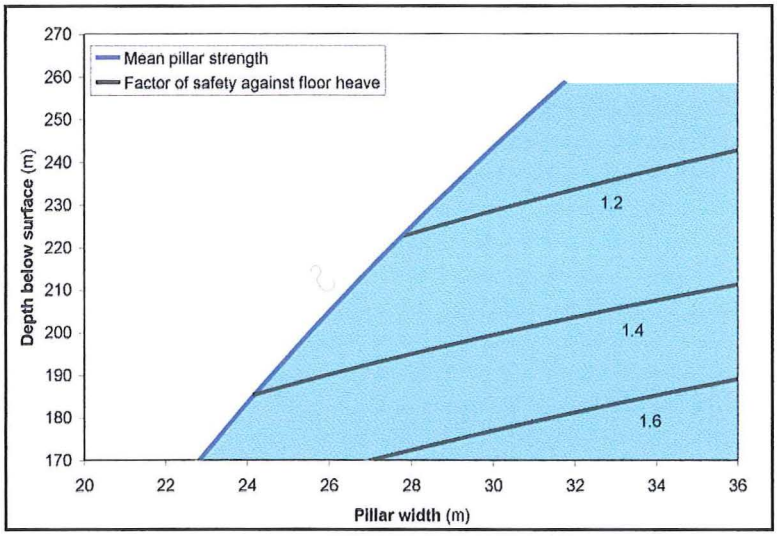

b)

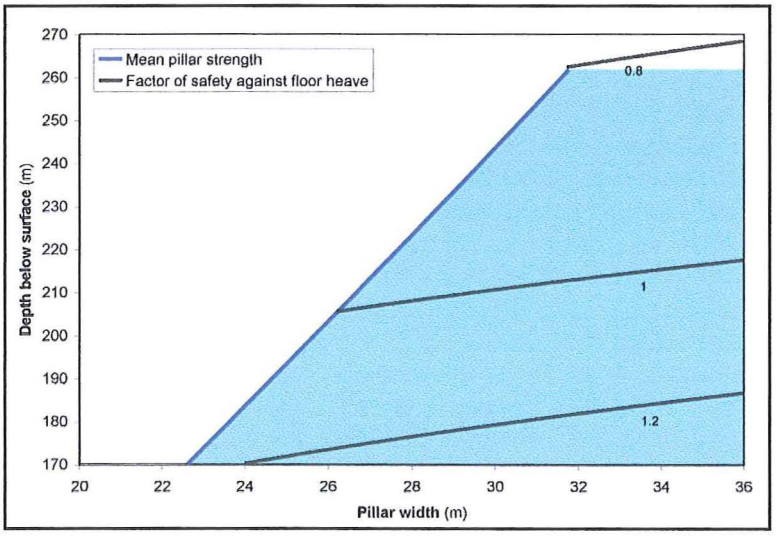

c)

Figure 4.16. Optimum pillar size for Terrace mine No. 4 seam with factor of safety against bearing capacity failure a) seam dip of 15°; b) seam dip of 20°; and c) seam dip of 25°. Shaded area gives pillars with FOS >1.6. Black lines give FOS against bearing capacity failure. The steeper these are, the easier it is to achieve the desired FOS by increasing pillar size.

It has been assumed in all previous examples that the fireclay remains dry from the protection of the coal retained in the floor. Yardley (1998) estimated that when the fireclay became wet the cohesion fell by almost 50% to 62 kPa. Calculations by this study estimate a saturated cohesion value of 84 kPa. Using the same conditions as example 4.2 (depth 170m, seam dip 15°), but with the fireclay saturated, FOS falls to 1.42 (compared to 2.11 with dry fireclay). At this point floor heave is still unlikely, but once the seam dip reaches 20° FOS falls to 1.03 and 0.72 once the dip reaches 25°. A summary of all scenarios for saturated fireclay is presented in Table 4.10.

Depth (m)	Pillar size	Seam Dip 15°	20°	25°
		Factor of safety		
170	28.0	1.42	1.03	0.72
180	29.1	0.14	1.00	0.70
190	30.1	1.34	0.96	0.67
200	31.3	1.27	0.90	0.63
210	32.3	1.24	0.88	0.61
220	33.2	1.19	0.84	0.58
230	34.2	1.16	0.82	0.56
240	35.1	1.12	0.79	0.54
250	36.1	1.10	0.78	0.53
260	37.1	1.07	0.75	0.51

Table 4.10. Factor of safety against beating capacity failure when fireclay is saturated.

4.8 Synthesis

- It is the view of the author that the sizing of pillars by any method must be conducted with caution due largely to the variability of coal strength and changing seam dips. The majority of pillar strength formulae were developed on coal seams in either South Africa or the U.S., thus they may not be directly applicable the New Zealand examples. However, studies in some Australian coalfields by Galvin (1995) confirm that these methods are applicable to Australian conditions. The methods of Bieniawski and Salamon appear applicable to a large range of conditions, and have been used successfully for many years worldwide. Finite element methods are not as simple to apply as the empirical methods, and add this the variability in a number of the input parameters such as coal strength data and then pillar design is open to interpretation.

- The pillar design equations of Bieniawski and Salamon were selected for use in this study as they are the only equations to have squat pillar variations which take into account the expected increase in strength at the core of the pillar once the *w/h* ratio increases to above 5. Pillar design must also take into account overburden thickness, coal strength and seam dip, and most pillar design equations are valid for seam dips up to 20°.

- Pillars in this study have been sized for 10m depth intervals, and in some cases for specific seam dips. Once seam dip exceeds 20°, as it often does in the Greymouth Coalfield, the factor of safety against pillar shearing needs to be taken into account. This is largely dependent on the friction angle of the coal involved, which is relatively constant across much of the coalfield. For a single weakness plane, the friction angle tends to be c. 24° but for multiple discontinuous weakness planes is much higher at c. 50°. As seam dip increases the stress distribution through the pillar changes. As dip increases the stress becomes increasingly concentrated on two corners of the pillar in the plane of seam dip while the other two corners become unloaded. Assuming multiple weakness planes, pillars are expected to remain stable with the factor of safety falling below 1.6 only when seam dip exceeds 30°.

- No pillars in this study are designed with *w/h* <2 due to the increased risk of failure at such dimensions, even though the factor of safety may appear adequate. Pillars of this size are at greater risk of failure along local defects, or by the strength of the pillar core being compromised due to penetration by spalling. The stress concentrations at the centre of narrow pillars are much greater than in wider pillars where the stress dissipates more rapidly, thus spalling penetrates further into the narrower pillar.

- Rectangular pillars of certain geometries are stronger than square pillars and have more favourable stress distributions. However, for the same factor of safety the initial percentage extraction will always be lower when rectangular pillars are used, and so square pillars are still favoured for use in partial extraction panels.

- Yardley (1996) concludes that 'pillar design cannot be considered in isolation from the rest of the mine design, for instance it is no use having stable pillars if the stress on the pillars exceeds the bearing capacity of the floor and the floor heaves'. This is especially true of the Terrace Mine where floor heave can be expected as mining depth and seam dip increases, due to the presence of a weak fireclay. Coal is stronger than the floor rocks at the Terrace Mine, so if the pillars are not of the required size, the floor may heave because of inability to support the load. At least one metre of coal needs to be retained in the floor of the Terrace mine (following the recommendation of Yardley, 1998) to ensure that the fireclay remains dry and lessen the chances of floor heave, as this material loses most of its strength and cohesion when it becomes saturated.

Chapter 5. Mining Implications

5.1 Mechanical Properties of Coal

Coal strength is very difficult to determine accurately due to its heterogeneous and discontinuous nature. A large degree of scatter is present in the results of all test methods, especially in the point load test, though this scatter decreased with increasing confinement in the triaxial tests. It is possible that the weakest samples are not represented in the strength test results, as many samples broke along cleats during preparation and were not tested. Cleats and bedding planes were seen to play a large part in the failure of the compressive strength test samples.

A great deal of the inherent weakness of coal, especially from Strongman and Spring Creek, is provided by cleating and the alternation of vitrain and clarain bands. Pronounced alternation of vitrain and durain bands in Spring Creek coal, especially the D seam, often caused shear failure in UCS testing at the intersection of these bands, especially when bedding is not perpendicular to the loading direction. In-situ the loading direction may have an angle of β up to 60° to the loading direction (i.e. seam dip = 30°) and so anisotropy is important. Anisotropy was most easily determined in Spring Creek samples where the bedding is more pronounced, as it was often impossible to determine bedding direction in Strongman No. 2 coal after block sampling. Minimum strength occurs when β = 30° (similar to most rock types; β is the minimum angle between loading direction and bedding orientation; Figure 5.1), with a decrease of c. 50%, from 13 MPa (when β = 80-90°) to c. 6 MPa (when β = 30°). This is due to the bedding planes in Spring Creek coal being very weak and subsequently slip along them occurs easily. This effect will be less pronounced at all other locations where the bedding is less obvious. As a result of the detailed data for the Spring Creek D seam mine pillars can be designed for specific dip intervals, but elsewhere it is not possible because of the lack of data on coal strength at specific loading directions.

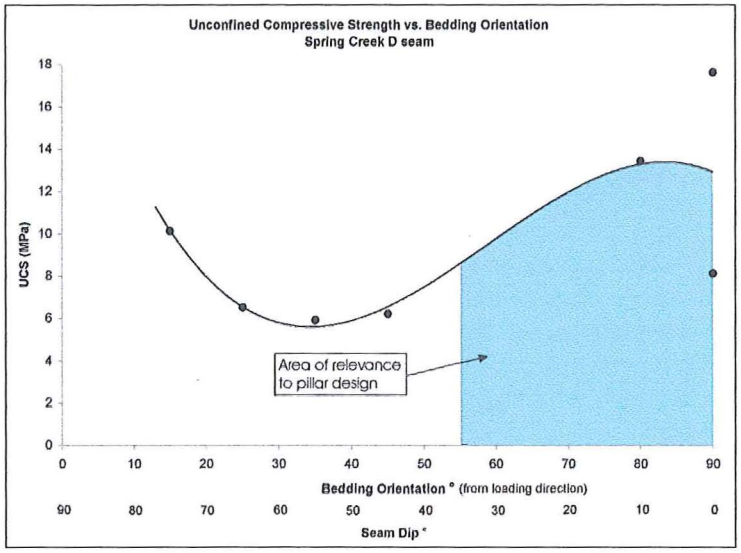

Figure 5.1. Variation of unconfined compressive strength resulting from changes in loading direction with respect to bedding orientation, β. Shaded area shows the loading directions likely to be encountered in mine pillars using a maximum seam dip of 35°.

The alternate banding in the Spring Creek coal prevented P and S waves from penetrating the samples for the determination of dynamic Young's Modulus. Though bedding was often not visible in Strongman No. 2 samples, and thus should have less effect, Young's modulus was still difficult to determine due to the discontinuous structure of the coal.

Cube samples were used as a comparison of each seam as they were deemed to be more reliable (less scatter in the results) than the point load test. Cube samples were seen to fail in the same manner as mine pillars, i.e. by spalling or fretting from the corners and sides of the samples where the stress concentration is greatest (Figure 5.2). Orientation of bedding and the presence of defects play less of a role in the failure of cube samples than core samples, though the number of defects in the samples will have an effect on its strength. Cube samples have a compressive strength which is on average two times higher than UCS. Core samples are still considered the best option for the determination of coal strength, but this is not possible at most locations due to the degree of cleating.

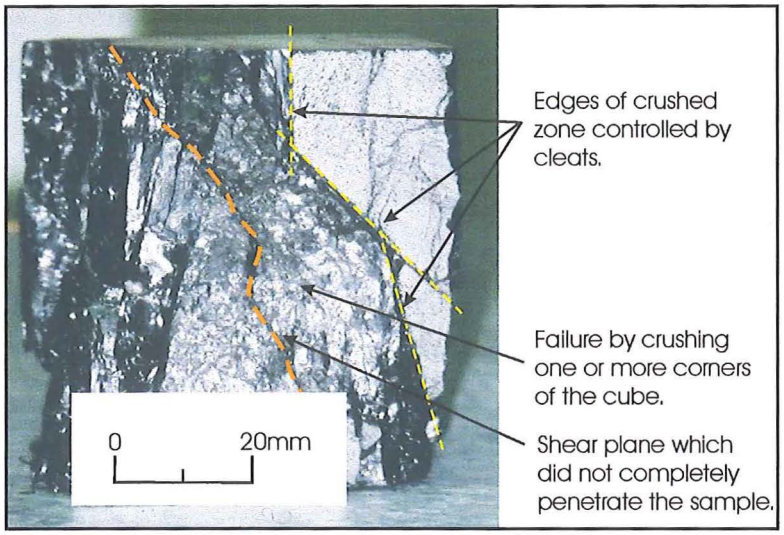

Figure 5.2. Common mode of failure in strong cube samples where one or more corners of the cube is crushed. Sample shown is from the Spring Creek Main Upper seam. Loading direction parallel to bedding, but this has no bearing on the failure mode, as samples of all orientations showed this type of failure.

Testing of cube samples (detailed in section 2.3) allowed the establishment of an equation by which a value for the unconfined compressive strength could be determined without needing core samples. Equations 5.1 and 5.2 developed in section 3.6 are a great advance in the determination of coal strength in the Greymouth Coalfield. This allowed the $UCS_{equivalent}/I_{s(50)}$ relationship to be established for all the seams involved in this study, thus allowing a more accurate determination of the compressive strength from point load test results where UCS tests were not possible. Equation 5.1 tends to overestimate coal strength as the strength decreases. To combat this equation 5.2 was introduced which lessens the overestimation significantly. Equation 5.2 gives similar results to those of Bell (1993a and b) for the Roa mine (the weakest coal in this study) with $UCS_{equivalent}$ of 1.32 MPa compared to 1.58 MPa for Bell. This equation provides a basis for the determination of the $UCS/I_{s(50)}$ relationship in other seams in the future.

$$UCS_{equivalent} = y\,(z.I_{s(50)}) \qquad \text{(equivalent to equation 3.12)} \qquad (5.1)$$

$$UCS_{equivalent} = y\,(z^{0.945}.I_{s(50)}) \qquad \text{(equivalent to equation 3.13)} \qquad (5.2)$$

where: y = core/cube strength ratio

z = cube/point load strength ratio

Table 5.1 gives a comparison of laboratory UCS values with of other methods of estimating UCS. Equation 5.2, derived from cube testing, is shown to give much more reliable estimates of $UCS_{equivalent}$ the using $UCS = 24.I_{s(50)}$ and also has a lower coefficient of variation the UCS_{actual} results.

Location	Seam	UCS_{actual}	Difference from UCS_{actual} (%)		Coefficient of Variation %		
		(MPa)	Eqn 5.2	$UCS = 24I_{s(50)}$	Eqn 5.2	UCS	$I_{s(50)}$
Spring Creek	Main Upper	7.0	+ 26	+91	30	38	55
	D	8.9	+ 26	+29	14	33	44
Strongman No. 2	E/OC	10.7	+ 16	+36	25	31	44

Table 5.1. Comparison of laboratory determined UCS values (UCS_{actual}) with other methods of estimating a UCS value.

From equation, UCS/point load relationships were determined for each seam (Table 5.2). these should be used to estimate $UCS_{equivalent}$ where no core samples are available.

Location	Seam	UCS=x.Is(50)
Bishop Block	Kimbell	*15.30*
	Morgan	*12.48*
Roa	Kimbell	*10.15*
Spring Creek	D	22.88
	Main Upper	17.18
Strongman No. 2	D	28.25
	E	23.31
Terrace	No. 4	*12.02*

Table 5.2. Summary of $UCS/I_{s(50)}$ relationships. Values in italics refer to those values derived from equation 5.2. *x* is the multiplier which is used to estimate UCS from point load strength.

5.2 Relationship between Coal Strength and other Properties

Various coal properties, including volatile matter, ash, fixed carbon, and coal rank, were plotted against unconfined compressive strength to establish other methods of accurately determining unconfined compressive strength when cores or cubes could not be used. For these plots $UCS_{equivalent}$ values were used in place of UCS for seams where no cores had been tested. The $UCS_{equivalent}$ values are calculated from equation 5.2. All of the above parameters show positive trends with coal strength, though some were better than others. In all cases the r^2 values between these properties and coal strength is greater than those between unconfined compressive strength and point load strength, making these better at estimating $UCS_{equivalent}$ values than point load strength.

$$UCS_{equivalent} = 4\times10^{11}x^{-6.04} \quad \text{where } x = \text{carbon content \%; } r^2 = 0.894 \qquad (5.3)$$

$$UCS_{equivalent} = 0.0002x^{2.98} \quad \text{where } x = \text{volatile matter \%; } r^2 = 0.800 \qquad (5.4)$$

$$UCS_{equivalent} = 9.65x - 7.11 \quad \text{where } x = \text{ash content \%; } r^2 = 0.200 \qquad (5.5)$$

Increasing volatile matter corresponds to increasing coal strength and has a high r^2 value (0.800). Volatile matter is, however, a function of coal rank, so the influence of cleats which are also dependant on coal rank is a critical factor. Carbon content shows a decrease as coal strength increases with an r^2 value of 0.894. Carbon and volatile matter vary with coal rank so there is no evidence to link their involvement with changes in coal strength, but they are however useful indicators of it. These trends are described by equations 5.3 and 5.4. Ash is independent of coal rank and shows a trend of increasing coal strength with ash content. This trend has a low r^2 value of 0.200 and is described by equation 5.5. Scatter in the results is generally low other than two outlying data points which reduce the r^2 value. Because of its independence from rank effects, ash is deemed to contribute to coal strength. Determining how this occurs however is beyond the scope of this study, but it may be due to increased cohesion.

Coal strength decrease with increasing coal rank is a well-recognised worldwide trend. This trend is pronounced in the Greymouth Coalfield where the rank gradient is especially high from west to east across the coalfield, increasing from high volatile bituminous C to low volatile bituminous. When UCS and point load are plotted against vitrinite reflectance (a rank indicator) a strong trend is shown. As the vitrinite reflectance increase from 0.62% to 1.76% a corresponding drop in compressive strength occurs, reducing from 24.8 MPa to 1.3 MPa for UCS and 0.64 MPa to 0.13 MPa for the point load strength. This is especially true of the UCS plot where the r^2 value is the highest (0.870; equation 5.6). The point load strength plot has the lower r^2 value of 0.613. A less pronounced but still noticeable decrease in coal strength would be expected across the Reefton and Garvey Creek Coalfields where the rank gradient is lower, all though this was not covered by the present study.

$$UCS_{equivalent} = 4.89x^{-2.24} \quad \text{where } x = \% \text{ vitrinite reflectance} \tag{5.6}$$

When the $UCS/I_{s(50)}$ relationships established by this equation are plotted against coal rank, a good correlation is seen between decreasing $UCS/I_{s(50)}$ and increasing coal rank. This has an r^2 value of 0.71 and can be described by equation 5.7, where x is percentage vitrinite reflectance.

$$UCS_{equivalent}/I_{s(50)} \text{ ratio} = 12.28x^{-0.84} \quad \text{where } x = \% \text{ vitrinite reflectance} \tag{5.7}$$

5.3 Pillar Design

5.3.1 Basis of Design

There are many pillar strength formulas presented in the literature, all of which give significantly different predictions leading to significantly different pillar sizes. However, only two of the popular equations provide a slender (w/h <5) and squat (w/h >5) pillar variation to take account of the increased confinement in the core of the pillar, and subsequently increases pillar strength, as the pillar size increases. These pillar design methods are those of Bieniawski (equations 5.8 and 5.9) and Salamon-Munro/Wagner (equations 5.10 and 5.11) which have been shown by field trials and case studies to be valid predictors of pillar strength. The squat pillar formulas lead to the use of significantly smaller pillars than would be required by other strength equations.

$$\sigma_p = \sigma_1 \, (0.64+0.36\frac{w}{h}) \tag{5.8}$$

$$\sigma_p = \sigma_1 (0.64+0.36\frac{w}{h})^{1.4} \tag{5.9}$$

$$\sigma_p = K\frac{w^{0.46}}{h^{0.66}} \tag{5.10}$$

$$\sigma_p = \sigma_1 \frac{R^{0.5933}}{V^{0.0667}} \left[\frac{0.5933}{e} \left[\left(\frac{w/h}{R} \right)^e - 1 \right] + 1 \right] \tag{5.11}$$

where: e = the rate of strength increase = 2.5

σ_1 = in-situ coal strength as per equation 4.5

w, h = pillar dimensions (m)

V = volume of pillar (m^3)

R = critical w/h ratio = 5

σ_p = pillar strength (MPa)

$$K = \frac{k}{\sqrt{12}}$$

$$k = \frac{145\sigma_c\sqrt{\frac{D}{25.4}}}{145}$$

σ_c = unconfined compressive strength (MPa)

D = diameter of cylindrical sample or cube side length (mm)

5.3.2 Pillar Design in the Greymouth and Reefton Coalfields

Panel pillars have designed to a factor of safety of 1.6. The optimum square pillar size for all seams and depths is presented in Table 5.3. The coal pillar sizes estimated for the Greymouth and Reefton coalfields are the best estimates of the author given the information available. Changes to the values given may need to be made depending on local conditions not taken into account by this study (e.g. small scale faults and shear zones). In locations other than the Spring Creek and Strongman No. 2 mines the unconfined compressive strength has been estimated by non-standard methods developed by this study, i.e. equation 5.2. Pillars have been designed using these methods which are thought to be more accurate than the UCS = $24.I_{s(50)}$ relationship, which has been shown to be inapplicable to most of the coalfield.

Location	Seam	Seam Dip	σ_1 (MPa)	Overburden (m)	Pillar Size (m)
Bishop Block	Kimbell		1.9	50-100m	6.0-17.4
	Morgan		1.7	100-150m	6.2-24.8
Roa	Kimbell	10-16°	0.3	25-170	13.5-55.8
Spring Creek	D	6-28°	2.2	200-220	25.5-27.1
	MNU	6-28°	1.7	250-300	31.2-34.9
Strongman No. 2	D	3-33°	4.2	70-170	6.7-15.1
	E	5-40°	4.2	70-125	6.7-11.5
Terrace	No. 4	15-25°	1.3	170-260	28.0-37.1

Table 5.3. Optimum square pillar size designed to a factor of safety of 1.6.

Pillars need to be designed for specific depth intervals as the changing overburden load with increasing depth will require successively larger pillars. By taking into account the information gathered with regard to coal strength at different loading orientations (Figure 5.1), pillars should in some cases should also be designed for specific seam dips,

especially where the bedding planes within the coal are weak (e.g. as at the Spring Creek Mine). Larger pillars would be required as the seam dip increases, but when seam dip is lower the pillars required are smaller. This requires specific data on how the coal reacts to different loading directions. For the Spring Creek D seam an increase in seam dip of 5° corresponds to an increased pillar size of 1.9m as shown in Figure 5.3. In seams where the bedding is less prominent this effect will be significantly reduced, but is still expected to have an influence.

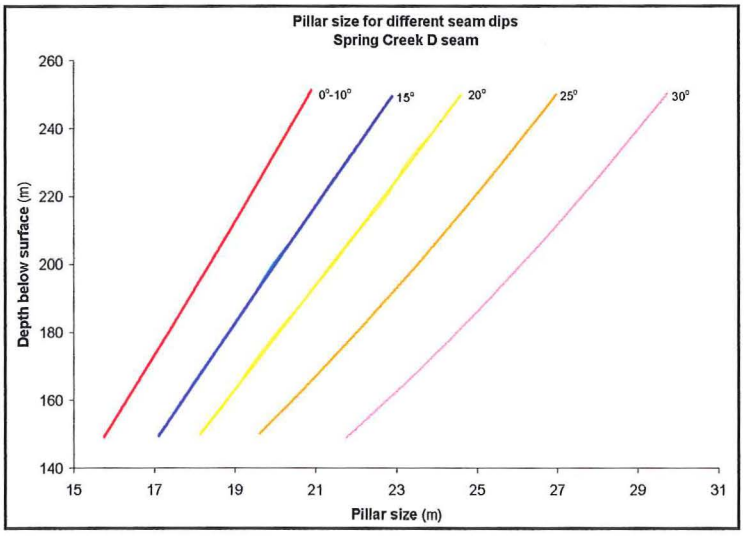

Figure 5.3. Pillar sizes for Spring Creek D seam at different seam dips. Strength difference for each seam dip is derived from Figure 5.2. Coal strength is considered to be constant when seam dip is 0-10° and then decreases with increasing seam dip.

Stresses within coal pillars dissipate rapidly with increasing width/height (*w/h*) ratio of the pillar. In all cases the maximum stresses are concentrated in the sides of the pillar adjacent to the excavation and at the corners where the pillar meets the roof and floor. When *w/h* ratio is low (especially <2) the maximum stress extends a long way into the pillar core which results in spalling penetrating further inwards thus reducing the strength of the pillar which is largely at the pillar core. Areas of least stress are in the centre of the roof and floor. These low stress zones are largely independent of *w/h* ratio and extend approximately 6m into the roof and floor. As the dip of the coal seam increases, the stress distribution within the pillar changes with the stress becomes increasingly concentrated on the corners of pillars in the plane of seam dip.

Rectangular pillars of equal volume to square pillars have significantly lower strength due to the effective width, w_{eff}, being used in calculating the pillar strength. Lower stress distributions can be achieved by increasing the length of the square pillars, whilst retaining the same width which distributes the load over a greater area and allows the pillar to take a greater load, giving a higher FOS. This, however, results in a lower initial extraction ratio.

Bearing capacity problems can be expected with increasing depth in the Terrace mine due to the weak fireclay in the floor. The development level currently stands at 170m (below the surface). The bearing capacity of the floor at this level has been calculated for the expected range of seam dips from 15° to 25° using equation 5.4 from Brady and Brown (1985; Summarised in Table 5.). When the seam dip is 15° the factor of safety against bearing capacity failure is 2.11-1.51 for depths of 170-260m, and is considered to be adequate. When seam dip is 20° the FOS drops to 1.13 at maximum depth and drops to 0.84 when seam dip is 25°. This assumes that 1.0m of coal is retained in the floor to keep the fireclay dry). As the seam dip increases, the bearing capacity of the fireclay is reduced. To counter this effect the pillar size needs to increase beyond the recommended size for a panel pillar in order to spread the load across a greater area, thus lessening the risk of bearing capacity failure. As the seam dip increases, increasing the pillar size has less effect. Consequently floor heave should be expected once the dip exceeds 20°.

$$q_{ult} = 1.2cN_c + 0.5\gamma BN_\gamma \qquad (5.11)$$

where: c = cohesion of fireclay ϕ = Friction angle of fireclay

B = pillar width (m) γ= unit weight of fireclay = 19.62 kPa

$N_c = (N_q\text{-}1)\cot\phi$, $N_\gamma = 1.8(N_q\text{-}1)\tan\phi$, and $N_q = \left(\frac{1+\sin\phi}{1-\sin\phi}\right)e^{\pi\tan\phi}$

Depth (m)	Pillar size	Seam Dip 15°	20°	25°
		Factor of safety		
170	28.0	2.11	1.62	1.24
180	29.1	2.04	1.57	1.19
190	30.1	1.95	1.49	1.13
200	31.3	1.84	1.40	1.06
210	32.3	1.79	1.36	1.02
220	33.2	1.72	1.30	0.97
230	34.2	1.66	1.25	0.93
240	35.1	1.60	1.21	0.90
250	36.1	1.57	1.18	0.87
260	37.1	1.51	1.13	0.84

Table 5.4. Optimum pillar size taken from Figure 4.8f for seams dips of 15°, 20° and 25° with the corresponding factors of safety against bearing capacity failure. For the worst case of 260m depth and 25° seam dip there is very little safeguard against bearing capacity failure. The pillar size values are the average of the Bieniawski and Salamon methods taken from Figure 4.8f.

Chapter 6. Summary and Conclusions

6.1 Project Objectives and Methodology

The objectives of this study have been to:

1) Determine the extent of any relationship between coal rank and strength, and establish the reasons for such a relationship.

2) Establish a relationship between unconfined compressive strength and point load strength for each seam studied.

3) Establish a database of the geotechnical properties of coal in the Greymouth Coalfield for use in future underground mine design.

4) Determine the extent to which pillar geometry affects coal pillar strength, and evaluate standard pillar design formulae for the Greymouth and Reefton Coalfields.

Samples for strength testing were prepared from lump samples taken from each location. Cores were drilled from these lump samples for unconfined and triaxial compressive strength tests, and the Brazilian tensile strength test. Other samples were prepared for cube compressive strength, point load strength and shear strength tests. As far as possible testing was conducted in accordance with the ISRM suggested methods. All deviations from the prescribed methods have been detailed in the text.

Relationships were developed between the unconfined compressive strength (UCS), cube compressive strength (CCS) and point load strength ($I_{s(50)}$) test results in order to develop an equation from which a $UCS_{equivalent}$ value could be estimated. This was required in areas where no core samples could be obtained.

$UCS_{equivalent}$ values were plotted against volatile matter, fixed carbon and vitrinite reflectance resulting is useful relationships for estimating coal strength which are more accurate than both the UCS = $24I_{s(50)}$ relationship and individual $UCS/I_{s(50)}$ ratios developed for individual seams.

Pillars have been designed to a factor of safety of 1.6 using two popular pillar strength equations which are considered to give the most accurate estimates of pillar strength. Knowledge of strength anisotropy allows pillars to be designed for specific seam dips in some cases.

6.2 Coal Strength

- Coal strength is highly variable both within and between seams, with variations of ± 100% of the mean within a single seam. All coal in this study is classified as very weak (1-5 MPa) to weak (5-25 MPa) using the classification of Hoek and Brown (1997). Increasing confinement under triaxial conditions served to decrease the scatter in the test results and increase the similarity of the strengths between all the seams tested. Cohesion (2.31 ± 0.47 MPa) and friction angles (50.3 ± 1.7°) are consistent between all the four seams tested by this method and show no relationship to each other.

- Coal strength from locations other than the Spring Creek and Strongman No. 2 mines has been estimated from equation 6.1.

$$UCS_{equivalent} = y\,(z.I_{s(50)}) \qquad (6.1)$$

where: $y = \dfrac{UCS_{control}}{CCS_{control}}$ $\qquad z = \dfrac{CCS}{I_{s(50)}}$

CCS = cube compressive strength.

6.3 Relationship between Coal Strength and other Coal Properties

- $UCS/I_{s(50)}$ relationships have very low r^2 values (-2.59-0.22) resulting from the large scatter seen in both the point load and UCS results. Point load strength tests results consistently had a range of 100% of the mean, so when this is applied to the UCS = $24.I_{s(50)}$ relationship the results will have such a spread that they become very difficult to interpret. Point load tests are of no use in determining coal strength as the variability in the results is too high and the r^2 value for $UCS/I_{s(50)}$ are too often negative to be of use in providing reliable estimate of coal strength.

- Cleat frequency has the single biggest influence on coal strength. The abundance of cleats increases with coal rank to a maximum abundance at medium-low volatile bituminous, before declining through semi-anthracite to anthracite. Coal strength shows a corresponding decrease as coal rank increases, dropping from a maximum of 24.8 MPa (Strongman E/UG) to 1.32 MPa at Roa.

- This study shows that there are many ways of estimating the compressive strength of coal and many factors that appear to have an influence on it. Unless UCS tests can be conducted on coal samples, the best solution to get a reliable estimate of coal strength in to determine it indirectly without conducting any strength tests.

- The most useful estimates of coal strength can be made from carbon and volatile matter contents (equations 6.2 and 6.3), and coal rank (equation 6.4). All of the methods have r^2 values between 0.800 and 0.894 and are thus much more reliable than $UCS/I_{s(50)}$ ratios which often have negative r^2 values.

$$UCS_{equivalent} = 4\times10^{11}x^{-6.04} \quad \text{where } x = \text{carbon \%; } r^2 = 0.894 \qquad (6.2)$$

$$UCS_{equivalent} = 0.0002x^{2.98} \quad \text{where } x = \text{volatile matter \%; } r^2 = 0.800 \qquad (6.3)$$

$$UCS_{equivalent} = 4.88x^{-2.25} \quad \text{where } x = \text{vitrinite reflectance \%; } r^2 = 0.870 \qquad (6.4)$$

6.4 Pillar Design

- The slender and squat pillar formulas of Bieniawski and Salamon-Munro/Wagner have been selected for pillar design in this study. The optimum square pillar size for panel pillars designed to a factor of safety of 1.6 is presented in Table 6.1.

- Pillars for the Spring Creek D seam should be designed for specific seam dip due to the anisotropy of the coal. This requires a 1.9m increase in pillar size for each 5° increase in seam dip. The required sizes for panel pillars at increasing dips is presented in Table 6.2.

Location	Seam	Seam Dip	σ_1 (MPa)	Overburden (m)	Pillar Size (m)
Bishop Block	Kimbell		1.9	50-100m	6.0-17.4
	Morgan		1.7	100-150m	6.2-24.8
Roa	Kimbell	10-16°	0.3	25-170	13.5-55.8
Spring Creek	D	6-28°	2.2	200-220	25.5-27.1
	MNU	6-28°	1.7	250-300	31.2-34.9
Strongman No. 2	D	3-33°	4.2	70-170	6.7-15.1
	E	5-40°	4.2	70-125	6.7-11.5
Terrace	No. 4	15-25°	1.3	170-260	28.0-37.1

Table 6.1. Optimum square pillar size designed to a factor of safety of 1.6.

Depth	Seam Dip				
	0-10°	15°	20°	25°	30°
	Required Pillar Size (m)				
200-220m	18.4-19.3	19.9-21.2	21.4-22.8	23.5-24.9	26.0-27.6

Table 6.2. Optimum square pillar size for different seam dips in the Spring Creek D seam.

- Bearing capacity problems can be expected with increasing depth in the Terrace mine due to the weak fireclay in the floor. The development level currently stands at 170m (below the surface) but will soon be extended to 260m. The bearing capacity of the floor at this level has been calculated for the expected range of seam dips of 15-25°. The FOS is considered adequate at all required depths when seam dip is 15°, being > 1.5. FOS drops rapidly as seam dip increases, never being higher than 1.25 when seam dip is 25°. To lessen the chances of floor heave the pillars will need to made larger than the recommended optimum size when the seam dip is above 20°. However, at the highest seam dips, large changes in the pillar size will only induce small changes in the factor of safety.

6.5 Recommendations for Further Work

6.5.1 Coal Strength Prediction

- To accurately predict the $UCS/I_{s(50)}$ relationship from the plot of $UCS/I_{s(50)}$ vs. vitrinite reflectance, a series of tests need to be conducted on coal from the Greymouth Coalfield in the range of 0.9%-1.6% vitrinite reflectance. The use of cube samples and equation 3.13 is recommended for this as core samples probably cannot be obtained from this area due to the expected weakness of the coal. The difficulty with this is that there is no development in this area at present, so outcrop samples would have to be used. The experience gained by this study is that outcrop samples (even 2m into the outcrop) from the Greymouth Coalfield are generally weathered because of the high rainfall in this region and the length of time that the coal has been exposed.

- Further cube and core samples taken from the Doherty Block (Map 1) or the F seam of the Strongman No. 2 mine would be useful in providing further refinement of the multiplier, *y*, used in equations 3.12 and 3.13. At present there is some scatter among the three seams tested, with *y* ranging from 0.35-0.53. Refining this parameter would in turn provide more accurate estimate of the strengths of the weaker seams which were estimated from this relationship.

6.5.2 Coal Strength Anisotropy

- It has been conclusively shown by this study that loading direction has a pronounced effect on the strength of the coal. It would be useful to further investigate the effect of this for other seams including the Strongman No. 2 D and E seam and the Main, Main Upper and Main Lower seams of the Spring Creek mine where the effects of bedding are more pronounced. This would allow pillar design for specific dip intervals to be used in these seams. The difficulties in this are, however, sample preparation for the desired loading direction, as many samples will break along cleats during preparation.

6.5.3 Determination of Fireclay Properties

- Testing of the friction angles and cohesion of the fireclay in the floor of the Terrace Mine should be conducted so that a more accurate analysis of the anticipated bearing capacity failures can be conducted. The friction angles used in the analysis conducted by this study were taken as 35°, as it was deemed by a previous study to be similar to that seen in the Huntly mine. Cohesion of the fireclay was back-calculated using this friction angle. An accurate determination of the actual cohesion and friction angle would allow for a more accurate estimate of the likelihood of bearing capacity problems, which may be significantly different to that estimated by this study.

References

Abel, J. F. 1988. Soft Rock Pillars. *Int. J. Min. and Geol. Eng.*, vol. 6, pp. 215-248.

Afrouz, A. 1975. Yield and Bearing Capacity of Coal Mine Floor. *Int J. Rock Mech. Min. Sci. Geomech. Abstr.*, vol. 12, pp. 241-253.

Ammosov, I. I., and Eremin, I. V. 1960. Fracturing in Coal (English vers., 1963), Israel Program in Scientific Translation, Tel Aviv, 111p.

Anderson, J. N. 2001. Engineering Geological Modelling for Opencast Mine Stability in Schists, Macraes Gold Mine, Otago. Unpublished M.Sc thesis, University of Canterbury, Christchurch, New Zealand.

Anon. 1996. Report on the 1996 New Zealand Branch AusIMM conference. *New Zealand Mining*, October 1996, pp. 28-33.

ASTM. 1979. Standard Methods of Test for Unconfined Compressive Strength of Rock Core Specimens. American Society for Testing Materials.

Atkinson, R. H., and Ko, H. Y. 1977. Strength Characteristics of US Coals. 18th Symposium on Rock Mechanics, pp. 2B3 1-6.

Barnes, G. E. 1995. Soil Mechanics: Principles and Practice. Macmillan. 365p.

Barry, J. M., Duff, S. W., and MacFarlan, D. A. B. 1994. Coal Resources of New Zealand. Ministry of Commerce Resource Information Report 16.

Bauschinger, J. 1876. Communication of the Mechanical-Technical Laboratories of the Technical University in Munich, vol. 6.

Beamish, B. B., and Vance, W. E. 1989. Some Aspects of Pillar Stability in Underground Coal Mines. Proc AusIMM Annual Conference, New Zealand Branch, Greymouth, 1989, pp. 105-114.

Bell, D. H. 1993a. Strength Testing of Coal Samples-Mt Davy pillar design. Letter to Coal Corporation, 13 August 1993.

Bell, D. H. 1993b. Strength Testing of Coal Samples-Mt Davy pillar design. Letter to Coal Corporation, 20 August 1993.

Bell, F. G., and de Bruyn, I. A. 1999. Subsidence Problems due to Abandoned Pillar Workings in Coal Seams. *Bull. Eng. Geol. Env.*, vol. 57, pp. 225-237.

Bieniawski, Z. T. 1967. Mechanisms of Brittle Fracture of Rock. National Mechanical Engineering Research Institute Council of Scientific and Industrial research. 226p.

Bieniawski, Z. T. 1968. The Effect of Specimen Size on Compressive Strength of Coal. *Int. J. Rock Mech. Min. Sci.*, vol. 5, pp. 325-335.

Bieniawski, Z. T. 1973. Engineering Classifications of Jointed Rock Masses. *Transactions of the South African Institute of Civil Engineers.* Vol. 15, pp. 335-344.

Bieniawski, Z. T. 1975. The Point-Load Test in Geotechnical Practice. *Eng. Geol.*, vol. 9, pp. 1-11.

Bieniawski, Z. T. 1983. New Design Approach for Room-and-Pillar Coal Mines in the USA. *Proc 5th Int. Congress on Rock Mechanics*, ISRM, Melbourne, Australia, 1983, vol. 2, pp. E27-36.

Bieniawski, Z. T. 1984. Rock Mechanics in Mining and Tunnelling. Balkema, 272p.

Bieniawski, Z. T. 1989. Engineering Rock Mass Classifications: A complete manual for Engineers and Geologists in mining, civil and petroleum engineering. John Wiley and Sons, New York. 251p.

Bieniawski, Z. T. 1992. A Method Revisited: Coal pillar strength formula based on field investigations. In: Iannacchione, A. T., Mark, C., Repsher, R. C. Tuchman, R. J., and Jones, C. C. 1992. Proc. Workshop on Coal Pillar Mechanics and Design. U.S Bureau of Mines Information Circular 9315. pp. 158-165.

Bieniawski, Z. T., and van Heerden, W. L. 1975. The Significance of In-Situ Tests on Large Rock Specimens. *Int. J. Rock Mech. Min. Sci.*, vol. 12, pp 101-113.

Bishop, D. J. 1992. Extensional Tectonism and Magmatism during the Middle Cretaceous to Paleocene, North Westland, New Zealand. *New Zealand J. of Geol. and Geophys.*, vol. 35 (1), pp. 81-91.

Boyd, R. J., and Lewis, D. W. 1995. Sandstone Diagenesis Relating to Varying Burial Depth and Temperature in Greymouth Coalfield, South Island, New Zealand. *New Zealand J. Geol. Geophys.*, vol. 38, pp. 333-348.

Bowman, R. G., Caffyn, P., and Duff, S. W. 1984. Greymouth Coalfield Report. New Zealand Coal Resources Survey Report, Ministry of Energy, Wellington, New Zealand. Part 1, 211 pp. + appendices.

Brady, B. H. G., and Brown, E. T. 1985. Rock Mechanics for Underground Mining. George, Allen & Unwin. 527p.

Broch, E. 1983. Estimation of Strength Anisotropy using the Point-Load Test. *Int. J. Rock. Mech. Min. Sci. & Geomech. Abstr.*, vol. 20 (4), pp. 181-187.

Broch, E., and Franklin, J. A. 1972. The Point-Load Strength Test. *Int. J. Rock Mech. Min. Sci.*, vol. 9, pp. 669-697.

Brook, N. 1993. The Measurement and Estimation of Basic Rock Strength. In: Hudson, J. A. (ed). Comprehensive Rock Engineering: Principles, practice and projects. Pergamon Press, vol. 3, pp. 41-65.

Brown, E.T (ed). 1981. Rock Characterisation, Testing and Monitoring. ISRM suggested methods. Pergamon Press, Oxford. 211p.

Bunting, D. 1911. Chamber Pillars in Deep Anthracite Mines, *Transactions of the AIME*, pp.739-748.

Bustin, R. M., Cameron, A. R., Grieve, D. A., Kalkreuth, W. P. 1985. Coal Petrology; Its principles, methods and applications. Short course notes. Geological Assoc. of Canada. 229p.

Caffyn, P. 1987. Doherty Block Report, Greymouth Coalfield. Unpublished report prepared for State Coal Mines, Ministry of Energy, Wellington, New Zealand.

Caffyn, P. 1992. Roa Geological Report, Greymouth Coalfield. Unpublished report compiled for L and M Mining Ltd. 14p.

Campbell, R. N. 2000. The Application of the Slope Stability Probability Classification System to Opencast Mining in the Waikato Coal Measures, New Zealand. Unpublished M.Sc thesis, University of Canterbury, Christchurch, New Zealand. 241p.

Chapple, A. P. 1998. An Engineering Geological Investigation into Pit Slope Stability at Macraes Gold Mine, Macraes Flat, Otago, New Zealand. Unpublished M.Sc thesis, University of Canterbury, Christchurch, New Zealand.

Coates, D. F, 1965. Rock Mechanics Principles. Mines Branch Monograph 874, Department of Energy, Mines and Resources, Ottawa, pp. 2-15.

Coates, D. F. 1966. Pillar Loading – a new hypothesis. Canada Department of Mines and Technical Surveys. Mines Branch Research Reports R168/170/180, February 1966.

D'Andrea, D. V., Fischer, R. L., and Fogelson, D. E. 1965. Prediction of Compressive Strength from Other Rock Properties. U.S. Dept. of the Interior, Bureau of Mines, Washington. 22p.

Deere, D. U., and Miller, R. P. 1966. Engineering Classification and Index Properties for Intact Rock: Tech. Rep. No. AFWL-TR-65-116, University of Illinois, Urbana.

Edbrooke, S. 1999. Mineral Commodity Report 18-Coal. *New Zealand Mining*, March 1999, pp. 9-23.

Evans, I., and Pomeroy, C. D. 1966. Strength, Fracture and Workability of Coal. Pergamon. 277p.

Field, A. 1998. Terrace Development Feasibility Report-June 1998. Unpublished report prepared for Solid Energy.

Fowke, N. 1998. Supplement to Geological Assessment of No. 4 Seam in and around Terrace Mine, Reefton. Unpublished report prepared for Solid Energy.

Gaddy, F. L. A. 1956. A Study of the Ultimate Strength of Coal as Related to Absolute Size of the Cubical Specimens Tested. *UPI Bulletin, Series No. 112*, August 1956, pp. 1-27.

Gage, M. 1952. The Greymouth Coalfield. *New Zealand Geological Survey bulletin 45.* 232p.

Gale, W. J., and Mills, K. W. 1995. Coal Pillar Design Guidelines-P351, Report AMI0157, Australian Mineral Industries Research Association Ltd, Melbourne. 52p.

Galvin, J. M. 1992. A Review of Coal Pillar Design in Australia. In: Iannacchione, A. T., Mark, C., Repsher, R. C. Tuchman, R. J., and Jones, C. C. 1992. Proc. Workshop on Coal Pillar Mechanics and Design. U.S Bureau of Mines Information Circular 9315. pp. 196-213.

Galvin, J. M. 1995. Pillar Design Procedure. *Strata Control Newsletter*, vol 7, School of Mines, University of New South Wales.

Galvin, J. M., and Wagner, H. 1982. Use of Ash to Improve Strata Control in Bord and Pillar Workings. In: Farmer, I. W. (ed). Strata Mechanics. *Proc. Symp. Strata Mech.*, pp. 264-270, Newcastle, 1982. Elsevier.

Ghose, A. K., Barat, D., and Bagchi, S. 1964. Some Preliminary Studies on the Impact Strength Index of Indian Coals. *J. Mines Metals Fuels*, vol 12, pp 153-155.

Gillard, G. R., and Moore, T. A. 1999. New Zealand Coal Characteristics in the Global Scene. *New Zealand Mining*, March 1999, pp. 9-23.

Greenwald, H. P., Hawarth, H. C., and Hartmann, I. 1939. Experiments on Strength of Small Pillars of Coal in the Pittsburgh Bed. *U. S. Bureau of Mines Technical Paper* 605, Rep Invest 3575. 22p.

Hansen, H., Kielland, A., Nielsen, K. E. C., and Thaulow, S. 1962. Compressive Strength of Concrete-Cube or Cylinder. *Bull. Reunion Intern. Lab. Essais Rech Mater. Constr.*, vol. 17, pp. 22-30.

Hawkes, I., and Mellor, M. 1970. Uniaxial Testing in Rock Mechanics Laboratories. *Eng. Geol.*, vol. 4, pp. 177-285.

Hebblewhite, B. K., Blackwood, R. L., Holt, G. E., Mikula, P. A., Richmond, A., Mallett, C., and Enever, J. 1986. Rock Mechanics and Stability of Excavations. In: Martin, C. H (ed). Australasian Coal Mining Practice. The Australasian Institute of Mining and Metallurgy Monograph Series No. 12, pp 148-161.

Hebblewhite, B. K., Galvin, J. M., and Foroughi, M. H. 1997. Geotechnical Mine Design Issues for Thick Seam Mining. *Proc 7th New Zealand Coal Conference*, pp. 402-411.

Hoek, E., and Brown, E. T. 1980. Underground Excavations in Rock. Institution of Mining and Metallurgy, London. 527p.

Hoek, E., and Brown, E. T. 1997. Practical Estimates of Rock Mass Strength. *Int. J. Rock Mech. Min. Sci.*, vol. 34 (8), pp. 1165-1186.

Hoek, E., Marinos, P., and Benissi, M. 1998. Applicability of the Geological Strength Index (GSI) Classification for Very Weak and Sheared Rock Masses. The case of the Athens Schist Formation. *Bull. Eng. Geol. Env.*, vol. 57 (2), pp. 151-160.

Holland, C. T. 1958. Cause and Occurrence of Coal Mine Bumps. *Proc. Amer. Inst. Min. Metall. Petr. Engrs.*, vol. 211.

Holland, C. T. 1964. The strength of Coal in Mine Pillars. *Proc 6th Symposium on Rock Mechanics*, University of Missouri, Rolla, pp. 450-466.

Holland, C. T. 1973. Mine Pillar Design. SME Mining Engineering Handbook, vol. 1, section 13-18, AIME, New York, pp. 97-118.

Hustrulid, W. A. 1976. A Review of Coal Pillar Strength Formulas. *Rock Mechanics*, vol. 8 (2), pp. 115-145.

Hustrulid, W. A., and Swanson, S. R. 1981. Filed Verification of Coal Pillar Strength Prediction Formulas. Final Report to Bureau of Mines, Contract #H0242059, April 1981.

ISRM. 1981. Basic Geotechnical Description of Rock Masses. *Int. J. Rock. Mech. Min. Sci.*, vol. 18, pp 85-110.

ISRM. 1985. Suggested Method for Determining Point Load Strength. Int. Soc. for Rock Mech. Commission on Testing Methods. *Int. J. Rock Mech. Min. Sci and Geomech. Abstr.*, vol 22 (2), pp.51-60.

Jeremic, M.L. 1985. Strata Mechanics in Coal Mining. Balkema, Rotterdam. 566p.

Johnson. 1897. Materials of Construction. (Cited in Babcock, C. O. 1981. Pillar Design Equations for Coal Extraction. U. S. Bureau of Mines information Circular no. 8973, pp. 36-48.

Kamp, P. J. J. 1986. Late Cretaceous-Cenozoic Tectonic Development of the Southwest Pacific Region. *Tectonophysics,* vol. 121 (2-4), pp. 225-251.

Kennedy, J. F. 1988. Engineering Geological Characterisation of the Brunner Coal Measures, Cedar Creek Area, Buller Coalfield. Unpublished M.Sc Thesis, University of Canterbury, Christchurch, New Zealand. 249p.

Kwasniewski, M. A. 1993. Mechanical Behaviour of Anisotropic Rocks. In: Hudson, J. A. (ed). Comprehensive Rock Engineering: Principles, practice and projects. Pergamon Press, vol. 1, pp. 285-312.

Laubscher, D. H. 1990. A Geomechanics Classification System for Rating of Rock Mass in Mine Design. *Journal South African Inst. of Mining and Metallurgy*, vol. 86 (10), pp. 257-273.

Logie, C. V., and Matheson, G. M. 1982. A Critical Review of the Current State-of-the-Art design of Mine Pillars. In: Brauner, C. O (ed). *Proc. 1st Int. Conf. Stability in Underground Mining*, Vancouver, pp. 359-382.

Lucas, T. 2002. Island Block High Wall Feasibility Study, Brunner Coal Measures, Reefton. M.Sc thesis, University of Canterbury, Christchurch, New Zealand (in prep).

Madden, B. J. 1988. The Performance of Coal Pillars Designed to the Squat Pillar Formula. In: Key Question in Rock Mechanics: *Proc. 29th US Symp. Rock Mech.*, pp. 699-708.

Madden, B. J. 1993. Calculation of Pillar Dimensions for Mt Davy Colliery. ACIRL report no. XGE 1662. Unpublished report prepared for Coal Corporation of New Zealand Ltd. 7p.

Madden, B. J., and Hardman, D. R. 1992. Long-term Stability of Bord and Pillar Workings in South Africa. In; *Proc. Symp. Effect of Underground Mining on Surface*, Sandton. SANGORM, pp. 25-32.

Marino, G. G., and Choi, S. 1999. Softening Effects on Bearing Capacity of Mine Floors. *J. Geotechnical and Geoenvironmental Eng.*, vol 125 (12), pp. 1078-1089.

Mathis, J. I. 1993. Strength of Laboratory-Sized Coal Specimens vs. Underground Coal Pillars. *Mining Engineering*, August 1993, pp. 1051-1053.

Medhurst, T. P., Brown, E. T. 1998. A Study of the Mechanical Behaviour of Coal for Pillar Design. *Int. J. Rock Mech. Min. Sci.*, vol. 35 (8), pp. 1087-1105.

Mills, K. W. 1986. In-Situ Mechanical Behaviour of Huntly Coal. School of Engineering Report No. 406. Dept. of Civil Engineering, University of Auckland, Auckland, New Zealand.

Morgan, P. G. 1911. The Geology of the Greymouth Subdivision, North Westland. *New Zealand Geological Survey Bulletin No. 13*, 159p.

Murray, D. R., and Orr, G. E. 1985. New Zealand State Coal Mines: Ohinewai Underground Prospect: Geotechnical testing of core samples from boreholes 9802, 9803, 9804, and 9805. Report 2-85/19, Central Laboratories, MWD, Lower Hutt, New Zealand, 123p.

MWD (Ministry of Works and Development). 1985. MWD Central Laboratories report. The complete reference for this report could not be found.

Nathan, S. 1978. Geological Map of New Zealand 1:63360 Sheet S44 Greymouth. Wellington, New Zealand Geological Survey, 36p.

Newman, J. 1985. Paleoenvironments, Coal Properties, and their Inter-Relationship in Paparoa and Selected Brunner Coal Measures on the West Coast of the South Island. Unpublished Ph.D Thesis, University of Canterbury. 242p.

Newman, J., and Newman, N. A. 1982. Reflectance Anomalies in Pike River Coals: Evidence of variability in vitrinite type, with implications for maturation studies and 'Suggate rank'. *N.Z. J. Geol. Geophys.*, vol. 25, pp. 233-243.

Newman, J., and Newman, N. A. 1992. Tectonic and Paleoenvironmental Controls on the Distribution and Properties of Upper Cretaceous Coals on the West Coast of the South Island, New Zealand. In: McCabe, P. J., and Parrish, J. T (eds). Controls on the Distribution and Quality of Cretaceous Coals. *Geol. Soc. America Special Paper* 267, pp. 347-368.

Nunweek, C. N. 2001. Depositional Controls on Peat Accumulation and Coal Characteristics, Dunollie and Brunner Coal Measures. Unpublished M.Sc thesis, University of Canterbury, Christchurch, New Zealand. 146p.

Obert, L., and Duvall, W. I. 1967. Rock Mechanics and the Design of Structures in Rock. John Wiley & Sons, New York, 650p.

Pariseau, W. G. 1977. Limit Design of Mine Pillars Under Uncertainty. *Proc. 16th Symp. on Rock Mech*, Minneapolis, ASCE, New York, pp. 287-301.

Pashin, J. C., Carroll, R. E., Hatch, J. R., and Goldhaber, M. B. 1999. Control of Cleating and Shearing in Coal. In: Mastalerz, M., Glikson, M., and Golding, S. D., (eds). 1999. Coalbed Methane: Scientific, Environmental and Economic Evaluation.

Pells, P. J. N. 1993. Uniaxial Strength Testing. In: Hudson, J. A. Comprehensive Rock Engineering: Principles, Practice and Projects. Vol. 3, Rock Testing and Site Characterisation. Pergamon Press, pp. 67-85.

Pells, P. J. N., and Ferry. M. J. 1983. Needless Stringency in Sample Preparation Standards for Laboratory Testing of Weak Rocks. Fifth International Congress on Rock Mechanics, Melbourne. Vol. 1, pp. A203-A207.

Peng, S. S .1993. Reply to article by Mathis. In: Mathis, J. I. Strength of Laboratory-Sized Coal Specimens vs. Underground Coal Pillars. *Mining Engineering*, August 1993, pp. 1051-1053.

Peng, S. S., and Dutta, D. 1992. Evaluation of Various Pillar Design Methods. In: Iannacchione, A. T., Mark, C., Repsher, R. C. Tuchman, R. J., and Jones, C. C. 1992. Proc. Workshop on Coal Pillar Mechanics and Design. U.S Bureau of Mines Information Circular 9315. pp. 269-276.

Quick, J. C. 1992. Fundamental Characterisation of New Zealand Bituminous Coal for Prediction of Carbonisation Behaviour-With special emphasis on fluorometric analysis. Unpublished Ph.D Thesis, University of Canterbury, 225p.

Ramamurthy, T. 1993. Strength and Modulus Responses of Anisotropic Rocks. In: Hudson, J. A. (ed). Comprehensive Rock Engineering: Principles practice and projects. Pergamon Press, pp. 313-329.

Richards, L. R. 2000. Bishop Block Project Pillar Design and Subsidence Assessment. Unpublished report prepared for Solid Energy.

Richards, L. R. 2002. Wairaki No. 6 Mine Subsidence and Barrier Pillars. Unpublished report prepared for Solid Energy.

Rockaway, J. D., and Stevenson, R. W. 1982. Geotechnical Evaluation of the Support of Coal Pillars in Underground Coal Mines. *Bull. Assoc. Eng. Geol.*, vol. 19 (1), pp. 5-14.

St George, J. D. 1995. Strength of New Zealand Coals in Relation to Pillar Stability. *Sixth New Zealand Coal Conference*. Coal Research Assoc. of New Zealand, Lower Hutt, New Zealand, pp. 365-372.

Salamon, M. D. G. 1992. Strength and Stability of Coal Pillars. In: Iannacchione, A. T., Mark, C., Repsher, R. C. Tuchman, R. J., and Jones, C. C. 1992. Proc. Workshop on Coal Pillar Mechanics and Design. U.S Bureau of Mines Information Circular 9315. pp. 94-121.

Salamon, M. D. G., and Munro, A. H. 1967. A Study of the strength of Coal Pillars. *J. S. Afr. Inst. Min. Metall.*, vol. 68, pp. 55-67.

Salamon, M. D. G., and Wagner, H. 1985. Practical Experiences in the Design of Coal Pillars. In: Green, A. R (ed). *Proc. 21st Int. Congr. Safety in Mines Research Institutes*, Sydney, pp. 3-9. Balkema.

Sheorey, P. R. 1993. Design of Coal Pillar Arrays and Chain Pillars. In: Hudson, J. A. (ed). Comprehensive Rock Engineering: Principles, practice and projects. Pergamon Press, vol. 2, pp. 631-670.

Sheorey, P. R., Biswas, A. K., and Choubey, V. D. 1989. An Empirical Failure Criterion for Rocks and Jointed Rock Masses. *Eng. Geol.*, vol. 26 (2), pp. 141-159.

Sheorey, P. R., Das, M. N., Barat, D., Prasad, R. K., and Singh, B. 1987. Coal Pillar Strength Estimations form Failed and Stable Cases. *Int. J. Rock Mech. Min. Sci. & Geomech. Abstr.*, vol. 24 (6), pp. 347-355.

Singh, M. M. 1981. Strength of Rock. Physical Properties of Rock and Minerals. McGraw-Hill, New York, pp. 81-121.

Sorenson, W. K., and Priseau, W. G. 1978. Statistical Analysis of Laboratory Compressive Strength and Young's Modulus Data for the Design of Production Pillars in Coal Mines. *Proc.19th Symp. on Rock Mech.*, vol. 1, pp. 30-37.

Stach, E., Mackowsky, M-Th., Teichműller, M., Taylor, G. H., Chandra, D., and Teichműller, R. 1982. Stach's Textbook of Coal Petrology, 3rd edition. Gebrűder Borntraeger Berlin. 535p.

Suggate, R. P. 1957. The Geology of the Reefton Subdivision. *New Zealand Geological Survey Bulletin No. 56.* 146p.

Szwilski, A. B. 1987. Evaluation of the Structural Properties of Coal Seams. *Mining Engineering*, Feb, pp. 115-118.

Trumbachev, V. F., and Melnikov, E. A. 1964. Distribution of Stresses in the Intervening Pillars at Medium and Steep Dips. In: Proc 4th Congr. Strat Control and Rock Mechanics, New York, pp. 316-322. Columbia University, New York.

Townsend, J. M., Jennings, W. C., Haycocks, C., Neall III, G. M. and Johnson III, L. P. 1977. A Relationship between the Ultimate Compressive Strength of Cubes and Cylinders for Coal Specimens. In: Wang, F., and Clark, G. B. 1977. Energy Resources and Excavation Technology. *Proc. 18th U.S Symp. on Rock Mech.* Colorado School of Mines Press, Golden, pp. 4A6-1 - 4A6-6.

Trueman, R., and Medhurst, T. P. 1994. The Influence of Scale Effects on the Strength and Deformability of Coal. IV CSMR/Integral Approach to Applied Rock Mechanics, vol. 1, ed. M Van Sint Jan. Sociedad Chilena de Geotechnica, Santiago, pp. 103-114.

Unrug, K. F., Nandy, S., and Thompson, E. 1987. Evaluation of Coal Strength for Pillar Calculations. Trans SME of AIME., vol. 280, pp. 2071-2075.

Van Heerden, W. L. 1973. In-Situ Determination of Complete Stress-Strain Characteristics of 1.4m Square Specimens with Width to Height Ratios up to 3.4. *CSIR Research Report* ME 1265.

Vicat, L. J. 1833. Researches on Physical Phenomena which Precede and Accompany Rupture or Deformation of a Certain Class of Solids. Ann. Ponts et Chaussees, pt. 2, 201p. (Cited in Babcock, C. O. 1981. Pillar Design Equations for Coal Extraction. U. S. Bureau of Mines information Circular no. 8973, pp. 36-48.

Wagner, H. 1974. Determination of the Complete Load-Deformation Characteristics of Coal Pillars. *Proc. 3rd Int. Congr. Rock Mech.*, ISRM, Denver, vol. 2B, pp. 1076-1082.

Wagner, H. 1992. Pillar Design in South African Collieries. In: Iannacchione, A. T., Mark, C., Repsher, R. C. Tuchman, R. J., and Jones, C. C. 1992. Proc. Workshop on Coal Pillar Mechanics and Design. U.S Bureau of Mines Information Circular 9315. pp. 283-301.

Wang, F. D., Skelly, W. A, and Wohlgemuth, J. 1977. In-Situ Coal Pillar Strength. *Proc 18th Symp. Rock Mechanics.*

Ward, S. 1997. Lithostratigraphy, Palynostratigraphy and Basin Analysis of the Late Cretaceous to Early Tertiary Paparoa Group, Greymouth Coalfield, New Zealand. Unpublished Ph.D Thesis, University of Canterbury. 200p.

Wellman, H. W. 1952. Interpretation and Discussion of Analysis. In: Gage, M. 1952. The Greymouth Coalfield. *New Zealand Geological Survey bulletin 45.* pp. 78-104.

Wilson, A. H. 1980. The Stability of Underground Workings in the Soft Rocks of the Coal Measures. Ph.D Thesis, University of Nottingham.

Wilson, A. H. 1983. The Stability of Underground Workings in the Soft Rocks of the Coal Measures. *Int. J. Mining Engineering*, vol. 1 (2), pp. 91-187.

Yardley, W. 1993. Assessment of Mining Conditions in Liverpool Mines and Mt Davy Stone Drive from Historic Records and Interviews with Former Employees on 2 June 1993 and 11 June 1993. In: Unknown report. Dated 16 June 1993, 7p.

Yardley, W. 1996. The Design of Coal Mine Pillars. *New Zealand Mining*, vol. 19, pp. 16-18.

Yardley, W. 1998. Floor Heave at Terrace Mine. In: Field, A. 1998. Terrace Development Feasibility Report-June 1998. Unpublished report prepared for Solid Energy.

Part 2

Appendices 1-9

Appendix 1.

A1.1 Sample Numbering System

Samples were given individual numbers depending on their location and the type of testing to which they were subjected. The name of each mine or the location from where samples were collected was given a one or two letter abbreviation as follows:

Bishop Block	BB
Roa Mine	R
Spring Creek Mine	SC
Strongman No. 2 Mine	SM
Terrace Mine	T

Each seam was then given an abbreviation put after the name of the mine.

D seam	D
E seam (Opencast)	E/OC
E seam (Underground)	E/UG
Kimbell	K
Main Upper	MNU
Morgan	M
No. 4 seam	4

These were then numbered for reference during each series of testing, 1, 2, 3... etc while cube samples were numbered C1, C2, C3...etc.

A1.2 Weathering Grades

Grade	Term	Description
VI	Residual soil	All rock material is converted to soil. The mass structure and material are destroyed. There is a large change in volume, but the soil has not been significantly transported.
V	Extremely/Completely weathered	All rock material is decomposed and/or disintegrated to soil. The original mass structure is largely intact.
IV	Highly weathered	More than half the rock is decomposed to a soil. Fresh or discoloured rock is present either as a continuous framework or as corestones.
III	Moderately weathered	Less than half of the rock is decomposed and/or disintegrated into a soil. Fresh or discoloured rock is present either as a continuous framework or as corestones.
II	Slightly weathered	Discoloration indicates weathering of rock material and discontinuity surfaces. All the rock material may be discoloured by weathering and may be somewhat weaker externally than it is in fresh condition.
I	Fresh rock	No visible signs of rock material weathering; perhaps slight discoloration on major discontinuity surfaces.

Table A1.1. Classification of weathering grades for rock masses (after Brown, 1981).

A1.3 Calculation of Statistical Parameters

Calculation of the mean and standard deviation quoted for each set of test results was conducted by disregarding the highest and lowest values as recommended in the ISRM standard test methods (Brown, 1981). In the case of the point load tests, the two highest and lowest values were disregarded.

The coefficient of variation is a measure of how much the standard deviation varies from the mean and is a good way of comparing the variance in sample populations with different means.

$$\text{Coefficient of variation} = \frac{std\ \ dev.}{mean} \times 100\%$$

Appendix 2. Unconfined Compressive Strength Determination of Core Samples

A2.1 Test Method

All samples tested were of 54mm (NX) diameter core, and where possible with L/D 2.5-3.0. Ends of the sample were made as flat as possible without being ground flat so to not risk breaking the sample. Sample diameter was measured in six locations (being two measurements at right angles at the base, mid-height and top of the sample) which are averaged and presented in Table A2.1 along with sample length. The unconfined compressive strength is calculated as follows:

$$UCS = \frac{P}{A} \text{ (MPa)} \qquad \text{where: P = failure load (kN)}$$

A = cross sectional area (mm^2)

A2.2 Data Tables

Sample No.	Bedding Orientation	Length (mm)	Average Core Diameter (mm)	Cross Sectional Area (mm^2)	L/D Ratio	Failure Load (kN)	UCS (MPa)	Moisture Content %	Bulk Density (g/mm^3)
Spring Creek D seam									
SC/D/1	⊥	131	54.03	2293	2.42	18.6	8.1	8.06	1.27
SC/D/2	45°	143	54.03	2293	2.65	14.2	6.2	11.28	1.27
SC/D/3	35°	139	54.05	2295	2.57	13.6	5.9	12.21	1.29
SC/D/6	⊥	128	53.97	2289	2.37	40.3	17.6	11.69	1.28
SC/D/7	80°	149	53.98	2289	2.76	30.7	13.4	7.91	1.27
SC/D/12	25°	128	54.11	2300	2.37	14.9	6.5	7.07	1.25
SC/D/13	15°	124	54.08	2297	2.29	23.1	10.1	7.77	1.30
Spring Creek Main Upper seam									
SC/MNU/5	15°	138	54.06	2295	2.55	10.5	4.6	9.40	1.36
SC/MNU/6	5°	148	54.09	2298	2.74	24.5	10.7	9.96	1.27
SC/MNU/7	85°	134	54.04	2294	2.48	31.3	13.6	7.62	1.26
SC/MNU/9	15°	162	54.03	2293	3.00	8.2	3.6	6.22	1.26
SC/MNU/11	10°	151	54.04	2297	2.79	18.8	8.2	7.79	1.28
SC/MNU/12		143	54.02	2292	2.65	15.9	7.0	7.08	1.27
SC/MNU/13	10°	148	54.12	2301	2.73	22.6	9.8	7.51	1.27
SC/MNU/14	10°	147	54.09	2298	2.72	11.5	5.0	8.81	1.27
SC/MNU/15	10°	133	54.03	2293	2.46	8.2	3.6	6.27	1.27
SC/MNU/16	15°	145	54.10	2299	2.68	10.6	4.6	4.99	1.26
SC/MNU/17	15°	150	53.98	2288	2.77	22.2	9.7	7.38	1.28

Strongman No. 2 D seam								
SM/D/1	†	131	54.01	2291	2.43	34.1	14.9	
SM/D/3		117	53.99	2290	2.98	44.0	19.2	
SM/D/4		124	54.04	2293	2.29	16.7	7.3	
SM/D/9		125	54.04	2293	2.31	21.5	9.4	
SM/D/11		131	54.14	2302	2.42	38.3	16.6	
SM/D/12		124	54.08	2297	2.29	59.0	25.7	
SM/D/13		158	54.15	2303	2.92	31.3	13.6	
SM/D/14	⊥	144	54.11	2300	2.66	47.5	20.7	
SM/D/15		144	54.18	2305	2.66	39.9	17.3	
SM/D/16		157	54.15	2303	2.90	1.2	0.5	
SM/D/23		117	53.99	2289	2.17	72.3	31.6	
SM/D/24	⊥	124	54.02	2292	2.30	53.3	23.3	
SM/D/25	‖	149	54.01	2291	2.76	60.7	26.5	
SM/D/26		135	54.00	2290	2.50			
SM/D/27	‖	113	54.16	2304	2.09	49.3	21.4	
SM/D/28	‖	117	54.08	2297	2.16	46.6	20.3	
SM/D/29	60°	131	54.03	2293	2.42	7.6	3.3	
Strongman No. 2 E seam								
SM/E/OC/2	†	158	53.95	2286	2.93	25.4	11.1	
SM/E/OC/3		142	53.94	2285	2.63	18.8	8.2	
SM/E/OC/4		150	53.96	2287	2.78	17.2	7.5	
SM/E/OC/5		159	53.95	2286	2.95	49.0	21.5	
SM/E/OC/6		160	53.99	2290	2.96	30.2	13.2	
SM/E/OC/7		137	53.84	2276	2.54	17.8	7.8	
SM/E/OC/10		157	54.00	2290	2.91	18.6	8.1	
SM/E/OC/12	‖	143	54.02	2292	2.65	22.8	9.9	
SM/E/OC/15	⊥	144	54.00	2290	2.67	38.5	16.8	
SM/E/UG/1	†	130	54.13	2295	2.40	17.1	7.4	
SM/E/UG/2		134	54.10	2298	2.48	51.0	22.2	
SM/E/UG/3		138	54.08	2297	2.55	44.8	19.5	
SM/E/UG/4		115	54.07	2296	2.13	66.8	29.1	
SM/E/UG/5		133	54.12	2301	2.46	69.8	30.4	
SM/E/UG/6		147	54.09	2298	2.72	65.6	28.5	

Table A2.1. Results of unconfined compressive strength tests on core samples. † Bedding orientation was often impossible to determine in samples from the Strongman No. 2 Mine.

A2.3 Plots of Unconfined Compressive Strength vs. L/D Ratio

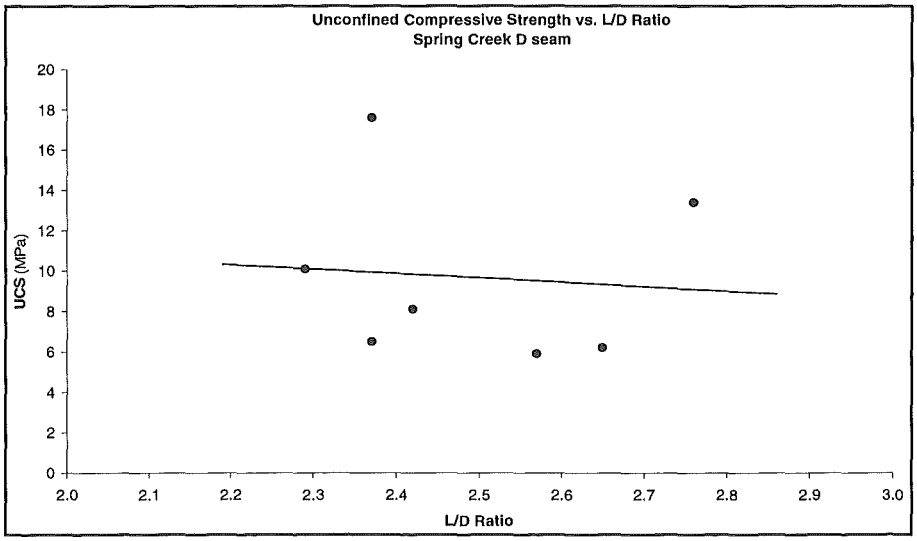

Figure A2.1. Unconfined compressive strength vs. L/D ratio for Spring Creek D seam.

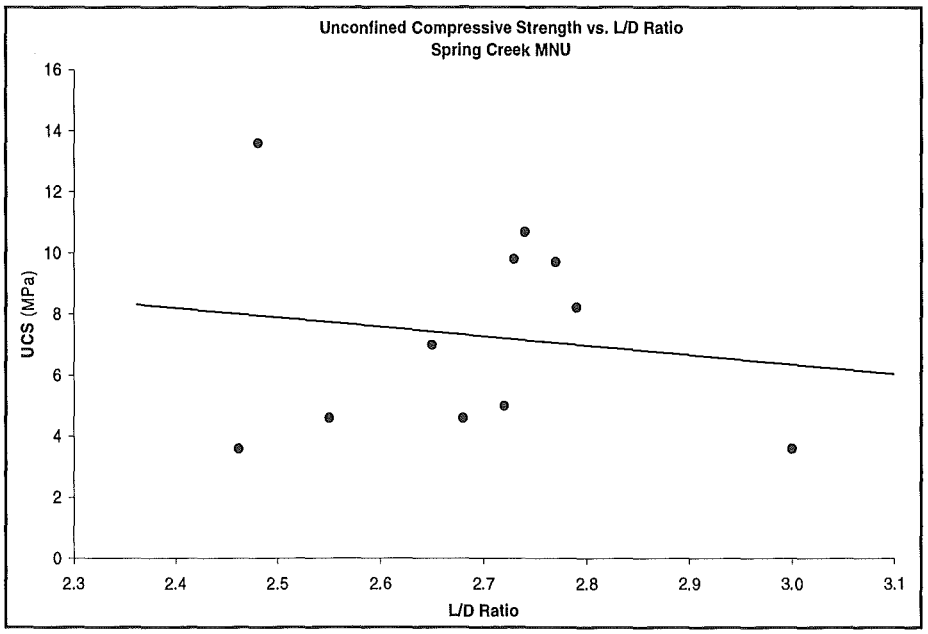

Figure A2.2. Unconfined compressive strength vs. L/D ratio for Spring Creek Main Upper seam.

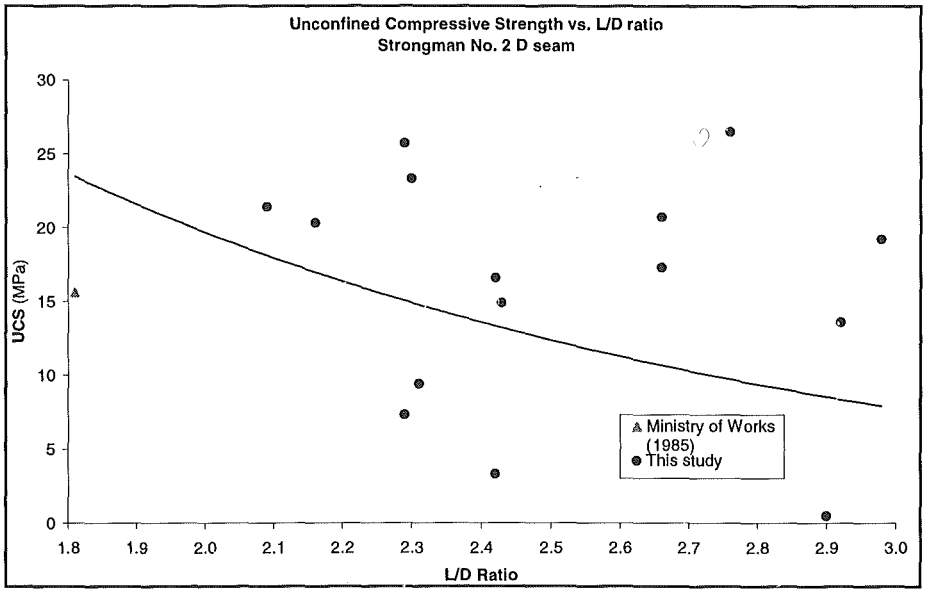

Figure A2.3. Unconfined compressive strength vs. L/D ratio for Strongman No. 2 D seam.

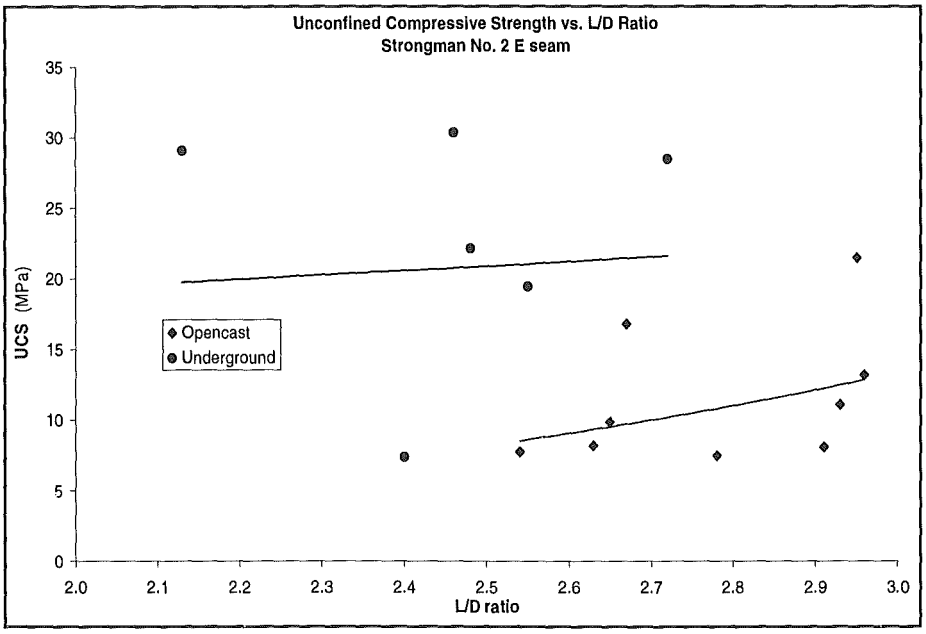

Figure A2.4. Unconfined compressive strength vs. L/D ratio for Strongman No. 2 E seam.

A2.4 Description of Samples and Mode of Failure

A2.4.1 Spring Creek D seam

SC/D/1: Series of cleats running parallel to each other, and perpendicular to bedding. Failed by axial splitting.

SC/D/2: Dominant feature is the crack which runs across the top. Very well defined bedding planes (40° to loading direction). Stepped failure along bedding planes. Alternating bright and dull bands controlled the failure.

SC/D/3: Dominated by bedding. There is one crack along a bedding plane which will probably be significant. Failed along the pre-existing fracture and also along a bedding plane (Figure A2.5a).

SC/D/6: Pretty well intact. Loading perpendicular to bedding. No important cracks. No failure mechanism recorded, but likely to be cataclasis.

SC/D/7: Cracks only on one side. Failed by axial splitting (Figure A2.5b).

SC/D/12: Numerous cracks which are concentrated on one side and run perpendicular to bedding.

SC/D/13: Couple of significant cleats which run up both sides. They are quite prominent but not as open as some others. A few other features run perpendicular to these. Failed by axial splitting.

A2.4.2 Spring Creek Main Upper seam

SC/MNU/5: Many cracks around the top on one side. Two very prominent bedding planes run down both sides. Failed on numerous planes by shearing.

SC/MNU/6: A couple of dominating fractures, one of which will control the failure. No failure mechanism recorded (Figure A2.5c).

SC/MNU/7: A couple of significant cracks which cut bedding. Cracks scattered around the sample. Some spalling from the sides, but is still otherwise intact. This is a reasonably common mode of failure (Figure A2.5d).

SC/MNU/9: One major cleat plane which is slightly undulating. More prominent on one side than the other. There are other smaller fractures.

SC/MNU/11: The dominating fractures runs down only one side and perpendicular to bedding. Appears to have failed along this fracture, by axial splitting along a bedding plane.

SC/MNU/12: There are a few fractures but none are as dominating as there has been in the other samples. Bedding is much less pronounced in Main Upper seam than D seam. Failed by combination of shearing and axial splitting.

SC/MNU/13: There are a few fractures in this one but they are small. Main factor may be bedding orientation (10° to loading direction). Failed by axial splitting in a brittle manner (hourglass shape; Figure A2.6a).

SC/MNU/14: One cleat is the dominating feature and may cause a premature failure. The rest of the sample is largely free of cleats. Just faint cracks. Failed by shearing with an axial component on the opposite side to the faint cracks (Figure A2.6b).

SC/MNU/15: There is a cleat which runs through the entire sample and there is another one at the top. Bedding perpendicular to fractures. No failure mechanism recorded.

SC/MNU/16: A few large cracks, concentrated on one side but there are a couple in the same orientation on the other side. The orientation of the defects led to a double shear failure. Both have completely failed (Figure 2.6c).

SC/MNU/17: Similar to sample SC/MNU/16. Most of the cleats are concentrated on one side. Failed by cataclasis (Figure A2.6d).

A2.4.3 Strongman No. 2 D seam

SM/D/1: Prominent large cleat running through the sample. Not quite continuous (~ ¾ of the way through). Runs down both sides ~60° to loading direction. Failed by cataclasis.

SM/D/4: Cleats run across the top of the sample ~25mm down and one goes off at 60° to it. Failed by axial splitting (Figure A2.7a).

SM/D/9: Cleats running in 2 different directions. Not as prominent as some other samples, but still may have an influence on the overall strength. Don't appear to run down both sides of the sample. Failed by axial splitting (Figure A2.7b).

SM/D/11: Contains no surface defects. Would expect the strength on this one to be higher. Failure by axial splitting (Figure A2.7c).

SM/D/12: No major surface cleats. Failed by slabbing from one side before it finally failed by cataclasis in an explosive manner.

SM/D/13: Scattered minor cracks with two non continuous large ones near the base of the sample. Failure by slabbing from sides and axial splitting.

SM/D/14: Only a few smaller defects visible. A small cleat plane at back of sample and cracks in the front. Loading direction perpendicular to bedding. Failed by axial splitting.

SM/D/15: Failure by very well defined axial splitting.

SM/D/16: Numerous large and prominent cleats. Would expect this sample to fail very soon. Specimen failed to take much load and literally fell apart along the numerous cleat planes.

SM/D/23: Sample is quite short and contains no cleats. Failed by cataclasis.

SM/D/24: Loading perpendicular to bedding. Only a small fracture running vertically for $^1/_3$ of the sample. Failed by axial splitting. Sample broke down the centre, with one side staying intact and the other side exploding. Combination of axial splitting and cataclasis.

SM/D/25: Loading parallel to bedding. Contains no cleats. Failure by axial splitting and cataclasis. Same as sample SM/D/24, 2 halves, only 1 intact.

SM/D/27: Contains only minor cleats. Loading parallel to bedding. Failed by slabbing off the sides.

SM/D/28: Loading parallel to bedding. Quite a few radial cracks concentrated on one side. Connected by a few axial cracks. Failed by slabbing off the sides.

SM/D/29: Sample contains large open cleats. Will fail early. Loading almost parallel to bedding, 60-70°. Failed to take any load beyond 7.6kN.

A2.4.4 Strongman No. 2 E seam

SM/E/OC/2: Large cleat which runs down both sides and will be very detrimental to the strength. Failure was along the cleat plane with a portion of axial splitting.

SM/E/OC/3: A few small cleats. Bottom left is the most important and should be the only one having a bearing on the strength. It did fail on the larger cleat, but this wasn't the main failure. Failed by axial splitting with a large split off the side being the main failure.

SM/E/OC/4: A lot of large cleats around the top of the sample. Would expect these to cause it to fail early. Mostly continue completely around the sample. As expected the top was sheared off with a crack running down the centre of the sample, though this had not failed.

SM/E/OC/5: No noticeable major features in it and correspondingly it had a very high strength. Failure began by slabbing of the sides. A few early pieces fell of, but the eventual main mode of failure was axial splitting.

SM/E/OC/6: Very large cleat which runs close to the edge and down both sides. Would expect this piece to slab off but it may not fail completely if this happens. Axial splitting was the main mode of failure. A large crack split the sample straight down the centre.

SM/E/OC/7: Very large cleat which runs down both sides. Failed by axial splitting along the major cleat and other axial cracks.

SM/E/OC/10: Only a few fractures which are not well defined. Cleat planes run 45° to loading direction. Failed across top on a cleat plane then down the centre by axial splitting.

SM/E/OC/12: No cleats, but loading direction parallel to bedding, so this may cause some loss of strength. Failed by axial splitting and slabbing from the sides of the sample.

SM/E/OC/15: Loading perpendicular to bedding. Only a few cracks in this one. Nothing too significant or continuous. Failed by cataclasis.

SM/E/UG/1: Large open cleats. Appears to have failed by a combination of mechanisms. Shearing and slabbing/axial splitting.

SM/E/UG/2: A few small cleats but they are faint. No failure mechanism recorded

SM/E/UG/3: A few small faint cleats. No failure mechanism recorded

SM/E/UG/4: Sample is short and absent of fractures so will probably be quite strong. Failed by cataclasis in an explosive manner.

SM/E/UG/5: Only one really faint crack. No failure mechanism recorded

SM/E/UG/6: Failed by axial splitting.

A2.5 Core Photos from Unconfined Compressive Strength Testing

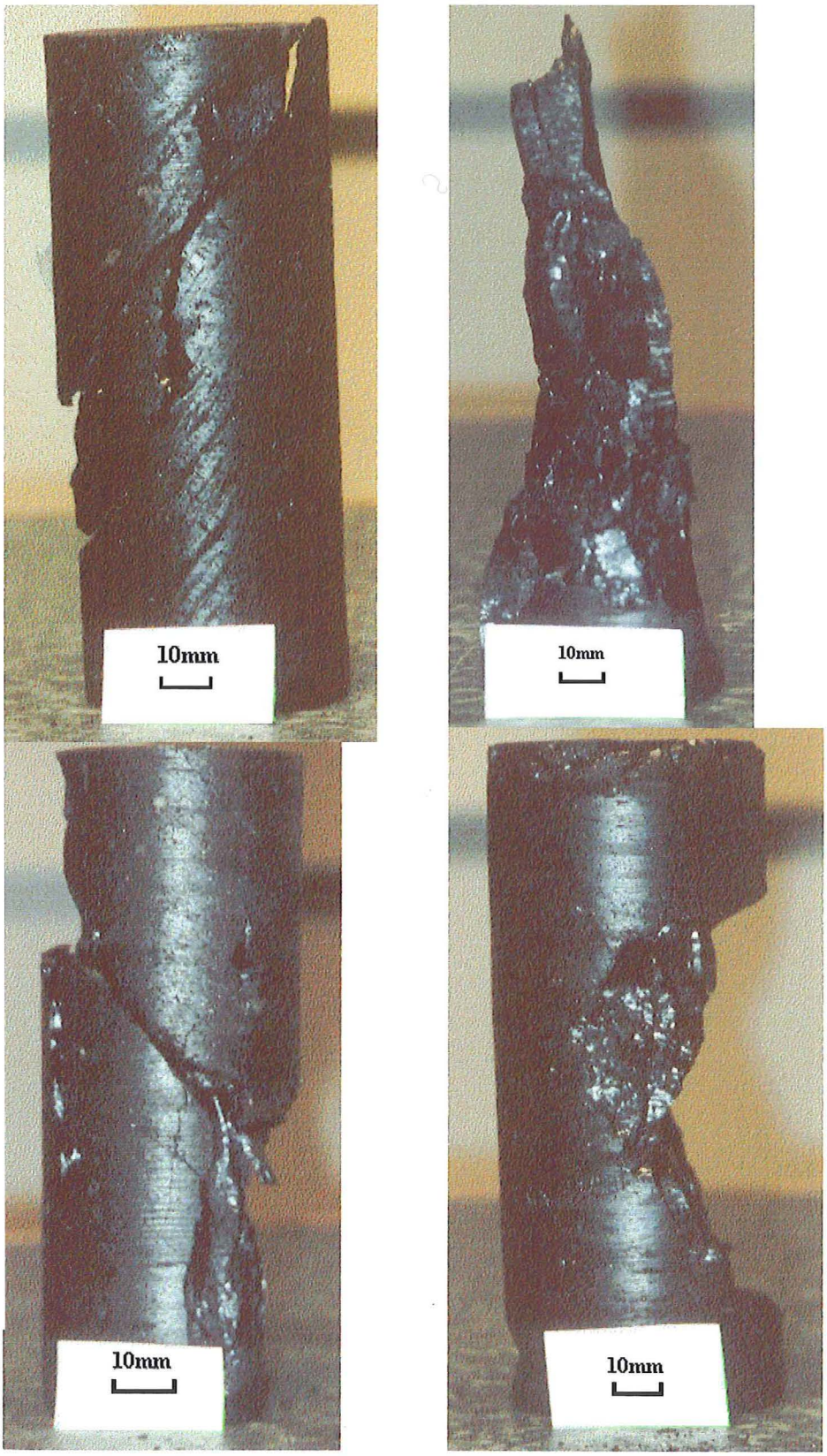

Figure A2.5a-d) Core photos from unconfined compressive strength testing. Sample numbers clockwise from top left SC/D/3, SC/D/7, SC/MNU/6 and SC/MNU/7.

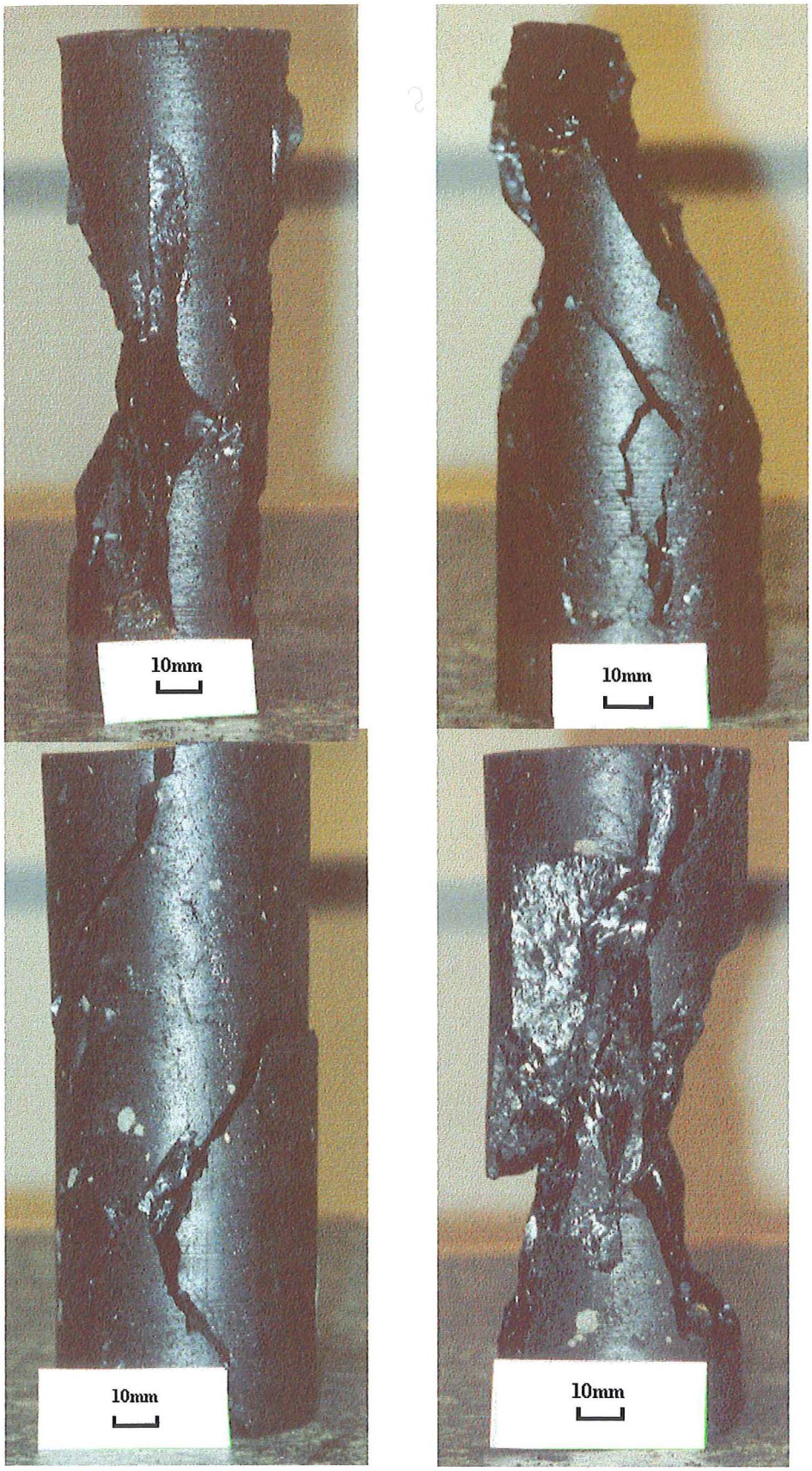

Figure A2.6a-d) Core photos from unconfined compressive strength testing. Sample numbers clockwise from top left SC/MNU/13, SC/MNU/14, SC/MNU/16 and SC/MNU/17.

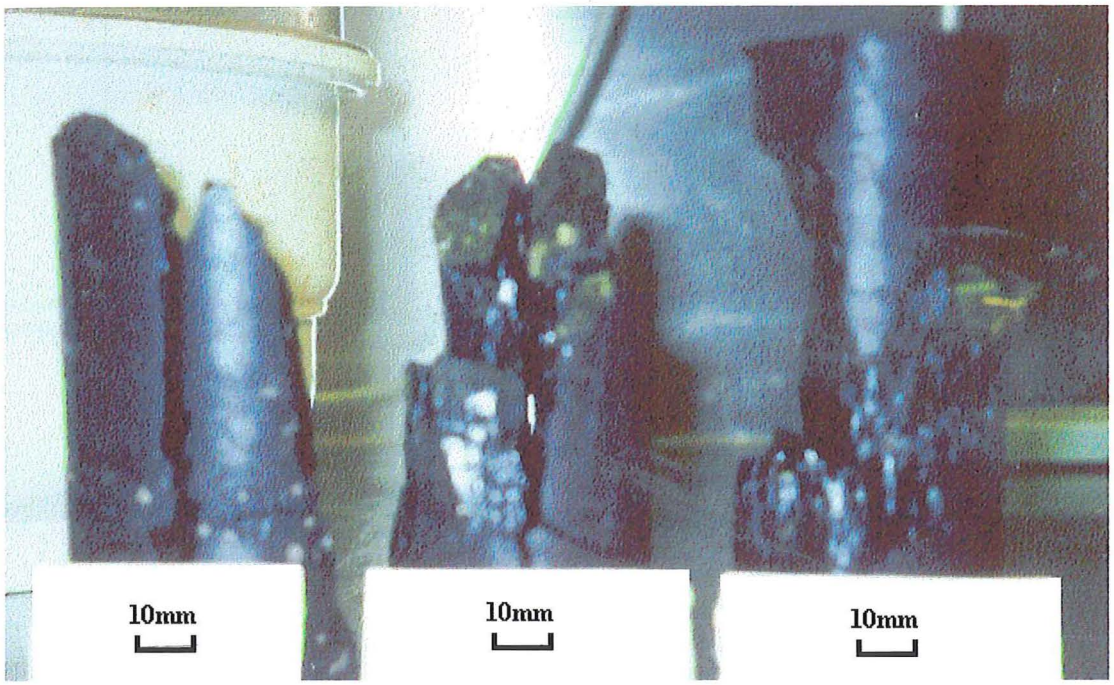

Figure A2.7a-c) Core photos from unconfined compressive strength testing. Sample numbers from left to right SM/D/4, SM/D/9 and SM/D/11.

A2.6 Young's Modulus

Location	Travel time (μs)		Velocity (m/s)		E_{dyn}	Poisson's
	P-wave	S-wave	P-wave	S-wave	(GPa)	ratio, ν
Strongman No. 2 D seam						
SM/D/23	49.3	166.5	2273.2	702.7	1.75	0.45
SM/D/24	73.2	169.9	1694.0	729.8	1.81	0.39
SM/D/25	67.9		2194.4			
SM/D/26	55.0		2454.5			
SM/D/27	46.0		2456.5			
E/UG						
SM/E/UG/2	64.4	185.8	2080.7	721.2	1.83	0.43
SM/E/UG/3	55.7	180.6	2477.6	764.1	2.08	0.45
SM/E/UG/4	54.0		2129.6			
SM/E/UG/5	61.1		2176.8			
SM/E/UG/6	59.5		2470.6			

Table A2.2. P and S wave velocities used in the determination of Young's Modulus and Poisson's Ratio.

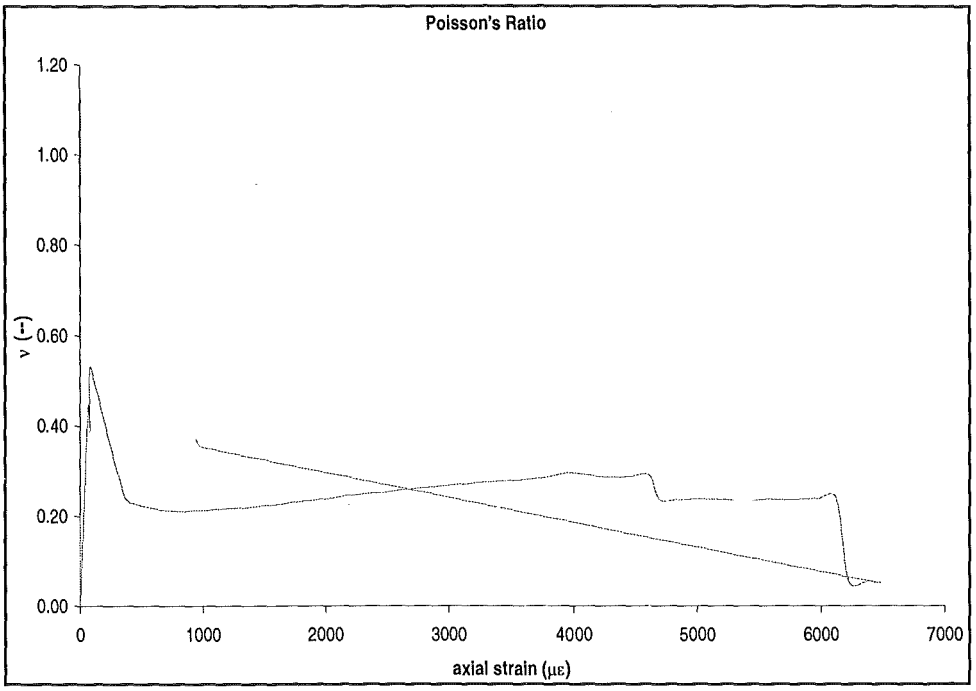

Figure A2.8. Plot of Poisson's Ratio vs. axial strain for Strongman No. 2 E seam opencast sample SM/E/OC/5.

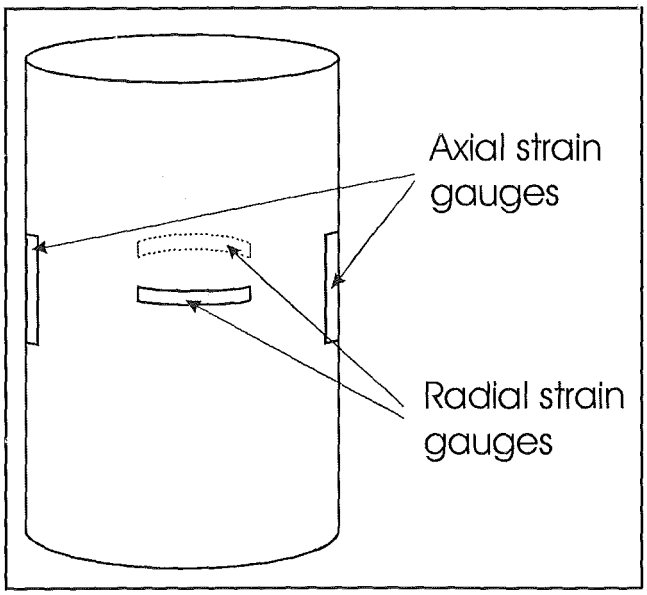

Figure A2.9. Arrangement of strain gauges for the determination of dynamic Young's Modulus.

Appendix 3. Unconfined Compressive Strength Determination of Cube Samples

A3.1 Test Method

There are no known standards for this test, so guidelines were taken from Townsend *et al.* (1977) who, like this study, experienced difficulties preparing perfect cube samples. This study used cube samples with an average side length of 63.5mm (2 ½"), with size limits set as follows:

$$0.95 < \text{width/height} < 1.05$$
$$0.95 < \text{width/depth} < 1.05 \qquad \text{(after Townsend } et\ al.\text{, 1977)}$$

Anything outside of this range was not considered. If greater than 10% of the cross sectional area of the surface to be loaded was missing the sample would also be disregarded. Otherwise this missing area would be filled with Plaster of Paris which appeared to have no significant effect on the strength of the coal. Cubes were prepared from lump samples using a diamond tipped saw. The sides of the samples were not ground flat as this would have caused the sample to break.

Cube compressive strength (CCS) is calculated as follows:

$$CCS = \frac{P}{A} \quad \text{(MPa)} \qquad \text{where: P = Failure load (kN)}$$

A = Cross sectional area of sample (mm^2)

The loading frame used for testing cube samples is the same as that used for the unconfined compressive strength.

A3.2 Data Tables

Sample No.	Bedding Orientation	Width ave. (mm)	Height ave. (mm)	Cross Sectional Area (mm^2)	Failure Load (kN)	Compressive Strength (MPa)	Plaster Cap Y/N	Moisture Content %	Bulk Density (g/cm^3)
Bishop Block Kimbell seam									
BB/K/C1		65.02	63.46	4228	42.0	9.9	Y	5.35	1.22
BB/K/C2	75°	63.06	63.90	3976	26.0	6.5	Y	3.35	1.21
BB/K/C3	75°	62.00	64.96	3843	16.9	4.4	Y	3.87	1.21
BB/K/C4	80°	62.67	65.82	3927	19.6	5.0	Y	3.34	1.25
BB/K/C5	80°	63.92	66.67	4086	32.0	7.8	Y	3.84	1.24
BB/K/C6	80°	63.39	63.25	4018	55.1	13.7	Y	3.56	1.24
BB/K/C7	⊥	66.58	64.56	4433	40.6	9.2	Y	3.62	1.23
BB/K/C8		64.16	66.38	4117	30.1	7.3	Y	4.81	1.25
BB/K/C9		64.32	63.87	4137	37.2	9.0		4.45	1.26
Bishop Block Morgan seam									
BB/M/C1	75°	62.83	63.33	3948	23.6	6.0	Y	3.00	1.20
BB/M/C2	70°	63.14	64.55	3987	4.6	1.2	Y	3.71	1.20
BB/M/C3	70°	63.59	67.19	4043	7.0	1.7	Y	4.80	1.21
BB/M/C4	45°	62.47	65.20	3903	27.4	7.0	Y	6.71	1.22
BB/M/C5	45°	63.62	68.05	4048	21.5	5.3	Y	4.16	1.24
BB/M/C6	10°	63.30	66.62	4007	8.1	2.0	Y	6.15	1.20
BB/M/C7	70°	66.19	64.31	4381	7.6	1.7	Y	5.34	1.18
Roa Kimbell seam									
K/C1	5°	64.41	64.63	3894	12.6	3.2	Y	1.44	1.13
K/C2	∥	60.63	61.69	3676	8.7	2.4	Y	1.55	1.33
K/C3	70°	64.35	66.35	4141	15.8	3.8	Y	2.18	
K/C4	30°	63.11	60.71	3983	23.3	5.8		2.49	1.17
K/C5	65°	63.29	64.86	4005	12.2	3.0	Y	2.90	1.22
K/C6		62.43	66.08	3897	9.7	2.5	Y	0.96	1.22
K/C7		64.33	65.80	4138	11.0	2.7		1.13	1.21
Spring Creek D seam									
SC/D/C1	⊥	65.63	61.72	4307	51.9	12.1	Y	7.11	1.26
SC/D/C2	⊥	62.23	64.63	3872	75.6	19.5		9.68	1.25
SC/D/C3	⊥	63.29	62.23	4005	99.6	24.9		9.44	
SC/D/C4	65°	60.33	60.51	3640	138.5	38.0		6.63	1.25
SC/D/C5	55°	62.68	61.10	3298	58.9	15.0	Y	9.36	1.24
Spring Creek Main Upper seam									
SC/MNU/C1	5°	61.81		3820	51.7	13.5		7.37	1.29
SC/MNU/C2	10°	62.26		3876	57.6	14.9		6.25	1.27
SC/MNU/C3	75°	62.84		3948	99.1	25.1		6.59	1.30
SC/MNU/C4	70°	63.02		3971	109.8	27.7		4.66	1.23
SC/MNU/C5	75°	62.92	64.21	3959	55.0	13.9		6.76	1.27
SC/MNU/C6	75°	62.86	64.41	3951	129.0	32.7	Y	6.87	1.30
SC/MNU/C7	70°	62.24	63.58	3873	68.5	17.7	Y	7.28	1.28
Strongman No. 2 E seam									
SM/E/OC/C1	⊥	62.78	63.90	3941	78.5	19.9		6.30	1.23
SM/E/OC/C3	⊥	64.38	65.05	4145	71.2	17.2	Y	3.78	1.22
SM/E/OC/C4	⊥	64.95	62.57	4218	108.9	25.8		3.93	1.25
SM/E/OC/C5	∥	64.30	62.19	4134	86.3	20.9	Y	3.46	1.24
SM/E/OC/C6	⊥	65.30	62.49	4264	66.0	15.5	Y	3.75	1.22
SM/E/OC/C7	85°	63.06	63.61	3976	63.6	16.0	Y	5.47	1.22
SM/E/OC/C8	80°	63.42	63.18	4022	143.3	35.6	Y	2.13	1.22

Terrace No. 4 seam									
T/C1		60.02	62.39	3602	36.8	10.2		11.42	1.34
T/C2	85°	67.65	64.70	4576	68.3	14.9	Y	13.58	1.25
T/C3	80°	61.25	62.14	3754	45.4	12.1	Y	10.83	1.25
T/C4	⊥	62.49	65.29	3905	52.3	13.4	Y	11.51	1.27
T/C5	⊥	63.06	62.45	3977	81.2	20.4	Y	12.18	1.32
T/C6	85°	65.46	65.24	4284	50.1	11.7		10.60	1.30

Table A3.1. Results of unconfined compressive strength tests on coal cubes

A3.3 Description of Samples and Mode of Failure

Generally the cubes tend to fail by stress concentration on one or more corners, except for Roa coal, where axial cracking appeared to be more prominent (Figure 2.14).

A3.3.1 Bishop Block Kimbell Seam

BB/K/C1: Very extensively cleated. Bedding direction could not be determined. One edge capped with plaster. Weathering has penetrated some of the cleat planes. Two failure types. Crushing of two corners and one side (essentially all corners) and shearing along a cleat plane. Shearing is not a common mode of failure in cubes.

BB/K/C2: Extensive open cleats in all directions. Some slight weathering on edges and along a durain band 3mm thick. There appears to be a very low angle shear across cleats as well as sample dilation and opening of cleats.

BB/K/C3: Very extensively cleated. Dominant cleats run parallel to bedding. Plaster covers half of top. Crushed one side and component of axial splitting. Failed similar to Roa coal where it takes load to a point then continues to shorten.

BB/K/C4: Complete plaster cap on top. Again prominent open cleating in all directions, but maybe not as bad as last one (BB/K/C2). One side plastered. Has a prominent dull/woody chunk in one corner and is slightly weathered around this. Weathering has penetrated some of the cleat planes. Appears to have failed by axial splitting and buckling which was all concentrated on one side, although three sides have been crushed. Bright bands were weathered where as woody piece was not.

BB/K/C5: Some weathering on one corner. Less cleated than the last two (BB/K/C2, BB/K/C4). Two dominant cleats running horizontal. Vertical cleats are more dominant above the horizontal ones, but less dominant below. Failed by axial splitting and buckling.

BB/K/C6: Loading perpendicular to bedding. Not as well cleated as others, but the main cleats are more prominent. Tends to be two big cleats parallel to bedding and one perpendicular to bedding in each sample. Only two small corners of plaster. Complicated failure where the corners were crushed with a large component of axial splitting.

BB/K/C7: The dominant cleats in this appear to be perpendicular to bedding. It is well cleated but the dominant open ones are not present. Has the appearance of being axially split before testing. Two corners crushed in failure. There has been some axial splitting and is also a shear plane

BB/K/C8: This one is much brighter than the others. Can see the weathering in some of the cleats. Cleats are most prominent in horizontal direction. Some are open. Can't determine bedding, but main cleats are 75° to loading direction. Failed by axial splitting, dilation, and buckling. Weathering doesn't appear to have penetrated too far into it.

A3.3.2 Bishop Block Morgan Seam

BB/M/C1: Big open dominating cleats, and a big lump of plaster. Failure of one corner but not what caused the main failure. That was caused by axial splitting, but not typical axial splitting. This one is inclined c. 20° rather than vertical.

BB/M/C2: Dominating feature is a durain band which is less cleated than the vitrain. The cleats also run in different directions in the vitrain and durain layers. Failed by axial splitting/bucking. Load got to 4.6kN then dropped back quickly.

BB/M/C3: Two thick 6-10mm durain bands which are not cleated. Bright bands are cleated, but not nearly as much as has been seen. Two main cleats, vertical sub-perpendicular to bedding. Top completely plastered and bottom on one corner. Failed by axial splitting. One thin side (~5mm) fell off. Took a small amount of load, then it dropped again. This is common in the weathered samples.

BB/M/C4: Has a complete plaster cap on top, but none on bottom. A very big continuous crack along a dull band cuts off a corner which is about $^1/_3$ of the sample. Shear failure of two corners.

BB/M/C5: Prominent cleats vertical, 45° to bedding. Some are open. Horizontal cleats much more frequent. Plaster capping on top and bottom. Two thin durain bands ~3mm thick. Failure by crushing of entire cube.

BB/M/C6: Big crack running vertically parallel to durain band. Others also running vertically on different sides.

BB/M/C8: Big thick uncleated durain bands with well-cleated vitrain bands. Vitrain bands generally only have vertical cleats. Durain bands up to 25mm thick. Complete plaster caps top and bottom. Loaded for a while and then loading began to go backwards. Sample buckled and collapsed.

A3.3.3 Roa-Kimbell seam

Coal from this seam gets to a point where it fails to take anymore load, but it stays largely intact and continues to deform (shorten and expand laterally). It displays a large number of vertical cracks and the whole cube eventually crumbles to very small fragments. There is virtually no residual strength in this material.

R/K/C1: Recording stopped at 12.6kN. Continued to deform but load did not increase.

R/K/C2: Has a significant amount of plaster to try and fix a very irregular surface.

R/K/C3: No significant cleats. Banding is easy to see. Once again there are thick durain bands (≤ 6mm). Very good sub-vertical axial cracking is displayed in this sample. These run across the top, diagonally across the sample.

R/K/C4: Nothing really remarkable. This one failed, though nothing came off it. It just became shorter and fatter. Width 66.94 x 64.70, height = 48.64mm. There are definitely a greatly increased number of cracks, and these have become quite open. There is obvious bulging in the sides of the sample.

R/K/C5: Very thick durain and vitrain bands, although not especially prominent. No significant cleats and plaster not that large. Axial cracks present as usual as well as the radial cracks which occur when there is too much horizontal deformation.

R/K/C6: Most surfaces are quite rough. Plaster on one corner, but nothing major. Radial cracking once again present. This one, like most of the others, failed to fail, but instead loaded to a point then continued to deform but took no more load. Cracks in this one are different to others. Axial cracks are divided by a few horizontal ones.

R/K/C7: Some spalling of the sides, but there was mainly shortening. As with K/C1, loading increased to a point then held constant, but cube continued to shorten.

A3.3.4 Spring Creek D seam

SC/D/C1: Bedding perpendicular to loading direction. Most significant feature is quite a substantial plaster cap. The plaster capped side remained essentially intact throughout, though cracks were opened a bit further. On the uncapped side one corner collapsed and a crack propagated across the rest of that side. Even with the plaster cap, it still had the lowest strength of the SC/D cubes.

SC/D/C2: Bedding perpendicular to loading direction. There is a large crack which essentially splits the sample in half. From this crack it may be possible to shear the sample in half. Failed sample kind of triangle shaped. Both sides came off.

SC/D/C3: Most prominent feature is bedding which is more prominent than Main Upper Seam. Dull bands are thin and less in number than bright bands.

SC/D/C4: Once again bedding is prominent, with a few more dull bands than in the last one. Sample pretty much stayed intact, and then suddenly exploded to leave virtually nothing.

SC/D/C5: Sample stayed largely intact after failure, but there were very large open cracks.

A3.3.5 Spring Creek Main Upper Seam

SC/MNU/C1: There are minor cracks on all sides of the cube. Cube fails by spalling off the sides. Only one side is unaffected. There appears to be a partial shear failure coming from one corner partway through the specimen.

SC/MNU/C2: There is a more substantial crack in this one which propagates through about 4 sides. The big crack did not play a large part in the failure, though there was some displacement of it. Interesting to note that this failed perpendicular to bedding even though loading was parallel to bedding.

SC/MNU/C3: A crack that pretty much cuts a corner. A significantly higher strength was obtained when this was tested perpendicular to bedding.

SC/MNU/C4: A small amount of the back left corner failed as well as one side coming away in pieces. A very simple failure. The remainder of the block is still very much intact.

SC/MNU/C5: Lots of axial cracks which are generally minor, but some open.

SC/MNU/C6: Bedding easy to see, but not especially prominent. Very violent failure. Left three medium sized pieces and a whole lot of crumbs.

SC/MNU/C7: The major crack appears to have had a role in the failure, but cannot take complete responsibility. There has also been some development of the other large crack.

A3.3.6 Strongman No. 2 E seam (opencast)

SM/E/OC/1: Cleating is quite extensive in a cubic type pattern. One prominent cleat runs completely around the sample ~$^2/_3$ of the way up. Bedding very difficult to see. Failed by crushing of two corners, but almost an entire side.

SM/E/OC/3: A prominent vertical cleat, and some going around the cube also. Should not be as strong as the others because the cleats are bigger. No failure mechanism recorded.

SM/E/OC/4: Cleating is much less prominent in this sample. One main cleat about ½ way up runs around three sides, with a lot of smaller vertical ones. Mode of failure is crushing of one corner. Dilation seen across the main cleat.

SM/E/OC/5: No significant cleats. Has plaster on most corners. Half of the sample collapsed.

SM/E/OC/6: Generally open cleats especially parallel to bedding. Most of the cleats are parallel to bedding but some perpendicular. Plaster on four corners. Failed by crushing one corner. More has come away from the bottom half than the top. Appears to be component of axial splitting.

SM/E/OC/7: Very similar to the others. Well cleated. Very thin edge of plaster on top. Two or three prominent cleat sets in this seam oriented parallel and perpendicular to bedding. In all samples one prominent cleat running around the sample. Two main failure areas. Crushing of one side, and incomplete failure on a different corner.

SM/E/OC/8: Loading perpendicular to bedding. Few cleats in this sample. A few vertical interconnected with a few parallel to bedding, but nothing too exciting. A thin edge of plaster on a side. Completely exploded leaving a small piece.

A3.3.7 Terrace (No. 4 seam)

T/C1: No notes available.

T/C2: Not many cleats. Very solid. Failed by cataclasis in an explosive manner.

T/C3: One fairly major cleat and two small plastered corners. No failure mechanism recorded.

T/C4: Lots of large cracks. Continued to load even though there was a large amount of spalling from the sides of the sample. Appeared to have failed on the large cracks eventually.

T/C5: Plaster in three different places. Failed by collapse of one side.

T/C6: Many significant large cleats and some plaster also. Main crack goes the entire way around the sample. It is quite open and has other cleats coming off it. Collapse was concentrated on one corner which failed early due to a piece falling of because of a couple of cleats running through it.

Appendix 4. Point Load Strength

A4.1 Test Methods

There are four recognised sample types for use in the point load test, these being axial, diametral, block and irregular lump tests. All tests carried out in this study were by either axial or irregular lump methods. Axial specimens are required to have a length/diameter ratio of 0.3-1.0. Lump samples are required to be 50±35mm with depth/width ratio between 0.3-1.0, and the length at least 0.5 width. In some cases samples smaller than 15mm were used to obtain sufficient samples from some seams, but this was avoided wherever possible. Often the lump samples were small and approaching the minimum dimensions with most in the range of 20-30mm. Samples were sufficiently weak that failure could not occur within the recommended 10-60 second period. Most samples in this study failed within 5 seconds. When calculating the average point load strength for each seam the two highest and lowest values have been disregarded as recommended by the ISRM (Brown, 1981).

Point load strength, $I_{s(50)}$, is calculated as follows:

$$I_s = \frac{P}{D_e^2}$$

where: $D_e^2 = D^2$ for diametral tests

$= 4A/\pi$ for axial, block and lump tests

$F = (D_e/50)^{0.45}$ F = size correction factor

$I_{s(50)} = F.I_s$ $I_{s(50)}$ = point load strength corrected to a reference diameter of 50mm

Strength anisotropy, $I_{a(50)}$, can be calculated as the ratio of point load tests conducted perpendicular and parallel to bedding. Attempts were made to determine the anisotropy from the point load tests but with the size of the samples being used the bedding

orientation was often difficult or impossible to determine. In most cases $I_{a(50)}$ was calculated from 5-10 samples per seam. Values of $I_{a(50)}$ are given in Table A4.2.

A4.2 Data Tables for Core Samples

Sample No.	Bedding orientation	P (kN)	D (mm)	W (mm)	A (mm^2)	D_e^2	D_e	I_s	F	$I_{s(50)}$ (MPa)
Spring Creek D seam										
SC/D/1	∥	0.71	26.0	31.6	822	1047	32.4	0.68	0.82	0.56
	∥	0.69	21.4	40.1	858	1093	33.1	0.63	0.83	0.52
	∥	0.39	16.6	19.3	320	408	20.2	0.96	0.67	0.64
	∥	0.45	15.3	25.7	393	501	22.4	0.90	0.70	0.63
	∥	0.24	15.7	29.6	465	592	24.3	0.41	0.72	0.30
	∥	0.41	17.2	19.9	342	436	20.9	0.94	0.68	0.63
SC/D/2	A	0.30	19.0	54.0	1026	1307	36.2	0.30	0.86	0.26
	∥	0.34	41.3	47.6	1966	2504	50.0	0.14	1.00	0.14
	∥	0.57	24.6	30.2	743	946	30.8	0.60	0.80	0.48
	∥	0.39	26.0	41.8	1086	1383	37.2	0.28	0.88	0.25
	∥	0.28	21.8	37.8	824	1050	32.4	0.27	0.82	0.22
	∥	0.26	22.6	45.3	1024	1304	36.1	0.20	0.86	0.17
	∥	1.08	30.4	38.8	1180	1503	38.8	0.72	0.89	0.64
SC/D/3	∥	0.61	28.6	26.7	764	973	31.2	0.63	0.81	0.51
	∥	1.14	39.1	33.5	1310	1669	40.8	0.68	0.91	0.62
	∥	0.67	22.0	40.9	900	1146	33.9	0.58	0.84	0.49
	∥	0.57	19.5	35.2	686	874	29.6	0.65	0.79	0.51
	∥	0.57	27.3	35.9	980	1248	35.3	0.46	0.86	0.39
	∥	0.45	21.7	44.8	972	1238	35.2	0.36	0.85	0.31
	A	0.77	28.2	54.0	1523	1940	44.0	0.40	0.94	0.38
SC/D/6	A	0.87	24.7	53.9	1331	1696	41.2	0.51	0.92	0.47
	∥	0.63	29.4	31.2	916	1167	34.2	0.54	0.84	0.45
	∥	0.77	25.3	36.2	916	1167	34.2	0.66	0.84	0.56
	∥	0.26	23.0	35.4	814	1037	32.2	0.25	0.82	0.21
	⊥	0.26	26.3	26.1	686	874	29.6	0.30	0.79	0.24
SC/D/7	∥	0.39	16.3	31.2	509	648	25.5	0.60	0.74	0.44
	∥	0.67	27.1	26.4	715	911	30.2	0.74	0.80	0.59
	⊥	0.65	25.3	45.2	1142	1455	38.1	0.45	0.89	0.40
	⊥	0.37	17.0	19.0	322	410	20.3	0.90	0.67	0.60
	∥	0.22	19.8	20.8	411	523	22.9	0.71	0.70	0.50
SC/D/12	∥	1.14	24.8	33.9	839	1069	32.7	1.07	0.83	0.88
	∥	0.75	20.2	25.7	518	660	25.7	1.14	0.74	0.84
	⊥	1.04	26.5	30.9	818	1041	32.3	1.00	0.82	0.82
	⊥	1.14	27.1	21.7	588	749	27.4	1.52	0.76	1.16
SC/D/13	∥	0.59	30.3	41.8	1267	1613	40.2	0.37	0.91	0.34
	∥	0.16	19.4	30.2	585	745	27.3	0.21	0.76	0.16
	∥	0.55	22.6	25.2	568	724	26.9	0.76	0.76	0.58
	∥	0.67	24.7	25.3	624	794	28.2	0.84	0.77	0.65
	∥	0.30	15.8	24.0	378	482	22.0	0.62	0.69	0.43
	∥	0.45	25.0	20.2	505	643	25.4	0.70	0.74	0.52
	∥	0.49	19.5	22.4	436	555	23.6	0.88	0.71	0.63
	∥	0.53	18.8	24.0	450	574	23.9	0.92	0.72	0.66
Spring Creek Main Upper seam										
SC/MNU/5	∥	0.35	20.2	34.4	695	885	29.8	0.40	0.77	0.31
	∥	0.45	25.6	33.3	851	1084	32.9	0.42	0.81	0.34
	∥	0.32	26.2	25.6	669	853	29.2	0.38	0.76	0.29
	∥	0.12	26.2	25.4	664	846	29.1	0.14	0.76	0.11
	∥	0.45	24.7	31.7	783	997	31.6	0.45	0.79	0.36

	I	0.61	25.8	28.0	722	920	30.3	0.66	0.78	0.52
	I	0.51	18.8	26.4	495	631	25.1	0.81	0.71	0.57
SC/MNU/6	A	0.79	20.3	53.9	1094	1394	37.3	0.57	0.86	0.49
	I	0.45	28.0	43.8	1226	1562	39.5	0.29	0.89	0.26
	I	0.83	28.1	25.0	701	893	29.9	0.93	0.77	0.72
	I	0.18	21.1	24.0	505	644	25.4	0.28	0.71	0.20
	I	0.20	32.7	34.5	1128	1437	37.9	0.14	0.87	0.12
	I	0.22	32.6	23.6	768	978	31.3	0.23	0.79	0.18
	I	0.18	37.7	35.2	1325	1688	41.1	0.11	0.91	0.10
SC/MNU/7	A	0.71	34.2	54.0	1847	2353	48.5	0.30	0.98	0.30
	A	0.51	21.8	54.0	1177	1500	38.7	0.34	0.88	0.30
	I	1.06	23.2	26.6	616	785	28.0	1.35	0.75	1.01
	I⊥	1.16	23.1	20.5	472	602	24.5	1.92	0.70	1.34
	I⊥	0.61	21.0	24.0	504	642	25.3	0.95	0.71	0.68
	I⊥	0.85	27.6	31.1	857	1092	33.0	0.78	0.81	0.63
	I⊥	0.81	26.1	34.4	897	1142	33.8	0.71	0.82	0.58
	I⊥	0.37	20.1	29.1	585	745	27.3	0.50	0.74	0.37
SC/MNU/9	I	1.65	38.6	43.5	1677	2137	46.2	0.77	0.96	0.74
	I	0.41	34.2	41.1	1404	1788	42.3	0.23	0.92	0.21
	I	1.00	18.8	31.3	588	750	27.4	1.33	0.74	0.98
	I	0.89	20.1	26.8	539	686	26.2	1.29	0.72	0.93
	I‖	1.12	40.6	39.9	1618	2061	45.4	0.54	0.95	0.52
	I	0.79	22.6	36.0	812	1035	32.2	0.76	0.80	0.61
	I⊥	1.52	27.4	37.3	1022	1302	36.1	1.17	0.85	0.99
	I⊥	1.81	25.4	38.3	972	1238	35.2	1.46	0.84	1.22
	I	1.67	38.1	41.9	1596	2034	45.1	0.82	0.95	0.78
	I	1.26	18.7	36.2	676	861	29.3	1.46	0.77	1.12
SC/MNU/11	A	0.75	25.3	54.1	1369	1744	41.8	0.43	0.91	0.39
	I	0.65	21.1	25.6	539	687	26.2	0.95	0.72	0.69
	I	0.69	19.4	21.1	408	520	22.8	1.33	0.68	0.90
	I	0.83	33.7	26.8	903	1151	33.9	0.72	0.82	0.59
	I	0.41	22.0	28.5	626	797	28.2	0.51	0.75	0.38
	I	0.61	20.8	20.7	430	547	23.4	1.12	0.68	0.77
SC/MNU/12	I	0.55	19.2	34.5	661	843	29.0	0.65	0.76	0.50
	I	0.49	32.1	34.5	1107	1411	37.6	0.35	0.87	0.30
	I‖	0.35	27.9	30.3	845	1077	32.8	0.32	0.81	0.26
	I	0.43	18.0	28.9	520	663	25.7	0.65	0.72	0.47
	I	0.55	19.5	31.5	614	782	28.0	0.70	0.75	0.52
	I	0.49	23.8	33.8	804	1025	32.0	0.48	0.80	0.38
SC/MNU/13	I	0.43	35.9	45.4	1628	2074	45.5	0.21	0.95	0.20
	I	0.71	22.5	30.9	694	884	29.7	0.80	0.77	0.62
	I	0.28	20.4	38.3	781	995	31.5	0.28	0.79	0.22
	I	0.59	25.8	33.9	875	1114	33.4	0.53	0.82	0.43
SC/MNU/14	A	0.73	16.2	54.2	878	1119	33.4	0.65	0.82	0.53
	I	0.67	23.9	38.5	920	1172	34.2	0.57	0.83	0.47
	I	0.47	21.8	23.1	502	640	25.3	0.73	0.71	0.52
	I	0.73	23.6	38.0	897	1142	33.8	0.64	0.82	0.53
	I	1.22	20.8	29.5	614	782	28.0	1.56	0.75	1.17
	I	0.35	23.9	26.7	637	811	28.5	0.43	0.75	0.32
	I⊥	0.34	23.8	24.6	585	746	27.3	0.46	0.74	0.34
	I⊥	0.49	20.3	23.1	469	597	24.4	0.82	0.70	0.57
SC/MNU/15	A‖	1.52	24.3	54.1	1315	1675	40.9	0.91	0.90	0.82
	A‖	1.34	24.9	54.0	1345	1713	41.4	0.78	0.91	0.71
	I‖	1.81	32.4	35.4	1147	1461	38.2	1.24	0.87	1.08
	I	0.57	27.1	29.4	797	1015	31.9	0.56	0.80	0.45
	I	1.50	21.9	41.0	898	1144	33.8	1.31	0.82	1.08
	I	1.34	21.8	32.7	713	908	30.1	1.48	0.78	1.15
	I	0.69	28.6	41.4	1183	1507	38.8	0.46	0.88	0.41
	I	0.83	28.8	30.9	890	1134	33.7	0.26	0.82	0.21
	I	0.75	22.8	30.5	694	884	29.7	0.85	0.77	0.66
SC/MNU/16	A‖	1.61	23.6	54.1	1277	1626	40.3	0.99	0.90	0.89
	I	1.59	35.3	37.4	1320	1682	41.0	0.95	0.91	0.86
	I	1.40	22.8	35.1	799	1018	31.9	1.38	0.80	1.10
	I	1.02	35.5	34.4	1221	1556	39.4	0.66	0.89	0.59
	I⊥	0.47	25.4	38.3	973	1239	35.2	0.40	0.84	0.34

SC/MNU/17	A	0.77	19.3	54.1	1044	1330	36.5	0.58	0.85	0.50
	A	0.53	21.5	54.1	1163	1482	38.5	0.36	0.88	0.32
	I	0.43	34.1	31.7	1079	1375	37.1	0.31	0.86	0.27
	I	0.85	26.7	28.6	764	973	31.2	0.87	0.79	0.69
	I	0.24	35.8	34.5	1233	1571	39.6	0.15	0.89	0.13
Strongman No. 2 D seam										
SM/D/23	I	0.91	21.1	24.9	525.4	669.3	25.9	1.35	0.74	1.00
	I	0.67	15.0	18.1	271.5	345.9	18.6	1.93	0.64	1.24
	I	0.39	24.8	16.3	404.2	515.0	22.7	0.76	0.70	0.53
	I	0.28	18.3	20.0	366.0	466.2	21.6	0.60	0.69	0.41
SM/D/24	I	0.20	15.6	25.9	404.0	514.7	22.7	0.39	0.70	0.27
	I	1.16	25.5	38.0	969.0	1234.4	35.1	0.94	0.85	0.80
	I	2.15	39.6	32.8	1298.9	1654.6	40.7	1.30	0.91	1.19
	I	0.79	28.1	31.3	879.5	1120.4	33.5	0.71	0.84	0.59
	I	0.53	26.5	27.3	723.5	921.6	30.4	0.58	0.80	0.46
SM/D/25	I	1.85	18.7	53.6	1002.3	1276.8	35.7	1.44	0.86	1.24
	I	1.48	21.8	34.8	758.6	966.4	31.1	1.53	0.81	1.24
	I	1.79	23.3	36.1	841.1	1071.5	32.7	1.67	0.83	1.38
SM/D/28	I	0.41	25.1	16.6	416.7	530.8	23.0	0.77	0.71	0.54
	I	1.08	36.9	34.1	1258.3	1602.9	40.0	0.67	0.90	0.61
	I	0.89	21.6	25.0	540.0	687.9	26.2	1.29	0.75	0.96
	I	0.69	20.2	22.6	456.5	581.6	24.1	1.18	0.72	0.85
SM/D/29	I	1.24	39.0	43.8	1708.2	2176.1	46.6	0.57	0.97	0.55
	I	0.73	29.5	42.6	1256.7	1600.9	40.0	0.46	0.90	0.42
	I	1.46	22.2	34.3	761.5	970.0	31.1	1.51	0.81	1.22
	I	0.89	45.7	35.8	1636.1	2084.2	45.7	0.43	0.96	0.41
	I	1.32	24.7	44.2	1091.7	1390.8	37.3	0.95	0.88	0.83
	I	1.06	24.7	21.4	528.6	673.4	25.9	1.57	0.74	1.17
	I	0.51	26.8	27.0	723.6	921.8	30.4	0.55	0.80	0.44
	I	1.00	25.4	20.8	528.3	673.0	25.9	1.49	0.74	1.11
	I	1.30	25.0	32.5	812.5	1035.0	32.2	1.26	0.82	1.03
	I	1.16	23.7	24.3	575.9	733.6	27.1	1.58	0.76	1.20
Strongman No. 2 E seam										
SM/E/UG/2	I	0.71	25.6	21.3	545	694.62	26.4	1.02	0.75	0.77
	I	0.81	23.8	36.0	857	1091.46	33.0	0.74	0.83	0.61
	I	0.95	18.0	20.9	376	479.24	21.9	1.98	0.69	1.37
	I	0.89	19.1	24.9	476	605.85	24.6	1.46	0.73	1.06
	I	1.87	29.1	26.7	777	989.77	31.5	1.88	0.81	1.53
SM/E/UG/3	I	1.12	20.0	19.7	394	501.91	22.4	2.23	0.70	1.55
	I	0.98	28.7	30.5	874	1113.27	33.4	0.88	0.83	0.73
	I	0.91	21.3	30.8	656	835.72	28.9	1.09	0.78	0.85
	I	1.18	15.5	21.0	326	414.65	20.4	2.84	0.67	1.90
SM/E/UG/4	I	1.48	18.0	22.5	405	515.92	22.7	2.87	0.70	2.01
	I	0.57	16.3	23.6	385	490.04	22.1	1.16	0.69	0.80
	I	0.63	23.9	24.8	593	755.06	27.5	0.83	0.76	0.63
SM/E/UG/5	I	0.77	16.2	29.8	483	614.98	24.8	1.25	0.73	0.91
	I	0.91	21.5	33.5	720	917.52	30.3	0.99	0.80	0.79
	I	2.19	21.3	28.6	609	776.03	27.9	2.82	0.77	2.17
	I	0.32	18.2	23.3	424	540.20	23.2	0.59	0.71	0.42
SM/E/UG/6	I	0.87	18.6	25.9	482	613.68	24.8	1.41	0.73	1.03
	I	0.34	16.6	26.0	432	549.81	23.4	0.62	0.71	0.44
	I	0.81	20.2	25.6	517	658.75	25.7	1.23	0.74	0.91
	I	1.42	19.2	29.8	572	728.87	27.0	1.95	0.76	1.48
	I	0.73	33.7	31.9	1075	1369.46	37.0	0.53	0.87	0.46
	I	2.05	19.5	31.7	618	787.45	28.1	2.60	0.77	2.01
	I	1.46	18.1	22.7	411	523.40	22.9	2.79	0.70	1.96
	I	1.16	30.0	28.3	849	1081.53	32.9	1.07	0.83	0.89

Strongman No. 2	A	1.04	23.5	54.0	1269	1617	40.2	0.64	0.91	0.58
E/UG	A	1.61	39.9	54.1	2159	2750	52.4	0.59	1.02	0.60
Axial tests	A	1.75	38.7	54.0	2090	2662	51.6	0.66	1.01	0.67
	A	2.13	29.4	54.1	1591	2026	45.0	1.05	0.95	1.00
	A	1.04	41.4	54.0	2236	2848	53.4	0.37	1.03	0.38
	A	1.50	46.2	54.0	2495	3178	56.4	0.47	1.06	0.50
	A	2.13	47.7	54.0	2576	3281	57.3	0.65	1.06	0.69
	A	2.38	49.9	54.0	2695	3433	58.6	0.69	1.07	0.74
	A	0.75	40.2	54.0	2171	2765	52.6	0.27	1.02	0.28
	A	1.06	40.1	54.1	2169	2764	52.6	0.38	1.02	0.39
	A	0.51	33.8	54.0	1825	2325	48.2	0.22	0.98	0.22
	A	2.62	48.8	54.1	2640	3363	58.0	0.78	1.07	0.83
	A	0.79	37.8	54.0	2041	2600	51.0	0.30	1.01	0.30
	A	2.54	38.0	54.0	2052	2614	51.1	0.97	1.01	0.98
	A	0.47	24.1	54.1	1304	1661	40.8	0.28	0.91	0.26
	A	1.54	38.7	54.0	2090	2662	51.6	0.58	1.01	0.59
	A	2.50	37.0	54.2	2005	2555	50.5	0.98	1.00	0.98
	A	0.12	34.9	54.0	1885	2401	49.0	0.05	0.99	0.05
	A	1.58	25.0	54.0	1350	1720	41.5	0.92	0.92	0.85
	A	1.50	34.8	54.0	1879	2394	48.9	0.63	0.99	0.62
	A	1.02	47.8	54.2	2591	3300	57.4	0.31	1.06	0.33
	A	1.73	32.7	54.1	1769	2254	47.5	0.77	0.98	0.75
Strongman No. 2	A	1.58	29.4	54.0	1588	2022	45.0	0.78	0.95	0.74
E/OC	A	1.73	33.6	54.0	1814	2311	48.1	0.75	0.98	0.74
Axial tests	A	2.91	32.2	54.1	1742	2219	47.1	1.31	0.97	1.28
	A	2.03	43.1	54.0	2327	2965	54.5	0.68	1.04	0.71
	A	2.46	41.1	53.9	2215	2822	53.1	0.87	1.03	0.89
	A	0.96	41.7	53.9	2248	2863	53.5	0.34	1.03	0.35
	A	2.50	29.8	54.0	1609	2050	45.3	1.20	0.96	1.15
	A	3.17	35.3	54.0	1906	2428	49.3	1.31	0.99	1.30
	A	1.95	40.1	54.0	2165	2758	52.5	0.71	1.02	0.73
	A	2.20	45.1	54.0	2435	3102	55.7	0.71	1.05	0.75
	A	1.18	34.9	54.0	1885	2401	49.0	0.49	0.99	0.49
	A	1.56	50.9	54.0	2749	3501	59.2	0.46	1.08	0.50
	A	1.83	35.3	54.0	1906	2428	49.3	0.75	0.99	0.75
	A	1.44	30.4	54.0	1642	2091	45.7	0.69	0.96	0.66
	A	1.42	28.9	54.0	1561	1988	44.6	0.71	0.95	0.67
	A	1.30	30.1	54.1	1628	2074	45.5	0.63	0.96	0.60
	A	0.87	17.0	54.0	918	1169	34.2	0.74	0.84	0.62
	A	0.30	45.9	54.0	2479	3157	56.2	0.10	1.05	0.11
	A	0.77	36.0	54.0	1944	2476	49.8	0.31	1.00	0.31
	A	1.20	26.8	54.1	1450	1847	43.0	0.65	0.93	0.61
	A	1.12	31.1	54.0	1679	2139	46.3	0.52	0.97	0.50
	A	0.85	32.1	53.9	1730	2204	46.9	0.39	0.97	0.38
	A	1.71	37.6	53.9	2027	2582	50.8	0.66	1.01	0.66
	A	1.04	31.5	53.9	1698	2163	46.5	0.48	0.97	0.46
	A	0.96	22.6	54.0	1220	1555	39.4	0.62	0.90	0.56
	A	0.75	37.3	54.0	2014	2566	50.7	0.29	1.01	0.29
	A	1.95	45.8	54.0	2473	3151	56.1	0.62	1.05	0.65
	A	1.10	35.5	54.0	1917	2442	49.4	0.45	0.99	0.45
	A	1.85	50.1	54.0	2705	3446	58.7	0.54	1.07	0.58
	A	2.05	43.1	54.0	2327	2965	54.5	0.69	1.04	0.72
	A	0.98	37.1	54.1	2007	2557	50.6	0.38	1.01	0.38
	A	1.00	26.5	54.1	1434	1826	42.7	0.55	0.93	0.51
	A	1.85	36.9	54.1	1996	2543	50.4	0.73	1.00	0.73
	A	1.12	32.2	54.1	1742	2219	47.1	0.50	0.97	0.49
	A	0.34	29.0	54.1	1569	1999	44.7	0.17	0.95	0.16

Table A4.1. Results of point load strength tests on failed core samples.

A4.3 Data Tables for Cube Samples

Sample No.	Bedding orientation	P (kN)	D (mm)	W (mm)	A (mm^2)	D_e^2	D_e	I_s	F	$I_{s(50)}$ (MPa)	ave.	$I_{a(50)}$
Bishop Block Kimbell seam												
BB/K/C1		0.10	22.21	33.97	754	961	31.0	0.10	0.81	0.08		
		0.51	26.65	35.77	953	1214	34.8	0.42	0.85	0.36		
		0.16	19.85	36.27	720	917	30.3	0.17	0.80	0.14		
		0.24	30.67	37.97	1165	1483	38.5	0.16	0.89	0.14		
		0.43	31.40	35.52	1115	1421	37.7	0.30	0.88	0.27		
		0.18	23.55	19.91	469	597	24.4	0.30	0.72	0.22		
		0.32	27.36	31.72	868	1106	33.2	0.29	0.83	0.24		
		0.24	18.36	36.56	671	855	29.2	0.28	0.79	0.22	0.21	
BB/K/C2		0.34	21.17	27.22	576	734	27.1	0.46	0.76	0.35		
		0.10	16.86	23.17	391	498	22.3	0.20	0.70	0.14		
	⊥	0.39	20.93	31.73	664	846	29.1	0.46	0.78	0.36		
	⊥	0.28	23.42	28.97	678	864	29.4	0.32	0.79	0.26		
		0.57	31.57	34.77	1098	1398	37.4	0.41	0.88	0.36		
		0.28	20.15	21.43	432	550	23.5	0.51	0.71	0.36	0.31	
BB/K/C3		0.30	27.29	45.82	1250	1593	39.9	0.19	0.90	0.17		
		0.18	16.69	22.80	381	485	22.0	0.37	0.69	0.26		
		0.16	23.93	35.44	848	1080	32.9	0.15	0.83	0.12		
		0.24	22.39	25.50	571	727	27.0	0.33	0.76	0.25		
		0.08	27.03	31.26	845	1076	32.8	0.07	0.83	0.06	0.17	
BB/K/C4		0.32	30.69	33.12	1016	1295	36.0	0.25	0.86	0.21		
		0.28	23.00	34.20	787	1002	31.7	0.28	0.81	0.23		
		0.18	20.35	33.29	677	863	29.4	0.21	0.79	0.16	0.20	
BB/K/C5	⊥	0.14	25.63	21.82	559	712	26.7	0.20	0.75	0.15		
	⊥	0.24	27.51	29.51	812	1034	32.2	0.23	0.82	0.19		
		0.45	26.26	30.59	803	1023	32.0	0.44	0.82	0.36		
	‖	0.32	19.68	21.78	429	546	23.4	0.59	0.71	0.42		
		0.22	28.01	24.71	692	882	29.7	0.25	0.79	0.20	0.26	0.40
BB/K/C6	⊥	0.35	35.17	48.18	1694	2159	46.5	0.16	0.97	0.16		
		0.30	29.71	33.41	993	1264	35.6	0.24	0.86	0.20		
	‖	0.22	16.45	21.01	346	440	21.0	0.50	0.68	0.34		
		0.14	16.46	18.31	301	384	19.6	0.36	0.66	0.24		
		0.14	19.42	24.17	469	598	24.5	0.23	0.72	0.17		
		0.24	26.32	43.12	1135	1446	38.0	0.17	0.88	0.15	0.21	0.47
BB/K/C7		0.20	23.95	21.93	525	669	25.9	0.30	0.74	0.22		
		0.14	24.72	29.51	729	929	30.5	0.15	0.80	0.12		
		0.26	16.67	22.97	383	488	22.1	0.53	0.69	0.37		
		0.24	24.09	21.88	527	671	25.9	0.36	0.74	0.27		
		0.12	29.71	34.73	1032	1314	36.3	0.09	0.87	0.08		
	‖	0.28	27.99	27.09	758	966	31.1	0.29	0.81	0.23		
		0.16	19.64	23.14	454	579	24.1	0.28	0.72	0.20		
	⊥	0.41	47.18	57.42	2709	3451	58.7	0.12	1.08	0.13		
	⊥‖	0.45	27.67	44.49	1231	1568	39.6	0.29	0.90	0.26		
	⊥	0.35	31.53	35.91	1132	1442	38.0	0.24	0.88	0.21		
		0.32	23.62	28.77	680	866	29.4	0.37	0.79	0.29	0.22	0.91
BB/K/C8		0.34	33.14	31.72	1051	1339	36.6	0.25	0.87	0.22		
		0.26	17.82	34.24	610	777	27.9	0.33	0.77	0.26		
		0.14	20.06	33.30	668	851	29.2	0.16	0.78	0.13		
	⊥	0.26	33.52	34.17	1145	1459	38.2	0.18	0.89	0.16		
	‖	0.32	27.51	33.93	933	1189	34.5	0.27	0.85	0.23		
		0.18	27.08	29.56	800	1020	31.9	0.18	0.82	0.14		
		0.22	26.04	37.95	988	1259	35.5	0.17	0.86	0.15		
		0.10	26.46	28.41	752	958	30.9	0.10	0.81	0.08	0.17	0.70
BB/K/C9		0.20	26.10	36.71	958	1221	34.9	0.16	0.85	0.14		
		0.22	29.23	36.84	1077	1372	37.0	0.16	0.87	0.14		
		0.41	41.27	44.87	1852	2359	48.6	0.17	0.99	0.17		
		0.32	35.72	38.46	1374	1750	41.8	0.18	0.92	0.17		
		0.16	22.22	44.15	981	1250	35.4	0.13	0.86	0.11		
		0.16	42.39	43.60	1848	2354	48.5	0.07	0.99	0.07		
		0.20	26.24	28.19	740	942	30.7	0.21	0.80	0.17		

	|	0.28	30.38	34.19	1039	1323	36.4	0.21	0.87	0.18	0.14	
Bishop Block Morgan seam												
BB/M/C1		0.18	16.26	30.46	495	631	25.1	0.29	0.73	0.21		
		0.26	30.19	23.08	697	888	29.8	0.29	0.79	0.23		
		0.08	20.04	22.64	454	578	24.0	0.14	0.72	0.10		
		0.41	38.33	39.01	1495	1905	43.6	0.22	0.94	0.20		
		0.30	41.93	35.77	1500	1911	43.7	0.16	0.94	0.15		
	⊥	0.20	39.20	40.97	1606	2046	45.2	0.10	0.96	0.09		
		0.20	35.90	38.91	1397	1779	42.2	0.11	0.93	0.10		
		0.18	20.58	23.03	474	604	24.6	0.30	0.73	0.22	0.16	
BB/M/C2		0.10	15.31	24.93	382	486	22.1	0.21	0.69	0.14		
	∥	0.20	19.59	34.25	671	855	29.2	0.23	0.79	0.18		
		0.24	28.96	42.63	1235	1573	39.7	0.15	0.90	0.14		
	<45	0.16	36.84	48.87	1800	2293	47.9	0.07	0.98	0.07		
	<45	0.16	39.59	49.53	1961	2498	50.0	0.06	1.00	0.06		
	∥	0.45	30.44	29.04	884	1126	33.6	0.40	0.84	0.33		
		0.28	34.32	34.34	1179	1501	38.7	0.19	0.89	0.17	0.16	
BB/M/C3		0.24	19.44	36.29	705	899	30.0	0.27	0.79	0.21		
		0.12	22.18	32.01	710	904	30.1	0.13	0.80	0.11		
	⊥	0.30	33.99	28.45	967	1232	35.1	0.24	0.85	0.21		
	⊥	0.14	21.65	29.57	640	816	28.6	0.17	0.78	0.13		
	⊥	0.28	23.17	22.02	510	650	25.5	0.43	0.74	0.32		
	∥	0.34	25.90	31.53	817	1040	32.3	0.33	0.82	0.27		
	⊥	0.35	17.69	26.36	466	594	24.4	0.59	0.72	0.43	0.24	1.01
BB/M/C4		0.35	20.41	24.59	502	639	25.3	0.55	0.74	0.40		
		0.14	16.46	25.02	412	525	22.9	0.27	0.70	0.19		
		0.16	25.10	39.93	1002	1277	35.7	0.13	0.86	0.11		
		0.30	18.95	38.63	732	933	30.5	0.32	0.80	0.26		
		0.12	28.62	32.38	927	1181	34.4	0.10	0.84	0.09		
		0.16	17.25	24.79	428	545	23.3	0.29	0.71	0.21	0.21	
BB/M/C5		0.10	25.97	27.90	725	923	30.4	0.11	0.80	0.09		
		0.12	24.45	24.64	602	767	27.7	0.16	0.77	0.12		
		0.26	16.04	25.34	406	518	22.8	0.50	0.70	0.35		
		0.18	35.94	44.93	1615	2057	45.4	0.09	0.96	0.08		
		0.24	28.62	36.30	1039	1323	36.4	0.18	0.87	0.16	0.16	
BB/M/C6		0.22	21.67	31.11	674	859	29.3	0.26	0.79	0.20		
		0.51	21.67	31.11	674	859	29.3	0.59	0.79	0.47		
		0.20	22.83	33.10	756	963	31.0	0.21	0.81	0.17		
		0.20	33.43	35.15	1175	1497	38.7	0.13	0.89	0.12		
		0.28	35.86	53.71	1926	2454	49.5	0.11	1.00	0.11		
		0.16	35.70	43.56	1555	1981	44.5	0.08	0.95	0.08	0.19	
BB/M/C7	⊥	0.16	22.14	34.51	764	973	31.2	0.16	0.81	0.13		
		0.20	24.34	26.35	641	817	28.6	0.24	0.78	0.19		
		0.12	26.70	36.75	981	1250	35.4	0.10	0.86	0.08		
		0.18	19.89	28.33	563	718	26.8	0.25	0.76	0.19		
		0.14	27.81	30.96	861	1097	33.1	0.13	0.83	0.11	0.14	
Roa Kimbell seam												
K/C1	|	0.08	23.4	33.6	786	1001	31.64	0.08	0.80	0.06		
	|	0.08	23.0	22.2	511	651	25.52	0.12	0.71	0.09		
	|	0.14	15.3	22.2	339	432	20.78	0.32	0.64	0.21	0.12	
K/C2	|	0.08	14.7	19.0	280	356	18.87	0.25	0.61	0.15		
	|⊥	0.08	20.5	21.4	438	558	23.62	0.14	0.69	0.10	0.13	
K/C3	|⊥	0.18	29.3	50.4	1480	1885	43.41	0.10	0.93	0.09		
	|⊥	0.16	30.1	26.5	798	1016	31.88	0.16	0.80	0.13		
	|∥	0.18	25.7	29.1	747	952	30.85	0.19	0.79	0.15		
	|	0.20	17.4	27.6	478	609	24.68	0.33	0.70	0.23		
	|45°	0.18	21.5	33.1	710	905	30.08	0.20	0.78	0.16	0.15	0.73
K/C4	|	0.16	23.5	28.3	666	848	29.12	0.19	0.76	0.14		
	|	0.08	15.2	25.4	386	492	22.18	0.16	0.67	0.11		
	|	0.10	19.5	21.0	409	521	22.84	0.19	0.68	0.13		
	|	0.10	18.8	21.9	412	525	22.91	0.19	0.68	0.13		
	|⊥	0.08	19.7	20.4	401	511	22.61	0.16	0.67	0.11	0.12	

K/C5	⊥	0.10	17.0	20.2	344	438	20.93	0.23	0.65	0.15		
	∥	0.08	11.3	18.2	207	263	16.22	0.30	0.57	0.17	0.16	
K/C6	∥	0.08	25.8	35.4	914	1164	34.12	0.07	0.83	0.06		
	∥	0.08	15.5	19.1	296	378	19.43	0.21	0.62	0.13	0.10	
K/C7	∥	0.10	13.4	17.9	240	305	17.47	0.33	0.59	0.19		
	∥	0.10	19.6	18.9	369	470	21.67	0.21	0.66	0.14		
	∥	0.14	18.3	16.8	307	391	19.78	0.36	0.63	0.23		
	∥	0.08	21.3	24.7	524	668	25.84	0.12	0.72	0.09	0.16	
Spring Creek D seam												
SC/D/C1	⊥	0.67	29.8	30.5	908	1157	34.0	0.58	0.82	0.48		
	⊥	0.61	30.4	33.6	1020	1300	36.0	0.47	0.85	0.40		
	∥	0.47	16.7	18.5	310	395	19.9	1.18	0.63	0.74		
	∥	0.35	27.6	20.1	556	708	26.6	0.49	0.73	0.36		
	∥	0.26	25.8	34.1	880	1121	33.5	0.23	0.82	0.19		
	∥	0.32	15.2	20.2	307	391	19.8	0.82	0.63	0.52	0.45	0.59
SC/D/C2	⊥	0.83	31.6	28.8	909	1158	34.0	0.72	0.82	0.59		
	⊥	0.22	13.1	25.9	339	431	20.8	0.51	0.64	0.33		
	∥	0.24	26.9	30.9	830	1058	32.5	0.23	0.81	0.19		
	∥	0.55	16.1	23.0	370	471	21.7	1.17	0.66	0.77	0.47	2.42
SC/D/C3	∥	0.16	16.4	23.8	389	495	22.3	0.32	0.67	0.21		
	∥	0.41	14.7	16.5	243	310	17.6	1.32	0.59	0.78		
	⊥	0.81	23.8	24.3	579	737	27.2	1.10	0.74	0.81	0.60	1.63
SC/D/C4	∥	0.89	20.7	36.6	758	966	31.1	0.92	0.79	0.73		
	∥	0.81	22.5	22.2	500	637	25.2	1.27	0.71	0.90		
	∥	0.79	20.2	21.2	428	545	23.3	1.45	0.68	0.99	0.87	
SC/D/C5	∥	0.55	18.0	26.0	468	596	24.4	0.92	0.70	0.64		
	∥	0.61	19.9	39.1	777	990	31.5	0.62	0.79	0.49		
	∥	0.63	18.3	25.1	459	585	24.2	1.08	0.70	0.75		
	∥	0.67	22.0	40.2	884	1127	33.6	0.59	0.82	0.48	0.59	
Spring Creek Main Upper seam												
SC/MNU/C1	⊥	0.67	25.9	31.1	805	1025	32.02	0.65	0.80	0.52		
	⊥	0.14	30.9	31.9	984	1254	35.41	1.12	0.84	0.94		
	⊥	0.95	29.8	24.4	726	924	30.40	1.03	0.78	0.80		
	∥	0.53	17.9	18.0	322	411	20.26	1.29	0.64	0.82		
	∥	0.32	21.9	28.6	628	799	28.27	0.40	0.75	0.30		
	∥	0.28	18.2	24.8	452	576	24.00	0.49	0.69	0.34		
	∥	0.85	30.3	29.8	904	1151	33.93	0.74	0.82	0.61	0.62	0.92
SC/MNU/C2	∥	0.43	31.1	30.6	952	1213	34.82	0.35	0.83	0.29		
	∥	1.12	29.9	47.8	1427	1818	42.63	0.62	0.92	0.57		
	∥	0.67	29.5	31.3	922	1175	34.28	0.57	0.83	0.47		
	∥	0.93	25.1	29.8	747	952	30.86	0.98	0.79	0.77		
	∥	0.69	17.3	19.4	336	428	20.69	1.61	0.64	1.04	0.63	
SC/MNU/C3	∥	0.73	26.4	29.3	775	987	31.42	0.74	0.79	0.59		
	∥	0.47	25.5	28.6	729	928	30.47	0.51	0.78	0.40		
	∥	0.67	26.7	32.6	869	1107	33.27	0.61	0.82	0.50		
	∥	0.83	28.2	31.2	879	1119	33.45	0.74	0.82	0.61		
	∥	0.32	27.7	32.8	910	1159	34.05	0.28	0.83	0.23		
	∥	1.12	20.7	28.5	591	752	27.43	1.49	0.74	1.10	0.57	
SC/MNU/C4	∥	0.95	18.0	34.0	612	779	27.91	1.22	0.75	0.91		
	∥	0.61	30.1	32.5	978	1246	35.30	0.49	0.84	0.41		
	∥	0.34	30.5	33.1	1009	1286	35.86	0.26	0.85	0.22		
	⊥	1.20	28.7	31.3	898	1144	33.82	1.05	0.82	0.86		
	∥	0.98	17.7	30.4	539	687	26.21	1.43	0.72	1.04		
	∥	0.43	19.2	29.7	572	728	26.98	0.59	0.73	0.43		
	∥	0.67	28.8	25.5	733	933	30.55	0.72	0.78	0.56	0.63	
SC/MNU/C5	⊥	0.53	30.5	41.9	1278	1628	40.34	0.33	0.90	0.30		
	∥	0.30	29.2	31.1	910	1159	34.05	0.26	0.83	0.21		
	∥	0.10	30.6	33.8	1035	1318	36.31	0.08	0.85	0.07		
	∥	0.63	31.1	63.4	1969	2508	50.08	0.25	1.00	0.25	0.21	

SC/MNU/C6	∥	0.26	16.4	30.8	506	645	25.39	0.40	0.71	0.29		
	∥	0.53	21.6	38.7	836	1065	32.64	0.50	0.81	0.40		
	∥	0.22	23.2	39.9	925	1179	34.33	0.19	0.83	0.16		
	∥	0.57	15.4	20.9	321	409	20.23	1.39	0.64	0.88	0.43	
SC/MNU/C7	∥	0.35	26.2	30.3	793	1011	31.79	0.35	0.80	0.28		
	∥	0.55	31.1	34.0	1059	1349	36.73	0.41	0.86	0.35		
	∥	0.61	20.9	28.7	599	763	27.63	0.80	0.74	0.59		
	∥	0.26	22.2	22.8	505	643	25.36	0.40	0.71	0.28		
	∥	0.34	22.0	20.5	451	574	23.96	0.60	0.69	0.42	0.39	
Strongman No. 2 E seam												
SM/E/OC/C1		0.41	27.65	32.38	895	1140	33.8	0.36	0.84	0.30		
		0.61	27.54	36.18	996	1269	35.6	0.48	0.86	0.41		
		0.51	23.63	29.36	694	884	29.7	0.58	0.79	0.46		
		0.65	19.56	21.95	429	547	23.4	1.19	0.71	0.84		
	⊥	0.28	19.23	28.30	544	693	26.3	0.40	0.75	0.30		
	⊥	0.67	17.51	27.08	474	604	24.6	1.11	0.73	0.81		
	∥	0.65	20.74	27.04	561	714	26.7	0.91	0.75	0.69	0.54	0.80
SM/E/OC/C3		0.71	40.55	44.05	1786	2275	47.7	0.31	0.98	0.31		
		0.26	21.83	28.23	616	785	28.0	0.33	0.77	0.26		
	⊥	0.51	26.35	34.88	919	1171	34.2	0.44	0.84	0.37		
	⊥	0.71	23.82	25.88	616	785	28.0	0.90	0.77	0.70		
	⊥	1.34	29.28	37.06	1085	1382	37.2	0.97	0.88	0.85		
		1.32	42.14	45.80	1930	2459	49.6	0.54	1.00	0.53		
		0.61	35.20	39.04	1374	1751	41.8	0.35	0.92	0.32	0.48	
SM/E/OC/C4	⊥	1.12	24.06	31.35	754	961	31.0	1.17	0.81	0.94		
	∥	0.37	23.15	27.19	629	802	28.3	0.46	0.77	0.36		
	⊥	0.61	21.35	28.21	602	767	27.7	0.80	0.77	0.61		
	⊥	1.50	28.28	29.78	842	1073	32.8	1.40	0.83	1.16		
	∥	1.24	23.31	26.39	615	784	28.0	1.58	0.77	1.22		
	⊥	0.57	23.31	30.60	713	909	30.1	0.63	0.80	0.50	0.80	1.01
SM/E/OC/C5	∥	0.65	28.34	42.11	1193	1520	39.0	0.43	0.89	0.38		
	⊥	0.63	18.29	28.06	513	654	25.6	0.96	0.74	0.71		
	∥	0.47	29.30	41.89	1227	1564	39.5	0.30	0.90	0.27		
	⊥	0.61	17.30	29.54	511	651	25.5	0.94	0.74	0.69		
	⊥	0.61	27.28	29.09	794	1011	31.8	0.60	0.82	0.49		
	⊥	0.41	22.41	29.03	651	829	28.8	0.49	0.78	0.39	0.49	1.75
SM/E/OC/C6		0.63	28.84	47.31	1364	1738	41.7	0.36	0.92	0.33		
		0.41	19.31	26.63	514	655	25.6	0.63	0.74	0.46		
		0.32	13.80	18.70	445	567	23.8	0.56	0.72	0.40		
		0.45	32.50	38.79	1261	1606	40.1	0.28	0.91	0.25		
		0.41	28.58	32.58	931	1186	34.4	0.35	0.85	0.29		
		0.35	20.79	29.27	609	775	27.8	0.45	0.77	0.35		
		0.35	22.56	32.17	726	925	30.4	0.38	0.80	0.30	0.34	
SM/E/OC/C7		0.43	24.87	35.16	874	1114	33.4	0.39	0.83	0.32		
		0.65	28.06	33.54	941	1199	34.6	0.54	0.85	0.46		
	⊥	0.73	26.32	30.03	790	1007	31.7	0.73	0.81	0.59		
		0.35	30.17	35.89	1083	1379	37.1	0.25	0.87	0.22	0.40	
SM/E/OC/C8	∥	0.83	25.81	39.83	1028	1310	36.2	0.63	0.86	0.55		
	⊥	0.47	17.54	26.78	470	598	24.5	0.79	0.72	0.57		
	⊥	0.37	23.70	25.76	611	778	27.9	0.48	0.77	0.37		
	∥	0.61	27.31	31.27	854	1088	33.0	0.56	0.83	0.46		
	∥	1.44	21.23	27.26	579	737	27.2	1.95	0.76	1.48		
	80°	0.77	25.41	23.15	588	749	27.4	1.03	0.76	0.78		
	∥	0.34	21.21	31.09	659	840	29.0	0.40	0.78	0.32	0.65	0.67
Terrace No. 4 seam												
T/C1	∥	0.37	43.4	39.0	1691	2154	46.4	0.17	0.97	0.17		
	∥	1.40	23.4	43.5	1018	1297	36.0	1.08	0.86	0.93		
	∥	1.30	22.8	43.9	1001	1276	35.7	1.02	0.86	0.88		
	∥	1.12	20.4	24.0	489	623	25.0	1.80	0.73	1.32		
	∥	0.85	26.3	27.6	724	923	30.4	0.92	0.80	0.74		
	∥	0.73	19.1	30.1	575	732	27.1	1.00	0.76	0.76		
	∥	0.87	15.9	29.3	466	594	24.4	1.47	0.72	1.06		
	∥	0.37	18.4	27.8	513	653	25.6	0.57	0.74	0.42	0.78	

T/C2	∥	0.87	17.5	36.3	633	807	28.4	1.08	0.78	0.84		
	∥	0.43	18.6	26.2	487	620	24.9	0.69	0.73	0.51		
	∥	0.45	16.0	19.0	304	387	19.7	1.16	0.66	0.76		
	∥	0.18	20.4	20.2	413	526	22.9	0.34	0.70	0.24	0.59	
T/C3	∥⊥	0.12	18.3	16.6	305	388	19.7	0.31	0.66	0.20		
	∥	0.10	19.4	22.9	445	567	23.8	0.18	0.72	0.13		
	∥<45°	0.20	19.0	26.1	497	633	25.2	0.32	0.73	0.23		
	∥	0.18	16.5	17.5	289	369	19.2	0.49	0.65	0.32		
	∥	0.30	24.1	24.2	584	744	27.3	0.40	0.76	0.31	0.24	
T/C4	∥‖	0.10	19.8	22.6	448	571	23.9	0.18	0.72	0.13		
	∥	0.43	17.3	19.1	331	422	20.5	1.02	0.67	0.68		
	∥	0.22	22.6	23.3	526	670	25.9	0.33	0.74	0.24		
	∥	0.18	15.6	27.9	437	556	23.6	0.32	0.71	0.23	0.32	
T/C5	∥	0.18	26.0	38.6	1002	1277	35.7	0.14	0.86	0.12		
	∥	0.14	21.8	28.3	618	787	28.0	0.18	0.77	0.14		
	∥	0.47	23.9	23.7	566	721	26.8	0.65	0.76	0.49		
	∥	0.61	22.1	22.8	505	644	25.4	0.95	0.74	0.70	0.36	
T/C6	∥‖	0.49	16.6	38.1	631	804	28.4	0.61	0.77	0.47		
	∥⊥	0.12	36.8	34.2	1259	1604	40.0	0.08	0.90	0.07		
	∥⊥	0.28	19.9	17.8	354	451	21.2	0.62	0.68	0.42		
	∥	0.39	16.9	20.8	351	447	21.2	0.87	0.68	0.59		
	∥	0.28	18.2	17.0	309	394	19.8	0.71	0.66	0.47		
	∥	0.28	27.1	34.4	931	1186	34.4	0.24	0.85	0.20	0.37	0.52

Table A4.2. Results of point load tests on failed cube samples.

Appendix 5. Triaxial Compressive Strength

A5.1 Test Method

All triaxial tests were carried out according to the ISRM suggested method detailed in Brown (1981), apart from sample no. SC/D/9. This sample had an L/D ratio of 1.98 which was corrected to an L/D of 2.0 using the ASTM equation outlined in section 2.2.2.3. Sample ends were not ground flat due their fragility. The ends were made as flat and parallel as possible when the samples were trimmed to the required length. Confining pressures of 2, 4, and 6 MPa for the samples was provided by the use of a Hoek and Franklin Cell shown in Figure A5.1. The loading frame used is the same as that used for the UCS tests. The full set of triaxial test results is presented in Table A5.1.

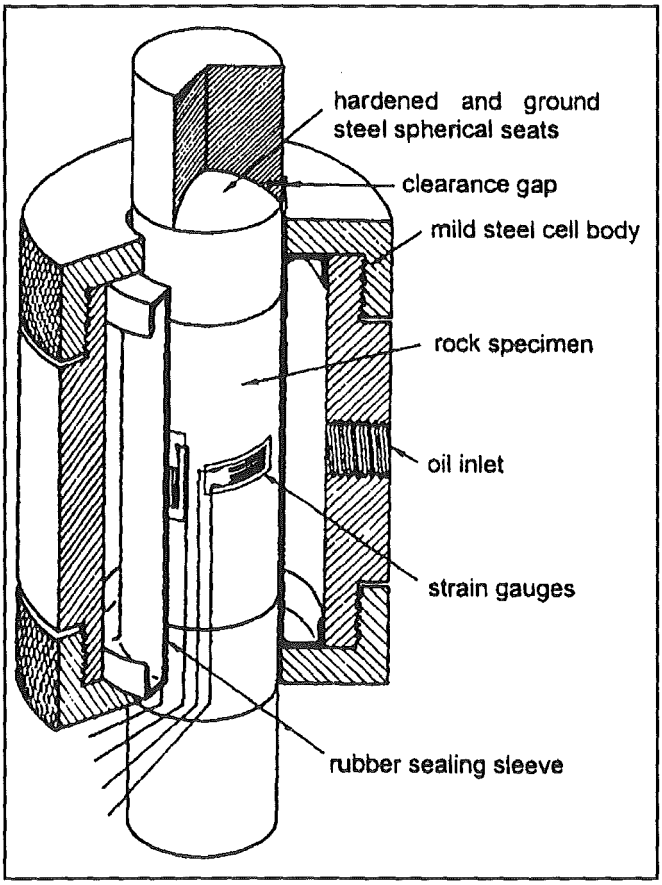

Figure A5.1. Cut-away view of the Hoek and Franklin Cell used to provide the confining pressure in the determination of the triaxial compressive strength (after Hoek and Brown, 1997).

A5.2 Data Tables

Sample No.	Bedding orientation	Length (mm)	Average Core Diameter (mm)	Cross Sectional Area (mm^2)	L/D Ratio	σ_3 (MPa)	Failure Load (kN)	σ_1 (MPa)	Moisture Content %	Bulk Density (g/mm^3)
Spring Creek D seam										
SC/D/4	35°	115	54.02	2292	2.13	2.0	53.4	23.3	-	1.27
SC/D/5	⊥	122	54.04	2294	2.26	2.0	74.9	32.7	6.65	1.27
SC/D/8	20°	110	54.03	2293	2.04	4.0	92.1	40.2	7.05	1.27
SC/D/9	30°	107	53.99	2289	1.98	4.0	100.7	44.0	7.64	1.26
SC/D/10	⊥	121	54.05	2295	2.24	6.0	132.0	57.5	8.10	1.27
SC/D/11	20°	110	54.06	2296	2.03	6.0	107.2	46.7	7.62	1.26
Spring Creek Main Upper seam										
SC/MNU/1	⊥	112	54.05	2295	2.07	2.0	126.3	55.0	6.02	1.27
SC/MNU/2	⊥	131	54.10	2299	2.42	4.0	108.7	47.3	6.40	1.26
SC/MNU/3	∥	126	54.08	2297	2.33	4.0	111.3	48.4	6.46	1.31
SC/MNU/4	∥	129	54.07	2296	2.39	2.0	78.2	34.1	6.76	1.29
SC/MNU/8	5°	108	54.02	2292	2.00	6.0	126.7	55.3	4.98	1.29
SC/MNU/10	10°	127	54.04	2294	2.35	6.0	120.7	52.6	5.03	1.28
Strongman No. 2 D seam										
SM/D/10		111	53.94	2285	2.06	2.0	98.1	42.9		
SM/D/17		115	54.14	2302	2.12	2.0	111.0	48.2		
SM/D/18		110	54.15	2303	2.03	2.0	70.7	30.7		
SM/D/2		117	54.00	2290	2.17	4.0	80.5	35.2		
SM/D/6	⊥	120	54.05	2295	2.22	4.0	40.8	40.8		
SM/D/7		123	54.13	2301	2.27	4.0	42.0	42.0		
SM/D/22		116	54.05	2295	2.15	4.0	144.0	62.7		
SM/D/19	20°	110	54.05	2295	2.04	6.0	128.2	55.9		
SM/D/20		113	54.17	2304	2.09	6.0	121.8	52.9		
SM/D/21		114	54.10	2299	2.11	6.0	143.9	62.6		
Strongman No. 2 E seam										
SM/E/OC/1	45°	120	53.94	2285	2.22	2.0	111.6	48.9		
SM/E/OC/16	∥	108	54.13	2301	2.00	2.0	96.5	41.9		
SM/E/OC/17		115	54.07	2295	2.13	2.0	58.2	25.4		
SM/E/OC/9	∥	117	54.02	2292	2.17	4.0	98.5	43.0		
SM/E/OC/11	⊥	127	54.03	2293	2.35	4.0	108.5	47.3		
SM/E/OC/13		110	53.97	2287	2.04	4.0	97.5	42.6		
SM/E/OC/19	30°	108	54.06	2295	2.00	4.0	118.4	51.6		
SM/E/OC/8	⊥	120	54.01	2291	2.22	6.0	151.6	66.2		
SM/E/OC/14	∥	130	54.02	2292	2.41	6.0	121.5	53.0		
SM/E/OC/18		108	54.06	2295	2.00	6.0	125.1	54.6		

Table A5.1. Results of triaxial compressive strength tests.

A5.3 Hoek-Brown and Mohr-Coulomb Parameters

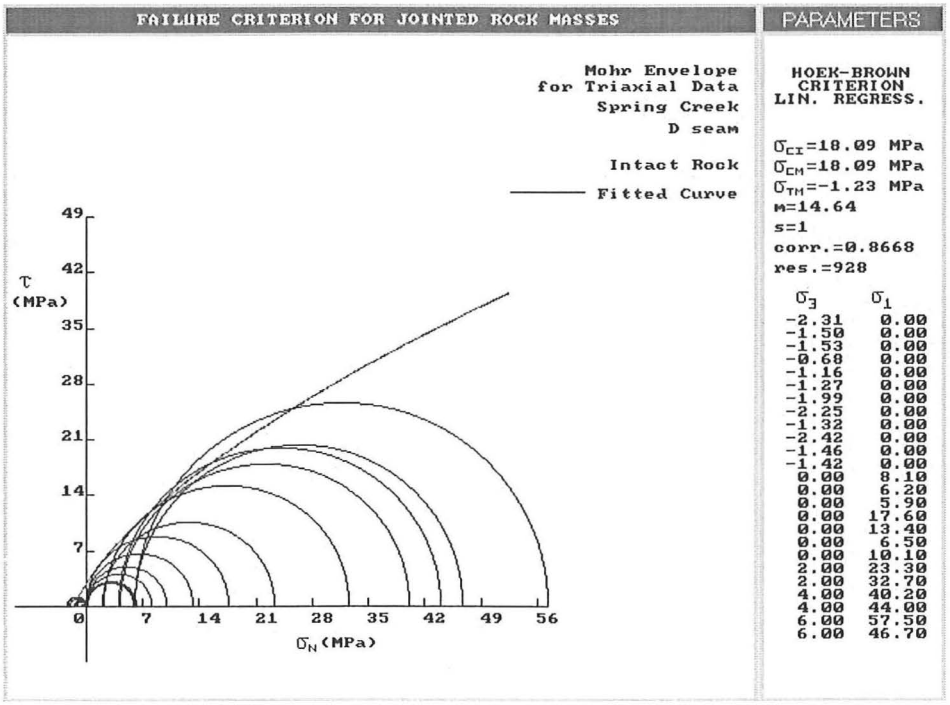

Figure A5.2. Hoek-Brown parameters for Spring Creek D seam.

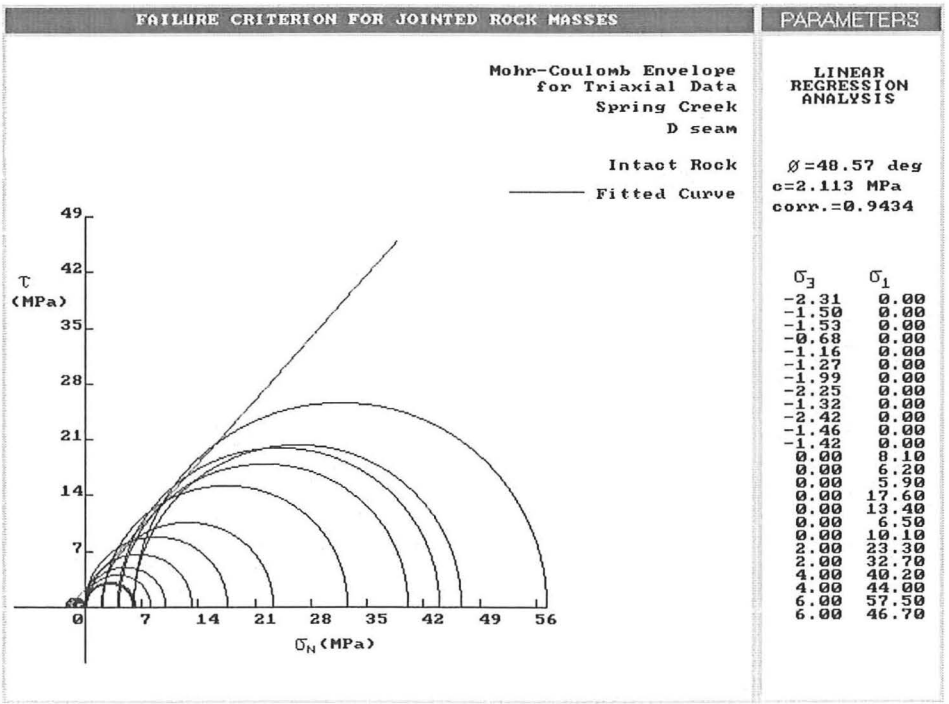

Figure A5.3. Mohr-Coulomb parameters for Spring Creek D seam.

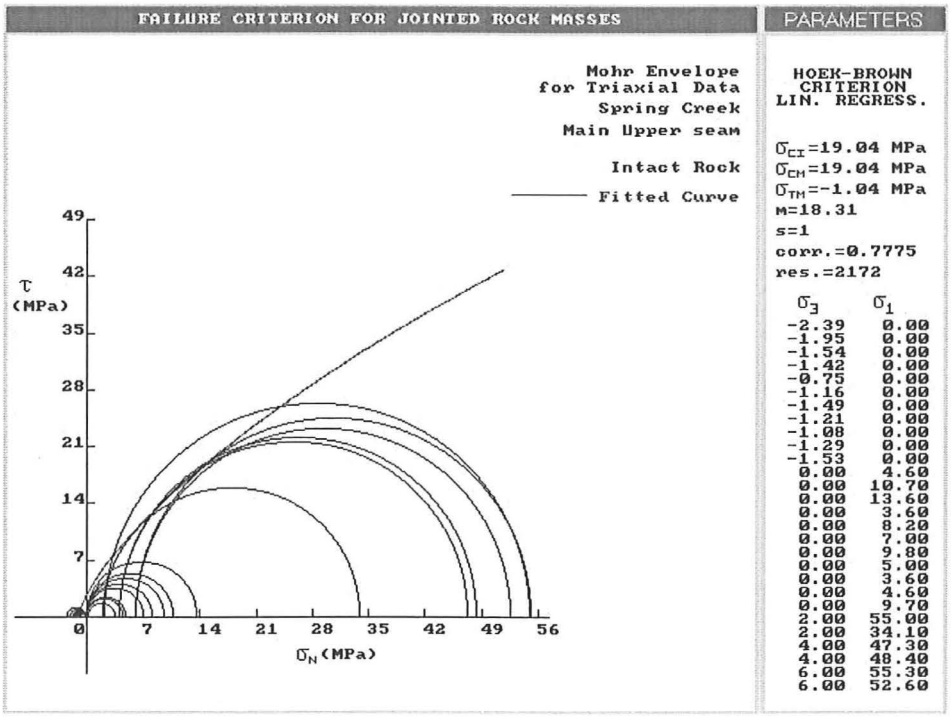

Figure A5.4. Hoek-Brown parameters for Spring Creek Main Upper seam.

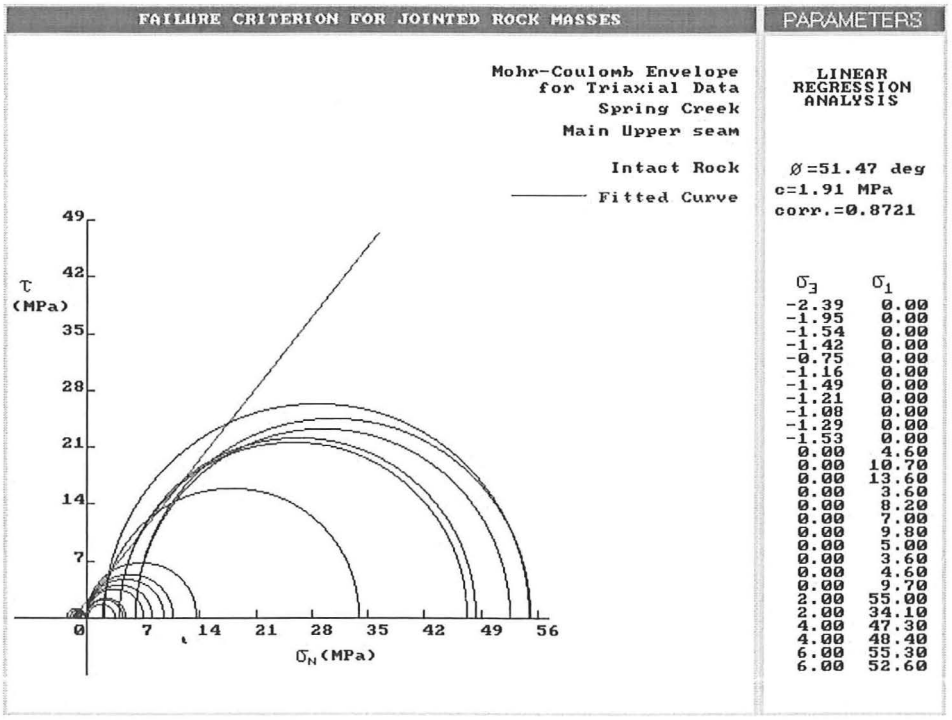

Figure A5.5. Mohr-Coulomb parameters for Spring Creek Main Upper seam.

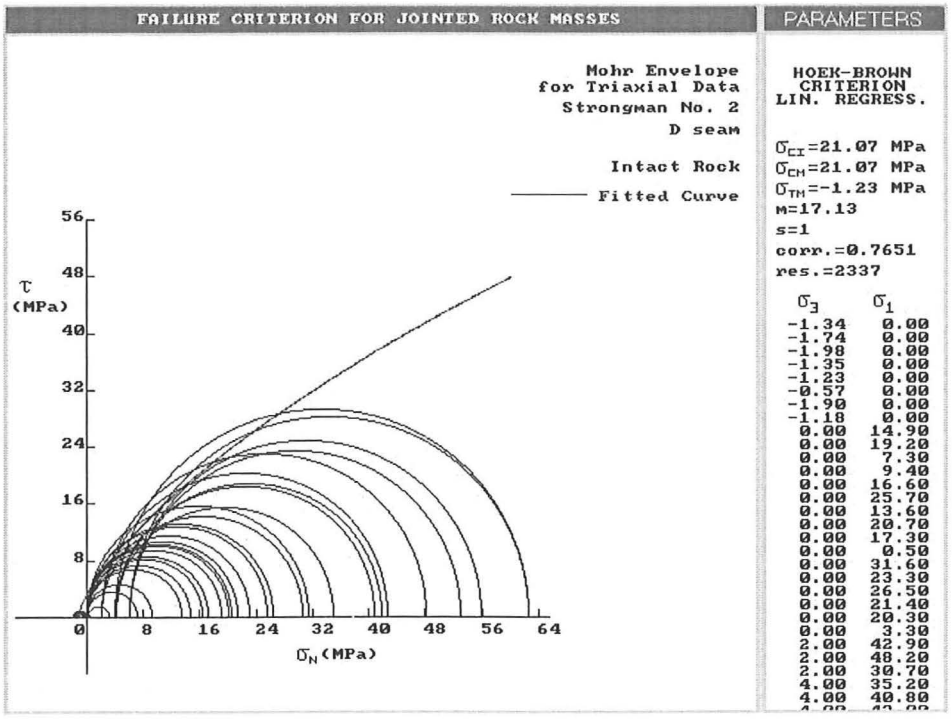

Figure A5.6. Hoek-Brown parameters for Strongman No. 2 D seam.

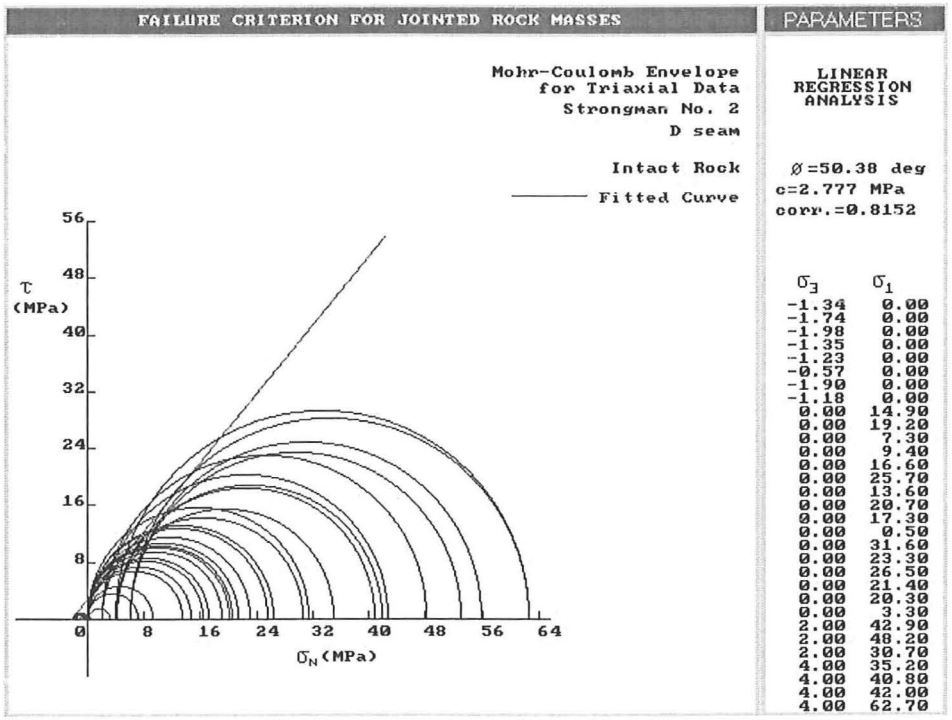

Figure A5.7. Mohr-Coulomb parameters for Strongman No. 2 D seam.

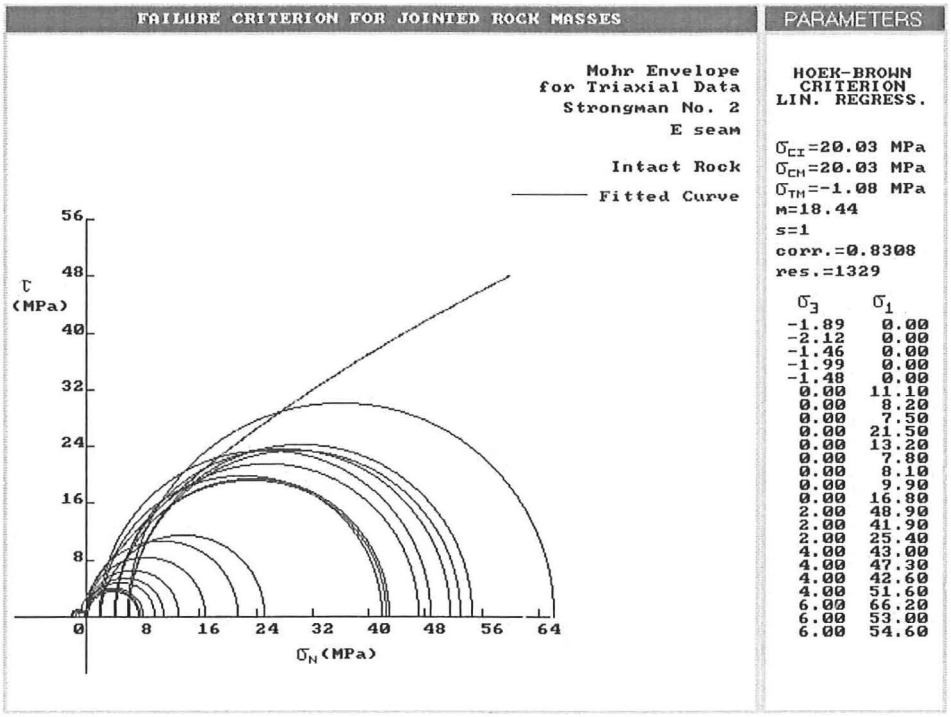

Figure A5.8. Hoek-Brown parameters for Strongman No. 2 E seam.

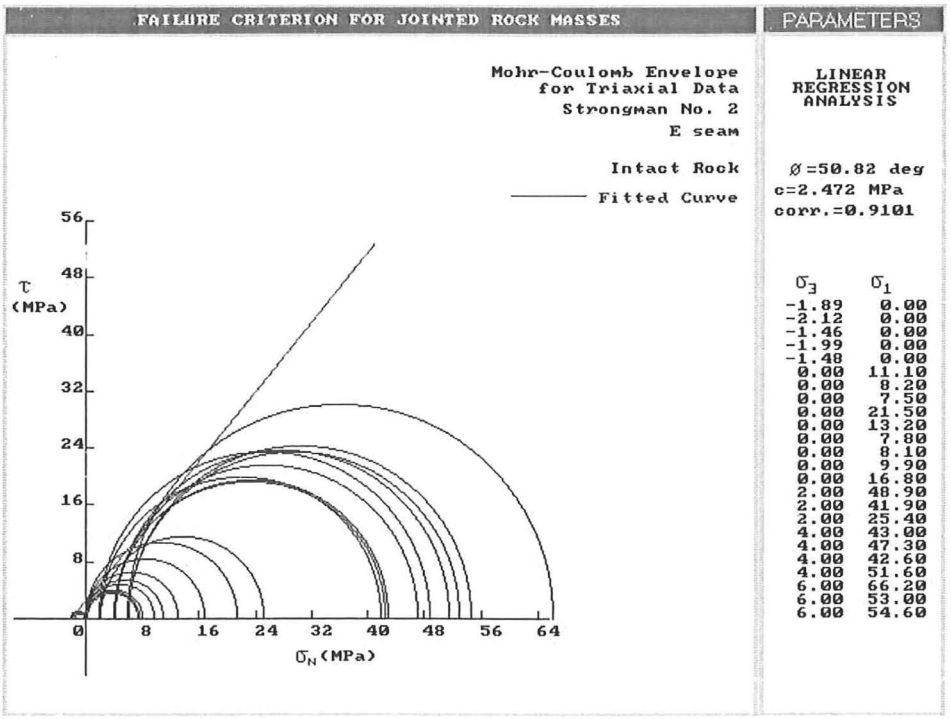

Figure A5.9. Mohr-Coulomb parameters for Strongman No. 2 E seam.

A5.4 Description of Samples and Mode of Failure

A5.4.1 Spring Creek D seam

SC/D/4: σ_3 = 2.0 MPa. Very pronounced bedding. Not really any significant cleats. Expect bedding to be the major feature. Failed by shearing along a low angle bedding plane (Figure A5.10a).

SC/D/5: σ_3 = 2.0 MPa. Mostly scattered fractures dipping ~60°. Bedding much less defined. Failure by incomplete shearing which is common in triaxial testing.

SC/D/8: σ_3 = 4.0 MPa. Two major cleats which are perpendicular to each other. A few prominent bedding planes. One crack which follows a bedding plane on the other side. The main fracture appears to have not played a significant role in the failure. It has instead failed along a cleat which followed one of the more dominant bedding planes. These are generally the durain bands which tend to be weaker.

SC/D/9: σ_3 = 4.0 MPa. Multiple closely spaced cleats, but none really entirely through going. Appears to have failed along a bedding plane (durain band), but is hard to tell (i.e. still intact).

SC/D/10: σ_3 = 6.0 MPa. Bedding perpendicular to loading direction and no significant cleats. Combination of shear and bedding plane failure.

SC/D/11: σ_3 = 6.0 MPa. Couple of large cleats running perpendicular to loading and bedding. Failed by shearing.

A5.4.2 Spring Creek Main Upper Seam

SC/MNU/1: σ_3 = 2.0 MPa. The most important feature is a faint cleat which runs down one side of the sample. Didn't fail along that crack. The orientation of bedding and the absence

of fractures led to a very high strength, with a slab eventually popping of the side. The top of this slab failed along a bedding plane which was a durain band (Figure A5.10b).

SC/MNU/4: σ_3 = 2.0 MPa. An absence of any large cracks, but there are more than in the last sample. Shear type failure, but not a typical one.

SC/MNU/2: σ_3 = 4.0 MPa. Loading direction perpendicular to bedding. Only one significant cleat. Biggest one of the last three samples. Combination of shear failure and failure along a bedding plane (failed through a durain band).

SC/MNU/3: σ_3 = 4.0 MPa. Pretty well absent of cracks. Bedding appears to be parallel to loading. Failure appears to have begun by shearing and has then failed along a bedding plane.

SC/MNU/8: σ_3 = 6.0 MPa. One main crack and some secondary ones. Failed by shearing through the major cleat plane.

SC/MNU/10: σ_3 = 6.0 MPa. Has failed by incomplete shearing.

A5.4.3 Strongman No. 2 D seam

SM/D/2: σ_3 = 4.0 MPa. Mode of failure has changed to a shear failure (Figure A5.10d).

SM/D/6: σ_3 = 4.0 MPa. Largely absent of defects. Loading direction appears to be perpendicular to bedding. Failure by shearing. Only one failure plane observed (Figure 5.10c).

SM/D/7: σ_3 = 4.0 MPa. Would be expected to fail early. Has a major cleat running up both sides. Another cleat runs parallel to this one and is also present on the other side but is less continuous. Failed by shearing directly through the cleat plane.

SM/D/10: σ_3 = 2.0 MPa. Cleat across the top and one smaller one down the side. Appears to have failed through a low angle cleat at very high strength.

SM/D/17: σ_3 = 2.0 MPa. Has a lot of large cleat planes scattered around it. None are really completely through going, but most do connect with others. Had a very high strength. Failed through a horizontal fracture, which would probably explain this.

SM/D/18: σ_3 = 2.0 MPa. Has a major cleat which runs across the top and down the sides. Would expect the strength to be much lower on this sample. Simple shear failure along the observed cleat plane. Lower strength as expected.

SM/D/19: σ_3 = 6.0 MPa. A few small cracks around the top. Bedding appears to be on a slight angle ~20° to loading direction (Figure A5.11a).

SM/D/20: σ_3 = 6.0 MPa. A few cracks around the sample but nothing too major or continuous. Although it has failed, there appears to be no actual failure plane although a number of hairline cracks have appeared.

SM/D/21: σ_3 = 6.0 MPa. Very good, pretty much intact core. One crack across the top and another across the base. Other than that, very good. Failed by shearing (Figure A5.11b).

SM/D/22: σ_3 = 4.0 MPa. One cleat which runs down both sides may cause premature failure. One across the top may be alright. After failure, the two main cleats are slightly more open. There is a new crack which runs around the main cleat, but there is no complete failure.

A5.4.4 Strongman No. 2 E seam

SM/E/OC/1: σ_3 = 2.0 MPa. Loading direction 45° to bedding. Only one large crack which runs partway down one side and across top. Could be influential due to shearing type failures expected in triaxial. No actual failure plane developed in this sample. A number of small cracks developed with one of the larger ones almost completely through going.

SM/E/OC/16: σ_3 = 2.0 MPa. Loading direction parallel to bedding. Nothing really to cause any problems except bedding direction. Perfect example of a shearing failure. Very smooth crack from corner to corner, though it doesn't run down both sides, so the sample is still intact.

SM/E/OC/17: σ_3 = 2.0 MPa. A couple of large cleats which will likely cause shearing failure. Expect this to be the weakest of the 2 MPa samples.

SM/E/OC/9: σ_3 = 4.0 MPa. Loading direction parallel to bedding. Only one cleat of significance. Significant factor could be loading direction with respect to bedding. Shearing failure through a bedding plane, although has not completely broken the sample.

SM/E/OC/11: σ_3 = 4.0 MPa. Cleats will cause an early shearing failure. Loading direction perpendicular to bedding. Failed through cracks and then along a bedding plane.

SM/E/OC/13: σ_3 = 4.0 MPa. Large cleat running ½ way around the top but no other significant features. Failed by a simple smooth shear. Complete failure.

SM/E/OC/19: σ_3 = 4.0 MPa. No really significant cracks. Bedding 30° from horizontal.

SM/E/OC/8: σ_3 = 6.0 MPa. A few small cleats, but only one of any significance. Loading direction perpendicular to bedding. Combination of shear failure and failure along a bedding plane. Neither were completely through going.

SM/E/OC/14: σ_3 = 6.0 MPa. No fractures. Loading direction parallel to bedding. Incomplete shear failure perpendicular to bedding plane. Another crack does follow a bedding plane.

SM/E/OC/18: σ_3 = 6.0 MPa. A crack connected across the top was $^1/_3$ of the way down each side which may cause some lower strength.

A5.5 Core Photos from Triaxial Testing

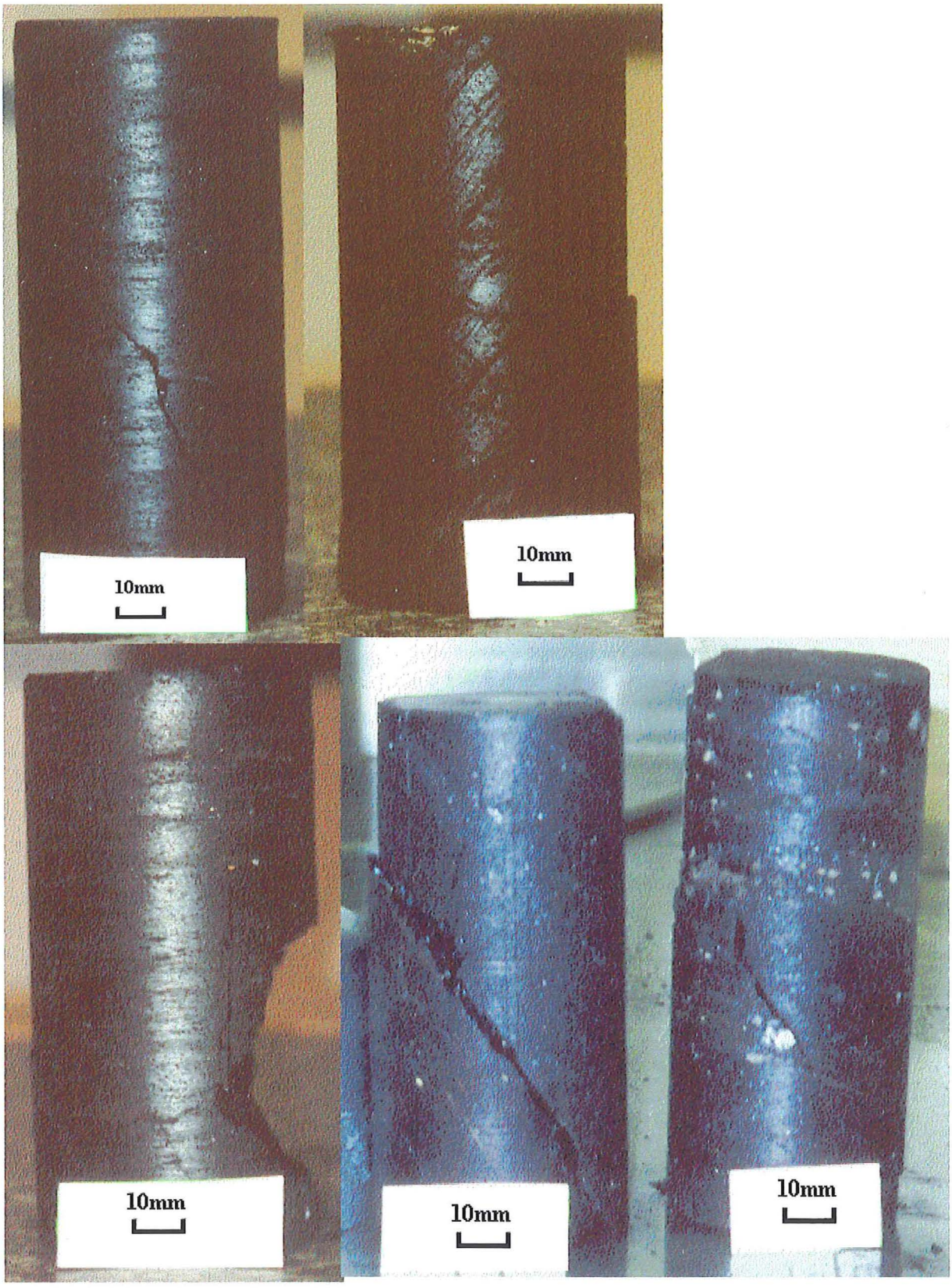

Figure A5.10a-e. Core photos from triaxial testing. Samples numbers clockwise from top left SC/D/4 (σ_3 = 2 MPa), SC/MNU/1 (σ_3 = 2 MPa), SM/D/6 (σ_3 = 4 MPa), SM/D/2 (σ_3 = 4 MPa) and SC/MNU/2 (σ_3 = 4 MPa).

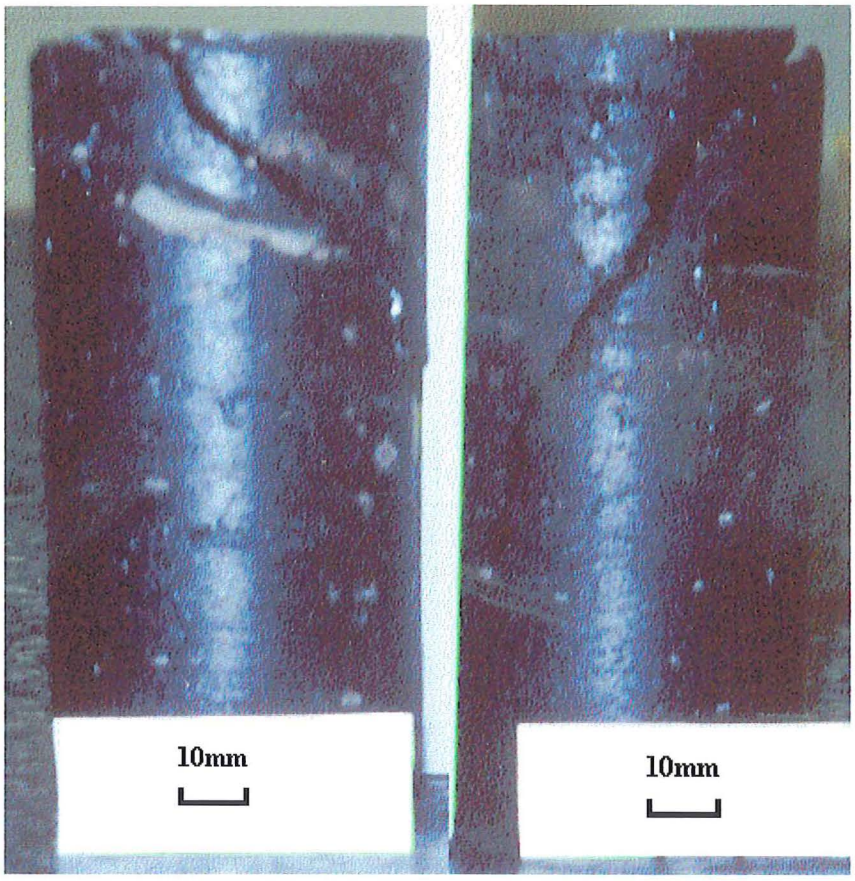

Figure A5.11a and b. Core photos from triaxial testing. Sample numbers from left SM/D/19 (σ_3 = 6 MPa) and SM/D/21 (σ_3 = 6 MPa).

Appendix 6. Brazilian Strength Test

A6.1 Test Method

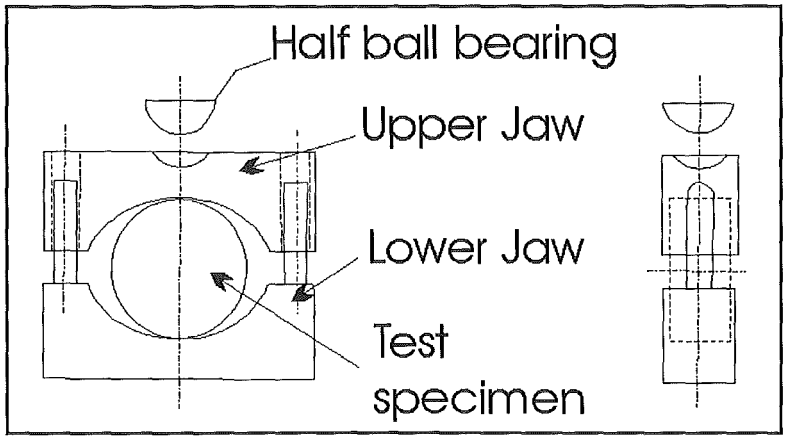

Figure A6.1. Apparatus used in Brazilian test (modified after Brown, 1981).

The following procedure for the Brazilian test is taken from Brown (1981). This test is used to indirectly determine the tensile strength of rocks. Samples used in this procedure are cylindrical with flat and parallel ends. Specimen diameter should not be less than 54mm and the thickness should equal the sample radius. Each specimen is to be wrapped in one layer of masking tape. Specimen should be loaded at a constant rate of 200 N/s or so that failure occurs within 15-30s. Ten samples are recommended per lithology being tested. The loading frame is the same as that used for the UCS testing. The tensile strength is calculated as follows:

$$\sigma_t = \frac{0.636P}{Dt} \quad \text{(MPa)}$$

where: P = load at failure (N).

D = diameter of the test specimen (mm).

t = thickness of the specimen measured at the centre (mm).

A6.2 Data Tables

Sample No.	Bedding orientation	P (kN)	D (mm)	t (mm)	Dt	σ_t (MPa)	Mean (MPa)
Spring Creek D seam							
1		5.7	54.37	28.81	1566.4	2.31	
2		3.8	54.71	29.54	1616.1	1.50	
3		3.7	54.32	28.37	1541.1	1.53	
4		1.7	54.29	29.32	1591.8	0.68	
5		2.8	54.53	28.18	1536.7	1.16	
6		3.1	54.45	28.48	1550.7	1.27	
7		5.0	54.71	29.21	1598.1	1.99	
8	⊥	5.0	54.35	26.00	1413.1	2.25	
9		3.2	54.37	28.34	1540.8	1.32	
10		6.1	54.47	29.43	1603.1	2.42	
11		3.8	54.25	30.61	1660.6	1.46	
12		3.7	54.24	30.60	1659.7	1.42	1.62
Spring Creek Main Upper seam							
1	⊥	5.8	54.14	28.54	1545	2.39	
2		5.1	54.58	30.50	1665	1.95	
3	⊥	3.8	54.36	28.90	1571	1.54	
4	⊥	3.3	54.29	27.16	1475	1.42	
5	∥	1.9	54.44	29.43	1602	0.75	
6		4.3	54.60	28.66	1565	1.75	
7		2.8	54.27	28.35	1539	1.16	
8	⊥	3.7	54.32	29.04	1577	1.49	
9	⊥	3.1	54.45	29.94	1630	1.21	
10	⊥	2.6	54.59	28.07	1532	1.08	
11	⊥	3.1	54.20	28.13	1525	1.29	
12	⊥	3.7	54.46	28.19	1535	1.53	1.44
Strongman No. 2 D seam							
1	⊥	3.1	54.52	27.43	1495.5	1.32	
2	⊥	3.6	54.28	24.22	1314.7	1.74	
3	⊥	4.4	54.36	26.01	1413.9	1.98	
4	⊥	3.0	54.48	25.89	1410.5	1.35	
5		2.9	54.31	27.70	1504.4	1.23	
6		1.5	54.64	30.64	1674.2	0.57	
7	⊥	4.2	54.50	25.74	1402.8	1.90	
8	⊥	2.6	54.36	25.82	1403.6	1.18	1.45
Strongman No. 2 E seam (OC)							
1	⊥	4.0	54.19	24.79	1343.4	1.89	
2		4.5	54.07	25.01	1352.3	2.12	
3		3.6	54.81	28.56	1565.4	1.46	
4	⊥	4.0	54.17	23.55	1275.7	1.99	
5		3.1	54.20	24.54	1330.1	1.48	1.79
E seam (UG)							
1	⊥	4.0	54.36	27.99	1521.5	1.67	
2	⊥	2.5	54.34	27.11	1473.2	1.08	
3	∥	5.4	54.08	25.50	1379.0	2.49	
4		5.3	54.13	26.07	1411.2	2.39	
5		3.5	54.34	26.22	1424.8	1.56	
6	⊥	4.2	54.22	25.51	1383.2	1.93	
7	⊥	1.0	54.09	25.56	1382.5	0.46	
8	⊥	3.5	53.95	24.97	1347.1	1.65	
9		3.6	54.21	26.32	1426.8	1.60	
10		5.2	54.39	31.07	1689.9	1.96	
11	⊥	6.0	54.93	26.90	1477.6	2.58	
12	∥	3.2	54.46	26.16	1424.7	1.43	1.82

Table A6.1. Results of Brazilian (indirect tensile strength) tests.

Appendix 7. Shear Strength

A7.1 Test Method

Shear strength tests were conducted as per the ISRM recommendations outlined in Brown (1981) using a portable direct shear box. Five specimens were tested for each of the Strongman No. 2 D and E seams. Two tests from each seam were considered to invalid. Each test specimen was sheared at normal loads of 2.5, 5.0 and 7.5 kN. This corresponds to a maximum normal load of 2.4 MPa, which is considerably lower than the maximum overburden pressures, but the weakness of the samples prevents higher normal loads being used. The full set of results from the test regime is presented in Table A7.1. Plots of shear stress vs. normal stress for both seams are presented in Figures A7.1 and A7.2. The shear and normal stresses are calculated as follows:

$$\text{Shear stress } \tau = \frac{P_s}{A}$$

$$\text{Normal stress } \sigma_n = \frac{P_n}{A}$$

where: P_s = total shear force

P_n = total normal force

A = area of shear surface overlap (>2500mm^2)

The following is the specifications of the Robertson Geologging Portable Direct Shear Box and low friction pressure maintainer:

Maximum load capacity:	Normal Load – 50 kN
	Shear Load – 50 kN
Maximum shear displacement:	25mm
Maximum hydraulic pressure:	68.95 MPa (10,000 PSI)

A7.2 Data Tables

Sample No.	Displacement Original	P_n (kN)	P_s (kN)	Travel (mm)	Area (mm^2)	τ (MPa)	σ_n (MPa)	JRC	c (MPa)	ϕ
Strongman No. 2 D seam										
SM/D/1	13.06	2.5	2.4	0.97	4156	0.58	0.60	10-12	0.37	26.6
	13.37	5.0	4.8	0.64		1.15	1.20			
	15.75	7.5	4.9	5.49		1.18	1.80			
SM/D/2	15.43	2.5	2.1	2.29	4665	0.45	0.54	8-10	0.02	33.6
	15.80	5.0	2.8	2.24		0.60	1.07			
	16.06	7.5	5.4	4.49		1.16	1.61			
SM/D/3	15.85	2.5	4.8	1.35	4033	1.19	0.62	12-14,16-18		
	16.01	5.0	3.8	2.55		0.94	1.24			
	15.42	7.5	2.8	3.07		0.69	1.86			
SM/D/4	16.06	2.5	3.1	1.96	3861	0.80	0.65	11		
	15.62	5.0	1.5	1.62		0.39	1.30			
	16.94	7.5	1.2	1.90		0.31	1.94			
SM/D/5	18.70	2.5	2.4	0.90	3134	0.77	0.80	15	0.48	18.3
	17.42	5.0	3.0	1.44		0.96	1.60			
	17.42	7.5	4.0	1.13		1.30	2.40			
Strongman No. 2 E seam										
SM/E/OC/1	14.10	2.5	4.0	1.71	4377	0.91	0.57	14-16		
	15.68	5.0	2.8	2.58		0.64	1.14			
	18.11	7.5	2.1	3.23		0.48	1.71			
SM/E/OC/2	13.86	2.5	1.8	4.51	4452	0.40	0.56	8-10, 4-6	0.26	15.9
	11.41	5.0	2.7	5.28		0.61	1.12			
	14.12	7.5	3.2	2.07		0.72	1.68			
SM/E/UG/1	11.20	2.5	1.0	4.1	3384	0.30	0.74	4	0.10	12.6
	12.17	5.0	1.2	0.7		0.35	1.48			
	11.82	7.5	2.1	1.21		0.62	2.22			
SM/E/UG/2	18.21	2.5	2.0	0.2	3420	0.58	0.73	15	0.43	11.6
	20.26	5.0	2.5	0.3		0.73	1.46			
	18.87	7.5	3.0	1.33		0.88	2.19			

Table A7.1. Results of shear strength tests.

A7.3 Plots of Shear Strength vs. Normal Stress

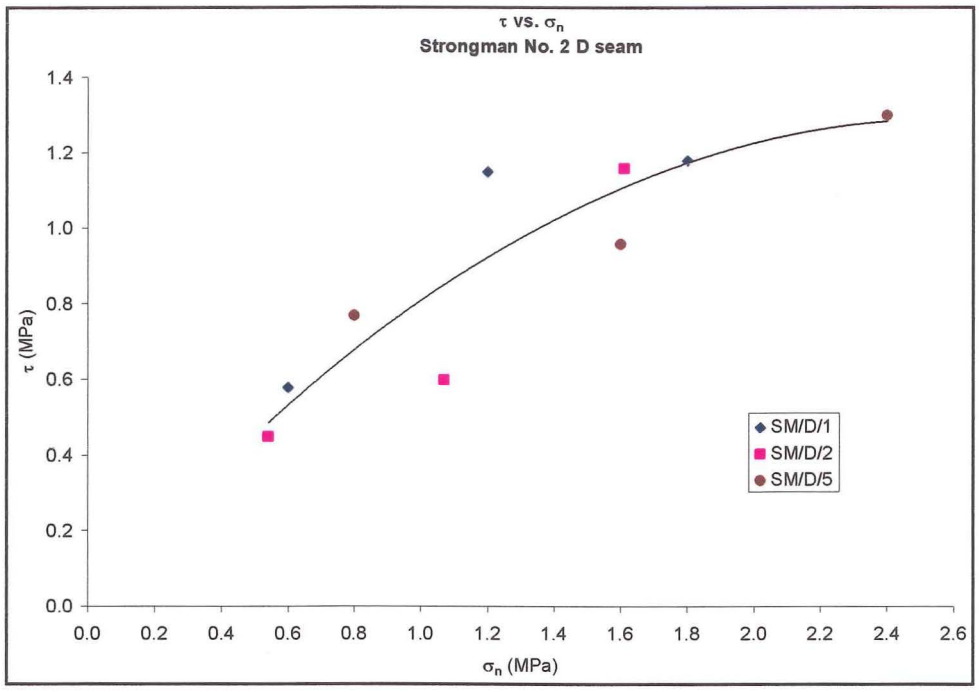

Figure A7.1. Shear stress vs. normal stress. Strongman No. 2 D seam

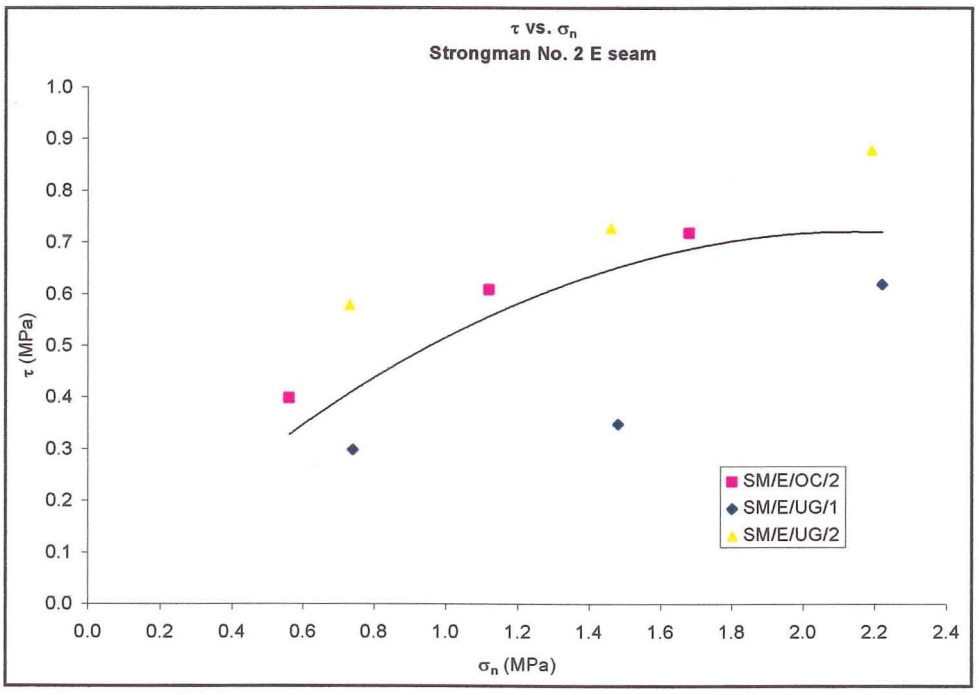

Figure A7.2. Shear stress vs. normal stress. Strongman No. 2 E seam.

Appendix 8. Proximate Analysis

A8.1 Bishop Block

The following proximate analyses were performed on samples taken by Solid Energy. The location where the samples were collected is the same adits described in section 1.5.1 where the samples used in this project were collected. Analysis performed by CRL Energy Ltd (report dated 21st August 2002) unless otherwise stated.

A8.1.1 Kimbell Seam (Sample location 1. Map 1)

Analysis-Air dried basis

Inherent Moisture	(ASTM D 5142-90 mod)	%	2.1
Ash	(ASTM D 5142-90 mod)	%	1.3
Volatile Matter	(ASTM D 5142-90 mod)	%	38.4
Fixed Carbon	by difference	%	58.2
Sulphur	(ASTM D 4239-85)	%	0.26
Swelling Index	(ISO 501-1981)		9.5

Mean Maximum Reflectance of Vitrinite	%	0.87

Analysis performed by SGS New Zealand Ltd (report dated 16th August 2000) on sample provided by Solid Energy.

A8.1.2 Kimbell Seam (Sample location 2. Map 1)

Analysis-Air dried basis

			Sample A	Sample B
Lab Reference			D00-577	D00-578
Inherent Moisture	(ASTM D 5142-90 mod)	%	3.3	3.1
Ash	(ASTM D 5142-90 mod)	%	3.7	2.1
Volatile Matter	(ASTM D 5142-90 mod)	%	34.2	35.0
Fixed Carbon	by difference	%	58.8	59.8
Sulphur	(ASTM D 4239-85)	%	0.3	0.28
Swelling Index	(ISO 501-1981)		2.5	3

Analysis-As received basis

Total Moisture	Calculated	%	7.4	5.3
Loss on Air Drying	(ISO 1988-1975)	%	4.2	2.3
Ash	(ASTM D 5142-90 mod)	%	3.5	2.1
Volatile Matter	(ASTM D 5142-90 mod)	%	32.8	34.2
Fixed Carbon	by difference	%	56.3	58.4
Sulphur	(ASTM D 4239-85)	%	0.29	0.27
Swelling Index	(ISO 501-1981)		2.5	3

A8.1.3 Morgan Seam

Analysis-Air dried basis

			Sample A	Sample B
Lab Reference			D00-579	D00-580
Inherent Moisture	(ASTM D 5142-90 mod)	%	1.4	1.3
Ash	(ASTM D 5142-90 mod)	%	3.1	2.0
Volatile Matter	(ASTM D 5142-90 mod)	%	37.8	38.0

Fixed Carbon	by difference	%	57.7	58.7
Sulphur	(ASTM D 4239-85)	%	0.31	0.32
Swelling Index	(ISO 501-1981)		9	9.5

Analysis-As received basis

Total Moisture	Calculated	%	7.8	6.7
Loss on Air Drying	(ISO 1988-1975)	%	6.5	5.5
Ash	(ASTM D 5142-90 mod)	%	2.9	1.9
Volatile Matter	(ASTM D 5142-90 mod)	%	35.3	35.9
Fixed Carbon	by difference	%	54.0	55.5
Sulphur	(ASTM D 4239-85)	%	0.29	0.30
Swelling Index	(ISO 501-1981)		9	9.5

Analysis of Kimbell seam sample (location 2) and Morgan seam sample performed by SGS New Zealand ltd (report dated 14th June 2000) on sample provided by Solid Energy.

A8.2 Roa Mine

Analysis-as received basis

Sample Number (this study)			R/K/C1	R/K/C3
Moisture	(ISO 5068)	%	0.7	0.4
Ash	(ISO 1171)	%	1.2	3.3
Volatile Matter	(ISO 562)	%	18.8	19.3
Fixed Carbon	by difference	%	79.3	77.0

Other samples were tested for ash only. The results of these are as follows:

R/K/C2	R/K/C4	R/K/C5	R/K/C6	R/K/C7
2.2%	1.6%	2.5%	1.3%	1.2%

A8.3 Spring Creek Mine

A8.3.1 D seam

Analysis-as received basis

Sample Number (this study)			SC/D/C1	SC/D/C5
Moisture		%	4.7	3.7
Ash	(ISO 5068)	%	1.0	1.8
Volatile Matter	(ISO 1171)	%	37.9	39.4
Fixed Carbon	(ISO 562)	%	56.4	55.1

A8.3.2 Main Upper seam

Analysis-as received basis

Sample Number (this study)			SC/MNU/C2	SC/MNU/C4
Moisture		%	3.8	4.0
Ash	(ISO 5068)	%	2.0	1.3
Volatile Matter	(ISO 1171)	%	40.2	41.6
Fixed Carbon	(ISO 562)	%	54.0	53.1
Mean Maximum Reflectance of Vitrinite		%	0.62	

Other samples were tested for ash only. The results of these are as follows:

SC/MNU/C1	SC/MNU/C3	SC/MNU/C5
2.0%	2.2%	1.6%

A8.4 Strongman No. 2 Mine

A8.4.1 D seam

Analysis-as received basis

Sample Number (this study)			SM/D/29
Moisture	(ISO 5068)	%	2.8
Ash	(ISO 1171)	%	2.2
Volatile Matter	(ISO 562)	%	41.0
Fixed Carbon		%	54.0

A8.4.2 E seam (Opencast)

Analysis-as received basis

Sample Number (this study)			SM/E/OC/C1	SM/E/OC/C4	SM/E/OC/C6
\Moisture	(ISO 5068)	%	3.2	2.1	2.4
Ash	(ISO 1171)	%	1.7	2.1	1.6
Volatile Matter	(ISO 562)	%	39.2	40.8	39.1
Fixed Carbon	by difference	%	55.9	55.0	56.9

Other samples were tested for ash only. The results of these are as follows:

SM/E/OC/C2	SM/E/OC/C3	SM/E/OC/C5	SM/E/OC/C7	SM/E/OC/C8
2.0%	2.1%	1.0%	1.4%	1.0%

A8.5 Terrace Mine

Lab Reference			68/429

Analysis-As received basis

Moisture	(ISO 5068-1983)	%	15.3
Ash	(ISO 1171-1981)	%	3.4
Volatile Matter	(ISO 562-1981)	%	37.4
Fixed Carbon	by difference	%	43.9

Analysis performed by CRL Energy Ltd on sample provided by this study (report dated 8th February 2002).

Appendix 9. Pillar Design

A9.1 Extraction Ratio

Roadway Width	Pillar Width																
	4	5	6	7	8	9	10	11	12	13	14	15	16	17	18	19	20
2.00	0.56	0.49	0.44	0.40	0.36	0.33	0.31	0.28	0.27	0.25	0.23	0.22	0.21	0.20	0.19	0.18	0.17
2.50	0.62	0.56	0.50	0.46	0.42	0.39	0.36	0.34	0.32	0.30	0.28	0.27	0.25	0.24	0.23	0.22	0.21
3.00	0.67	0.61	0.56	0.51	0.47	0.44	0.41	0.38	0.36	0.34	0.32	0.31	0.29	0.28	0.27	0.25	0.24
3.50	0.72	0.65	0.60	0.56	0.52	0.48	0.45	0.42	0.40	0.38	0.36	0.34	0.33	0.31	0.30	0.29	0.28
4.00	0.75	0.69	0.64	0.60	0.56	0.52	0.49	0.46	0.44	0.42	0.40	0.38	0.36	0.34	0.33	0.32	0.31
4.50	0.78	0.72	0.67	0.63	0.59	0.56	0.52	0.50	0.47	0.45	0.43	0.41	0.39	0.37	0.36	0.35	0.33
5.00	0.80	0.75	0.70	0.66	0.62	0.59	0.56	0.53	0.50	0.48	0.46	0.44	0.42	0.40	0.39	0.37	0.36
5.50	0.82	0.77	0.73	0.69	0.65	0.61	0.58	0.56	0.53	0.51	0.48	0.46	0.45	0.43	0.41	0.40	0.38
6.00	0.84	0.79	0.75	0.71	0.67	0.64	0.61	0.58	0.56	0.53	0.51	0.49	0.47	0.45	0.44	0.42	0.41

Roadway Width	Pillar Width																
	21	22	23	24	25	26	27	28	29	30	31	32	33	34	35	36	37
2.00	0.17	0.16	0.15	0.15	0.14	0.14	0.13	0.13	0.12	0.12	0.12	0.11	0.11	0.11	0.11	0.10	0.10
2.50	0.20	0.19	0.19	0.18	0.17	0.17	0.16	0.16	0.15	0.15	0.14	0.14	0.14	0.13	0.13	0.13	0.12
3.00	0.23	0.23	0.22	0.21	0.20	0.20	0.19	0.18	0.18	0.17	0.17	0.16	0.16	0.16	0.15	0.15	0.14
3.50	0.27	0.26	0.25	0.24	0.23	0.22	0.22	0.21	0.20	0.20	0.19	0.19	0.18	0.18	0.17	0.17	0.17
4.00	0.29	0.28	0.27	0.27	0.26	0.25	0.24	0.23	0.23	0.22	0.22	0.21	0.20	0.20	0.19	0.19	0.19
4.50	0.32	0.31	0.30	0.29	0.28	0.27	0.27	0.26	0.25	0.24	0.24	0.23	0.23	0.22	0.21	0.21	0.21
5.00	0.35	0.34	0.33	0.32	0.31	0.30	0.29	0.28	0.27	0.27	0.26	0.25	0.25	0.24	0.23	0.23	0.22
5.50	0.37	0.36	0.35	0.34	0.33	0.32	0.31	0.30	0.29	0.29	0.28	0.27	0.27	0.26	0.25	0.25	0.24
6.00	0.40	0.38	0.37	0.36	0.35	0.34	0.33	0.32	0.31	0.31	0.30	0.29	0.28	0.28	0.27	0.27	0.26

Roadway Width	Pillar Width																
	38	39	40	41	42	43	44	45	46	47	48	49	50	51	52	53	54
2.00	0.10	0.10	0.09	0.09	0.09	0.09	0.09	0.08	0.08	0.08	0.08	0.08	0.08	0.07	0.07	0.07	0.07
2.50	0.12	0.12	0.11	0.11	0.11	0.11	0.10	0.10	0.10	0.10	0.10	0.09	0.09	0.09	0.09	0.09	0.09
3.00	0.14	0.14	0.13	0.13	0.13	0.13	0.12	0.12	0.12	0.12	0.11	0.11	0.11	0.11	0.11	0.10	0.10
3.50	0.16	0.16	0.15	0.15	0.15	0.14	0.14	0.14	0.14	0.13	0.13	0.13	0.13	0.12	0.12	0.12	0.12
4.00	0.18	0.18	0.17	0.17	0.17	0.16	0.16	0.16	0.15	0.15	0.15	0.15	0.14	0.14	0.14	0.14	0.13
4.50	0.20	0.20	0.19	0.19	0.18	0.18	0.18	0.17	0.17	0.17	0.16	0.16	0.16	0.16	0.15	0.15	0.15
5.00	0.22	0.21	0.21	0.21	0.20	0.20	0.19	0.19	0.19	0.18	0.18	0.18	0.17	0.17	0.17	0.16	0.16
5.50	0.24	0.23	0.23	0.22	0.22	0.21	0.21	0.21	0.20	0.20	0.20	0.19	0.19	0.19	0.18	0.18	0.18
6.00	0.25	0.25	0.24	0.24	0.23	0.23	0.23	0.22	0.22	0.21	0.21	0.21	0.20	0.20	0.20	0.19	0.19

Roadway Width	Pillar Width																
	55	56	57	58	59	60	61	62	63	64	65	66	67	68	69	70	71
2.00	0.07	0.07	0.07	0.07	0.06	0.06	0.06	0.06	0.06	0.06	0.06	0.06	0.06	0.06	0.06	0.05	0.05
2.50	0.09	0.08	0.08	0.08	0.08	0.08	0.08	0.08	0.07	0.07	0.07	0.07	0.07	0.07	0.07	0.07	0.07
3.00	0.10	0.10	0.10	0.10	0.09	0.09	0.09	0.09	0.09	0.09	0.09	0.09	0.08	0.08	0.08	0.08	0.08
3.50	0.12	0.11	0.11	0.11	0.11	0.11	0.11	0.10	0.10	0.10	0.10	0.10	0.10	0.10	0.09	0.09	0.09
4.00	0.13	0.13	0.13	0.12	0.12	0.12	0.12	0.12	0.12	0.11	0.11	0.11	0.11	0.11	0.11	0.11	0.10
4.50	0.15	0.14	0.14	0.14	0.14	0.13	0.13	0.13	0.13	0.13	0.13	0.12	0.12	0.12	0.12	0.12	0.12
5.00	0.16	0.16	0.15	0.15	0.15	0.15	0.15	0.14	0.14	0.14	0.14	0.14	0.13	0.13	0.13	0.13	0.13
5.50	0.17	0.17	0.17	0.17	0.16	0.16	0.16	0.16	0.15	0.15	0.15	0.15	0.15	0.14	0.14	0.14	0.14
6.00	0.19	0.18	0.18	0.18	0.18	0.17	0.17	0.17	0.17	0.16	0.16	0.16	0.16	0.16	0.15	0.15	0.15

Table A9.1. Percentage extraction for different pillar and roadway widths.

A9.2 Pillar Stress

	Extraction Ratio %														
Depth (m)	0.05	0.10	0.15	0.20	0.25	0.30	0.35	0.40	0.45	0.50	0.55	0.60	0.65	0.70	0.75
20	0.53	0.56	0.59	0.63	0.67	0.71	0.77	0.83	0.91	1.00	1.11	1.25	1.43	1.67	2.00
30	0.79	0.83	0.88	0.94	1.00	1.07	1.15	1.25	1.36	1.50	1.67	1.88	2.14	2.50	3.00
40	1.05	1.11	1.18	1.25	1.33	1.43	1.54	1.67	1.82	2.00	2.22	2.50	2.86	3.33	4.00
50	1.32	1.39	1.47	1.56	1.67	1.79	1.92	2.08	2.27	2.50	2.78	3.13	3.57	4.17	5.00
60	1.58	1.67	1.76	1.88	2.00	2.14	2.31	2.50	2.72	3.00	3.33	3.75	4.29	5.00	6.00
70	1.84	1.94	2.06	2.19	2.33	2.50	2.69	2.92	3.18	3.50	3.89	4.38	5.00	5.83	7.00
80	2.11	2.22	2.35	2.50	2.67	2.86	3.08	3.33	3.64	4.00	4.44	5.00	5.71	6.67	8.00
90	2.37	2.50	2.65	2.81	3.00	3.21	3.46	3.75	4.09	4.50	5.00	5.63	6.43	7.50	9.00
100	2.63	2.78	2.94	3.13	3.33	3.57	3.85	4.17	4.55	5.00	5.56	6.25	7.14	8.33	10.00
110	2.89	3.06	3.24	3.44	3.67	3.93	4.23	4.58	5.00	5.50	6.11	6.88	7.86	9.17	11.00
120	3.16	3.33	3.53	3.75	4.00	4.29	4.62	5.00	5.45	6.00	6.67	7.50	8.57	10.00	12.00
130	3.42	3.61	3.82	4.06	4.33	4.64	5.00	5.42	5.91	6.50	7.22	8.13	9.29	10.83	13.00
140	3.68	3.89	4.12	4.38	4.67	5.00	5.38	5.83	6.36	7.00	7.78	8.75	10.00	11.67	14.00
150	3.95	4.17	4.41	4.69	5.00	5.36	5.77	6.25	6.82	7.50	8.33	9.38	10.71	12.50	15.00
160	4.21	4.44	4.71	5.00	5.33	5.71	6.15	6.67	7.27	8.00	8.89	10.00	11.43	13.33	16.00
170	4.47	4.72	5.00	5.31	5.67	6.07	6.54	7.08	7.73	8.50	9.44	10.63	12.14	14.17	17.00
180	4.74	5.00	5.29	5.63	6.00	6.43	6.92	7.50	8.18	9.00	10.00	11.25	12.86	15.00	18.00
190	5.00	5.28	5.59	5.94	6.33	6.79	7.31	7.92	8.64	9.50	10.56	11.88	13.57	15.83	19.00
200	5.26	5.56	5.88	6.25	6.67	7.14	7.69	8.33	9.09	10.00	11.11	12.50	14.29	16.67	20.00
210	5.53	5.83	6.18	6.56	7.00	7.50	8.08	8.75	9.55	10.50	11.67	13.13	15.00	17.50	21.00
220	5.79	6.11	6.47	6.88	7.33	7.86	8.46	9.17	10.00	11.00	12.22	13.75	15.71	18.33	22.00
230	6.05	6.39	6.76	7.19	7.67	8.21	8.85	9.58	10.45	11.50	12.78	14.38	16.43	19.17	23.00
240	6.32	6.67	7.06	7.50	8.00	8.57	9.23	10.00	10.91	12.00	13.33	15.00	17.14	20.00	24.00
250	6.58	6.94	7.35	7.81	8.33	8.93	9.62	10.42	11.36	12.50	13.89	15.63	17.86	20.83	25.00
260	6.84	7.22	7.65	8.13	8.67	9.29	10.00	10.83	11.82	13.00	14.44	16.25	18.57	21.67	26.00
270	7.11	7.50	7.94	8.44	9.00	9.64	10.38	11.25	12.27	13.50	15.00	16.88	19.29	22.50	27.00
280	7.37	7.78	8.24	8.75	9.33	9.99	10.77	11.67	12.73	14.00	15.56	17.50	20.00	23.33	28.00
290	7.63	8.06	8.53	9.06	9.67	10.34	11.15	12.08	13.18	14.50	16.11	18.13	20.71	24.17	29.00
300	7.89	8.33	8.82	9.38	10.00	10.69	11.54	12.50	13.64	15.00	16.67	18.75	21.43	25.00	30.00

Table A9.2. Overburden stress for varying extraction ratios for any depth likely to be encountered in the Greymouth Coalfield.

Depth (m)	Percentage extraction					
	0.05	0.10	0.15	0.20	0.25	0.30
150	3.55	3.75	3.97	4.22	4.50	4.82
160	3.79	4.00	4.24	4.50	4.80	5.14
170	4.03	4.25	4.50	4.78	5.10	5.46
175	4.14	4.38	4.63	4.92	5.25	5.63
180	4.26	4.50	4.76	5.06	5.40	5.79
190	4.50	4.75	5.03	5.34	5.70	6.11
200	4.84	5.11	5.41	5.75	6.13	6.57
210	5.08	5.37	5.68	6.04	6.44	6.90
220	5.37	5.67	6.00	6.38	6.81	7.29
225	5.49	5.80	6.14	6.53	6.96	7.46
230	5.62	5.93	6.28	6.67	7.11	7.62
240	5.89	6.21	6.58	6.99	7.46	7.99
250	6.26	6.47	6.85	7.28	7.77	8.32
260	6.51	6.79	7.19	7.64	8.15	8.73
270	6.68	7.05	7.46	7.93	8.46	9.06
275	6.80	7.18	7.60	8.08	8.62	9.23

Table A9.3. Overburden stress for the Terrace mine No. 4 seam. Gravels with ρ = 2.0 kg/m^3 comprise the top 80m of overburden. Rock below this has ρ = 2.5 kg/m^3. Overburden stress has been calculated by adjusting the overburden density at 20m intervals.

A9.3 Pillar Strength

The values given in the following tables were calculated using strengths determined in Chapter Two or by using equation 3.13. These values were used in the determination of the pillar design charts presented in Figures 4.8a-g. Bieniawski refers to the use of equations 4.10 ($w/h < 5$) and 4.12 ($w/h \geq 5$). Salamon refers to the use of equations 4.9 ($w/h < 5$) and 4.13 ($w/h \geq 5$). Pillar strengths have been calculated using the following assumptions: Strongman No. 2, Spring Creek and the Bishop Block have roadways 5m wide and an initial mining thickness of 3m. The Roa mine uses roadways 2m wide and has an initial mining thickness of 2.5m. The Terrace mine also has roadways 3m wide but uses an initial mining thickness of 3m.

Bishop Block	σ_1 = 2.1		**Bishop Block**	σ_1 = 1.8	
Kimbell seam	K = 3.58		**Morgan seam**	K = 3.13	
Pillar	Pillar Strength (MPa)		Pillar	Pillar Strength (MPa)	
width	Salamon	Bieniawski	width	Salamon	Bieniawski
6	3.95	2.86	6	3.46	2.45
7	4.24	3.11	7	3.71	2.66
8	4.51	3.36	8	3.95	2.88
9	4.76	3.61	9	4.16	3.10
10	5.00	3.86	10	4.37	3.31
11	5.22	4.12	11	4.57	3.53
12	5.44	4.37	12	4.75	3.74
13	5.64	4.62	13	4.93	3.96
14	5.84	4.87	14	5.10	4.18
15	6.02	7.32	15	5.26	6.28
16	6.21	7.83	16	5.43	6.71
17	6.43	8.35	17	5.62	7.16
18	6.67	8.88	18	5.83	7.61
19	6.94	9.41	19	6.06	8.07
20	7.23	9.96	20	6.32	8.54
21	7.54	10.51	21	6.59	9.01
22	7.88	11.08	22	6.89	9.50
23	8.24	11.65	23	7.21	9.98
24	8.63	12.23	24	7.55	10.48
25	9.05	12.82	25	7.91	10.99
26	9.49	13.41	26	8.29	11.50
27	9.95	14.01	27	8.70	12.01
28	10.44	14.63	28	9.13	12.54
29	10.96	15.24	29	9.58	13.07
30	11.51	15.87	30	10.06	13.60

Table A9.4. a) strength of coal pillars in Bishop Block Kimbell seam; b) strength of coal pillars in Bishop Block Morgan seam.

Spring Creek D seam	σ_1 = 2.2 K = 3.75		**Spring Creek Main Upper seam**	σ_1 = 1.7 K = 2.95	
Pillar width	Pillar Strength (MPa) Salamon	Bieniawski	Pillar width	Pillar Strength (MPa) Salamon	Bieniawski
15	6.30	7.67	20	7.57	8.06
16	6.51	8.20	21	7.90	8.51
17	6.73	8.75	22	8.25	8.97
18	6.99	9.30	23	8.63	9.43
19	7.27	9.86	24	9.04	9.90
20	7.57	10.43	25	9.48	10.38
21	7.90	11.02	26	9.94	10.86
22	8.25	11.61	27	10.42	11.35
23	8.63	12.20	28	10.94	11.84
24	9.04	12.81	29	11.48	12.34
25	9.48	13.43	30	12.05	12.85
26	9.94	14.05	31	12.65	13.36
27	10.42	14.68	32	13.28	13.88
28	10.94	15.32	33	13.94	14.40
29	11.48	15.97	34	14.62	14.93
30	12.05	16.62	35	15.34	15.46
31	12.65	17.29	36	16.08	16.00
32	13.28	17.96	37	16.86	16.54
33	13.94	18.63	38	17.66	17.09
34	14.62	19.32	39	18.50	17.65
35	15.34	20.01	40	19.36	18.21
36	16.08	20.71			

Table A9.5. a) strength of coal pillars in Spring Creek D seam; b) strength of coal pillars in Spring Creek Main Upper seam.

Roa Mine Kimbell seam	σ_1 = 0.32 K = 0.557		**Terrace mine No. 4 seam**	σ_1 = 1.31 K = 2.27	
Pillar width	Pillar Strength (MPa) Salamon	Bieniawski	Pillar width	Pillar Strength (MPa) Salamon	Bieniawski
10	0.88	0.67	18	4.23	5.54
11	0.92	0.71	19	4.40	5.87
12	0.95	0.76	20	4.58	6.21
13	0.99	1.16	21	4.78	6.56
14	1.03	1.26	22	5.00	6.91
15	1.08	1.35	23	5.23	7.27
16	1.13	1.45	24	5.47	7.63
17	1.19	1.55	25	5.74	7.99
18	1.25	1.65	26	6.02	8.37
19	1.32	1.76	27	6.31	8.74
20	1.39	1.86	28	6.62	9.12
21	1.47	1.97	29	6.95	9.51
22	1.56	2.08	30	7.30	9.90
23	1.65	2.19	31	7.66	10.29
24	1.75	2.30	32	8.04	10.69
25	1.86	2.42	33	8.44	11.10
26	1.97	2.53	34	8.85	11.50

27	2.09	2.65
28	2.21	2.77
29	2.34	2.89
30	2.48	3.01
31	2.62	3.13
32	2.77	3.26
33	2.93	3.39
34	3.09	3.51
35	3.26	3.64
36	3.44	3.77
37	3.63	3.90
38	3.82	4.03
39	4.02	4.17
40	4.23	4.30
41	4.44	4.44
42	4.66	4.58
43	4.89	4.72
44	5.13	4.86
45	5.37	5.00
46	5.62	5.14
47	5.88	5.28
48	6.15	5.43
49	6.42	5.57
50	6.71	5.72
51	7.00	5.86
52	7.29	6.01
53	7.60	6.16
54	7.92	6.31
55	8.24	6.47
56	8.57	6.62
57	8.91	6.77
58	9.26	6.93
59	9.61	7.08
60	9.97	7.24
61	10.35	7.40
62	10.73	7.56
63	11.12	7.72
64	11.52	7.88
65	11.92	8.04
66	12.34	8.20
67	12.76	8.36
68	13.20	8.53
69	13.64	8.69
70	14.09	8.86
71	14.55	9.03
72	15.02	9.19
73	15.49	9.36
74	15.98	9.53

35	9.28	11.91
36	9.74	12.33
37	10.20	12.75
38	10.69	13.17
39	11.20	13.60
40	11.72	14.03
41	12.26	14.47
42	12.83	14.91
43	13.41	15.35
44	14.01	15.80
45	14.63	16.25
46	15.27	16.70

Strongman No. 2 $\sigma_1 = 4.2$

D and E seams K = 7.2

Pillar width	Pillar Strength (MPa) Salamon	Bieniawski
6	7.95	5.71
7	8.53	6.22
8	9.08	6.72
9	9.58	7.22
10	10.06	7.73
11	10.51	8.23
12	10.94	8.74
13	11.35	9.24
14	11.74	9.74
15	12.10	10.25
16	12.49	10.75
17	12.93	11.26
18	13.42	11.76

Table A9.6. a) strength of coal pillars in the Roa mine Kimbell seam; b) strength of coal pillars in the Terrace mine No. 4 seam; c) strength of coal pillars in the Strongman No. 2 mine D and E seams.

A9.4 Pillar Design

A9.4.1 Optimum Pillar Size

The overburden load which pillars must support is dependant on the extraction ratio, *e*, which depends on the mining height, roadway width and pillar size. Roadway widths and mining heights are summarised in Table A9.7. Pillars for main roadways (M & M entrances) must remain stable for a much longer period and subsequently are designed to a higher factor of safety of 2.0. Optimum pillar sizes for M & M entrances are summarised in Table 4.4.

Mine	Mining Height (m)	Roadway width (m) Sub-levels	M & M entrances
Bishop Block	3	5	6
Roa	2	2	4
Spring Creek	3	5	6
Strongman No. 2	3	5	6
Terrace	3	2	3

Table A9.7. Summary of mining heights (upon first extraction) and roadway widths for each of the mines used in this study.

A9.4.2 Pillar Design in Dipping Seams

Pillars can be designed for specific dip intervals in the Spring Creek D seam due to the strength data gained in section 2.2.2 and presented in Figure 2.6. Not enough information is known about the strength of other seams with respect to loading orientation for this to be conducted. The effect is expected to be similar in the Main Upper seam where the bedding is also very pronounced, but the effect will be significantly less in other seams where bedding is often difficult to determine.

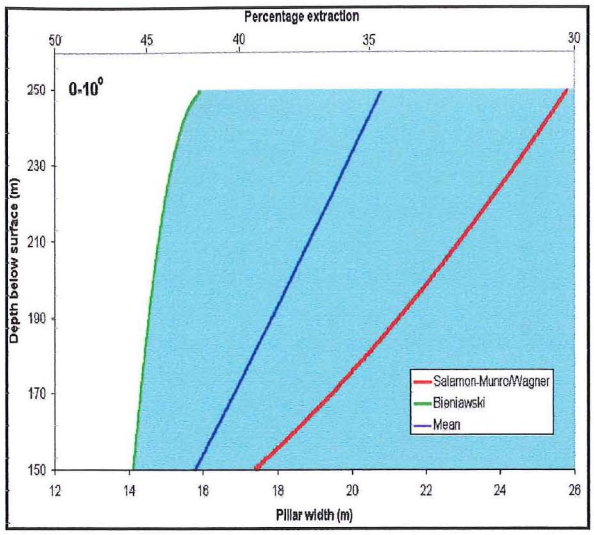

a)

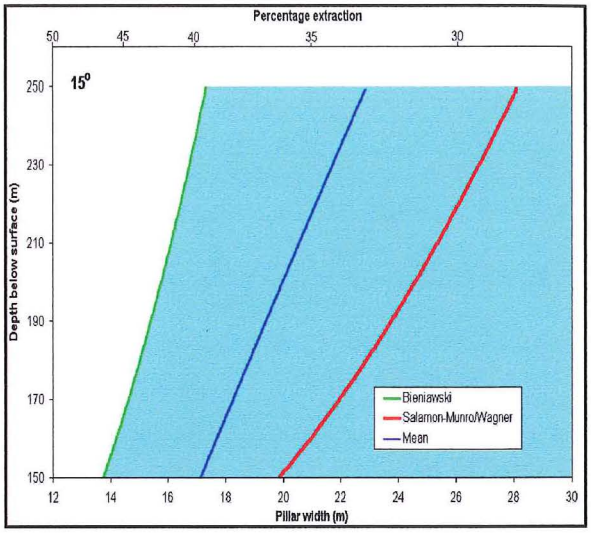

b)

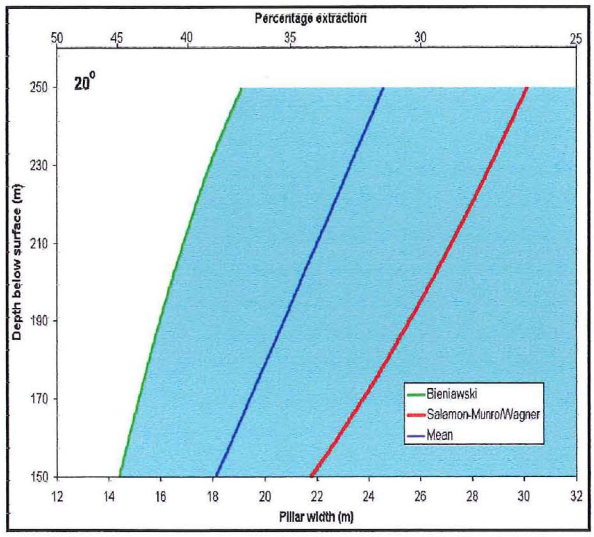

c)

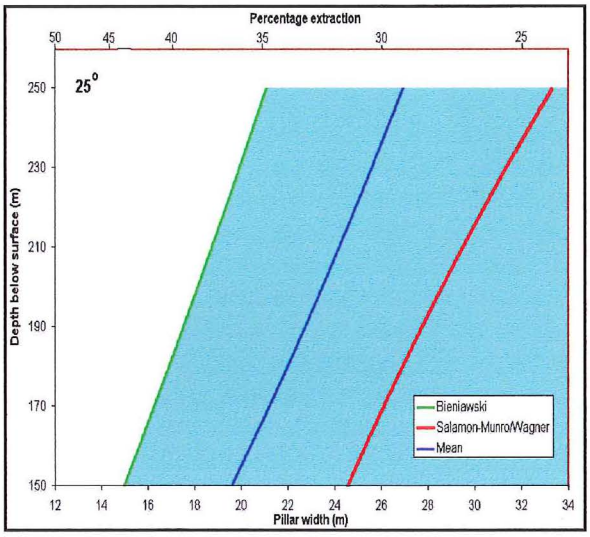

d)

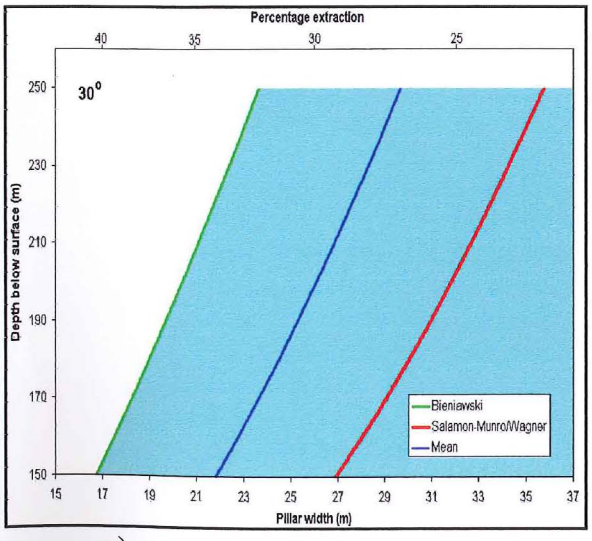

e)

Figure A9.1a-e. Pillar sizes for Spring Creek D seam at different seam dips. Strength difference for each seam dip derived from Figure 2.6. Coal strength is considered to be constant when seam dip is 0°-10° and then decreases with increasing seam dip. a) Seam dip 0°-10°; b) seam dip 15°; c) seam dip 20°; d) seam dip 25°; e) seam dip 30°.

Depth (m)	Optimum Square Pillar Size for Spring Creek D seam				
	Seam Dip				
	0-10°	15°	20°	25°	30°
150	15.8	17.1	18.2	19.6	21.8
160	16.3	17.7	18.8	20.4	22.8
170	16.8	18.3	19.4	21.3	23.8
180	17.4	18.9	20.0	21.9	24.4
190	17.9	19.4	20.7	22.8	25.3
200	18.4	19.9	21.4	23.5	26.0
210	18.9	20.6	22.1	24.3	26.9
220	19.3	21.2	22.8	24.9	27.6
230	19.7	21.8	23.2	25.6	28.3
240	20.4	22.3	23.9	26.3	29.0
250	20.9	22.9	24.6	30.0	29.7

Table A9.8. Optimum pillar size for Spring Creek D seam using specific depth and seam dip intervals. These sizes do not take into account the factor of safety against shearing in steeply dipping seams as this needs to be calculated separately (section 4.5). Designed to a factor of safety of 1.6.